# *Deep-water circulation and detrital provenance in the South Pacific, from the present day until 240 000 years ago. Evidence from Nd, Sr and Pb isotopes and Rare Earth Elements*

Mario Molina Kescher

Dissertation

Kiel 2014

# Deep-water circulation and detrital provenance in the South Pacific, from the present day until 240 000 years ago. Evidence from Nd, Sr and Pb isotopes and Rare Earth Elements

**Dissertation**
**zur Erlangung des Doktorgrades**

**Dr. rer. nat.**

**Der Mathematisch-Naturwissenschaftlichen Fakultät**

**der Christian-Albrechts-Universität zu Kiel**

**Mario Molina Kescher**

**Kiel, 2014**

1. Gutachter und Betreuer: Prof. Dr. Martin Frank
2. Gutachter: Dr. Katharina Pahnke

Eingereicht am: 12. Juni 2014
Datum der Disputation: 18. Juli 2014
Zum Druck genehmigt:

Gez. Prof. Dr. Wolgang J. Duschl, Dekan

## Erklärung

Hiermit versichere ich an Eides statt, dass ich diese Dissertation selbständig und nur mit Hilfe der angegebenen Quellen und Hilfsmittel erstellt habe. Ferner versichere ich, dass der Inhalt dieses Dokumentes weder in dieser, noch in veränderter Form, einer weiteren Prüfungsbehörde vorliegt. Die Arbeit ist unter Einhaltung der Regeln guter wissenschaftlicher Praxis der Deutschen Forschungsgemeinschaft entstanden.

Kiel, den

Mario Molina Kescher

# Contents

## *Abstract*

Present and past climate of the Earth has strongly depended on oceanic circulation and marine biological productivity. The formation of deep and bottom waters in high latitudes as a consequence of density changes and their pathways through the global ocean, the so called thermohaline circulation (THC) have been of primary importance for the redistribution of heat, for the Earth's albedo through control on the sea ice distribution, and it serves as a reservoir of greenhouse gases such as $CO_2$. The understanding of the mechanisms that have driven the THC in the past is crucial to reliably predict future climatic variations. For example, large amounts of $CO_2$ were stored in the deep ocean during glacial periods, which depended on the structure of the water column but also on the availability of nutrients for primary producers in the surface ocean. Besides macronutrients, phytoplankton depends also on dust input to the ocean, which releases iron, one of the most important micronutrients, in particular in High Nutrient Low Chlorophyll areas.

These issues have been poorly studied in the South Pacific, despite its importance for these processes. It represents a key area for the interchange of deep waters from all ocean basin because it is the main entrance and exit of deep waters to the largest of all oceans, the Pacific, which is also one of the principal $CO_2$ reservoirs on Earth. For the study of present and past deep-water circulation regimes and the provenance of the dust input in this region, Rare Earth Element (REE) distributions and radiogenic isotopes of neodymium (Nd), lead (Pb) and strontium (Sr) have been analyzed in water and sediment samples obtained from a meridional transect of the South Pacific, spanning all the way from South America to New Zealand. Radiogenic isotopes have been proved to be very reliable traces for studying different surface earth processes, such as, in the case of Nd and Pb, the advection of water masses. These are labeled with characteristic isotope compositions through weathering of the lithologies of the surrounding continents in their formation regions, allowing to track the pathway of a certain water mass in the present day water column (not in the case of Pb due to anthropogenic inputs), as well as their presence and mixing in the past at a particular location given that these signatures are recorded by the sediments. Nd, Sr and Pb isotopes also allow identifying the provenance of lithogenic particles that arrive the bottom of the ocean brought by currents or wind due to the specific signature that different rocks carry as a consequence of their type and age. The concentrations of the REE including Nd in seawater also allow to distinguish water masses as well as vertical processes such as scavenging as their relative distributions vary coherently in the water column due to different affinities to particles.

Chapter 4 of this study presents the first seawater REE concentrations and Nd isotope compositions in intermediate and deep waters of the South Pacific. The results show that Nd isotopes faithfully trace the different water masses displaying more negative Nd isotope compositions for those water masses originating in the Southern Ocean, such as Lower Circumpolar Deep Water (LCDW) and Antarctic Intermediate Water (AAIW), with $\varepsilon_{Nd}$ around -8.3; and more positive signatures for North Pacific Deep Water (NPDW)($\varepsilon_{Nd}$ = -5.9), which exits the South Pacific in the east, close to South America. Nd isotope compositions also allowed identifying a remnant of North Atlantic Deep Water (NADW) entering the western South Pacific as part of LCDW. Dissolved REE concentrations indicate that NPDW were affected by scavenging processes underneath the high productivity area of the equatorial eastern Pacific that lowered the concentrations of the more particle reactive light REE (LREE) of this water mass before reaching the South Pacific. At the same time LREE are also released from oxides in the sediments of the Southeast Pacific Basin.

Chapter 5 compares bottom seawater (chapter 4) and surface sediment Nd isotope compositions to identify the most reliable technique to obtain seawater-derived Nd isotopes from the sediment for the study of past circulation changes recorded in the sediment. Four different archives were tested in order to obtain the authigenic seawater Nd isotope signal that precipitates from seawater into the sediment in the form of early-diagenetic Fe-Mn oxide coatings: 'decarbonated' and 'non-decarbonated' bulk sediment leachates as well as 'uncleaned' planktonic foraminifera, which were also compared to the compositions of fossil fish teeth. None of them registered exactly the same Nd isotope compositions as those of the present day bottom waters due to the low sedimentation rates in the South Pacific that result in very old surface sediments (up to 24 kiloyears before present), which therefore integrate Nd isotope compositions from different circulation states of the ocean. However, independent evidence (REE patterns and Al/Ca ratios measured on unclean foraminifera), clearly indicates that the Nd isotope compositions of unclean foraminifera, fish teeth and 'non-decarbonated' leachates originated from bottom seawater, allowing the use of these methods to study past changes of deep water circulation. This study also suggests that contributions of the continental margins of the South Pacific to the Nd isotope composition of seawater, the so called 'boundary exchange' was small. The sources of fine lithogenic particles that arrive the South Pacific are studied in this chapter by combining Nd and Sr isotopes from the detrital fraction of the sediment. The results show that the lithogenic material found in the western and central Pacific originates from Southeast Australia and South New Zealand and was transported by the dominant Westerlies.

The influence of these sources is also dominant in the eastern South Pacific, although in this region the proportions of detrital material from the Andes increase and contributions from Antarctica can also not be excluded.

The last chapter of this thesis presents a reconstruction of the deep-water circulation and detrital provenances in the central South Pacific of the last 240 kyr based on Nd, Pb and Sr isotopes. The results show small but significant glacial-interglacial variations in the Nd and Pb isotope composition of the circumpolar deep water (CDW), which has been the dominating water mass in this region, caused by a decrease in the contribution of NADW during glacial stages. A deepening of the flow and advective incorporation of NPDW during glacial periods is not supported by the results of this study due to the location of the cores, which have remained within CDW. The combined detrital Nd-Sr isotope compositions indicate a dominance of Southeastern Australia and South New Zealand derived material, similar to the surface sediments over the past 240,000 years. Nevertheless, a small shift towards the Antarctic end-member during glacial periods is identified, which may indicate a stronger influence of Antarctic-derived material during cold periods, most probably transported northwards as suspended load of oceanic currents.

## *Zusammenfassung*

Das Klima der Erde in der Gegenwart wird, wie auch in der Vergangenheit, stark von der ozeanischen Zirkulation und der marinen biologischen Produktivität beeinflusst. Die durch Änderungen der Dichte des Meerwassers verursachte Tiefenwasserbildung in den hohen Breiten und das dadurch getriebene globale Zirkulationsmuster der gesamten Wassersäule, die so genannte Thermohaline Zirkulation (THZ), spielt eine entscheidende Rolle als Wärmeverteiler, für die Albedo durch die Kontrolle der Eisausdehnung und auch als Speicher für Treibhausgase wie $CO_2$. Das Verständnis der Mechanismen, die die THZ in der Vergangenheit gesteuert haben, ist entscheidend um zukünftige Änderungen des Klimas zu prognostizieren. Zum Beispiel wurden große Mengen an $CO_2$ während der Glazialzeiten in der Tiefsee gespeichert, was zum Einen von der Tiefenwasserzirkulation abhängig war, zum anderen aber auch von der Verfügbarkeit von Nährstoffen für die Primärproduzenten an der Meeresoberfläche. Abgesehen von den Makronährstoffe ist das Phytoplankton auch von Staubeinträgen in den Ozean abhängig, die Eisen freisetzen, einer der wichtigsten Mikronährstoffe, besonders in sogenannten 'High Nutrient Low Chlorophyll'-Gebieten.

Der Süd-Pazifik wurde trotz seiner Bedeutung für diese Prozesse bis jetzt wenig untersucht obwohl er eine entscheidende Rolle für den Austausch und die Mischung von Tiefenwasserspielt. Dort finden Zufluss und Abfluss aller Tiefen-wassermassen in und aus dem Pazifik statt, dass das global größte Ozeanbecken ist und damit auch einer der wichtigsten $CO_2$ Speicher der Erde ist. Um die gegenwärtige und vergangene Tiefenwasserzirkulation des Süd-Pazifiks und die Herkunft der Staubeinträge in dieser Region untersuchen zu können, wurden Konzentrationen der Seltenerdelemente (REE) und radiogene Isotopenverhältnisse von Neodym (Nd), Blei (Pb) und Strontium (Sr) an Wasser- und Sedimentproben gemessen, die entlang eines meridionalen Transekts über den Süd-Pazifik von Südamerika bis Neuseeland gewonnen wurden. Radiogene Isotopenverhältnissen haben sich als verlässliche Tracer für die Untersuchung verschiedener Prozessen an der Erdoberfläche erwiesen wie zum Beispiel, in Falle von Nd und Pb, als Advektionsindikatoren verschiedener Wassermassen. Diese werden von charakteristischen Isotopenverhältnissen gekennzeichnet, die sie durch Verwitterungeinträge von den umliegenden Kontinenten in ihren Entstehungsgebieten erhalten. Dies erlaubt die Verfolgung von bestimmten Wassermassen und deren Mischung sowohl in der heutigen Wassersäule (allerdings nicht im Fall von Pb- Isotopen, die von anthropogenen Einträgen kontaminiert wurden) als auch in der Vergangenheit dank der Speicherung der Meerwasserisotopenverhältnisse im Sediment. Dank der charakteristischen Nd-, Pb- und Sr-Isotopenverhältnisse der Gesteine als Folge ihres Typs

und Alters ist auch die Bestimmung der Herkunft des lithogenen Anteils der Sedimente möglich, der durch Wind und Strömungen transportiert wird. Die Konzentrationen der Seltenerdelemente inklusive Nd im Meerwasser erlauben ebenfalls die Identifizierung von Wassermassen sowie von vertikalen Prozesse wie 'Scavenging', da deren Konzentrationen in Abhängigkeit ihrer Ionenradien durch unterschiedliche Affinitäten zu Partikeln in der Wassersäule variieren .

Kapitel 4 dieser Arbeit zeigt die ersten systematischen Daten von Seltenerdelement-Konzentrationen und radiogenen Nd-Isotopenzusammensetzungen von Tiefen- und Zwischenwässern des Süd-Pazifiks. Die Ergebnisse zeigen, dass die Nd-Isotopie des Tiefenwassers im Südpazifik als verlässlicher konservativer Wassermassentracer dienen kann, da Wassermassen aus dem Antarktischen Zirkumpolarstrom, wie das untere zirkumpolare Tiefenwasser (LCDW) oder das antarktische Zwischenwasser (AAIW), negativere $\varepsilon_{Nd}$-Signaturen um -8.3 zeigen. Dagegen zeigen die aus dem Nordpazifik stammenden Beiträge des Nordpazifischen Tiefenwassers (NPDW), die den Pazifischen Ozean an seinem östlichen Rand entlang Südamerika verlassen, positivere Werte ($\varepsilon_{Nd}$ = -5.9). Ein weiteres wichtiges Ergebnis ist die Identifikation von Zumischungen des Nordatlantischen Tiefenwassers (NADW) im oberen Teil des LCDW im westlichen Südpazifik. Die Konzentrationen der Seltenen Erden zeigen, dass NPDW von Scavengingprozessen unter der Hochroduktivitätszone des äquatorialen östlichen Pazifiks beeinflusst wird bevor es den Südpazifik erreicht. Dies verringert die Konzentrationen der stärker partikelreaktiven leichten REE (LREE). Zusätzlich wird aber auch beobachtet, dass LREE im südöstlichen Pazifischen Becken von Mn-Fe-Oxihydroxiden im Sediment freigesetzt werden.

Kapitel 5 prüft die Verlässlichkeit von Extraktionsmethoden um Meerwasser-Nd-Isotopen-Signaturen aus Tiefseesedimenten zu gewinnen. Dazu wurde eine detaillierte Kalibration durchgeführt, in deren Rahmen die $\varepsilon_{Nd}$-Signaturen des Meerwassers mit den aus den Oberflächensedimenten extrahierten Werten verglichen wurden. Hierzu wurden vier verschiedene Extraktions-Methoden angewandt und verglichen um sicherzustellen, dass verlässliche Daten für die Rekonstruktionen der Zirkulation der Vergangenheit erhoben werden können. Die Tiefenwasser-Nd-Isotopie der authigenen, frühdiagenetischen 'Fe-Mn-coatings' wurde durch verschiedene Laugungsmethoden extrahiert: Laugung des Gesamtsediments mit und ohne vorherige Entfernung der Karbonatfraktion, sowie Auflösung handverlesener planktonische Foraminiferengehäuse. Diese Ergebnisse wurden mit den $\varepsilon_{Nd}$-Signaturen fossiler Fischzähne verglichen. Keine dieser Methoden spiegelte die exakten Nd-

Isotopenzusammensetzungen des heutigen Bodenwassers exakt wider. Dies ist eine Folge der sehr niedrigen Sedimentationsraten im Südpazifik, die zu extremen Oberflächensedimentaltern von bis zu 24,000 Jahren führt was die Integration von Nd Isotopenzusammensetzungen verschiedener Zirkulationsmuster der Vergangenheit in den Oberflächensedimenten führt. Die REE-Muster und Al/Ca Verhältnisse der Mn-Fe Coatings der planktonischen Foraminiferengehäuse zeigen dass sowohl die Nd- Isotopenzusammensetzungen der Foraminiferengehäuse, der gelaugten Sedimente ohne vorheriger Entfernung der Karbonatfraktion und fossile Fisch Zähne aus dem Bodenwasser stammen. Diese Studie zeigt auch, dass Kontinentalränder des Südpazifiks zumindest an der Lokation dieser Studie nicht mit dem Bodenwasser austauschen und keinen Einfluss haben auf die Nd-Isotopenzusammensetzung des Tiefenwassers. Die kombinierten Nd- und Sr-Isotopenzusammensetzungen der lithogenen Fraktion des Sediments erlauben die Bestimmung der Herkunft der detritischen Partikel im Untersuchungsgebiet. Diese stammen hauptsächlich aus Südostaustralien und dem südlichen Neuseeland und wurden von den dominierenden 'Westwinden' geliefert, wobei aber auch der Einfluss der Anden vor allem in östlichen Südpazifik klar identifizierbar ist. Dort kann auch ein Einfluss von Material aus der Antarktis nicht ausgeschlossen werden.

Das letzte Kapitel dieser Arbeit präsentiert die Änderungen in der Tiefenwasserzirkulation des Südpazifiks auf glazial/interglazialen Zeitskalen während der letzten 240,000 Jahre, sowie die Änderungen der Herkunftsgebiete der detritischen Partikel anhand ihrer Nd-, Pb- und Sr-Isotopensignaturen. Die Ergebnisse zeigen systematische Veränderungen der Meerwasser-Nd- und Pb-Isotopenzusammensetzungen, die den klimatischen Zyklen folgen, wobei ein geringerer Anteil zugemischten NADWs im Zirkumpolaren Tiefenwassser (CDW) während der Glazialzeiten angezeigt wird. Die zeitlichen Variationen waren relativ niedrig, was mit dem erwarteten geringeren Anteil von NADW im Südpazifik als Folge der erhöhten Verdünnung der Wassermassen aus dem Nordatlantik übereinstimmt. Eine stärkere Produktion von NPDW während Glazialzeiten konnte anhand der Lokation der Sedimentkerne nicht bewiesen werden, da diese unter dem Einfluss von CDW lagen. Die kombinierten Nd- und Sr-Isotopenzusammensetzungen der lithogenen Fraktion des Sediments der letzten 240 000 Jahre zeigen die Dominanz von lithogenem Material aus Südostaustralien und dem südlichen Neuseeland, wobei ein stärkerer Einfluss von Antarktischem Detritus während Glazialzeiten nachweisbar ist, was durch Suspension in ozeanische Strömungen transportiert wurde.

## *Preface*

Our planet is unique in the solar system as it fulfills the requirements needed for life on its surface, which is possible thanks to an equilibrium of the main components of the Earth system: Geosphere, atmosphere, hydrosphere, and biosphere. These elements are sophistically linked and coupled to each other. Humans have an extraordinary ability to perceive, manipulate and govern our medium compared to other species on this planet, which eventually leaves in our hands the future of our and many others species. Therefore, a detailed understanding of the operation and connections of the different systems that rule the climate of our planet is crucial. This thesis aims to provide further insight into some of the mechanisms that affect the hydrosphere in one of the less studied regions of the oceans, the deep South Pacific, combining knowledge from different fields related to the Earth system sciences, such as geochemistry, biological and chemical oceanography, and sedimentology.

# 1) Introduction

The climate of the Earth is what in the end defines most of the different ecosystems on this planet and is therefore crucial for most of the life on its surface. The climate of the Quaternary has ultimately been driven by orbital changes that modify the radiation reaching the Earth's surface from the Sun. This orbital forcing occurs at characteristic frequencies of about 100, 41 and 23 kilo years (kyr), the so-called 'Milankovitch Cycles' (Hays et al., 1976; Berger et al., 1984). Nevertheless, the effect of this forcing is not enough to explain the amplitude observed in the glacial-interglacial variations of the last million years (cf. Bard and Frank, 2006), which are therefore consequence of many forces and feedbacks occurring within the Earth's climate system.

## 1.1. Role of the ocean in Earth's climate

The hydrological cycle, from which the oceans compose about 97%, is one of the key components of the Earth system that regulates the climate. Among other important functions, the ocean has three major tasks, which are intrinsically coupled to each other:

1) Redistributor of heat through oceanic currents from lower latitudes, where the radiation of the sun is perpendicular to the Earth surface and therefore stronger, to higher latitudes where the planet looses heat in form of long waves (Fig. 1.1).

2) Relevant modulator of the albedo as the extent of highly reflecting ice sheets and the production of clouds through evaporation influences considerably the reflection of radiation that is returned back to space.

3) The ocean is also the most important reservoir of heat, $CO_2$ and nutrients of the planet. $CO_2$ is a greenhouse gas that influences the retention of outgoing radiation. Its concentrations in the atmosphere have varied tightly with global temperatures during glacial and interglacial stages (Fig 1.2.) and it has been sequestered in the deep ocean during cold periods and released back to the atmosphere during warm stages. The storage of $CO_2$ in the deep ocean has been linked to primary production at the sea surface, as the microorganisms that live there assimilate large amounts of carbon to build up their organic matter and carbonate shells, which finally sink to the bottom of the oceans when they die thereby sequestering important amounts of $CO_2$ in the abyss. This process has been named the 'biological pump' (Broecker, 1982) and is directly dependent on the availability of nutrients that reach the surface ocean.

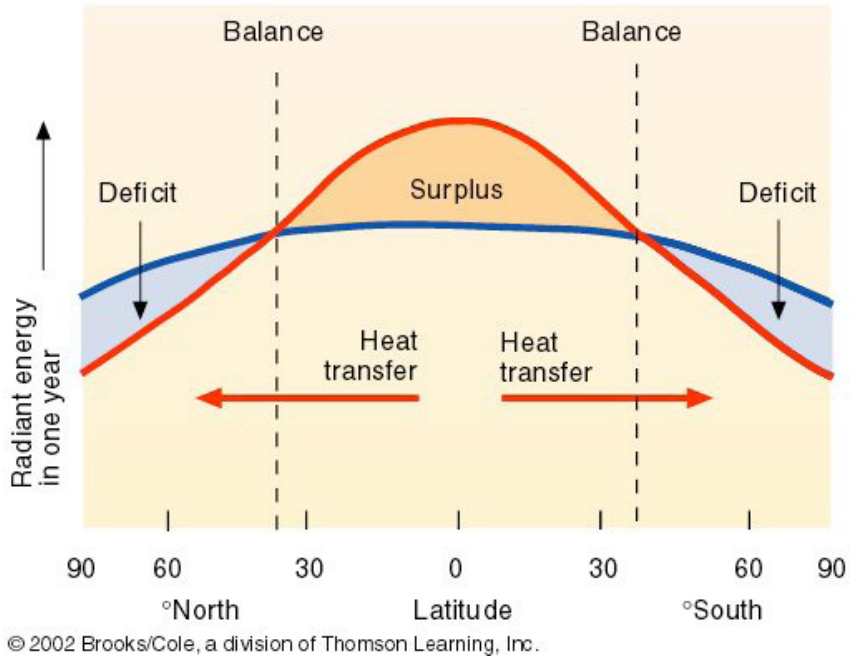


***Figure 1.1.*** *Radiative balance of the Earth. Red line represents incoming solar radiation to the planetary surface, whereas the blue line indicates loss of heat towards the space. Atmosphere and ocean transfer heat from lower to higher latitudes (red arrows). Copyright ©2005 Brooks/Cole, a division of Thomson Learning, Inc.*

The presence of essential nutrients for phytoplankton such as nitrate ($NO_3$) or, in the case of diatoms, also silicic acid ($H_4SiO_4$), depends directly on the structure of the water column and the circulation patterns of intermediate and deep water (Falkowski et al., 1998; Sarmiento et al., 2004; 2007), given that most of the nutrients that sink to the subsurface ocean together with the shells of the microorganisms will return to the surface through oceanic advection as they get remineralised again at greater depths where bacteria consume the sinking organic matter, returning these nutrients to dissolved form. This respiration process consumes oxygen at the same time. Therefore, the concentrations of nutrients and oxygen in deep waters are generally inversely related.

Other continentally derived micronutrients that are essential for the life cycle of primary producers, such as Iron (Fe) arrive at the surface ocean through wind in the form of dust, which mainly originates from arid regions such as deserts (e. g. Prospero, 2002). Therefore its availability was increased during glacial periods (e. g. Lamy et al., 2014) as the moisture/rain generally decreases globally as a consequence of the decrease in evaporation because of the lower global temperatures and due to the enhanced wind speeds caused by the more pronounced pole to equator temperature gradients.

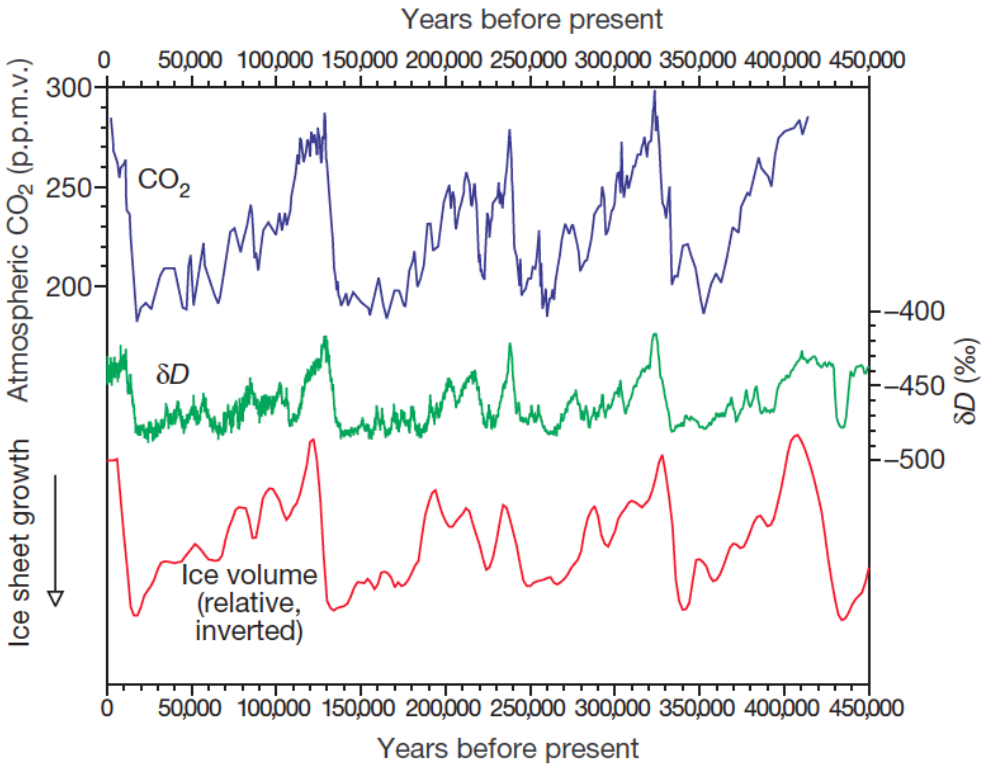


***Figure 1.2.*** *Glacial-Interglacial variations of the last ~400,000 years in atmospheric $CO_2$ (blue) and air temperature over Antarctica (green) obtained from an Antarctic ice core (Vostok), and global ice volume variations (red) deduced from oxygen isotopes registered in benthic foraminifera of deep-sea cores. The peaks of maximum ice extension (note the reverse plot) represent glacial stages. Figure from Sigman and Boyle, 2000.*

### 1.1.2. Thermohaline circulation

The currents and circulation pathways of all oceans are ultimately connected at all depths through the so-called thermohaline circulation (Fig. 1.3), which is controlled by density changes in surface waters at high latitudes (e. g. Broecker, 1991; Rahmstorf, 2006). There are two main regions of deep-water formation: 1) The North Atlantic and the Greenland-Norwegian Seas, where warm and salty surface waters originating in the Gulf of Mexico, as a consequence of strong evaporation, arrive via the Golf Stream. They finally sink as they cool and thus density increases, thereby forming North Atlantic Deep water (NADW)(Dickson and Brown, 1994). This deep-water mass flows south until the Southern Ocean where it mixes with the Antarctic Circumpolar Current (ACC), which connects all ocean basins and homogenizes the entire water column along its eastward flow (Rintoul et al., 2001). 2) Around Antarctica is where the densest of all water masses form: Antarctic Bottom Water (AABW) (Orsi et al 1999). This water mass originates from sea ice formation at the Antarctic coast. This process leaves behind brines that increase considerably the salinity of surface waters that finally sink. AABW also joins the ACC. The deep to bottom waters that form in high latitudes and get mixed with all other deep-water

masses in the Southern Ocean finally fill the abyssal Indian and Pacific oceans, returning at some point again to the ACC and ultimately upwelling to the surface, where the cycle starts again. This entire process lasts about 1500 years (Schmittner et al., 2013).

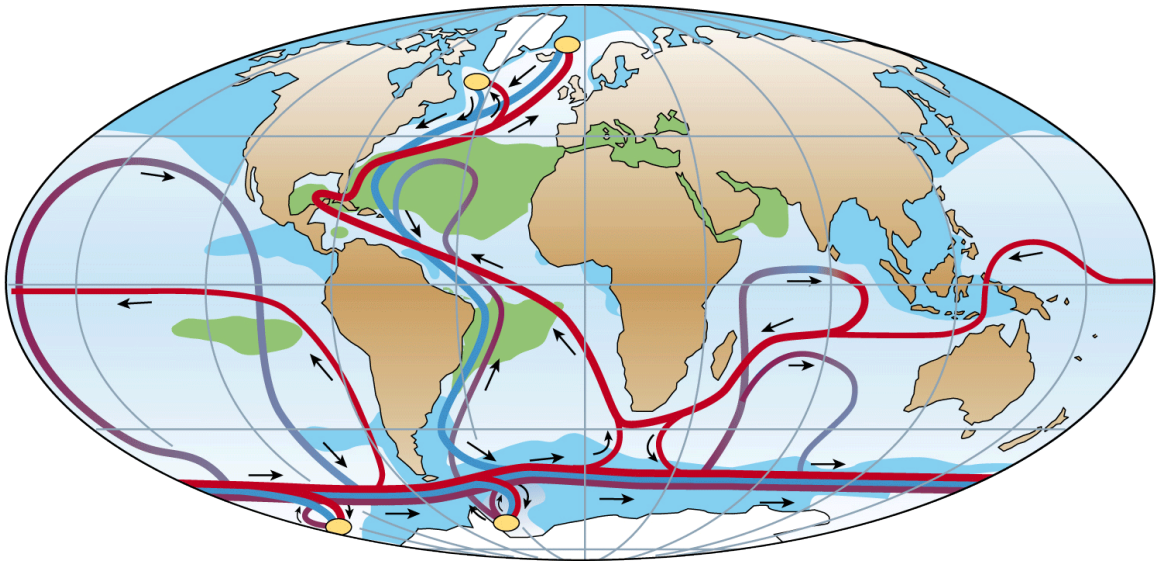

***Figure 1.3**. Simplified sketch of the global thermohaline circulation pathway, whereby yellow dots represent regions of deep-water formation; red path: near-surface ocean circulation; blue path: deep-water circulation and; purple path: bottom currents. The surface salinity gradient is also represented: green > light blue > blue. Figure from Rahmstorf, 2002.*

During recent glacial periods, many pieces of evidence (Duplessy et al., 1988; Rutgers et al., 2000; Ninneman and Charles, 2002; Piotrowski et al., 2004, 2005, 2008, 2009, 2012; Curry and Oppo, 2005) suggest a remarkably different structure of the thermohaline circulation (Fig. 1.4). It was dominated by a shoaling of NADW in the Atlantic Ocean, which resulted in the occupation of the deepest parts of this basin by AABW during cold stages. There were even short periods of complete shut down of NADW during Heinrich events, as a consequence of massive fresh water input in the North Atlantic due to ice sheets melting (e. g. Rahmstorf, 2002). However, less is known about the structure of the water column in the Pacific Ocean, where a deepening of North Pacific Deep Water (NPDW) was inferred (e.g. Matsumoto et al., 2002). The reconstruction of past deep-water circulation regimes in the South Pacific is one of the main objectives of this work.

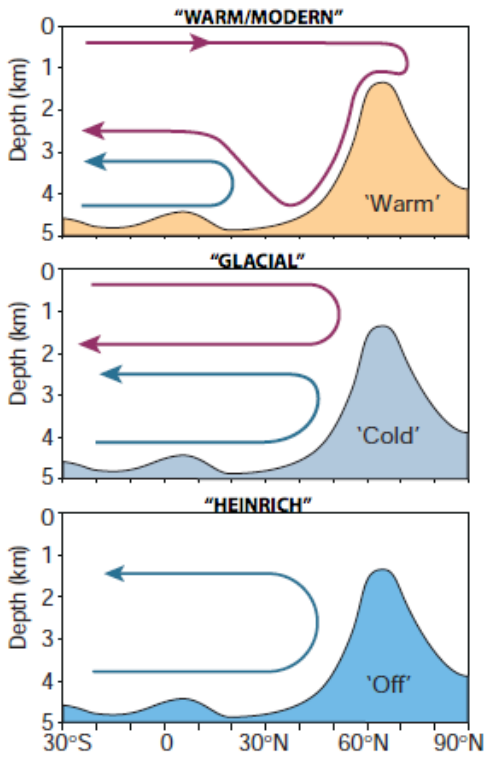


***Figure 1.4**. Simplified sketches of three different structures of the water column of the Atlantic ocean during recent glacial and interglacial stages. Red paths represent NADW and blue paths represent AABW. Figure from Rahmstorf, 2002.*

### 1.2. The South Pacific

The South Pacific is a key area for the global thermohaline circulation as well as for the capacity of the ocean to store $CO_2$ because it represents the main entrance and exit of deep waters feeding the largest basin of the global ocean, the Pacific. The deep currents entering in the western South Pacific ventilate the basin as there is no bottom water formation in the North Pacific. These deep waters travel around the entire Pacific loosing oxygen and gaining nutrients and $CO_2$ as a consequence of respiration and remineralisation until they leave the Pacific again at middepths of the eastern South Pacific. This process is crucial for the oceanic $CO_2$ storage as growing evidence suggests that large amounts of $CO_2$ have escaped from the returning middepth waters in the Southern Ocean during interglacial periods, perhaps as a consequence of limited consumption of nutrients by the phytoplankton (e. g. Sigman et al., 2010). This process is therefore directly linked to the availability of nutrients, which itself is dependent on: 1) the water column structure and; 2) the dust input regimes. These are two of the main foci of this work.

Detailed descriptions of the oceanography (water masses, hydrographic properties and flow directions) and of the geological background (sedimentation rates, dominant winds and dust input) of the mid-latitude (~40°S) South Pacific are provided in chapters 3 (section 3.1.1.) and 4 (4.1.1.) respectively.

## 1.3. Tracers of Ocean circulation and weathering

For being able to elucidate present and past circulation, as well as weathering regimes it is necessary to track changes in these processes with tracers or proxies. In the case of present variations of the ocean circulation these tracers have to be analysed directly from the different water masses the water column is composed of, whereas for studying past changes the proxy-signatures have to be extracted from the sediments that accumulate and remain undisturbed over long periods of time in the deep-sea sediments thus recording the proxy-signatures of past oceanic states.

### 1.3.1. Rare Earth Elements

The Rare Earth Elements (REE) are a group of natural chemical elements that include the lanthanides (including Nd) and yttrium (Y), which has very similar geochemical properties. The REE are weathered on the continents and supplied to the ocean via rivers or dust where they vary coherently as a function of their increasing particle reactivity with increasing ionic radii. This property allows studying processes occurring in the water column (e. g. Nozaki, 2001), such as scavenging or the differentiation of water masses with different REE concentrations and different relative abundances. Within the REE there are some exceptions to this behaviour, such as cerium (Ce), which is highly insoluble in seawater, but which, on the other hand, permits the study of other oceanic processes, such as the oxidation state of seawater and sediment. A detailed description of dissolved REE as tracers for oceanic processes is provided in Chapter 3 (section 3.1.).

### 1.3.2. Radiogenic isotopes of trace metals

The isotopic composition of certain metals can also be used as tracers for Earth surface processes thanks to a combination of their fractionation during continental crust/mantle formation and their radioactivity, which produces daughter isotopes of other elements. This way, characteristic isotope ratios of some elements develop that depend on the age and type of a rock. When rocks are weathered, their characteristic isotopic ratios are transferred to the ocean in particulate or dissolved form This allows the identification of particular water masses depending

on the isotope signature acquired in their formation region or the provenance of lithogenic particles found in the sediment. Some isotopic systems also are influenced by hydrothermal inputs. As biological processes or evaporation in the oceans do not fractionate radiogenic isotopes they serve as independent water mass tracers in addition to other nutrient type proxies, such as carbon isotopes ($\delta^{13}C$) or Cadmium to Calcium ratios (Cd/Ca) (cf. Frank, 2002). Detailed descriptions of the different isotopic systems used in this study are presented below.

### 1.3.2.1 Neodymium (Nd) isotopes.

During the formation of continental crust, the REE Nd is preferentially retained in the melts and thus ultimately in the crustal rocks, whereas the REE samarium (Sm) preferentially stays behind in the mantle during this process. Sm is radioactive and decays into a stable isotope of Nd ($^{143}Nd$) at a very slow rate (half time of $^{147}Sm$ = 106 Gyr). This results in higher proportions of radiogenic $^{143}Nd$ with respect to primordial $^{144}Nd$ in young mantle derived rocks compared to old continental rocks. Therefore, different continental regions and geological formations are characterized by distinctive $^{143}Nd/^{144}Nd$ ratios (Fig. 1.5). Nd isotope compositions are expressed as $\varepsilon_{Nd}$ values: $\varepsilon_{Nd}=[(^{143}Nd/^{144}Nd_{(sample)}/ (^{143}Nd/^{144}Nd_{(CHUR)}-1]*10^4$, whereby CHUR stands for the Chondritic Uniform Reservoir ($^{143}Nd/^{144}Nd$=0.512638, Jacobsen and Wasserburg, 1980).

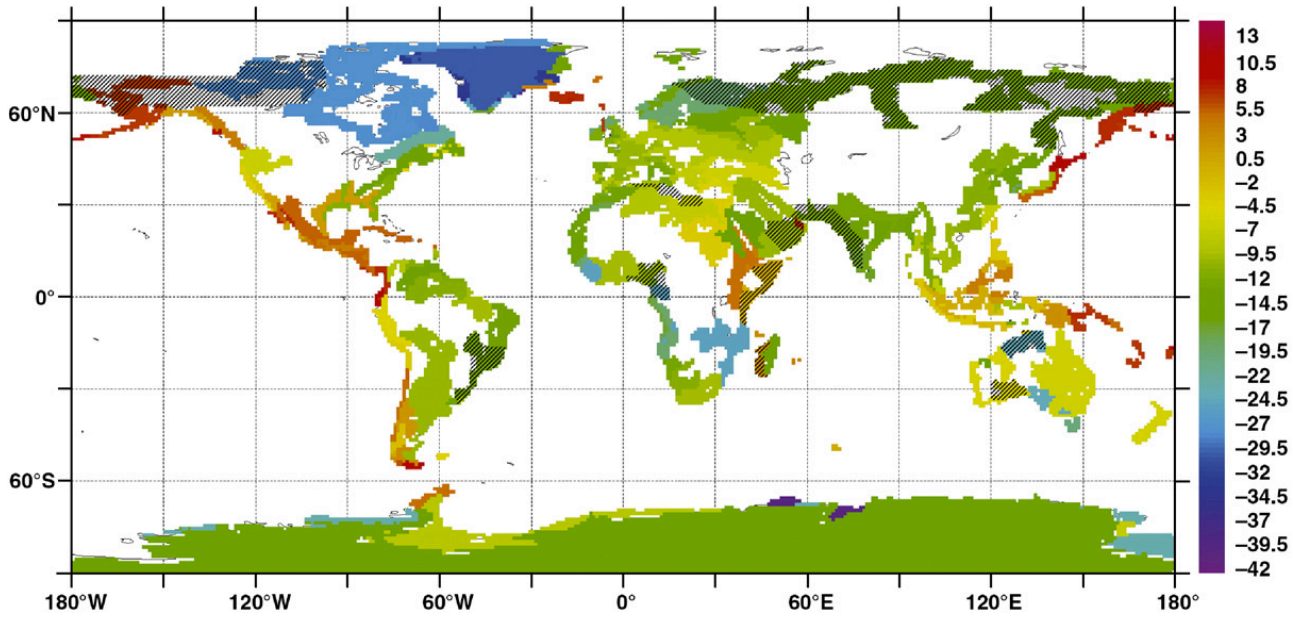


***Figure 1.5****.Global Nd isotope compositions ($\varepsilon_{Nd}$) of the rocks and sediments at continental margins. Figure from Jeandel et al. 2007.*

The sources of Nd in the oceans are weathering, dust input and exchange with the shelf sediments, which in the case of stable Nd concentrations has been termed 'boundary exchange' (Lacan and Jeandel, 2005). The residence time of Nd in the ocean is similar to the oceanic mixing

time (Tachikawa et al., 2003; Arsouze et al., 2009; Rempfer et al., 2011). Further details on the use of Nd isotopes as present and past water mass tracer and as detrital provenance proxy are provided in chapters 3 (section 3.1), 4 (section 4.1), and 5 (section 5.1).

#### 1.3.2.2. Strontium (Sr) isotopes

The systematics of Sr isotopes are based on the fractionation of rubidium (Rb) and Sr between continental crust and mantle. In this case, Rb is strongly enriched in the continental crust compared to Sr, which stays preferentially in the mantle. As $^{87}Rb$ decays into $^{87}Sr$, the ratio of this isotope to the primordial isotope of Sr ($^{86}Sr$) is higher in continental rocks than in mantle-derived rocks. The sources of Sr to the ocean during recent glacial/interglacial periods are: continental weathering, hydrothermal inputs, ground water discharge and weathering of continental shelf carbonates that were exposed during lower sea level of glacials periods (Krabenhöft et al., 2010). The long residence time of Sr in seawater (~2 million years), consequence of its low particle reactivity, impedes its use as water mass tracer but allows its use as provenance tracer for lithogenic material arriving in the ocean, although here Sr isotopes also present some disadvantages, such as: 1) Incongruent weathering, due to the different resistance to chemical weathering intensities of minerals with different Sr isotope compositions (e.g Derry and France-Lanord, 1996); or 2) Fractionation of Sr isotopes due to grain size effects, as $Sr^{87}/Sr^{86}$ ratios increase as the size of the particles decreases (Innocent et al., 2000). The correlation of detrital Sr and Nd isotopes helps to avoid these inconveniences and provides a powerful tool for tracking detrital provenances. Today's $^{87}Sr/^{86}Sr$ ratio in seawater is 0.70916. This value changed in the past as a consequence of long-term changes in weathering inputs, such as the Himalayan uplift (Richter et al., 1992; Derry and France-Lanord, 1996).

#### 1.3.2.3. Lead (Pb) isotopes

Pb is the end-product of all three Uranium (U) decay series (Fig. 1.6), leading to three stable radiogenic isotopes ($^{206}Pb$, $^{207}Pb$ and $^{208}Pb$) that are used in comparison to the only primordial isotope $^{204}Pb$. As in the case of Nd and Sr, the use of the Pb isotope system as water mass and provenance tracer is based on the fractionation of mother and daughter elements during the formation of the continental crust (Dickin, 1998). Whereby radiogenic isotopes are enriched with respect to primordial Pb in igneous rocks. Pb sources in the ocean are also continental weathering and hydrothermal inputs. One of the main differences to the Nd isotope system is that Pb isotopes undergo incongruent weathering due to the α-recoil effect, which results in structural damage of the minerals as consequence of the emission of radiation during the production of radiogenic Pb isotopes within the U-series chains. As a consequence, the

radiogenic Pb isotopes are preferentially mobilized during weathering. The short residence time of Pb in seawater (~50 to 200 years) (Schaule and Patterson, 1981; von Blanckenburg and Igel, 1999) due to its high particle reactivity results in very heterogeneous Pb isotope ratios in seawater, allowing to track small variations in the composition of a single water mass. Industrial activity and the use of leaded gasoline in the past decades as derived in the alteration of the natural isotope ratios of Pb in the atmosphere and oceans (Schaule and Patterson, 1981; Weiss et al., 2003), which, nevertheless, do not impede the use of this isotopic system for pre-anthropogenic studies.

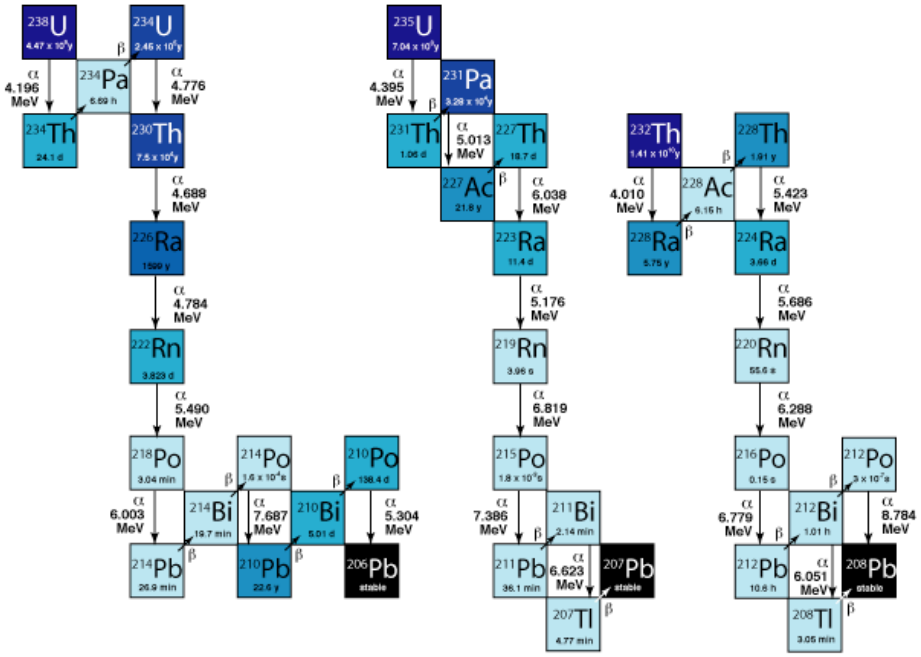


***Figure 1.6*** *Uranium-series decay chains of the radioactive $^{238}U$ and $^{235}U$ and the $^{232}Th$ isotope systems. Figure from gemoc.mq.edu.au.*

### 1.4. Outline and objectives of this thesis

Radiogenic isotopes have progressively gained more attention as oceanographic, paleoceanographic or paleoclimate tools within the past few decades. Particularly Nd isotopes have frequently been used as proxies of present and past water mass advection, (cf. Frank, 2002; Goldstein and Hemming, 2003). Nevertheless there are still discrepancies and unresolved questions, such as the processes controlling influence of the continental margins in the oceanic Nd cycle (Lacan and Jeandel, 2005), which can bias the purely advective character of this tracer, especially in the Pacific Ocean, which is surrounded by highly soluble volcanogenic material (reference). Therefore, it is essential to better understand the behavior of Nd concentrations and isotope compositions in the present ocean and to investigate and confirm its quasi-conservative behavior in every area of the ocean. In this respect, the South Pacific has been poorly investigated until recently. Cruise SO213 (Tiedemann et al., 2014), which crossed the entire South Pacific basin along a meridional section, was therefore an ideal occasion to collect seawater samples and analyze the oceanic Nd cycle and its relationship to ocean circulation in this area. A large variety of water masses from different origins prevails in this region providing at the same time an excellent opportunity to study dissolved REE distributions as indicators of scavenging processes in the water column and as present day circulation tracers. These issues are presented and discussed in chapter 3. 'Boundary exchange' processes are further investigated in Chapter 4 by analyzing the Nd isotope compositions of the sediments and the immediately adjacent bottom waters of the New Zealand Margin, which is a key region for studying this issue as a strong Deep Western Boundary Current (DWBC) flows in this area, potentially interacting with the sediment and thereby modifying the seawater Nd isotope composition.

Another problem that Nd isotopes face in their application as paleoceanographic proxy is the reliable extraction of their seawater signatures from the sediment, where they are stored in early diagenetic Fe-Mn oxide coatings of particles including foraminifera. These coatings are difficult to separate from detrital particles that contain high amounts of Nd. Therefore, chapter 4 also compares different methods to extract seawater $\varepsilon_{Nd}$ signatures from surface sediments (core-tops) of the South Pacific and compares them to dissolved Nd isotope compositions (chapter 3) obtained from bottom waters overlying the same areas.

Besides the present day structure of the water column of the South Pacific and the processes that govern its chemical oceanography (chapter 3), another important objective of this

thesis was the reconstruction of the past circulation regime of the last 240 kyrs in this region (chapter 5). For this purpose Nd and Pb isotope changes recorded by two sediment cores in the central South Pacific were used to reconstruct the evolution of the advection and mixing of prevailing deep-water masses. These results are complemented by measurements of the carbon isotope composition of benthic foraminifera, which have been used for many decades as proxy for deep-water advection despite many uncertainties.

As explained above, dust input to the ocean has been a main driver of the primary productivity and therefore $CO_2$ storage in the deep ocean. In this work we contribute to decipher the sources of the lithogenic material that has arrived in the South Pacific transported by wind and, to a lesser extent, by currents. Analyses of the Nd and Sr isotope compositions of the lithogenic material in the sediments serve to reconstruct changes in source areas from recent times (core-tops; chapter 4) back to 240 ka in the central South Pacific (Chapter 5).

### 1.5. Contributions to this thesis and resulting publications

Martin Frank and Dirk Nürnberg wrote and submitted the proposal to the *Bundesministerium für Forschung und Bildung* (BMBF), through which this project was funded (No.:03G0213B). Ralf Tiedemann (Alfred Wegener Institute for Polar and Marine Research - AWI), Dirk Nürnberg and Frank Lamy (AWI) led cruise SO213, during which all samples of this study were collected and in which I participated.

Chapter 3 of this thesis was published in the journal *Geochimica et Cosmochimica Acta* (volume 127, pages 171-189, 2014), authored by Mario Molina-Kescher, Martin Frank, and Ed Hathorne under the title: South Pacific dissolved Nd isotope compositions and rare earth element distributions: Water mass mixing versus biogeochemical cycling. I collected and prepared all samples in the laboratory, measured the Nd isotope and concentration data, and wrote the manuscript. Ed Hathorne performed the measurements of the REE concentrations. Ralf Tiedemann provided the nutrient concentration data. Martin Frank and Ed Hathorne contributed to the discussions and improved the text of the manuscript. The manuscript was also improved by the contributions of three reviewers and the associate editor of *Geochimica et Cosmochimica Acta*, Mark Rehkämper.

Chapter 4 of this thesis has recently been submitted to the journal *Geochemistry, Geophysics, Geosystems,* authored by Mario Molina-Kescher, Martin Frank and Ed Hathorne under the title: Nd and Sr isotope compositions of different phases of surface sediments in the South Pacific: extraction of seawater signatures, boundary exchange, and detrital/dust provenance. I collected and prepared all samples in the laboratory, measured the Nd and Sr isotope data, and wrote the manuscript. Student assistant Ingmar Schindlbeck helped picking the foraminiferal samples. Ed Hathorne performed the measurements of the REE concentrations and Al/Ca ratios. Martin Frank and Ed Hathorne contributed to the discussions and improved the text of the manuscript.

Chapter 5 of this thesis will be prepared for submission to the journal *Earth and Planetary Science Letters* in the following months. I collected and prepared all samples in the laboratory, measured the Nd, Pb and Sr isotope data, and wrote the chapter. Ingmar Schindlbeck picked the foraminiferal samples and helped with sample preparation. Thomas Ronge (AWI) and Raul Tapia (GEOMAR) analyzed oxygen and carbon isotopes on benthic foraminifera and developed the age models of sediment cores SO213-59-2 and SO213-60-1, respectively.

## References


Arsouze T., Dutay J.-C., Lacan F. and Jeandel C. (2009) Reconstructing the Nd oceanic cycle using a coupled dynamical biogeochemical model. *Biogeosciences* **6(12),** 2829–2846.

Bard E. and Frank M., (2006) Climate change and solar variability: What's new under the sun? *Earth Planet. Sci. Lett.* **248**, 1-14

Berger A., Imbrie J., Hays J., Kukla G. and Saltzman B. (1984) Milankovitch and Climate. *Journal of Climatology* **5,** 344–345

Broecker W. S. (1982) Ocean chemistry during glacial time. *Geochim. Cosmochim. Acta* **46**, 1689-1706.

Broecker W. S. (1991) The great ocean conveyor, *Oceanography*, **4**,79–90.

Curry W.B. and Oppo D. W. (2005). Glacial water mass geometry and the distribution of $\delta^{13}C$ of $\sum CO2$ in the western Atlantic Ocean. *Paleoceanography* **20**, PA1017, http://dx.doi.org/doi:1010.1029/2004PA001021.

Derry L. A. and France-Lanord C. (1996) Neogene Himalayan weathering history and river $^{87}Sr/^{86}Sr$: impact on the marine Sr record. *Earth Planet. Sci. Lett*. **142**, 59–74.

Dickin A.P. (1998) Radiogein isotope geology, second edition. Cambridge University Press.

Dickson R. R. and Brown J. (1994) The production of North Atlantic Deep Water: Sources, rates and pathways. *J. of Geophysical res.* **99,** 12,319-12,341

Duplessy J.-C., Shackleton N.J., Fairbanks R.G., Labeyrie L., Oppo D.W., Kallel N., 1(988). Deepwater source variations during the last climatic cycle and their impact on the global deepwater circulation. *Paleoceanography* **3**, 343–360.

Falkowski P. G., Barber R. T. and Smetacek V. (1998) Biogeochemical controls and feedbacks on ocean primary production. *Science* **281**, 200-206.

Frank M. (2002) Radiogenic isotopes: tracers of past ocean circulation and erosional input. *Rev. Geophys.* **40**, 1001.

Goldstein S. L. and Hemming S. R. (2003) Long-lived Isotopic Tracers in Oceanography. Paleoceanography, and Ice-sheet Dynamics, *Treatise on Geochemistry. Pergamon, Oxford.* pp. 453–489.

Hays J. D., Imbrie J. and Shackleton N. J. (1976) Variations in the Earth's orbit: Pacemaker of the Ice Ages. *Science* **194**, 1121-1132.

Innocent C., Fagel N. and Hillaire-Marcel C. (2000) Sm-Nd isotope systematics in deep-sea sediments: clay-size versus coarser fractions. *Marine Geology* **168**, 79–87.

Jacobsen S. B. and Wasserburg G. J. (1980) Sm–Nd isotopic evolution of chondrites. *Earth Planet. Sci. Lett.* **50**, 139–155.

Jeandel C., Arsouze T., Lacan F., TeÅLchine P. and Dutay J.-C. (2007) Isotopic Nd compositions and concentrations of the lithogenic inputs into the ocean: a compilation, with an emphasis on the margins. *Chem. Geol.* **239**, 156–164.

Krabbenhöft A., Eisenhauer A., Böhm F., Vollstaedt H., Fietzke J., Liebetrau V., Augustin N., Peucker-Ehrenbrink B., Müller M.N., Horn C., Hansen B.T., Nolte N. and Wallmann K. (2010) Constraining the marine strontium budget with natural strontium isotope fractionations

($^{87}Sr/^{86}Sr^*$, $\delta^{88/86}Sr$) of carbonates, hydrothermal solutions and river waters. *Geochim. Cosmochim. Acta* **74**, 4097–4109

Lacan F. and Jeandel C. (2005) Neodymium isotopes as a new tool for quantifying exchange fluxes at the continent–ocean interface. *Earth Planet. Sci. Lett*. **232**, 245–257.

Lamy F., Gersonde R., Winckler G., Esper O., Jaeschke A., Kuhn G., Ullermann J., Martinez-Garcia A., Lambert F. and Kilian, R. (2014) Increased Dust Deposition in the Pacific Southern Ocean During Glacial Periods. *Science* **343**, 403. DOI: 10.1126/science.1245424

Ninnemann U.S. and Charles, C.D. (2002). Changes in the mode of Southern Ocean circulation over the last glacial cycle revealed by foraminiferal stable isotopic variability. *Earth Planet. Sci. Lett*. **201** (2), 383.

Nozaki Y. (2001) Encyclopedia of Ocean Sciences (eds. J. H. Steel et al.). Vol. 2, Academic Press. pp. 840–845.

Orsi A. H., Johnson G. C. and Bullister J. L. (1999) Circulation, mixing, and production of Antarctic Bottom Water. *Prog. Oceanogr*. **43**, 55–109.

Piotrowski A.M., Banakar V.K., Scrivner A.E., Elderfield H., Galy A. and Dennis, A. (2009). Indian Ocean circulation and productivity during the last glacial cycle. *Earth Planet. Sci. Lett*. **285**, 179–189.

Piotrowski A.M., Goldstein S.L., Hemming S.R. and Fairbanks R.G. (2004). Intensification and variability of ocean thermohaline circulation through the last deglaciation. *Earth Planet. Sci. Lett*. **225**, 205–220.

Piotrowski A. M., Goldstein S. L., Hemming S. R. and Fairbanks R. G. (2005). Temporal relationships of carbon cycling and ocean circulation at glacial boundaries, *Science*, **307**, 1933–1938, doi:10.1126/science.1104883.

Piotrowski A. M., Goldstein S. L., Hemming S. R., Fairbanks R. G. and Zylberberg D. R. (2008). Oscillating glacial northern and southern deep water formation from combined neodymium and carbon isotopes*, Earth Planet. Sci. Lett.*, **272**(1–2), 394–405, doi:10.1016/j.epsl.2008.05.011.

Piotrowski A. M., Galy A., Nicholl J. A. L., Roberts N., Wilson D. J., Clegg J. A. and Yu J. (2012). Reconstructing deglacial North and South Atlantic deep water sourcing using foraminiferal Nd isotopes. *Earth Planet. Sci. Lett*. **357-358**, 289-297.

Prospero J. M., Ginoux P., Torres O., Nicholson S. E. and Gill T. E. (2002) Environmental Characterization of global sources of atmospheric soil dust identified with the nimbus 7 total ozone mapping spectrometer (TOMS) absorbing aerosol product, *Reviews of Geophysics*, **40**, DOI: 10.1029/2000RG000095

Rahmstorf S. (2006) Thermohaline Ocean Circulation. In: Encyclopedia of Quaternary Sciences, Edited by S. A. Elias. Elsevier, Amsterdam.

Rempfer J., Stocker T. F., Joos F., Dutay J.-C. and Sidall M. (2011) Modelling Nd-isotopes with a coarse resolution ocean circulation model: sensitivities to model parameters and source/sink distributions. *Geochim. Cosmochim. Acta* **75**, 5927–5950.

Richter F. M., Rowley D. B. and DePaolo D. J. (1992) Sr isotope evolution of seawater: The role of tectonics. *Earth Planet. Sci. Lett.*, **109**, 11-23

Rintoul S., Hughes C. and Olbers D. (2001) The Antarctic Circumpolar Current System. *Ocean Circulation and Climate* / G. Siedler, J. Church and J. Gould, eds. New York : Academic Press. p., ISBN: 0-12-641351-7

Rutberg R. L., Hemming S. R., Goldstein S. L., (2000). Reduced North Atlantic Deep Water flux to the glacial Southern Ocean inferred from neodymium isotope ratios, *Nature*, **405**, 935–938, doi:10.1038/35016049.

Sarmineto J. L., Gruber N., Brzezinski M. A. and Dunne J. P. (2004) High-latitude controls of thermohaline nutrients and low latitude biological productivity. *Nature* **427**, 56-60.

Sarmiento J. L., Simeon J., Gnanadesikan A., Gruber N., Key R. M. and Schlitzer R. (2007) Deep ocean biogeochemistry of silicic acid and nitrate. *Global Biogeochem. Cycles* **21**. http://dx.doi.org/10.1029/2006GB002720.

Schaule B.K. and Patterson C.C. (1981) Lead concentrations in the northeast Pacific: evidence for global anthropogenic perturbations. *Earth Planet. Sci. Lett*. **54**, 97-116.

Schmittner A., Chiang J. C.H. and Hemming S. R. (2013) Introduction: The Ocean's Meridional Overturning Circulation, in Ocean Circulation: Mechanisms and Impacts - Past and Future Changes of Meridional Overturning (eds A. Schmittner, J. C. H. Chiang and S. R. Hemming), American Geophysical Union, Washington, D. C.. doi: 10.1029/173GM02

Sigman D. M. and Boyle E. A. (2000) Glacial/interglacial variations in atmospheric carbon dioxide. *Nature* **407**, 859-869

Sigman D. M., Hain M. P. and Haug G. H. (2010) The polar ocean glacial cycles in atmospheric $CO_2$ conentration. *Nature* **466**, 47–55**.** doi:10.1038/nature09149

Tachikawa K., Athias V. and Jeandel C. (2003) Neodymium budget in the modern ocean and paleo-oceanographic implications. *J. Geoph. Res.* **108** (C8).

Tiedemann R., Lamy F., cruise participants (2014) FS Sonne Fahrtbericht/Cruise Report SO213 - SOPATRA: South Pacific Paleoceanographic Transects - Geodynamic and Climatic Variability in Space and Time, Leg 1: Valparaiso/Chile - Valparaiso/Chile, 27.012.2010 - 12.01.2011, Leg 2: Valparaiso/Chile - Wellington/New Zealand, 12.01.2011 - 07.03.2011. doi:10.2312/cr_so213

von Blanckenburg and F. Igel H. (1999) Lateral mixing and advection of reactive isotope tracers in ocean basins: observations and mechanisms. *Earth Planet. Sci. Lett.* **169** (1e2), 113e128.

Weiss D., Boyle E.A., Wu J., Chavagnac V., Michel A. and Reuer M.K. (2003) Spatial and temporal evolution of lead isotope ratios in the North Atlantic Ocean between 1981 and 1989. *J. Geophys. Res.* **108** (C10), 3306. doi:10.1029/2000JC000762

## 2) Methods and materials

The methods and materials used for the studies presented in this thesis are based on previously well-established methodologies and are described in detail in chapters 3 (section 3.2), 4 (section 4.2) and 5 (section 5.2). Therefore this section only presents an overview of the samples taken and techniques used in this study, and provides additional information that is not included in the above chapters, such as details of the column chemistry and mass spectrometry.

All data presented in this thesis were obtained from seawater and sediment samples recovered during cruise SO213 aboard of the German research vessel FS SONNE, which took place from December 2010 to March 2011on two subsequent legs, which covered the distance between central Chile and New Zealand (Fig. 2.1). This expedition was part of the collaborative SOPATRA (SOuth PAcific paleoceanographic TRAnsects) project between the GEOMAR Helmholtz Centre for Ocean Research Kiel and the Alfred Wegener Institute for Polar and Marine Research (AWI) in Bremerhaven (expedition details are provided in Tiedemann et al., 2014).

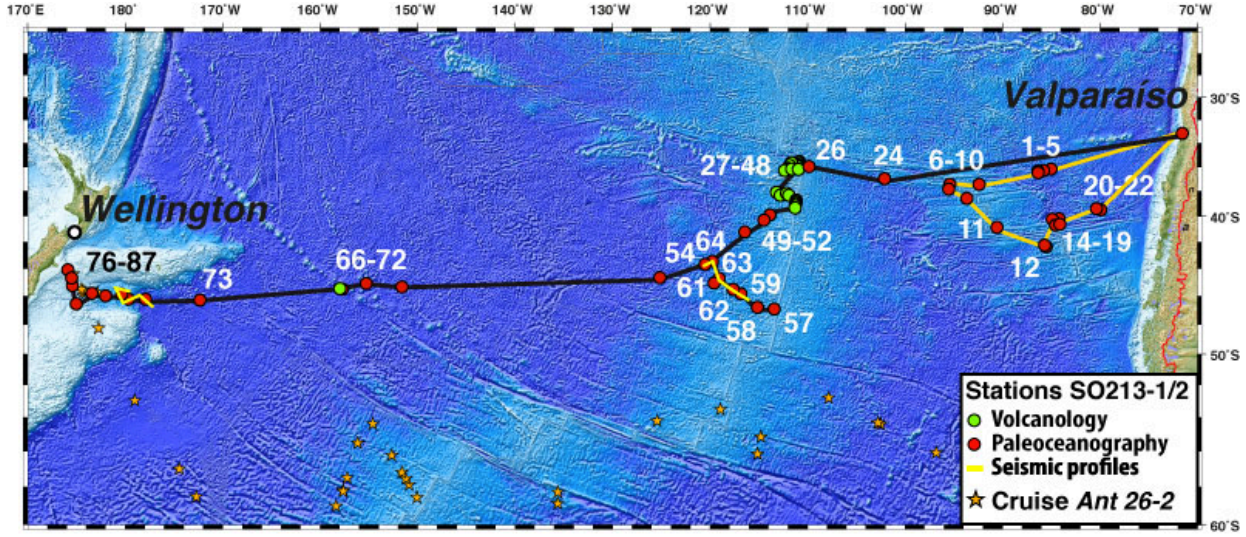


***Figure 2.1****. SO213 cruise track of Leg 1 (dark yellow line) and 2 (black line). GEBCO map made by WTD on board RV SONNE. Figure from Tiedemann et al., 2014 (FS Sonne Fahrtbericht / Cruise Report SO213)*

Chapter 3 of this thesis focuses on REE concentrations and Nd isotope compositions obtained from seawater samples from different water depths covering the sections shown in figure 2.1. Between 10 and 20 litres of seawater per sample was needed for these analyses. The REE were pre-concentrated on the ship using an Fe co-precipitation technique and further isolated and purified in the home laboratory in Kiel before determining the REE concentrations with an online pre-concentration method with an Agilent 7500-CX inductive coupled plasma

mass spectrometer (OC-ICP-MS). The Nd isotope compositions and Nd concentrations (via isotope dilution) were determined on a Nu Plasma multi-collector inductive coupled plasma mass spectrometer (MC-ICP-MS). This study also presents nutrient concentration data that were produced at the AWI, Bremerhaven, by the working group of R. Tiedemann.

The findings of chapters 4 and 5 are based on Nd, Sr and Pb isotope analysis of different sedimentary phases, which include Fe-Mn hydroxide coatings and detritus, were also measured on the same MC-ICP-MS. Chapter 4 presents Nd and Sr isotope data obtained from surface sediments (core-tops), also covering the entire distance between central Chile and New Zealand, using different methods to obtain the authigenic, seawater-derived Nd isotope compositions stored in Fe-Mn oxide coatings. These methods include two different ways of leaching bulk sediments, as well as dissolution of not reductively cleaned (unclean) planktonic foraminifera and fish teeth. Nd and Sr isotope compositions of the detrital fraction of the sediment were also measured for this study. Chapter 5 is based on two down-core records from the central South Pacific. For this study, authigenic Nd and Pb isotope compositions were obtained from 'unclean' planktonic foraminifera, 'non-decarbonated' bulk sediment leachates, and lithogenic Nd and Sr isotope compositions from the detritus. This study also presents oxygen and carbon isotope data that were produced by R. Tapia and T. Ronge (AWI, Bremerhaven).

The exact locations of the samples, the devices used for their procurement and the treatments applied to them to initially isolate REE and Nd from seawater and to separate and purify Nd, Sr and Pb from the different sedimentary phases are described in detail in section 3.2 for the water samples, in section 4.2 for the surface sediments, and in section 5.2 for down-core sediments. The specific separation and purification of Nd, Sr and Pb prior to the measurement of their isotopic ratios on the MC-ICP-MS was performed by ion chromatography (column chemistry), which followed the same procedures regardless of the origin of the samples and are described in detail in the following section. The MC-ICP-MS analyses are also similar for all kinds of samples of this study and are explained in detail in section 2.2.

### 2.1. Column chemistry

For the analysis of Nd, Sr and Pb isotope ratios on a MC-ICP-MS, it is essential to previously isolate the elements to be measured. Therefore, after dissolution and pre-concentration from their original phases (see sections 3.2, 4.2 and 5.2), these elements have to be chromatographically separated and purified in order to avoid interferences of other isotopes

during the measurement. In the case of sedimentary Pb, one third of the total amount of the dissolved samples was passed through anion exchange columns, filled with 50 µl of AG1-X8 resin, mesh size 100-200 µm (Galer and O'Nions, 1989; Lugmair and Galer, 1992) following the steps shown in table 2.1. For the isolation of Nd and Sr, the rest of the sample (in the case of the seawater samples the entire sample was used only for Nd) was taken through cation exchange columns filled with 0.8 ml AG50WX12 resin, mesh size 200-400 µm, to separate alkaline elements (including Sr) from Rare Earth Elements (including Nd) following the elution scheme in table 2.2. The solutions containing Nd and Sr were further purified using Eichrom® Ln Spec resin (50-100 µm mesh size, 2mL resin bed)(Barrat et al., 1996; Le Fevre and Pin, 2005) and Eichrom Sr Spec resin (50-100 µm mesh size, 50µL resin bed) (Horwitz et al., 1992), respectively (see tables 2.3 and 2.4).

| **Stage** | **Volume** | **Acid** |
|---|---|---|
| clean column | 1 x 1 res. | 1M HNO3 |
| clean column | 2 x 1 res. | MQ |
| **LOAD RESIN** | **0.05 ml** | **RESIN** |
| clean resin | 3 x 1ml | 0.25 HNO3 |
| condition resin | 2 x 100µl | Solution A |
| **LOAD SAMPLE** | 300µl | Solution A |
| Elute | 2 x 100µl | Solution A |
| Elute | 150µl | Solution A |
| Elute | 200µl | Solution B |
| **COLLECT Pb** | **300µl** | **Solution B** |
| Used resin to waste | Backwash | MQ |
| Clean column | Clean column | MQ |
| store columns | store columns | 1M HCl |
| Solution A: 5ml 1M HNO3 + | 1ml 2M HBr + | 4ml MQ |
| Solution B: 5ml 1M HNO3 + | 0.15ml 2M HBr + | 4.85 ml MQ |

***Table 2.1.*** *Ion chromatographic separation and purification of Pb using columns filled with 50µl of exchange resin AG1-X8 (100-200 µm).*

| **Stage** | **Volume** | **Acid** |
|---|---|---|
| clean columns | 8ml | 6M HCl |
| condition columns | 0.5ml | 1M HCL |
| condition columns | 1ml | 1M HCL |
| **LOAD SAMPLE** | **0.5** | **1M HCL** |
| wash in sample | 3 x 0.6ml | 1M HCL |
| elute matrix | 5ml | 3M HCl |
| **COLLECT Sr** | **5ml** | **3M HCl** |
| MQ buffer | 2 x 1ml | MQ |
| elute Ba | 8ml | 2.5M HNO3 |
| **COLLECT REEs** | **6ml** | **6M HNO3** |
| clean columns | 6ml | 6M HNO3 |
| MQ buffer | 2 x 1ml | MQ |

***Table 2.2.*** *Cation chromatographic separation of REE and Sr using columns filled with 0.8 ml of exchange resin AG50W-X12 resin (200-400 µm)*

| Stage | Volume | Acid |
|---|---|---|
| clean columns | 8ml | 6M HCl |
| condition columns | 0.5ml | 0.1M HCl |
| condition columns | 1ml | 0.1M HCl |
| **LOAD SAMPLE** | **0.5ml** | **0.1M HCl** |
| wash in sample/elute Ba | 0.5ml | 0.1M HCl |
| elute REEs | 7.5ml | 0.25M HCl |
| **COLLECT Nd** | **5ml** | **0.25M HCl** |
| clean columns | 8ml | 6M HCl |
| pass/condition for storage | 1+1ml | 0.3M HCl |

***Table 2.3.*** *Chromatographic separation and purification of neodymium from Ba and the other REEs using columns filled with 2ml Ln Spec resin (50-100 µm)*

| Stage | Volume | Acid |
|---|---|---|
| clean column | 1 x 1 res. | 0.1M H2SO4 |
| clean column | 2 x 1 res. | MQ |
| **LOAD RESIN** | **0.05ml** | **RESIN** |
| clean resin | 1ml | 0.1M H2SO4 |
| clean resin | 2 x 1 res. | MQ |
| condition resin | 2 x 50µl | 3M HNO3 |
| condition resin | 2 x 75µl | 3M HNO3 |
| **LOAD SAMPLE** | **100µl** | **3M HNO3** |
| elute sample | 1 x 50µl | 3M HNO3 |
| elute sample | 300µl | 3M HNO3 |
| **COLLECT Sr** | **500µl** | **MQ** |
| salvage used resin | backwash resin | MQ |
| clean columns to waste | | Acetone |
| rinse columns to waste | | MQ |
| store columns | | 1M HCl |

***Table 2.4.*** *Chromatographic purification of strontium using columns filled with 50µl Sr-spec resin (50-100µm)*

| Stage | Volume | Acid |
|---|---|---|
| Pre – clean | 8 ml | 6M $HNO_3$ / 0.5M HF |
| Change acid | 2 x 1ml | MQ |
| Pre – clean | 0.5 ml | 1M HCL / 0.5M HF |
| Pre - condition | 1 ml | 1M HCL / 0.5M HF |
| **Load sample (and collect Hf)** | **0.5 ml** | **1M HCL / 0.5M HF** |
| **(Collect Hf)** | **2 ml** | **1M HCL / 0.5M HF** |
| Elute Fe | 5 ml | 3M HCl |
| Change acid | 2 x 1ml | MQ |
| elute Ba | 12 ml | 2M HNO3 |
| **Collect Ac/REE** | **6 ml** | **6M HNO3** |
| clean columns | 6 ml | 6M HNO3/ 0.5M HF |
| Pass and store | 1 ml | MQ |

***Table 2.5.*** *Cation chromatographic separation of REE for isotope dilution (ID) measurements of Nd conc. using columns filled with 0.8 ml of exchange resin AG50W-X8 resin (200-400 µm)*

## 2.2. Mass spectrometry

The measurements of the isotope compositions of Nd, Sr, and Pb were carried out on a Nu Plasma MC-ICP-MS at GEOMAR, Kiel. The instrument was configured at low mass resolution in static mode. The efficiency of the Faraday cups on this instrument was calibrated for gain before every measurement session. All samples were dissolved in 2% $HNO_3$ for introduction into the plasma of the instrument via a desolvating nebulizer.

### 2.2.1. Determination of Nd concentration via isotope dilution

Seawater REE concentrations were measured through OC-ICP-MS, but in order to obtain a better precision for the seawater Nd concentrations, these were also determined by an isotope dilution (ID) method (details in Stichel, 2010 and Chen, 2013), which comprises the addition of a known amount of spike that is artificially enriched in the isotope $^{150}Nd$ ($^{150}Nd/^{144}Nd$ = 199.6356) compared to the natural ratio ($^{150}Nd/^{144}Nd$ = 0.235873) to aliquots of the samples (0.5 l). After equilibration and preconcentration the samples were then subject of a one step chromatographic separation (table 2.5)(see also section 3.2.2.1.). The measured isotope ratios are a combination of the relative abundances present in the spike and the samples, which are at the end dependent of the amount of spike added and the amount of the element in the sample. To minimize the uncertainty of an ID measurement it is ideal to reach the optimum abundance ratio between isotopes $^{150}Nd$ and $^{144}Nd$, which in the case of our spike is 6.86 (see Stichel, 2010 and Chen, 2013). Therefore, it is crucial to estimate the amount of Nd expected for a particular sample as well as possible before adding the spike. In this case, precise guesses were achieved given that the OP-ICP-MS measurements for REE concentrations (section 2.2.3.) were performed prior to the ID measurements.

### 2.2.2. Measurement of isotope ratios

Prior to any isotope measurement a concentration test of the samples was carried out. This test consists in the analysis of standards diluted to different and known concentrations together with cuts of the samples diluted to the expected concentrations. These are then calculated using the regression line given by the by the currents and concentrations of the standards (Fig. 2.2). Ideally, the cuts should fall within the range of the standards, as shown in figure 2.2. Typical concentrations for the analyses of this study are shown in table 2.6.

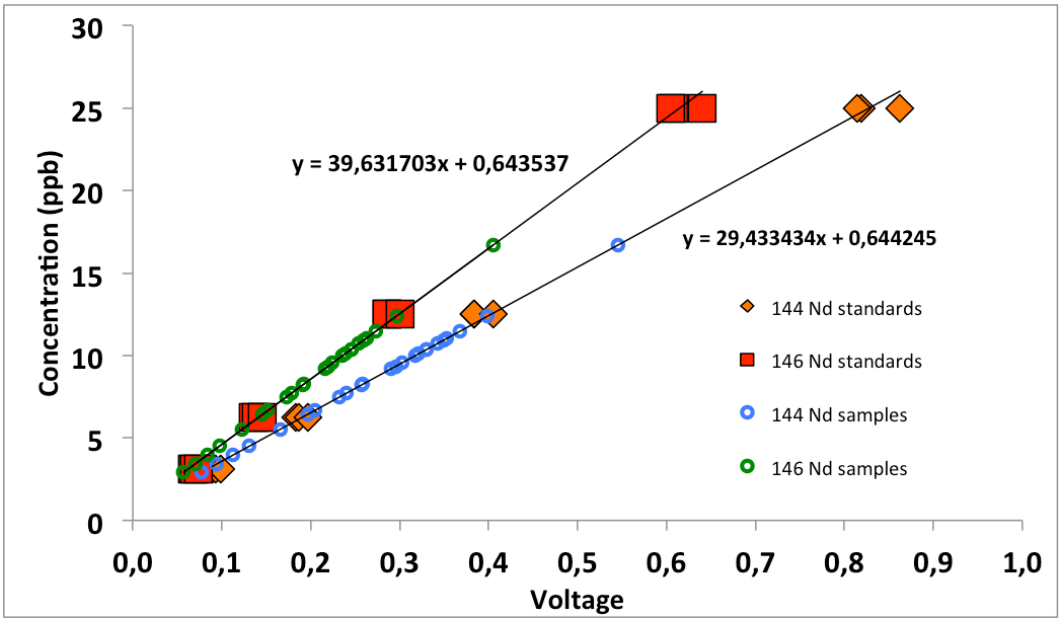


***Figure 2.2**. Example of a concentration test on 'uncleaned' foraminifera samples. In this case the analyzed cuts were diluted 1:8 with respect to the original sample.*

| Type of sample | Typical concentration (ppb) | | |
|---|---|---|---|
| | ***Nd*** | ***Sr*** | ***Pb*** |
| fish teeth | 10 - 30 | - | - |
| seawater | 10 - 60 | - | - |
| uncleaned foraminifera | 30 - 60 | - | - |
| decarbonated leachate | 50 - 200 | - | - |
| non-decarbonated leachate | 100 - 300 | 300 -2000 | 60 - 400 |
| detritus | 200 - 1200 | 1000 - 4000 | - |

***Table 2.6.** Typical concentrations (ppb) adjusted by dilution and measured during the concentration test for the different kinds of samples analyzed in this thesis.*

For the measurements of the isotope ratios, samples and standards were diluted to the same concentrations in order to reach similar beam intensities during the measurement (Fig. 2.3). This allows a realistic estimation of the external reproducibility of the samples, which is twice the standard deviation (2σ) of the measured isotope ratios of all standards measured during a session. Standards were usually intercalated every 2 to 6 samples. The standards used in this study, their official values and the external reproducibilities for the measurements of this study are reported in chapters 3 (section 3.2), 4 (section 4.2) and 5 (section 5.2).

In the case of samples with concentrations above 20 ppb in 1 ml solution, the analysis were carried out applying an autorun method using an autosampler over night, whereas samples with lower concentrations were manually measured in time resolved mode. In this case the samples were diluted to concentrations that allowed a beam intensity above at least 0.1 V per Faraday cup, which is the minimum voltage per cup required for a reliable measurement. Therefore, the

internal error measured for the low concentrated samples of this study was always better than $1x10^{-5}$.

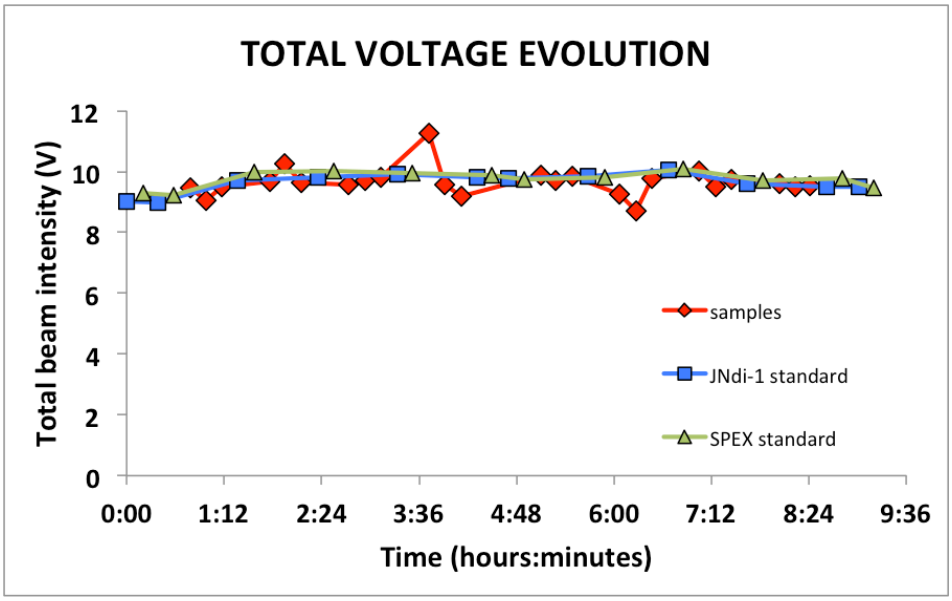


***Figure 2.3****. Example of the total voltage evolution of Nd samples and standards diluted to 60ppb during an overnight autorun session on the MC-ICP-MS.*

Isobaric interferences on the Nd and Sr isotopes caused by $^{144}Sm$ and $^{86}Kr$, $^{87}Rb$, respectively were corrected by subtracting their expected contributions, which were deduced from measuring the ratios of other primordial isotopes of these elements. Instrumental mass bias was corrected for Nd and Sr isotopes applying an exponential mass fractionation law using the ratios of two of their primordial isotopes, which are 0.7219 and 0.1194 for $^{146}Nd/^{144}Nd$ and $^{88}Sr/^{86}Sr$, respectively.

Given that Pb has only one primordial isotope ($^{204}Pb$), it is not possible to define a primordial ratio between two Pb isotopes to correct for mass fractionation in the instrument. We thus used a standard-bracketing method for the measurements of Pb isotope ratios following Albarède et al., (2004). As the abundance of $^{204}Pb$ is considerably lower than those of $^{206}Pb$, $^{206}Pb$ and $^{208}Pb$ (table 2.7), the beam intensity of $^{208}Pb$ has to be at least 5 V in order to reach 0.1 V on the Faraday cup detecting the $^{204}Pb$ beam. Similarly, $^{88}Sr$ represents ~83% of the total amount of Sr (table 2.7), therefore, for reaching a minimum of 0.1 V on cap $^{86}Sr$, the beam intensity for $^{88}Sr$ had to be around 8 V, but not exceed 10 V, which would overload the cup and invalidate the measurement. The relative natural abundances of the isotopes of Nd (table 2.7.) are more evenly distributed than these of Pb and Sr, this facilitates the measurement in term of minimum voltages and cup overloading.

| Isotope | Mass of Atom (u) | % Abundance |
|---|---|---|
| $^{142}$Nd | 141.907719 | 27.2 |
| $^{143}$Nd | 142.90981 | 12.2 |
| $^{144}$Nd | 143.910083 | 23.8 |
| $^{145}$Nd | 144.912569 | 8.3 |
| $^{146}$Nd | 145.913112 | 17.2 |
| $^{148}$Nd | 147.916889 | 5.7 |
| $^{150}$Nd | 149.920887 | 5.6 |
| $^{204}$Pb | 203.973029 | 1.4 |
| $^{206}$Pb | 205.974449 | 24.1 |
| $^{207}$Pb | 206.975881 | 22.1 |
| $^{208}$Pb | 207.976636 | 52.4 |
| $^{84}$Sr | 83.913425 | 0.6 |
| $^{86}$Sr | 85.909262 | 9.9 |
| $^{87}$Sr | 86.908879 | 7.0 |
| $^{88}$Sr | 87.905614 | 82.6 |

***Table 2.7.*** *Isotopic masses and natural abundances of the different isotopic systems used in this study. Data from Rosman and Taylor, 1999.*

### 2.2.3. Determination of REE concentrations in seawater and 'uncleaned' foraminifera

The REE concentrations of seawater and 'uncleaned' foraminifera samples were determine on an Agilent 7500ce ICP-MS using an online pre-concentration technique that separates matrix elements, such alkaline elements, from REE using a resin with ethylenediaminetriacetic acid and iminodiacetic acid functional groups. This pre-concentration process was carried out in a 'seaFAST' system (Elemental Scientific Inc.), which was coupled to the ICP-MS (Hathorne et al., 2012). Only 8 ml of filtered and acidified seawater were necessary for these measurements (further details in section 3.2.2.2). In the case of 'uncleaned' foraminifera, the samples were subject of a preceding calcium (Ca) concentration test, after which the samples were diluted to a Ca concentration of 25ppm for the measurements (details in section 4.2.3).

**References:**


Albarède F., Telouk P., Blichert-Toft J., Boyet M., Agranier A. and Nelson B. (2004) Precise and accurate isotopic measurements using multiple-collector ICPMS. *Geochim. Cosmochim. Acta* **68** (12), 2725–2744.

Barrat J. A., Keller F., Amosse´ J., Taylor R. N., Nesbitt R. W. and Hirata T. (1996) Determination of Rare Earth Elements in sixteen silicate reference samples by ICP-MS after Tm addition and ion exchange separation. *Geostand. Geoanal. Res.* **20**, 133–139.

Chen T. (2013) The geochemical cycling and paleoceanographic application of combined oceanic Nd-Hf isotopes. *Dissertation*. Christian-Albrechts-Universität zu Kiel.

Hathorne E.C., Haley B.A., Stichel T., Grasse P., Zieringer M. and Frank M. (2013) Online preconcentration ICP-MS analysis of rare earth elements in seawater. *Geochem. Geophys. Geosyst.* **13**, Q01020, doi:10.1029/2011GC003907

Horwitz E. P., Chiarizia R. and Dietz M. L. (1992) A novel strontium-selective extraction chromatographic resin. *Solvent Extr. Ion Exch.* **10**, 313–336. http://dx.doi.org/10.1080/07366299208918107

Galer S.J.G. and O'Nions R.K. (1989) Chemical and isotopic studies of ultramafic inclusions from the San Carlos volcanic field, Arizona: a bearing on their petrogenesis. *J. Petrol.* **30** (4), 1033–1064.

Le Fevre B. and Pin C. (2005) A straightforward separation scheme for concomitant Lu–Hf and Sm–Nd isotope ratio and isotope dilution analysis. *Anal. Chim. Acta* **543**, 209–221.

Lugmair G.W. and Galer S.J.G. (1992) Age and isotopic relationships among the angrites Lewis Cliff 86010 and Angra dos Reis. *Geochim. Cosmochim. Acta* **56**, 1673–1694.

Rosman K. J. R. and Taylor P. D. P. (1999) Report of the IUPAC Subcommittee for Isotopic Abundance Measurements. *Pure Appl. Chem.* **71**, 1593-1607

Stichel T. (2010) Tracing water masses and continental weathering by neodymium and hafnium isotopes in the Atlantic sector of the Southern Ocean. *Dissertation*. Christian-Albrechts-Universität zu Kiel.

Tiedemann R., Lamy F., cruise participants (2014) FS Sonne Fahrtbericht/Cruise Report SO213 - SOPATRA: South Pacific Paleoceanographic Transects - Geodynamic and Climatic Variability in Space and Time, Leg 1: Valparaiso/Chile - Valparaiso/Chile, 27.012.2010 - 12.01.2011, Leg 2: Valparaiso/Chile - Wellington/New Zealand, 12.01.2011 - 07.03.2011. doi:10.2312/cr_so213

# 3) South Pacific dissolved Nd isotope compositions and rare earth element distributions: Water mass mixing versus biogeochemical cycling

**Abstract**

Despite its enormous extent and importance for global climate, the South Pacific has been poorly investigated in comparison to other regions with respect to chemical oceanography. Here we present the first detailed analysis of dissolved radiogenic Nd isotopes ($\varepsilon_{Nd}$) and Rare Earth Elements (REEs) in intermediate and deep waters of the mid-latitude (~40°S) South Pacific along a meridional transect between South America and New Zealand. The goal of our study is to gain better insight into the distribution and mixing of water masses in the South Pacific and to evaluate the validity of Nd isotopes as a water mass tracer in this remote region of the ocean. The results demonstrate that biogeochemical cycling (scavenging processes in the Eastern Equatorial Pacific) and release of LREEs from the sediment clearly influence the distribution of the dissolved REE concentrations at certain locations. Nevertheless, the Nd isotope signatures clearly trace water masses including AAIW (Antarctic Intermediate Water) (average $\varepsilon_{Nd}$=-8.2 ±0.3), LCDW (Lower Circumpolar Deep Water) (average $\varepsilon_{Nd}$=-8.3 ±0.3), NPDW (North Pacific Deep Water) (average $\varepsilon_{Nd}$=-5.9 ±0.3), and the remnants of NADW (North Atlantic Deep Water) (average $\varepsilon_{Nd}$=-9.7 ±0.3). Filtered water samples taken from the sediment-water interface under the deep western boundary current off New Zealand suggest that boundary exchange processes are limited at this location and highlight the spatial and temporal variability of this process.

These data will serve as a basis for the paleoceanographic application of Nd isotopes in the South Pacific.

*This chapter was published in the journal Geochimica et Cosmochimica Acta (volume 127, pages 171-189, 2014), authored by Mario Molina-Kescher, Martin Frank, and Ed Hathorne under the title: South Pacific dissolved Nd isotope compositions and rare earth element distributions: Water mass mixing versus biogeochemical cycling*

## 3.1. Introduction

The Rare Earth Elements (REEs) are a coherent group of chemical elements (here the lanthanides and yttrium), for which the relative distribution or "pattern" is sensitive to oceanic processes such as scavenging and advection of water masses (e.g. Elderfield et al., 1988; Nozaki, 2001). The study of dissolved REEs in seawater has regained attention in recent years, in particular as a result of the use of Nd isotopes as a water mass tracer in oceanographic and paleoceanographic studies (e.g. Rickli et al., 2009; Roberts et al., 2010; Horikawa et al., 2010; Elderfield et al., 2012; Piotrowski et al., 2012; Martin et al., 2012; Stichel et al., 2012) This is possible because of the quasi-conservative behavior of Nd within distinct deep and intermediate water masses and due to the fact that Nd isotopes are not affected by biological fractionation (e.g. Frank, 2002; Goldstein and Hemming, 2003 and references therein). Studies based on Nd isotope compositions and REE distributions have helped to better understand present and past ocean circulation as well as weathering inputs and their relationship to climate on different time scales (e.g. Bertram and Elderfield, 1992; Piepgras and Jacobsen, 1992; Nozaki, 2001; Frank, 2002; Goldstein and Hemming, 2003; Scher and Martin, 2004; Lacan and Jeandel, 2005; Pahnke et al., 2008; Carter et al., 2012; Piotrowski et al., 2012; Singh et al, 2012).

The REEs can be divided into the light REEs (LREE) from La to Sm, the Middle REEs (MREE) from Eu to Dy, and the Heavy REEs (HREE) from Ho to Lu. Y behaves similarly to Ho because of the similar ionic radii (e.g. Nozaki, 2001). REE concentrations generally increase with water depth, similar to nutrients, as a consequence of particle scavenging in the surface and gradual remineralization of sinking particles, leading to REE release in deeper waters. Dissolved REEs fractionate coherently within the water column as a function of their ionic radii (e.g. Byrne and Kim, 1990). The LREEs are more particle reactive and therefore have shorter residence times than the HREEs, leading to differences in the REE profiles with water depth. Different water masses also present different absolute REE concentrations and ratios between REEs depending on the composition of their primary continental sources, as well as the age of a particular water mass or the scavenging intensity it has experienced. Cerium is exceptional in that it oxidizes to Ce(IV) in the water column thus becoming highly insoluble (Moffett, 1990). The main features of the shale-normalized patterns of seawater, which represent the fractionation of REEs with respect to the continental sources, are a gradual increase in abundance from the LREE to the HREE and a marked Ce depletion compared to its neighboring

REEs (Elderfield, 1988; Byrne and Kim, 1990; Piepgras and Jacobsen, 1992; Nozaki 2001 and references therein).

Radiogenic Nd isotope ratios ($^{143}Nd/^{144}Nd$) are generally expressed in the $\varepsilon_{Nd}$ notation: $\varepsilon_{Nd} = [(^{143}Nd/^{144}Nd_{sample}/^{143}Nd/^{144}Nd_{CHUR})-1]*10.000$, where CHUR stands for Chondritic Uniform Reservoir ($^{143}Nd/^{144}Nd=0.512638$, Jacobsen and Wasserburg, 1980). Seawater acquires its dissolved Nd isotope signature through continental weathering either via riverine or dust input and via exchange with the continental margins (Lacan and Jeandel, 2005), which includes groundwater discharge (Johannesson et al. 2007) and reactions with resuspended sediments (cf. Frank, 2002). Water masses originating from regions where young mantle derived material is weathered, such as around the Pacific Ocean, have higher, more radiogenic $\varepsilon_{Nd}$ values, ranging from -2 to -4 in the North Pacific (Piepgras and Jacobsen, 1988; Amakawa et al., 2004a; Amakawa et al., 2009). In contrast, contributions from old continental rocks result in more negative (unradiogenic) values. This is for example the case for the old cratonic rocks located in eastern Canada and northern Europe, which results in an $\varepsilon_{Nd}$ value near -13 for North Atlantic Deep Water (NADW) (Piepgras and Wasserburg, 1987; Rickli et al., 2009). Those two most important end members mix within the Antarctic Circumpolar Current (ACC) resulting in intermediate present day $\varepsilon_{Nd}$ values near -8.5 (Piepgras and Wasserburg, 1982; Stichel et al., 2012). A prerequisite for the use of $\varepsilon_{Nd}$ signatures as water mass traces is the seawater residence time of Nd, which has been estimated to be between 300 and 1000 years (Tachikawa et al., 2003; Arsouze et al., 2009; Rempfer et al., 2011) and which is thus shorter than the global oceanic mixing time.

Nevertheless, the exact source and sink terms of Nd are still debated because of the apparent mismatch between Nd isotopes, which in the open ocean follow the advection and mixing of water masses, and Nd concentrations, which show a general increase with water depth and thus document vertical transport. This apparent contradiction has been named the Nd paradox (e.g. Goldstein and Hemming, 2003), which is most likely explained by reversible particle scavenging (Siddall et al., 2008), particularly in high productivity areas (e.g. Grasse et al., 2012) or near large river mouths (Singh et al., 2012). Another poorly understood aspect of marine Nd isotopes are the so-called boundary exchange processes that consider continental margins to be both an important source and sink of Nd in the oceans (Tachikawa et al., 2003; Lacan and Jeandel, 2005; Rempfer et al., 2011). These processes have been shown to change the isotope composition of Nd in seawater without significantly modifying its concentration (Lacan and Jeandel, 2005).

In the South Pacific the behavior of dissolved REE concentrations and Nd isotope compositions have not been systematically investigated until now. As pointed out in a recent global seawater Nd isotope compilation (Lacan et al., 2012) there is a general lack of data in the entire Pacific, in particular south of 30°S. Recent studies have contributed the first seawater Nd isotope data from the Pacific sector of the Southern Ocean and the Drake Passage (Carter et al., 2012; Stichel et al., 2012), as well as from the western (Grenier et al., 2013) and eastern equatorial Pacific (Grasse et al., 2012; Jeandel et al., 2013) but there are still only very few data for the large South Pacific basin.

The goal of this study is to better understand the behavior of dissolved REEs and Nd isotopes and their applicability as water mass tracers in the mid-latitude South Pacific. The South Pacific plays an important role for the global ocean circulation given that it represents the entrance and exit area for all deep waters of the largest ocean basin. We aim to elucidate the main factors controlling the distribution of REEs and Nd isotopes including advection, biogeochemical processes (scavenging), and boundary exchange processes. Although consisting of only 24 samples, this study covers the most important water masses in the southern Pacific and provides the first systematic evaluation of $\varepsilon_{Nd}$ signatures and REE concentrations in this area, which will also serve as an important basis for reconstructions of past ocean circulation in the southern Pacific using Nd isotopes (e.g. Basak et al., 2010; Elderfield et al., 2012; Noble et al., 2013).

### 3.1.1. Hydrography and water column properties.

Our study focuses on the body of water between New Zealand and South America between 35° and 50°S (Fig. 3.1a), the hydrography of which is dominated by waters originating from the Antarctic Circumpolar Current (ACC). A number of oceanographic studies have taken place in this remote region, many of them building on the knowledge acquired along longitudinal sections during the pioneering SCORPIO expeditions in the late 1960s (Stommel et al., 1973) and the more recent World Ocean Circulation Experiment (WOCE). One of the main features observed is a general southward flow of water masses between 1000 and 3500 metres depth that are ultimately entrained in circumpolar waters of the ACC (Reid, 1973, 1986, 1997; Warren, 1973; Tsuchiya and Talley 1996, 1999; Tsimplies et al., 1998; Wijffels et al., 2001). This flow is compensated by ACC derived northward moving water masses above and below.

The ACC is composed of deep waters admixed from the three major ocean basins, which results in the formation of Circumpolar Deep Water (CDW). The southeast Pacific sector of the Southern Ocean is also where equatorward flowing Antarctic Intermediate Water (AAIW)

forms (Bostock et al., 2010) by winter air-sea exchange and cooling of Antarctic Surface Water (AASW) resulting in denser Subantarctic Mode Water (SAMW), which through further cooling is converted into AAIW (Sloyan and Rintoul, 2001). These fresh, oxygen-rich water masses occupy the depth range of 200 to 1500 m in the South Pacific and are transported along the anticyclonic pathway of the subtropical gyre, thereby ventilating the lower subtropical thermocline. Modified SAMW/AAIW returns poleward at the western boundary of the South Pacific and joins the AAC close to New Zealand near 170°W, 45°S.

Mixing with North Atlantic Deep Water (NADW) in the Atlantic sector of the Southern Ocean changes the properties of the upper part of CDW and thus divides it into Upper Circumpolar Deep Water (UCDW) and Lower Circumpolar Deep Water (LCDW). Nevertheless, the influence of NADW admixed in the Atlantic sector is still detectable in the western South Pacific between 180°E and 160°W by its salinity maximum and low nutrient concentrations near 3000 m (Fig 3.1c,d)(Reid and Lynn, 1971).

LCDW dominates the deeper water column flowing equatorward across the Southwest Pacific Basin (Fig 3.1b). It develops a deep western boundary current in its westernmost sector, which is considered responsible for the ventilation of the deep Pacific (Stommel and Arons, 1960; Reid et al., 1968). This is a consequence of the high oxygen content that LCDW acquires through admixture of one of its main sources, the Antarctic Bottom Water (AABW), which forms by sinking around Antarctica (Warren, 1973; Mantyla and Reid, 1983; Orsi et al., 1999). There is a strong vertical mixing component that tends to homogenize the hydrographic properties of LCDW characterized by low temperature, high salinity and high oxygen concentrations within the ACC.

UCDW enters the South Pacific near 120°W (Kawabe and Fujio, 2010) and its composition differs from that of LCDW mainly in its lower oxygen content, which originates from previous mixing with Indian Ocean deep waters (Callahan, 1972). However, in the depth range of UCDW in the South Pacific (1500 m– 3500 m) $O_2$ concentrations of UCDW are still higher than those of the water masses originating from the North Pacific and therefore UCDW is difficult to unambiguously identify by its hydrographic properties in our study area.

Mid-depth southward flow mainly occurs close to the South American continent in the form of North Pacific Deep Water (NPDW) (Fig. 3.1d), the precursors of which are ultimately LCDW and UCDW (Kawabe and Fujio, 2010). However, the original properties of those waters masses have been strongly modified during advection through the entire Pacific Ocean. The LCDW and UCDW become enriched in nutrients and depleted in oxygen due to respiration and

remineralisation processes of organic matter as the water masses age. As a consequence, these waters are transformed into NPDW long before returning to the Southern Ocean (Shaffer et al., 2004; Wijffels et al., 2001; Kawabe and Fujio, 2010). Mid-depth waters with central Pacific characteristics are detectable by their lower [$O_2$] in the Southwest Pacific basin between 1500 and 3500 m depth (Fig 3.5). This water body, from hereon referred to as South Pacific Gyre derived Deep Water (SPGDW), is the result of the mixing between UCDW that enters the South Pacific flowing across the East Pacific Rise and mid-depth central Pacific waters as a consequence of the middepths dynamics of the South Pacific Gyre (Reid, 1986), which supplies these less oxygenated waters in addition to pure UCDW to our study area.

The absence of deep water formation with characteristic hydrographic fingerprints in the North Pacific results in small differences of salinity and temperature in deep and intermediate waters throughout the Pacific. In the case of the South Pacific it is thus often difficult to distinguish northern and southern derived mid-depth water masses based on their hydrographic properties. In contrast, oxygen concentrations show marked differences between waters of northern and southern origin as a consequence of respiration during transport and aging of water masses. Oxygen concentrations are therefore a more suitable tool to distinguish waters from these sources and to track the return flow of mid-depth waters to the Southern Ocean.

### 3.2. Samples and Methods.

For this study, 26 seawater samples from depths between 300 m and 5150 m were collected for analysis of REE concentrations and Nd isotope ratios along a longitudinal transect between 36°S and 45°S extending over approximately 10 000 km from central Chile to New Zealand (Fig. 3.1a). Samples were collected during Expedition SO213 of the German RV SONNE, which consisted of two legs from December 2010 to March 2011.

#### 3.2.1. Sample collection

24 samples were collected from 5 profiles consisting of 4 to 5 depths using Niskin bottles attached to a CTD-rosette, which allowed the recovery of a volume of 18 to 20 l of seawater for every sample. The five bottom water samples obtained with the CTD-rosette were collected at approximately 2 m above the seafloor. In addition, off New Zealand 2 bottom water samples

were recovered using a multicorer device (MuC) for the extraction of short undisturbed surface sediment cores that also allows the collection of bottom water immediately above the sediment-water interface (e.g. Haley et al., 2004). This water collected in the tubes of the device

was carefully extracted without suspending the sediment and was subsequently filtered and treated in the same way as the other seawater samples. This method allowed the collection of about 10 l of bottom water for each of the two samples and enables the investigation of boundary exchange processes. Unfortunately this sampling method does not allow the acquisition of in situ hydrological properties, which were thus inferred from the World Ocean Atlas 2009 (WOA 09) (Fig. 3.1, table 3.1).

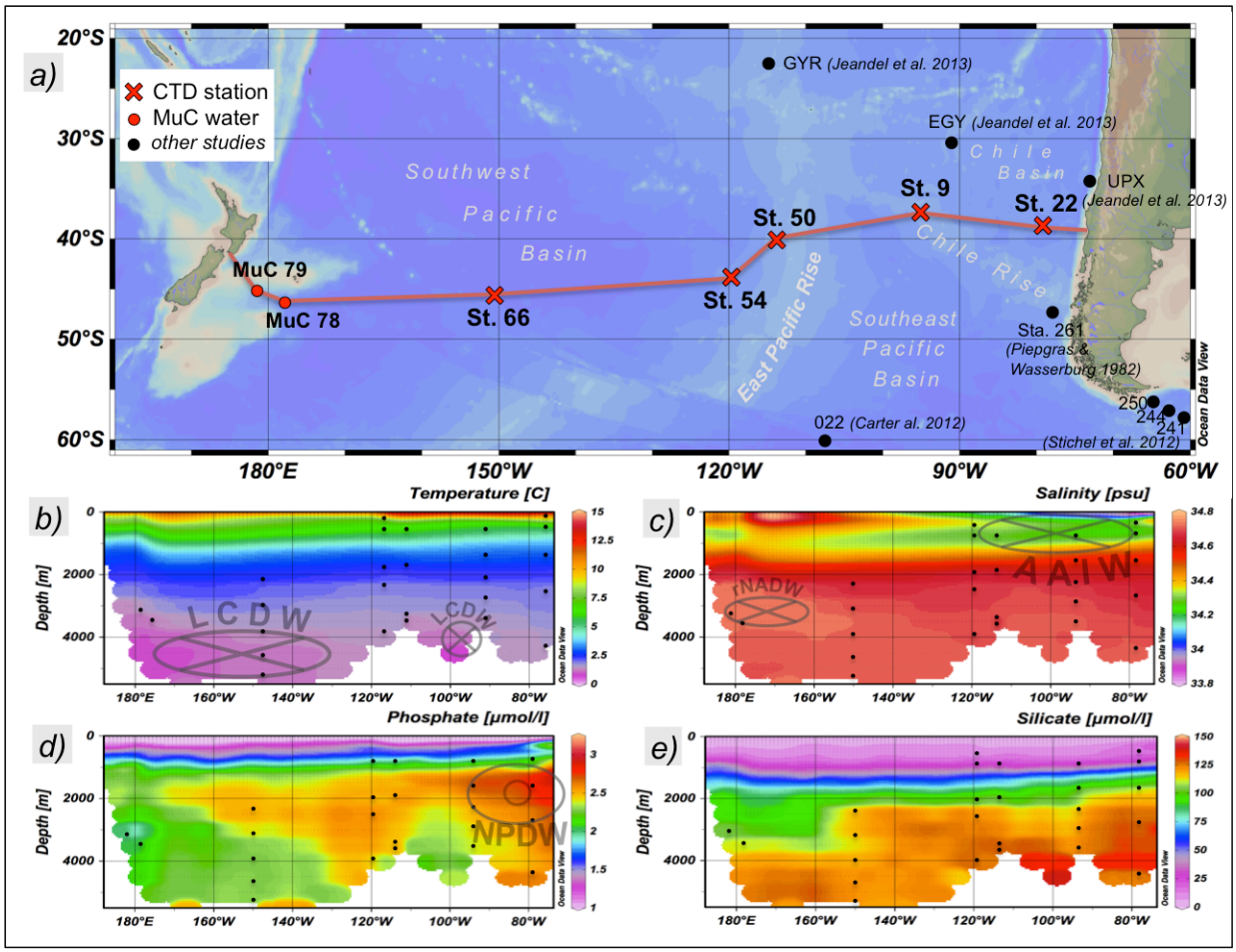


***Figure 3.1.*** *Cruise track and locations of water sampling stations of expedition SO213 together with the most important hydrological properties (Data from the World Ocean Atlas 09). a) Sampled locations: red crosses represent full depth CTD profiles and red dots represent bottom water samples obtained with a Multicorer (MuC). Black dots represent locations from other studies cited in the text. The most important bathymetric features are also indicated. The hydrological properties along the cruise track (red line) are provided in b) Temperature (°C), c) Salinity (psu), d) Phosphate (µmol/l), e) Silicate (µmol/l). Oxygen (ml/l) is presented in figure 3.5.*
*The flow directions of the waters masses are also shown by transparent circles on the section plots of the properties, whereby crosses represent the sense of movement into the page and centred circles represent movement out of the page. Specific water masses are illustrated in the section plots according to hydrographic properties that allow their identification. Water mass abbreviations: LCDW (Lower Circumpolar Deep Water), rNADW (residual North Atlantic Deep Water), AAIW (Antarctic Intermediate Water) and NPDW (North Pacific Deep Water). Small black dots on the sections indicate the locations of the samples of this study.*

### 3.2.2. Analytical procedures

All samples were filtered through 0.45 μm filters (nitrocellulose acetate) and were acidified to pH ~2.2 within the first two hours after collection. The majority of the water volume of every sample was used for the determination of the Nd isotope compositions but an aliquot of 0.5 to 2 litres of the same samples was separated for the determination of REE concentrations.

#### 3.2.2.1. Determination of Nd isotope compositions and Nd concentrations by isotope dilution.

The procedure applied for the extraction and isolation of the dissolved Nd is based on Fe co-precipitation of the REEs and was described in detail by Stichel et al. (2012). Briefly, after discarding the supernatant the Nd in the FeOOH-precipitate was separated from the other elements by four principal steps: Rinsing with deionized water for removal of major seawater ions, liquid-liquid extraction using diethyl ether for separation of the Fe, and a two step ion chromatographic purification of Nd: First the REEs are separated from other elements using Biorad® AG50W-X12 resin (200-400 μm mesh-size, 0.8mL resin bed resin) (Barrat et al., 1996) and then the Nd is separated from the other REEs using Eichchrom® Ln Spec resin (50-100μm mesh-size, 2mL resin bed)(Le Fevre and Pin, 2005).

For the determination of the dissolved Nd concentrations an isotope dilution (ID) method was applied as described in Stichel et al. (2012), in which $^{150}Nd/^{149}Sm$ spike is added to an aliquot (0.5 L) prior to subsequent treatment. The Nd preconcentration, also based on Fe co-precipitation, and subsequent purification with only a single chromatographic separation was applied for the purification of the Nd using a 1.4 ml resin bed of BIORAD® AG50W-X8, 200–400 μm mesh-size.

A Nu plasma MC-ICPMS at GEOMAR was used for the determination for both $^{143}Nd/^{144}Nd$ ratios and ID Nd concentration measurements. Instrumental mass fractionation was corrected by applying an exponential fractionation law using a $^{146}Nd/^{144}Nd$ ratio of 0.7219. The initial concentrations of the samples in the solutions for isotopic analysis ranged between 70 ppb and 120 ppb, which were first measured in autosampler sessions with samples and standards diluted to 50 ppb or 60 ppb allowing duplicate measurements. Some duplicates were considerably less concentrated (10 to 30 ppb) and were therefore measured in time resolved mode. Typical total ion beam intensities for samples and standards ranged from 1.5 V to 9 V for different measurement sessions with the low voltages realized by time resolved measurements. The results of the Nd isotope measurements were normalized to the accepted value of 0.512115 for the JNdi-1 standard (Tanaka et al., 2000), which was measured every two to six samples during

each session together with an in-house standard. Standards and samples were diluted to the same concentration resulting in standard deviations (external reproducibility) of repeated standard measurements that ranged between 0.2 and 0.4 εNd units (2σ) for the autosampler sessions and between 0.3 and 1 εNd units (2σ) for the time resolved measurements. All duplicate isotope analyses resulted in identical εNd values within these uncertainties, whereby the results presented in table 3.1 correspond to those measurements with the lower uncertainties of the individual analyses. Blank corrections were not applied as the blanks for both Nd isotope compositions and concentrations averaged 14 pg, representing around 1% of the concentrations of the samples. The entire protocol to measure seawater Nd isotopes in our laboratory corresponds to the one intercalibrated as part of the international GEOTRACES program (van de Flierdt et al., 2012).

#### 3.2.2.2. Determination of REE concentrations

REE concentrations were obtained using an online pre-concentration (OP) ICP-MS technique modified from Hathorne et al. (2012). Aliquots of 8 mL of filtered and acidified seawater were analysed using a "seaFAST" system (Elemental Scientific Inc.) coupled to an Agilent 7500ce ICP-MS. The improved technique applied here utilises artificial standards with REE patterns similar to seawater, which were prepared using a seawater matrix, from which all REEs had been removed by Fe co-precipitation (Hathorne et al., 2012). The external precision based on repeated measurement of GEOTRACES inter-calibration samples (van de Flierdt et al., 2012) in the course of this study is reported in table 3.2. These values are within the uncertainties of between 6% and 22% (2σ) of the measurements of the individual REEs (Hathorne et al., 2012) identical to the consensus values reported by van de Flierdt et al. (2012).

#### 3.2.2.3. Determination of nutrient concentrations

Dissolved silicate and phosphate concentrations were measured at the Alfred Wegener Institute Bremerhaven following standard procedures (Grasshoff, 1999).

## 3.3. Results

All the results presented in this study are available in the database of PANGAEA® (www.pangaea.de)

| | Depth | [Nd] | Nd IC | Ext. reprod. | θ | Salinity | $\sigma_\theta$ | [Oxygen] | [Phosphate] | [Silicate] |
|---|---|---|---|---|---|---|---|---|---|---|
| | m | pmol/kg | $\varepsilon_{Nd}$ | 2sd | °C | PSU | kg/m³ | ml/l | µmol/l | µmol/l |
| **Stations** | | | | | | | | | | |
| **St. 22** *(SO213-22-2)* | 300 | 11.2 | -7.5 | 0.3 | 5.19 | 34.25 | 26.87 | 3.46 | 1.70 | 14.42 |
| *39°12'S, 79°55'W* | 650 | 10.4 | -8.2 | 0.4 | 2.69 | 34.54 | 27.15 | 5.17 | 2.45 | 79.44 |
| *4144 m depth* | 1500 | 12.9 | -5.4 | 0.4 | 1.77 | 34.64 | 27.78 | 2.63 | 2.30 | 103.99 |
| | 2600 | 16.1 | -5.8 | 0.3 | 1.37 | 34.68 | 28.01 | 3.26 | 2.19 | 109.91 |
| | 4142 | 21.0 | -6.6 | 0.4 | 1.00 | 34.70 | 28.12 | 3.79 | 2.06 | 112.82 |
| **St. 9** *(SO213-09-2)* | 750 | 11.4 | -9.0 | 0.3 | 7.49 | 34.27 | 27.14 | 5.15 | 1.90 | 10.25 |
| *37°41'S, 95°28'W* | 1500 | 14.0 | -6.4 | 0.3 | 5.13 | 34.23 | 27.74 | 2.70 | 1.75 | 12.53 |
| *3771 m depth* | 2200 | 18.9 | -6.8 | 0.3 | 2.58 | 34.56 | 27.96 | 3.24 | 2.54 | 90.29 |
| | 2800 | 21.0 | -8.5 | 0.2 | 1.51 | 34.66 | 28.05 | 3.55 | 2.34 | 113.40 |
| | 3769 | 39.1 | -9.1 | 0.3 | 0.94 | 34.70 | 28.11 | 3.83 | 2.19 | 115.68 |
| **St. 50** *(SO213-50-1)* | 770 | 11.2 | -8.8 | 0.4 | 5.59 | 34.27 | 27.10 | 5.26 | 1.66 | 12.17 |
| *40°17'S, 114°26'W* | 1800 | 15.3 | -8.3 | 0.2 | 2.12 | 34.61 | 27.88 | 3.64 | 2.29 | 79.83 |
| *3483 m depth* | 3380 | 23.2 | -6.9 | 0.2 | 1.10 | 34.68 | 28.09 | 3.71 | 2.34 | 113.97 |
| | 3481 | 23.1 | -6.9 | 0.3 | 1.09 | 34.68 | 28.09 | 3.72 | 2.19 | 113.70 |
| **St. 54** *(SO213-54-2)* | 350 | 11.0 | -7.9 | 0.3 | 7.10 | 34.37 | 26.94 | 5.63 | 1.29 | 5.29 |
| *43°42'S, 120°30'W* | 800 | 9.7 | -7.8 | 0.4 | 5.57 | 34.28 | 27.11 | 5.09 | 1.70 | 14.32 |
| *3844 m depth* | 1900 | 14.1 | -7.6 | 0.2 | 2.11 | 34.61 | 27.89 | 3.57 | 2.21 | 83.21 |
| | 2400 | 18.6 | -6.9 | 0.2 | 1.59 | 34.66 | 28.00 | 3.43 | 2.22 | 106.47 |
| | 3842 | 25.9 | -6.5 | 0.2 | 0.95 | 34.69 | 28.12 | 3.84 | 2.16 | 113.54 |
| **St. 66** *(SO213-66-1)* | 2200 | 14.4 | -6.0 | 0.2 | 1.96 | 34.63 | 27.92 | 3.32 | 2.31 | 98.06 |
| *45°23'S, 151°42'W* | 3000 | 17.7 | -6.6 | 0.2 | 1.41 | 34.69 | 28.05 | 3.57 | 2.24 | 104.87 |
| *5157 m depth* | 3800 | 22.5 | -8.3 | 0.3 | 0.89 | 34.72 | 28.15 | 4.16 | 2.11 | 102.09 |
| | 4500 | 30.0 | -8.3 | 0.2 | 0.50 | 34.71 | 28.20 | 4.35 | 2.10 | 110.75 |
| | 5155 | 30.6 | -8.3 | 0.3 | 0.44 | 34.71 | 28.21 | 4.37 | 2.07 | 111.48 |
| **Multicorer samples** | | | | | | | | | | |
| **MuC - 78** | 3410 | 22.8 | -9.0 | 0.3 | 1.1* | 34.72* | 28.12* | 4.64* | 2.06* | 111.26* |
| *46°15'S, 179°37'W* | | | | | | | | | | |
| **MuC - 79** | 3144 | 21.9 | -10.3 | 0.3 | 1.4* | 34.73* | 28.08* | 4.53* | 1.90* | 103.53* |
| *45°51'S, 179°34'E* | | | | | | | | | | |

***Table 3.1.*** *Nd concentrations, Nd isotope compositions (IC) with external reproducibilities (2σ) and hydrographic data presented from east to west. [Nd] correspond to isotope dilution (ID) measurements. Values marked with * correspond to data obtained from the World Ocean Atlas 09 (WOA 09). θ = Potential temperature. $\sigma_\theta$ = Potential density. PSU = Practical Salinity Units.*

### 3.3.1. Hydrography at the sampling sites

The distribution of water masses described in the introduction is generally consistent with the hydrographic data obtained for the five full water depth profiles (Fig. 3.2). The similarity of the temperature-salinity characteristics of northern and southern derived deep waters requires the water mass characteristics in figure 3.2a to be defined by oxygen concentration against potential density ($\sigma_\theta$). With this approach the major water masses present at our sampling sites can be distinguished with the exception of UCDW, which is more difficult to identify in some cases (e.g. St. 09) as it is essentially identical to Pacific-derived waters with the same density range.

Station 22 exhibits a marked $O_2$ minimum of 3.46 ml/l at 26.87 kg/m$^3$ sampled at 300 m depth indicating the presence of Equatorial SubSurface Water (ESSW) (Fig. 3.2a). In the potential density range from 26.9 to 27.3 kg/m$^3$ the low salinities and high $O_2$ concentrations mark the presence of SAMW and AAIW, which was sampled at all stations except station 66. Below this depth, there is a clear bifurcation to waters with oxygen concentrations as low as 2.6 ml/l in the easternmost profiles 22 and 9, reflecting the southward flow of NPDW. This difference disappears at around 28.0 kg/m$^3$, where all profiles converge again coinciding with the presence of Antarctic derived waters. Profile 22 remains slightly less oxygenated than the rest of the stations indicating a stronger Pacific influence at this location. Pure LCDW has only been sampled in the deepest of all five profiles at station 66 located in the central southwest Pacific basin. UCDW can be identified by its lower oxygen content (3.5 ml/l) and higher potential density with respect to LCDW and is least diluted in profiles 50 and 54 located above the East Pacific Rise, where the influence of water masses originating from the north is smaller but not absent. The presence of pure circumpolar deep waters (UCDW/LCDW) in the deepest part of profile 9 documented in the sections of figure 3.1 (data from the World Ocean Atlas 09), is not reflected in figure 3.2 because of the difficulty of distinguishing UCDW based on hydrographic data. In the density range of UCDW the lower [$O_2$] in profile 66 indicates the southward flow of central Pacific waters (SPGDW).

The nutrient profiles (Fig. 3.2b and 3.2c) show depleted concentrations for both silicate and phosphate in surface waters, which increase with depth. Nevertheless while silicate concentrations reach their maxima in the bottom waters, phosphate maxima are present between 1500 and 3500, especially for samples 22-1500 (St. 22, 1500 m water depth) and 9-1500 (St. 9, 1500 m water depth) coinciding with the main core of NPDW.

Figures 3.1c,e,f and 3.2b,c indicate that the two multicorer samples are located under the influence of the last remnant of NADW, as indicated by the high salinity and low nutrient content.

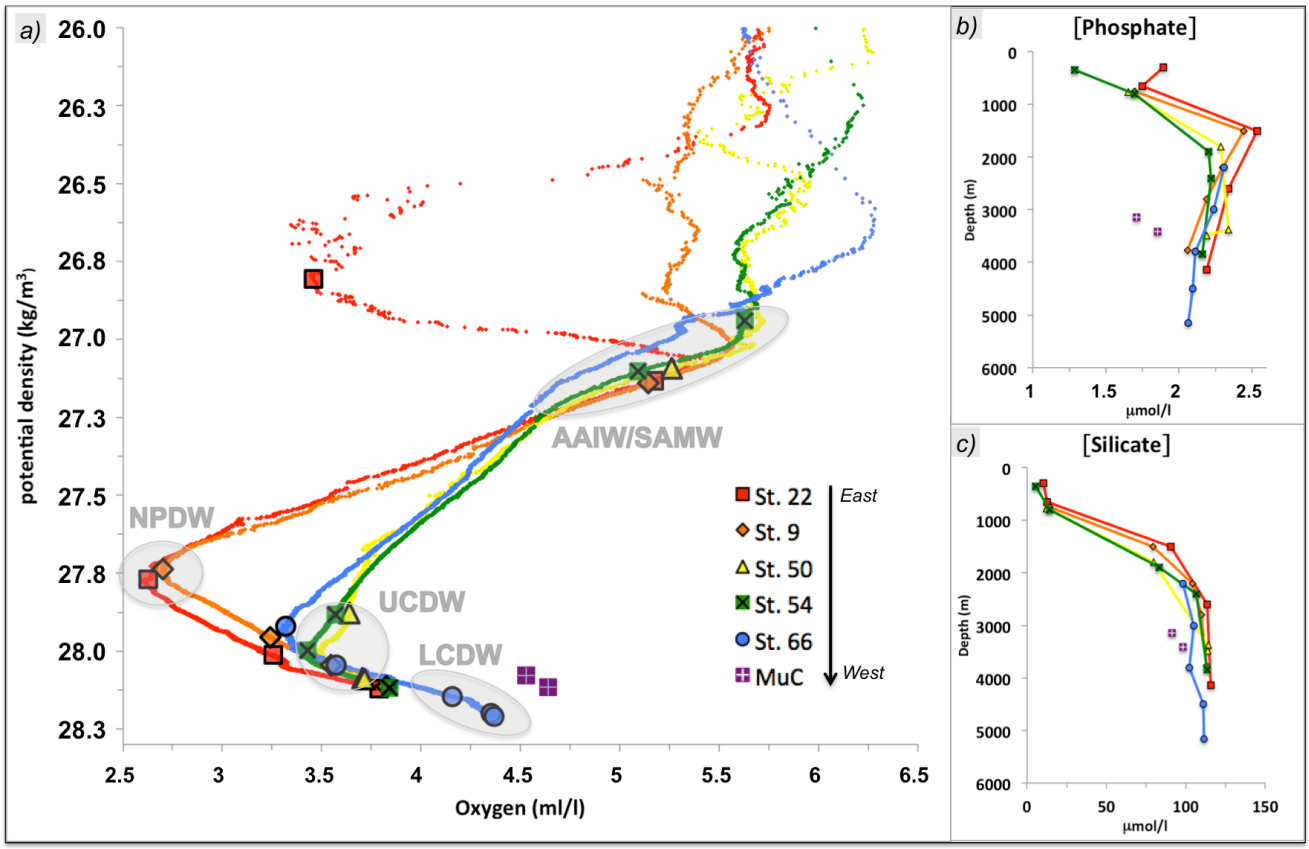


***Figure 3.2.*** *a) Potential density versus oxygen for the five CTD profiles and multicorer water samples (MuC) obtained during cruise SO213. From east to west: St. 22 (red), St. 9 (orange), St. 50 (yellow), St. 54 (green), St. 66 (blue) and MuC (purple). Data for the MuC samples were taken from the World Ocean Atlas 09 (WOA 09). The identified major water masses are indicated by grey circles: SAMW/AAIW (SubAntarctic Mode Water / Antarctic Intermediate Water), NPDW (North Pacific Deep Water), UCDW (Upper Circumpolar Deep Water) and LCDW (Lower Circumpolar Deep Water). Symbols represent the distinct water samples in the colours of their respective stations. b) and c) Phosphate and silicate concentrations versus depth in µmol/l for the five CTD profiles and the multicorer water samples (MuC). R. Tiedemann (AWI) provided the nutrient data, except for the data for the MuC samples, which were taken from WOA 09.*

### 3.3.2. REE distribution

The REE concentrations, with the exception of Ce, (Fig. 3.3, table 3.2) increase with water depth as expected for open ocean waters. The increase is generally linear with depth for the light and middle REEs, whereas for the heavier REEs the shape of the profiles gradually becomes more convex, similar to that of dissolved silicate concentrations (Fig. 3.2c) but significantly less pronounced. In contrast Ce concentrations show little systematic variation with water depth ranging between 5 and 17 pmol/kg. The only exception to the generally steady increase of

dissolved REE concentrations with depth is the bottom sample of station 9 (9-3769), which shows anomalously high concentrations of all LREEs, in particular of Ce.

The REE patterns normalised to Post-Achaean Australian Sedimentary rocks (PAAS) (Taylor and McLennan, 1985) are presented in figure 3.4 and are generally typical for open ocean seawater samples. All patterns exhibit a negative Ce anomaly and a progressive enrichment from LREEs to HREEs that becomes more pronounced with water depth.

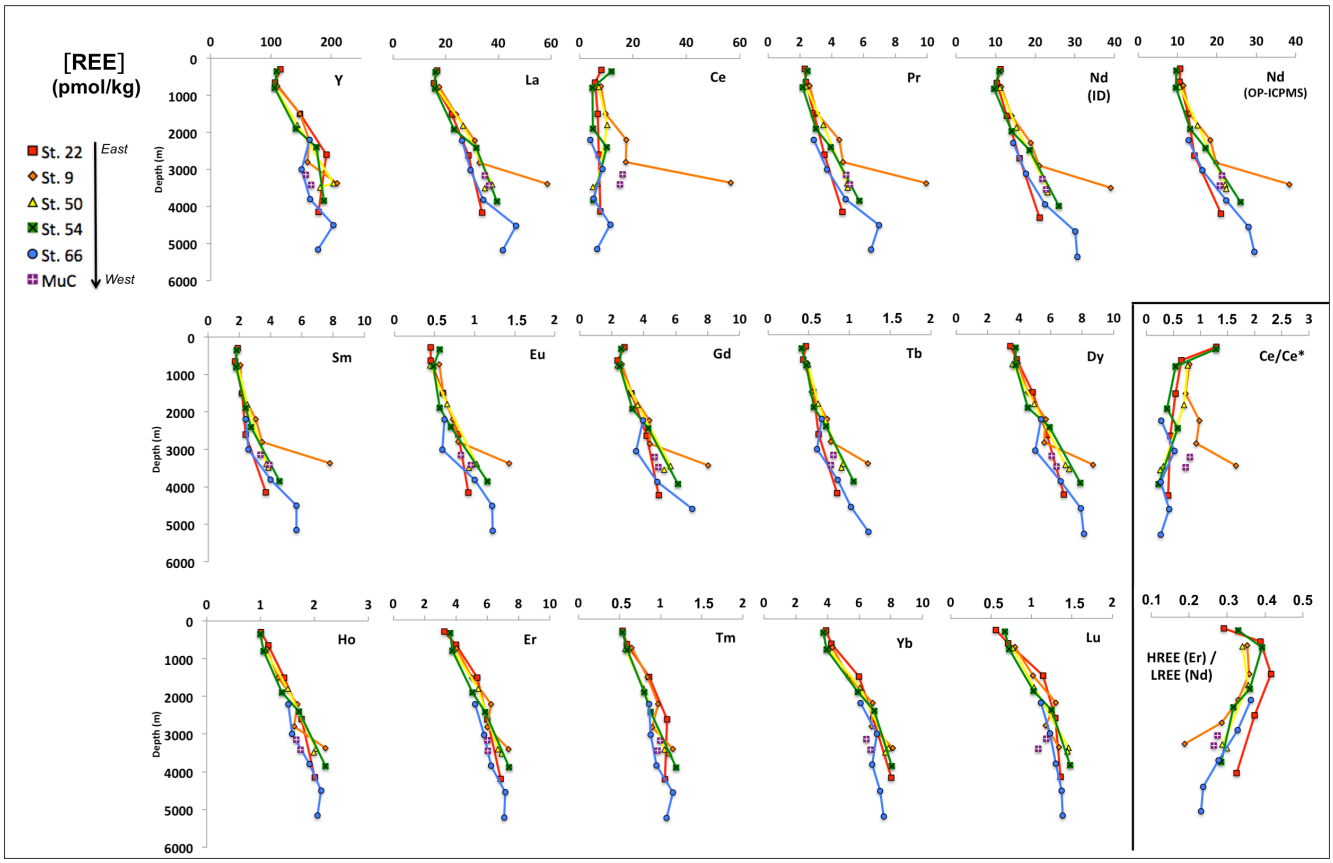


***Figure 3.3.*** *REE concentrations (pmol/l), HREE/LREE (Er/Nd) ratios and Ce anomalies (Ce/Ce*=2[Ce]/([La]+[Pr])) versus water depth (m). Samples from the five CTD profiles and the two multicorer water samples (MuC) are presented, from east to west: St. 22 (red), St. 9 (orange), St. 50 (yellow), St. 54 (green), St. 66 (blue) and MuC (purple). All REE concentrations were obtained by OP-ICP-MS, while Nd concentrations were obtained by both isotope dilution (ID) and OP-ICP-MS. Er/Nd ratios were calculated using the more precise ID method for the Nd concentrations.*

| | Depth (m) | Y (pmol / kg) | La (pmol / kg) | Ce (pmol / kg) | Pr (pmol / kg) | Nd (pmol / kg) | Nd (ID) (pmol / kg) | Sm (pmol / kg) | Eu (pmol / kg) | Gd (pmol / kg) | Tb (pmol / kg) | Dy (pmol / kg) | Ho (pmol / kg) | Er (pmol / kg) | Tm (pmol / kg) | Yb (pmol / kg) | Lu (pmol / kg) | HREE / LREE (Er/ Nd) | Ce anomaly Ce/ Ce* |
|---|---|---|---|---|---|---|---|---|---|---|---|---|---|---|---|---|---|---|---|
| **Stations** | | | | | | | | | | | | | | | | | | | |
| **St. 22** | 300 | 115 | 16.9 | 8.25 | 2.32 | 10.7 | 11.2 | 1.87 | 0.45 | 2.79 | 0.46 | 3.43 | 1.00 | 3.27 | 0.54 | 3.92 | 0.56 | 0.29 | 1.29 |
| *39°12'S* | 650 | 107 | 15.6 | 5.84 | 2.36 | 10.6 | 10.4 | 1.71 | 0.45 | 2.36 | 0.43 | 3.86 | 1.14 | 4.02 | 0.59 | 4.24 | 0.71 | 0.39 | 0.65 |
| *79°55'W* | 1500 | 148 | 22.3 | 6.78 | 2.87 | 12.7 | 12.9 | 2.16 | 0.61 | 3.23 | 0.55 | 4.84 | 1.44 | 5.36 | 0.86 | 5.98 | 1.14 | 0.42 | 0.54 |
| *4144 m* | 2600 | 192 | 28.6 | 7.15 | 3.55 | 14.3 | 16.1 | 2.39 | 0.79 | 4.20 | 0.62 | 5.77 | 1.76 | 6.00 | 1.08 | 6.87 | 1.29 | 0.37 | 0.45 |
| *depth* | 4142 | 178 | 33.8 | 7.74 | 4.68 | 21.0 | 21.0 | 3.70 | 0.92 | 4.94 | 0.85 | 6.85 | 2.00 | 6.85 | 1.06 | 8.02 | 1.36 | 0.33 | 0.40 |
| **St. 9** | 750 | 110 | 17.5 | 7.97 | 2.60 | 11.5 | 11.4 | 2.05 | 0.56 | 2.62 | 0.48 | 3.91 | 1.11 | 4.03 | 0.65 | 4.32 | 0.80 | 0.35 | 0.79 |
| *37°41'S,* | 1500 | 148 | 24.1 | 9.89 | 3.06 | 13.1 | 14.0 | 2.14 | 0.61 | 3.27 | 0.54 | 4.54 | 1.33 | 5.02 | 0.84 | 5.30 | 1.02 | 0.36 | 0.73 |
| *95°28'W* | 2200 | 163 | 31.1 | 17.5 | 4.48 | 18.3 | 18.9 | 3.05 | 0.73 | 4.37 | 0.72 | 5.71 | 1.68 | 6.24 | 0.97 | 6.85 | 1.30 | 0.33 | 0.98 |
| *3771 m* | 2800 | 160 | 33.0 | 17.3 | 4.72 | 19.8 | 21.0 | 3.43 | 0.80 | 4.39 | 0.77 | 5.59 | 1.62 | 6.02 | 0.90 | 6.79 | 1.18 | 0.29 | 0.92 |
| *depth* | 3769 | 209 | 58.6 | 56.6 | 9.92 | 38.3 | 39.1 | 7.80 | 1.43 | 8.04 | 1.22 | 8.70 | 2.21 | 7.37 | 1.15 | 8.11 | 1.34 | 0.19 | 1.65 |
| **St. 50** | 770 | 106 | 16.5 | 7.20 | 2.38 | 10.5 | 11.2 | 1.89 | 0.45 | 2.36 | 0.49 | 3.58 | 1.09 | 3.81 | 0.57 | 4.04 | 0.77 | 0.34 | 0.76 |
| *40°17'S,* | 1800 | 143 | 26.7 | 10.5 | 3.49 | 15.1 | 15.3 | 2.49 | 0.66 | 3.64 | 0.62 | 4.94 | 1.50 | 5.43 | 0.79 | 6.06 | 1.03 | 0.36 | 0.69 |
| *114°26'W* | 3380 | 204 | 37.7 | 6.79 | 4.98 | 22.1 | 23.2 | 3.73 | 1.03 | 5.69 | 0.92 | 6.93 | 2.02 | 6.67 | 1.05 | 7.86 | 1.46 | 0.29 | 0.32 |
| *3483 m* | 3481 | 181 | 35.0 | 5.09 | 5.01 | 22.4 | 23.1 | 3.86 | 0.93 | 5.29 | 0.90 | 7.19 | 1.99 | 6.93 | 1.10 | 7.65 | 1.45 | 0.30 | 0.25 |
| *depth* | | | | | | | | | | | | | | | | | | | |
| **St. 54** | 350 | 110 | 16.2 | 12.0 | 2.49 | 9.67 | 11.0 | 1.80 | 0.56 | 2.61 | 0.41 | 3.78 | 0.99 | 3.62 | 0.54 | 3.76 | 0.67 | 0.33 | 1.29 |
| *43°42'S,* | 800 | 106 | 15.9 | 4.86 | 2.16 | 9.55 | 9.7 | 1.77 | 0.48 | 2.49 | 0.47 | 3.77 | 1.05 | 3.79 | 0.59 | 3.96 | 0.72 | 0.39 | 0.54 |
| *120°30'W* | 1900 | 141 | 23.2 | 5.10 | 2.99 | 13.2 | 14.1 | 2.39 | 0.56 | 3.30 | 0.56 | 4.54 | 1.40 | 5.06 | 0.80 | 5.92 | 1.03 | 0.36 | 0.39 |
| *3844 m* | 2400 | 176 | 31.6 | 10.3 | 3.95 | 17.2 | 18.6 | 2.72 | 0.70 | 4.28 | 0.71 | 5.92 | 1.71 | 5.87 | 0.88 | 6.95 | 1.25 | 0.32 | 0.58 |
| *depth* | 3842 | 188 | 39.5 | 5.22 | 5.72 | 25.9 | 25.9 | 4.58 | 1.16 | 6.13 | 1.05 | 7.89 | 2.21 | 7.40 | 1.19 | 8.06 | 1.48 | 0.29 | 0.23 |
| **St. 66** | 2200 | 164 | 26.2 | 4.05 | 2.88 | 12.8 | 14.4 | 2.38 | 0.62 | 3.97 | 0.66 | 5.40 | 1.51 | 5.23 | 0.86 | 6.09 | 1.12 | 0.36 | 0.28 |
| *45°23'S,* | 3000 | 151 | 29.4 | 8.67 | 3.70 | 16.3 | 17.7 | 2.55 | 0.60 | 3.51 | 0.60 | 5.03 | 1.59 | 5.79 | 0.88 | 7.13 | 1.23 | 0.33 | 0.52 |
| *151°42'W* | 3800 | 164 | 34.3 | 5.24 | 4.86 | 22.3 | 22.5 | 3.98 | 1.00 | 4.86 | 0.86 | 6.64 | 1.91 | 6.24 | 0.95 | 6.83 | 1.30 | 0.28 | 0.27 |
| *5157 m* | 4500 | 204 | 46.7 | 11.5 | 6.98 | 28.0 | 30.0 | 5.66 | 1.22 | 7.04 | 1.01 | 7.92 | 2.12 | 7.14 | 1.15 | 7.31 | 1.37 | 0.24 | 0.43 |
| *depth* | 5155 | 178 | 41.7 | 6.53 | 6.47 | 29.5 | 30.6 | 5.63 | 1.22 | - | 1.23 | 8.10 | 2.06 | 7.08 | 1.07 | 7.54 | 1.39 | 0.23 | 0.27 |
| **Multicorer samples** | | | | | | | | | | | | | | | | | | | |
| **Muc - 78** | 3410 | 166 | 36.5 | 15.1 | 5.15 | 20.7 | 22.8 | 3.92 | 0.95 | 4.91 | 0.77 | 6.36 | 1.75 | 6.04 | 0.96 | 6.70 | 1.09 | 0.26 | 0.73 |
| *46°15'S, 179°37'W* | | | | | | | | | | | | | | | | | | | |
| **MuC -79** | 3143 | 157 | 34.9 | 16.1 | 4.89 | 21.3 | 21.8 | 3.34 | 0.83 | 4.69 | 0.80 | 6.07 | 1.67 | 6.01 | 1.00 | 6.44 | 1.18 | 0.28 | 0.81 |
| *45°51'S, 179°34'E* | | | | | | | | | | | | | | | | | | | |
| **GEOTRACES BATS intercalibration** | | | | | | | | | | | | | | | | | | | |

| | Y (pmol /kg) | La (pmol /kg) | Ce (pmol /kg) | Pr (pmol /kg) | Nd (pmol /kg) | Sm (pmol /kg) | Eu (pmol /kg) | Gd (pmol /kg) | Tb (pmol /kg) | Dy (pmol /kg) | Ho (pmol /kg) | Er (pmol /kg) | Tm (pmol /kg) | Yb (pmol /kg) | Lu (pmol /kg) |
|---|---|---|---|---|---|---|---|---|---|---|---|---|---|---|---|
| ***BATS 2000m*** | | | | | | | | | | | | | | | |
| *average value:* ***(n=5)*** | 127 | 22.3 | 4.59 | 3.71 | 16.5 | 3.28 | 0.78 | 4.15 | 0.70 | 5.14 | 1.42 | 4.77 | 0.69 | 4.51 | 0.75 |
| *2s:* | 16.3 | 1.44 | 2.86 | 0.32 | 0.76 | 0.31 | 0.09 | 0.73 | 0.07 | 0.46 | 0.11 | 0.27 | 0.05 | 0.36 | 0.05 |
| ***BATS 15m*** | | | | | | | | | | | | | | | |
| *average value:* ***(n=5)*** | 124 | 14.1 | 10.8 | 2.97 | 13.6 | 2.91 | 0.79 | 4.38 | 0.77 | 5.42 | 1.40 | 4.53 | 0.67 | 4.19 | 0.65 |
| *2s:* | 16.8 | 1.64 | 2.89 | 0.18 | 0.84 | 0.30 | 0.06 | 0.54 | 0.06 | 0.64 | 0.14 | 0.44 | 0.04 | 0.30 | 0.09 |

***Table 3.2.*** *REE concentrations (pmol/l), Er/Nd ratios, Ce anomalies (Ce/Ce*=2[Ce]/([La]+[Pr])) and GEOTRACES inter-calibration measurements (BATS) for this study. [REE] correspond to OP-ICPMS measurements, whereby isotope dilution (ID) results for [Nd] are also shown. Er/Nd ratios were calculated using the more precise ID*

### 3.3.3. Nd concentrations

The Nd concentrations (Fig. 3.3, tables 3.1 and 3.2) obtained by OP-ICP-MS (table 3.2) are on average 5%, lower than those obtained using the more precise Isotope Dilution (ID) technique (table 3.1) but identical within the 95% confidence limits of the technique (Table 3.2). The maximum difference between the techniques was 12% for sample 54-350, similar to previous considerations of its uncertainties (Hathorne et al., 2012).

Nd concentrations are nearly constant around 10 pmol/kg in the shallowest two samples (22-300 and 54-350) and at ~800 m depth. Below that Nd concentrations increase with depth at all stations. Excluding the anomalous maximum of sample 9-3769 (39 pmol/kg), the Nd concentrations of the bottom samples vary between 21 pmol/kg (st. 22) and 30.6 pmol/kg for the deepest sample (66-5155). The increase in profile 66 is steady until 4500 m depth (30 pmol/kg) but below only shows a small increase until 5155 m depth. The multicorer samples have dissolved Nd concentrations similar to other samples from similar depths. Between approximately 2000 m and 3000 m depth, the increase in the concentrations is less pronounced for profiles 22 and 66. These two stations are influenced by north and equatorial Pacific-derived waters at this depth range, where Nd concentrations > 30 pmol/kg are expected (Piepgras and Jacobsen, 1988; Amakawa et al., 2004a; Amakawa et al., 2009). The fact that the observed concentrations are by 10 to 15 pmol/kg lower may indicate pronounced scavenging processes in the equatorial Pacific as discussed below (section 3.4.3.).

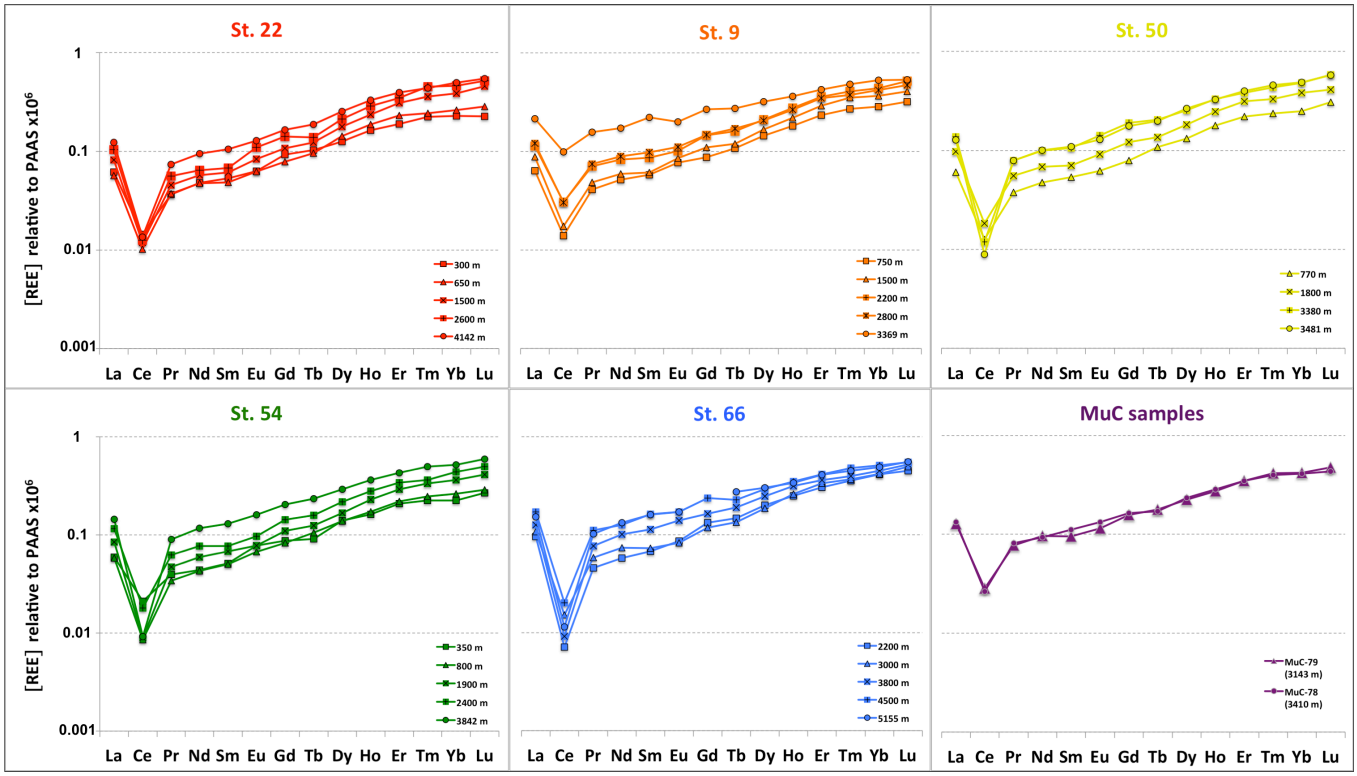


***Figure 3.4.*** *Rare Earth Element (REE) patterns normalized to Post-Achaean Australian Sedimentary rocks (PAAS) (Taylor and McLennan, 1985) for the five CTD profiles and the two Multicorer seawater samples (MuC). From east to west: St. 22 (red), St. 9 (orange), St. 50 (yellow), St. 54 (green), St. 66 (blue) and MuC (purple). Note that Gd is missing in sample 66-5155.*

### 3.3.4. Nd isotope compositions

The Nd isotope compositions of the samples range from -10.3 ±0.3 to -5.4 ±0.4 $\varepsilon_{Nd}$ units (Fig. 3.5, table 3.1). Intermediate waters, the domain of AAIW and its precursor SAMW (300 m to 1500 m depth) show a range of $\varepsilon_{Nd}$ signatures between -7.5 ±0.3 and -9.0 ±0.3. Below the influence of AAIW the most radiogenic Nd isotope compositions where found in the easternmost part of the study area, where the influence of waters derived from the north is greater. This is particularly the case for station 22 (80°W), which is located close to the South American continent and includes the main core of NPDW yielding the most radiogenic signatures of this study at 1500 m ($\varepsilon_{Nd}$ = -5.4 ±0.4) and 2600 m ($\varepsilon_{Nd}$ = -5.8 ±0.3) water depth. NPDW was also sampled further west (95°W) at station 9 (1500 m water depth) and therefore was more diluted with a slightly less radiogenic Nd signature of -6.4 ±0.3. Below that depth, profile 9 shows a trend towards unradiogenic values with depth (-6.8 ±0.3 to -9.1 ±0.3), progressively reaching the domain of waters of circumpolar origin that occupy the deep Southeast Pacific Basin (Fig. 3.1b to f). Similarly, the westernmost profile at station 66 (150°W) also shifts towards less radiogenic values with depth (-6.0 ±0.2 at 2200 m to -8.3 ±0.3 at 5155 m). In this case the hydrographic data

suggest the most positive $\varepsilon_{Nd}$ values coincide with the presence of SPGDW and the most negative $\varepsilon_{Nd}$ signatures with the core of LCDW. The $\varepsilon_{Nd}$ signal is constant at -8.3 ±0.3 from 3800 m to the bottom, reflecting the latter water mass.

Profiles 50 and 54, located above the East Pacific Rise (120°W to 110°W), include UCDW samples at 1800 m (-8.3 ±0.2) and 1900 m (-7.6 ±0.2) respectively. These profiles exhibit isotopic variations tending to more radiogenic values with depth, from -8.8 ±0.4 to -7.0 ±0.3 for station 50 and from -7.9 ±0.3 to -6.5 ±0.2, for station 54.

The bottom water signatures measured for the two deep samples obtained from the multicorer waters off New Zealand are amongst the most negative ones of this study, yielding $\varepsilon_{Nd}$ signatures of -9.0 ±0.3 for sample MuC-78 (3410 m depth) and -10.3 ±0.3 for sample MuC-79 (3143 m depth).

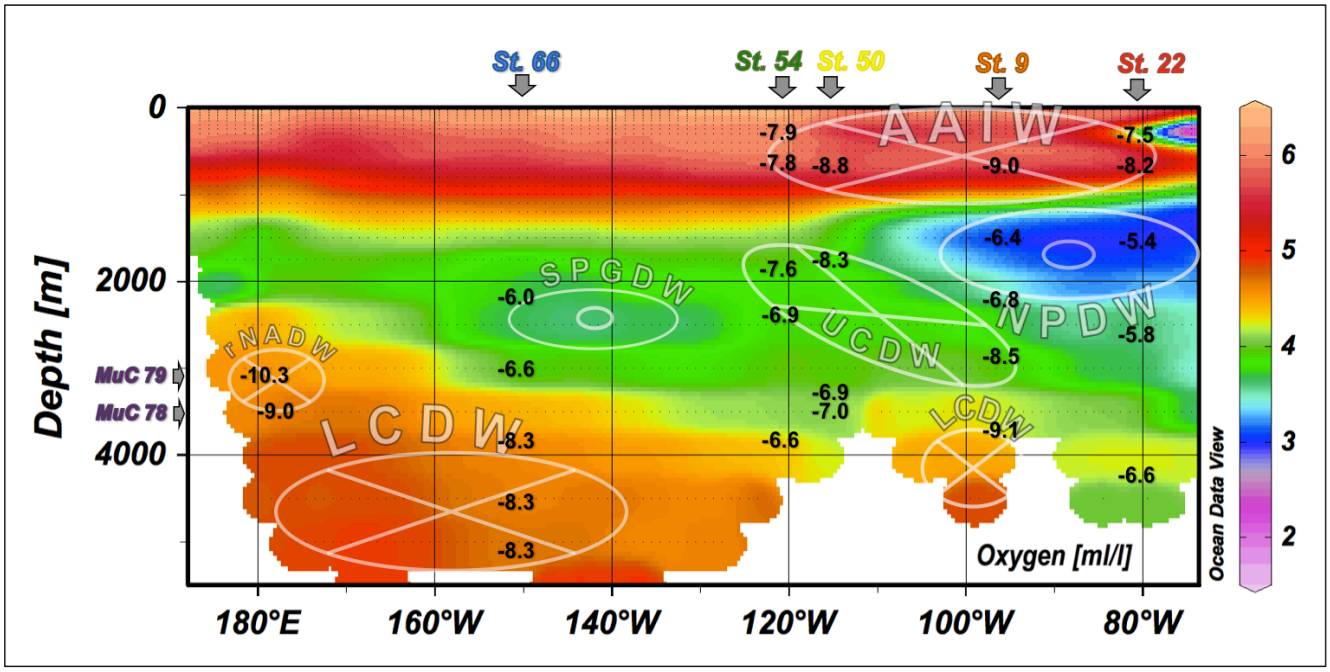


***Figure 3.5*** *Section (see figure 3.1a) of oxygen concentrations (ml/l) and measured $\varepsilon_{Nd}$ signatures (black numbers) at their corresponding depths. The flow direction of the main water masses present in the study area are also shown by transparent circles, where crosses represent the sense of movement into the picture and centred circles represent movement out of the picture. Water mass abbreviations: LCDW (Lower Circumpolar Deep Water), rNADW (residual North Atlantic Deep Water), AAIW (Antarctic Intermediate Water), UCDW (Upper Circumpolar Deep Water), SPGDW (South Pacific Gyre derived Deep Water) and NPDW (North Pacific Deep Water). Oxygen concentrations were obtained from the World Ocean Atlas 09.*

## 3.4. Discussion

### 3.4.1. Advection and water mass mixing in relation to Nd isotopes and Nd concentrations.

Comparing the Nd concentrations observed in the Southern Pacific water column presented in this study with available data from other ocean basins our vertical [Nd] gradients are less pronounced than in the north Pacific and rather resemble Southern and Indian Ocean profiles (Lacan et al., 2012 and references therein) reflecting the larger influence of Circumpolar Current derived waters in our study area. This implies efficient vertical mixing in the water column of the Antarctic Circumpolar Current and confirms a major role of advection in controlling the distribution of REEs. The physical processes that govern the distribution of the different water masses are clearly reflected by their Nd isotope characteristics as discussed below.

#### 3.4.1.1 AAIW

Stations 22, 9, 50, and 54 are located just north of the formation region of AAIW, which is represented by 6 samples from between 300 m and 800 m water depth. The average $\varepsilon_{Nd}$ signature of AAIW samples in this study is -8.2 ±0.3, which matches the signatures previously obtained for this water mass in the Atlantic sector of the Southern Ocean (Stichel et al., 2012; Jeandel et al., 1993). Figure 3.6 shows endmember mixing calculations between different water masses based on their $\varepsilon_{Nd}$ and [Nd] signatures and it is evident that all intermediate depth samples correspond to almost pure AAIW and that admixture of NPDW at this depth is below 10%.

Station 22 shows the most radiogenic value of all AAIW samples at 300 m depth ($\varepsilon_{Nd}$ = -7.5 ±0.3) and corresponds to an oxygen minimum (see Fig. 3.5) interpreted to be consequence of its location (80°W) within the extension of the poleward flow of the Peru-Chile Undercurrent, which transports oxygen depleted Equatorial SubSurface Water (ESSW) (Tsuchiya and Talley, 1999). A much more radiogenic dissolved Nd isotope signature of ESSW (-4.5 ±0.5) was determined by Jeandel et al. (2013) at their station UPX (see Fig. 3.1a) near our station 22. Their location is, however, very close to the Chilean coast (~60 km) and was most likely strongly affected by boundary exchange with the nearby continent.

Figure 3.7, summarizes all available data of dissolved Nd isotope compositions on a N-S transect along the pathway of modified NPDW in the eastern Pacific (see section 3.4.1.2.). AAIW gradually loses its signature by mixing as it flows to the north, changing from -8.4 ±0.4 in the

Southern Ocean (Stichel et al., 2012) to -6.5 ±0.5 at 32°S (St. EGY, from Jeandel et al., 2013). Above and below AAIW more radiogenic and oxygen poor equatorial waters prevail: Eastern South Pacific Intermediate Water (ESPIW): -4.0 ±0.5 (St. EGY, Jeandel et al., 2013) and modified NPDW: -5.4 ±0.4 (sample 22-1500, this study).

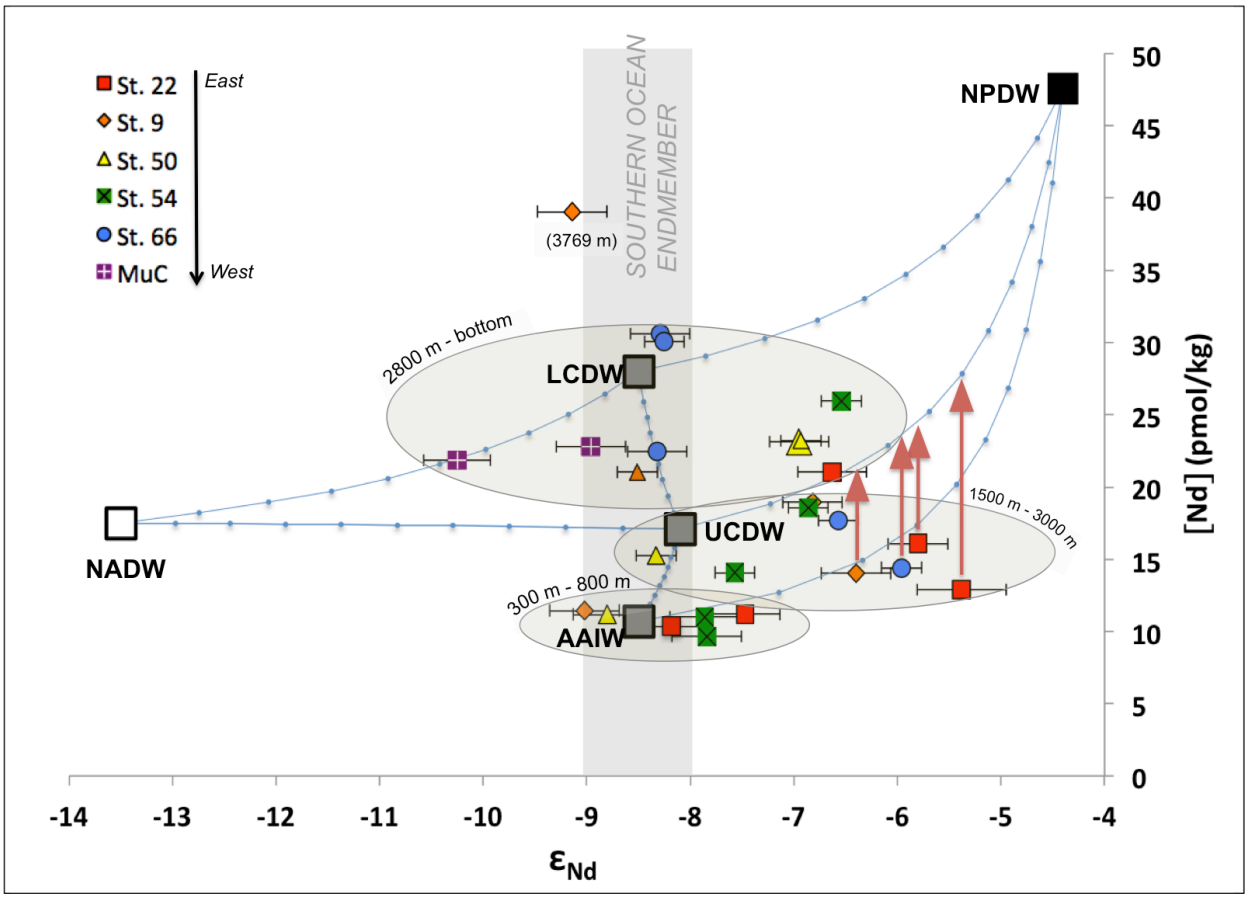


***Figure 3.6.*** *Endmember mixing lines (blue) of Nd concentrations and isotope compositions between different water masses divided into 10% steps (blue dots). Large squares represent the endmembers, with those originating in the Southern Ocean marked by a grey bar. Symbols represent the results of this study, coded by stations. The results are grouped by ranges of water depth (grey circles). Red arrows illustrate the offset caused by scavenging on the samples located within NPDW and SPGDW (see section 3.4.3). The values of the endmembers correspond to [Nd] in pmol/kg and* $\varepsilon_{Nd}$ *at their origins: NADW ([Nd]=17.5,* $\varepsilon_{Nd}$*=-13.5, Piepgras & Wasserburg (1987)), LCDW ([Nd]=28,* $\varepsilon_{Nd}$*=-8.5, Carter et al. (2012)), UCDW ([Nd]=17.1,* $\varepsilon_{Nd}$*=-8.1, averaged from Carter et al. (2012) and Stichel et al. (2012)), AAIW ([Nd]=10.7,* $\varepsilon_{Nd}$*=-8.5, averaged from Stichel et al. (2012) and this study) and NPDW ([Nd]=47.6,* $\varepsilon_{Nd}$*=-4.4, averaged from the locations closest to the formation region of modified NPDW according to Kawabe & Fujio (2010) based on the results of Amakawa et al. (2009) and Piepgras & Wasserburg (1988)). Nd concentrations presented in this figure were obtained by the Isotope Dilution (ID) technique.*

### 3.4.1.2 LCDW and NPDW

The only significant advection of deep waters filling the entire deep Pacific takes place in the Southwest Pacific Basin in the form of LCDW. This northward transport is mainly

compensated by the mid-depth return flow of NPDW in the eastern South Pacific. These water masses are responsible for the main deep water volume transport in the region at some 13 Sverdrup (Sv) each (Kawabe and Fujio, 2010). They also present the largest differences in $\varepsilon_{Nd}$ signatures between individual water masses (excluding the multicorer samples), as well as in hydrographic properties within the study area. The Nd isotope signatures of all samples below ~ 1400 m are compared with temperature and salinity (potential density) and oxygen concentrations in order to evaluate their conservative behaviour in figure 3.8.

LCDW is characterised by high salinities and low temperatures ($\sigma_\theta$ range: 28.15-28.21 kg/m$^3$), as well as high oxygen content (4.2-4.4 ml/l) and occupies the deepest regions of the study area. Here we do not consider the multicorer samples (180°W) to be LCDW given that these are clearly influenced by advection of North Atlantic derived waters (section 3.4.1.3). Thus homogenized LCDW was sampled below 3500 m depth of profile 66 (150°W) with a constant $\varepsilon_{Nd}$ signature of -8.3 (±0.3). This value is the same as found previously for pure LCDW in the Drake Passage (Piepgras and Wasserburg, 1982; Stichel et al., 2012) and is identical within uncertainties to the average $\varepsilon_{Nd}$ value observed for the same water mass at the zero meridian in the Atlantic Sector of the Southern Ocean -8.7 (±0.4)(Stichel et al., 2012) and in the Bellingshausen and Amundsen seas -8.7 (±0.2)(Carter et al., 2012).

Apart from the main flow entering the Southwest Pacific basin, LCDW also occupies the bottom of the southeast Pacific basin (Fig. 3.1b to 3.1f) below 3000 m depth (Warren 1973). Although profile 9 (95°W) does not reach the deepest parts of this basin (see Fig. 3.8) and thus mainly represents shallower UCDW (section 3.4.1.3), an influence of LCDW on the deepest sample of this station (9-3769) can not be excluded. This sample has a Nd isotope composition of -9.1 ±0.3, which points to the presence of circumpolar deep waters, although being slightly less radiogenic than typical signatures of LCDW in other basins. This sample has anomalously high LREE concentrations likely reflecting a significant sedimentary input (see section 3.4.4.1). However, Nd isotope signatures of detrital components of South Pacific sediments in this region are more radiogenic at values > -5 (e.g. Jeandel et al., 2007, GEOROC database and references therein) suggesting the LREE enrichment does not originate from local detrital material.

NPDW is the second major water mass endmember below the influence of AAIW in the South Pacific. Based on the hydrographic data ($\sigma_\theta$: 27.60-28.00 kg/m$^3$, [$O_2$]: 2.6-3.3 ml/l), profiles 22 and 9, show the major influence of North Pacific derived waters within the study area between 1500 and 2600 m depth. This is also documented by their $\varepsilon_{Nd}$ values, clearly marking

the influence of radiogenic source waters from the North Pacific: -5.4 ±0.4 and -5.8 ±0.3 for station 22 at 1500 m and 2600 m depth, respectively and -6.4 ±0.3 for sample 9-1500.

Kawabe and Fujio (2010) described in detail the distribution of NPDW within the entire Pacific ocean and identified two characteristic types; one that occupies wide areas of the deep water column of the North Pacific and one that flows in a southeasterly direction from the central North Pacific to the Antarctic, which they named modified NPDW given that it experienced admixture of significant amounts of LCDW and UCDW. This modified version of NPDW flows to the east and then south adjacent to the American continents, passing our section at stations 22 and 9.

Amakawa et al. (2009) reported an average $\varepsilon_{Nd}$ value of -3.9 ±0.7 for pure NPDW using data from different studies of dissolved Nd isotope compositions in the North Pacific (Piepgras and Jacobsen; 1988; Amakawa et al., 2004a; Amakawa et al., 2009). The $\varepsilon_{Nd}$ signatures track the flow path of modified NPDW from the central Pacific to the Drake Passage (Fig. 3.7). Despite the coarse resolution of the data, in particular between 20°S and 20°N, a clear gradual trend to less radiogenic $\varepsilon_{Nd}$ values from North to South can be observed in figure 3.7 with the exception of middepth waters at station 093 (Grasse et al., 2012) in the Eastern Equatorial Pacific (EEP). For this station, dissolution of particles of volcanic origin from South America was invoked as a cause for the signatures even more radiogenic than in the central North Pacific. On the other hand, between 30°S and 60°S (Fig. 3.7), CDW and AAIW become gradually more radiogenic (CDW evolving from -8.4 ±0.4 in the Southern Ocean (Stichel et al., 2012) to -6.6±0.3 at 14°S (St. 093; Grasse et al., 2012)) as they flow to the north sandwiching the remnants of modified NPDW (-5.4 ±0.4). Horikawa et al. (2011) observed a similar Nd isotope evolution of NPDW along their eastern Pacific (EP) transect obtained from fish teeth in surface sediments.

Jeandel et al. (2013) tentatively attributed the more radiogenic Nd isotope signatures of their unfiltered samples (-6.8 ±0.8, -3.7±0.7 and -5.2 ±0.4) at middepths (2000 to 3200 m) to a potential hydrothermal contribution from the East Pacific Rise. Given the location of their stations GYR and EGY in the central and eastern South Pacific (see figures 3.1 and 3.7) and the evolution of modified NPDW along the flow path described above, admixture of NPDW provides an alternative explanation for their radiogenic values between 2000 to 3200 m depth. Further detailed investigations, such as in the frame of the planned GEOTRACES sections in the Pacific Ocean, are required to better characterize the evolution of NPDW in terms of Nd isotopes and to elucidate potential hydrothermal effects.

Kawabe and Fujio (2010) suggested that modified NPDW forms at 15-25 °N, 155°W, where the average $\varepsilon_{Nd}$ signature below 2000 m from Amakawa et al. (2009) and Piepgras and Jacobsen (1988) is -4.4 corresponding to a Nd concentration of 47.6 pmol/kg. Assuming these values as endmembers for modified NPDW, and taking into account the effect of LREE scavenging that occurs in the eastern equatorial Pacific (see section 3.4.3), simple mixing calculations (Fig. 3.6) suggest that the fraction of NPDW still amounts to 30% to 50% at stations 22 and 9 located within the trajectory of this water mass. The remaining 50% to 70% consist of intermediate and middepth waters from the Southern Ocean (AAIW and UCDW).

The impact of the two major water masses (LCDW and NPDW) on the Nd isotope compositions and Nd concentrations in the South Pacific have been modelled (Rempfer et al., 2011). Simulated Nd isotope distributions covering our study area obtained from this model (Fig. 3.9a) predict the cores of both water masses roughly at the positions observed in this study, with simulated LCDW ($\varepsilon_{Nd}$ ~ -7) dominating below 3000 m predominantly at the western end, and simulated NPDW ($\varepsilon_{Nd}$ ~ -4) adjacent to South America occupying mid-depth waters. The absolute values obtained from the model are one to two $\varepsilon_{Nd}$ units more radiogenic compared to observations, probably resulting from an overestimation of weathering or boundary exchange contributions from South America in the model.

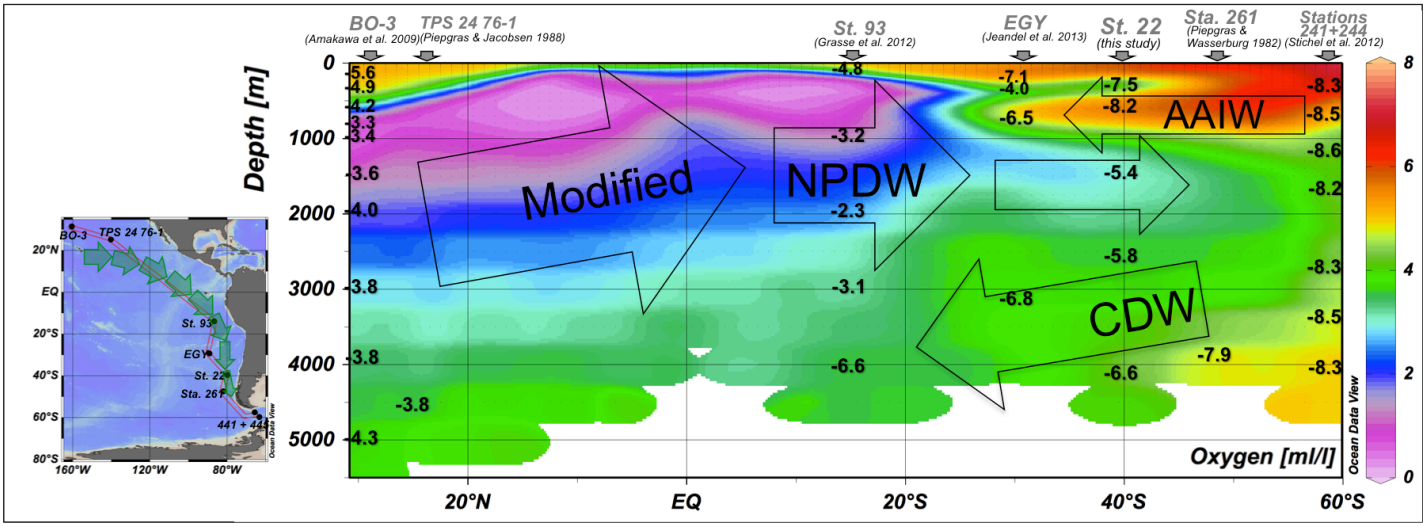


***Figure 3.7.*** *North-South section along the flow path of modified NPDW after Kawabe and Fujio (2010) (green arrows on section), showing oxygen concentrations (ml/l), represented by the colour gradient, and $\varepsilon_{Nd}$ signatures (black numbers) at their corresponding depths from this and other studies of seawater Nd isotope compositions of the Pacific Ocean. The flow direction of the main water masses are also shown by transparent arrows. Water mass abbreviations: CDW (Circumpolar Deep Water), AAIW (Antarctic Intermediate Water) and NPDW (North Pacific Deep Water). Oxygen concentrations were taken from the database of the World Ocean Atlas 09.*

#### 3.4.1.3 UCDW, SPGDW, and NADW

Apart from the volumetrically most important water masses LCDW and NPDW, the presence and/or influence of three other water masses can be traced using Nd isotopes, namely: UCDW, SPGDW and NADW. These water masses are not captured in the modelled section of figure 3.9 due to the low resolution of the model.

Pure mid-depth circumpolar waters (UCDW) are difficult to identify in the South Pacific due to the predominance of Pacific-derived waters in the same depth range (see section 3.1.1). Thus, UCDW can only be clearly identified based on its Nd isotope composition at 1) Station 9 located in the southeast Pacific basin where the deepest part is occupied by ACC-derived waters (Warren, 1973)(Fig. 3.5) and 2) above the East Pacific Rise sampled at stations 50 and 54 (Fig. 3.5), where the main inflow of UCDW into the Pacific takes place (Kawabe and Fujio, 2010). Sample 9-2800 shows a $\varepsilon_{Nd}$ value of -8.5 ±0.2. The presence of UCDW at these location and depth has been reported by Tsuchiya and Talley (1999) and can also be inferred from the low phosphate contents in figures 3.1e and 3.2b. Sample 9-3769 ($\varepsilon_{Nd}$ = -9.1 ±0.3) is also under the influence of UCDW (Fig. 3.1b to f), and has a slightly less radiogenic signature than average CDW. Samples 50-1800 and 54-1900 reflect pure circumantarctic isotopic compositions of -8.3 ±0.2 and -7.6 ±0.2 respectively. The signatures of these samples located above the East Pacific Rise reflect the dominance of southern sourced mid-depth waters in this region over north and central Pacific sources. These observations are also in agreement with the $\varepsilon_{Nd}$ measurements by Carter et al. (2012) (at their station 022 located 20° south of our study area (Fig. 3.1a) pure CDW averages -8.4 ±0.3 $\varepsilon_{Nd}$ units between 1500 and 3500 m).

Another example for the close correspondence of hydrological properties and Nd isotope signatures is the evolution of mid-depth waters of the central Pacific below the South Pacific Subtropical Gyre. In the Southwest Pacific basin between 1500 m to 3000 m water depth, SPGDW is produced because the dynamics of the South Pacific Subtropical Gyre also affects the deeper water column. UCDW that enters the Pacific across the East Pacific Rise mixes with central Pacific middepth waters, and is then transported from the equator to the south causing mixed hydrographic properties between Antarctic-derived waters and NPDW (Reid, 1986). Sampled at St. 66 (150°W) at 2200 m, this water mass yields an $\varepsilon_{Nd}$ value of -6.0 ±0.2 and an oxygen concentration of 3.3 ml/l, more radiogenic and less oxygenated than samples obtained at the same depth further east where UCDW flows into the Pacific: St. 50 (Depth: 1800 m, $\varepsilon_{Nd}$ = -8.3 ±0.2, [$O_2$]=3.6 ml/l) and St. 54 (Depth: 1900 m, $\varepsilon_{Nd}$ = -7.6 ±0.2, [$O_2$]=3.6 ml/l).

The Nd isotopes also allow the detection of the influence that NADW exerts on circumpolar deep waters (section 3.1.1). Residual NADW is still discernible in the western South Pacific at a depth near 3000 m between 180°E and 160°W by its salinity maximum, as well as low silicate and phosphate contents (Figures 3.1c,e,f and 3.2b,c). Reid and Lynn (1971) tracked the pathway of this water mass by its oceanographic properties, passing our sampling location, into the North Pacific. Boundary exchange does not seem to significantly influence the Nd isotope compositions of our bottom water samples from New Zealand's Bounty Trough (MuC-78 and MuC-79) given that the $\varepsilon_{Nd}$ values of New Zealand rocks range between -5 and +1 (Jeandel et al., 2007). Therefore, the unradiogenic values of -9.0 ±0.3 (MuC-78) and -10.3 ±0.3 (MuC-79) reflect the advection of residual NADW. The difference of 1.3 $\varepsilon_{Nd}$ units between these two samples may result from a larger fraction of this water mass present at the location of sample MuC-79, as inferred from its more negative $\varepsilon_{Nd}$ value, as well as its lower nutrient concentrations and higher salinity (see table 3.1 and figures 3.1e,f and 3.2b,c).

Figure 3.6 indicates that sample MuC-79 ($\varepsilon_{Nd}$ =-10.25, [Nd]=21.8 pmol/kg), falls on the mixing line of LCDW and NADW, indicating mixing proportions of around 50% for the two water masses at 3100 m, 179°E, 45°S. Mixing proportions of LCDW and NADW using temperature and salinity at this station give a maximum of 25% of NADW indicating a stronger dilution of NADW along its flow path to the South Pacific than deduced from Nd isotope mixing calculations. The quantitative discrepancies most likely result from boundary exchange or reversible scavenging processes along the long flow path of NADW from its sources to this location.

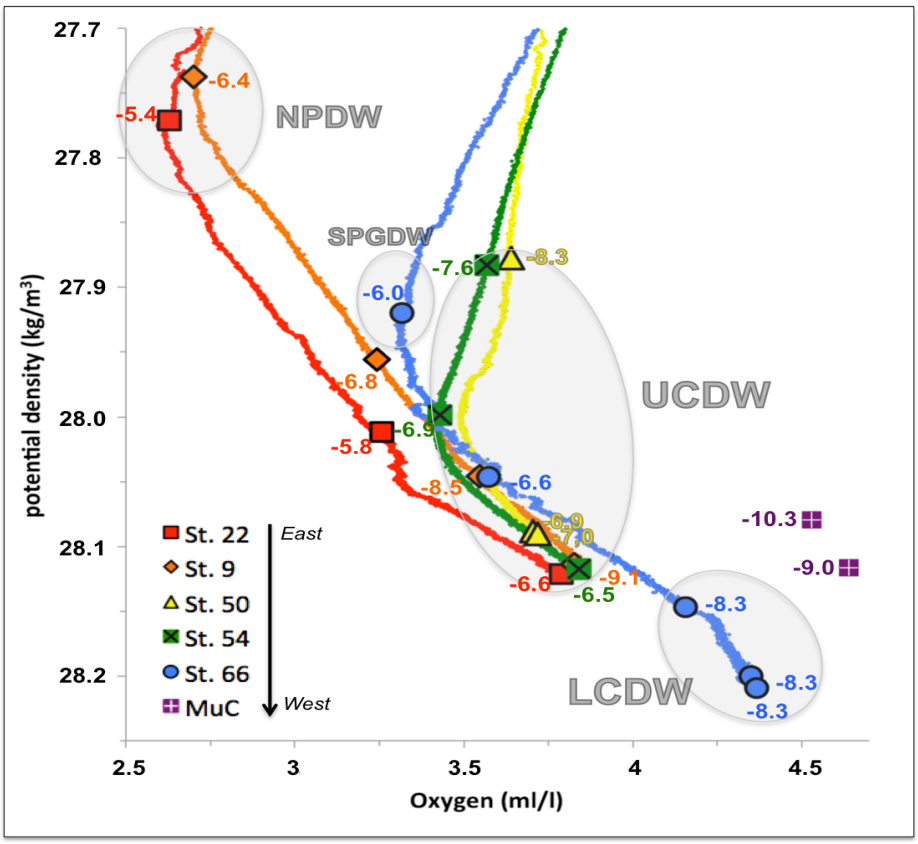


***Figure 3.8.*** *Nd isotope compositions of all samples (symbols) below the influence of AAIW (~1400 m) together with potential density and oxygen concentrations from the five CTD profiles and the two multicorer water samples (MuC) of this study. Hydrographic data from the MuC samples was obtained from World Ocean Atlas 09. From east to west: St. 22 (red), St. 9 (orange), St. 50 (yellow), St. 54 (green), St. 66 (blue) and MuC (purple). The identified water masses are indicated by grey circles: NPDW (North Pacific Deep Water), SPGDW (South Pacific Gyre derived Deep Water), UCDW (Upper Circumpolar Deep Water) and LCDW (Lower Circumpolar Deep Water).*

### 3.4.1.4. Admixture of northern and southern derived middepth water masses

Apart from the distinct water masses described above, many of the samples of this study reflect mixing of waters of different hydrographic properties. Following potential density and oxygen concentrations (Fig. 3.8), all five profiles converge on the mixing line of NPDW and LCDW. UCDW samples of profile 3.9 also fall within this mix. making UCDW difficult to distinguish. Excluding the pure UCDW samples (section 3.4.1.3), mixing between northern- and southern-derived waters is reflected by Nd isotope compositions ranging from -5.8 ±0.3 to -7.0 ±0.3 (Fig. 3.8). The endmember mixing calculations in figure 3.6 clearly indicate strong mixing between northern and southern sourced middepths waters for seven out of nine samples in the depth range of 1500 m to 3000 m, although being depleted in Nd concentrations (see section 3.4.3), yielding estimated NPDW contributions between 10 % and 50 %. The major influence of Pacific derived waters at middepths and of northward flowing Southern Ocean waters above and

below deduced from hydrographic properties (section 3.1.1), is also reflected in the Nd isotope compositions (figure 3.6), further supporting the use of Nd isotopes as a reliable water mass tracer in the open South Pacific.

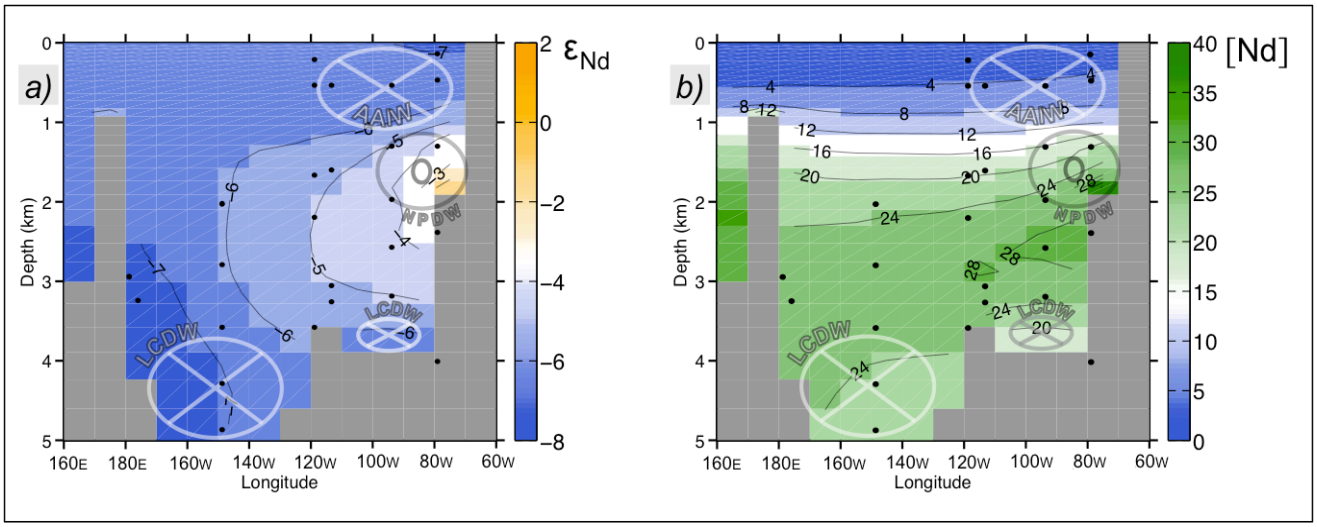


***Figure 3.9.*** *Modelled Nd isotopic compositions (left panel) and Nd concentrations (right panel) from a transect located between 38° S and 42° S and the same longitude range as our study area (Rempfer et al., 2011). Figure provided by J. Rempfer. Black dots show the locations of the samples obtained in this study (see Fig. 3.5 for comparison). The flow direction of the water masses captured by the model are shown by transparent circles, where crosses represent the sense of movement into the picture and centred dots represent movement out of the picture. Water mass abbreviations: LCDW (Lower Circumpolar Deep Water), AAIW (Antarctic Intermediate Water) and NPDW (North Pacific Deep Water).*

### 3.4.2. Advective processes deduced from REEs

Further evidence for the quasi conservative behaviour of REEs in the South Pacific can be inferred from the REE distributions. Normalization of the trivalent REEs to a reference water is a useful way to identify the distinct REE compositions of a particular water mass and provides important information on its origin as well as the oceanic processes that define it (e. g. Alibo and Nozaki, 2004). Regardless of the chosen reference water, the advantage over PAAS-normalized patters is that common features present in all seawater samples, such as the progressive enrichment from light to heavy REEs, are removed (Nozaki et al., 1999). The REE concentrations of NPDW sampled in the western North Pacific (34°N, 139°E)(Alibo and Nozaki, 1999) at around 2500 m depth have previously been used for normalization as these waters represent the oldest part of the global thermohaline circulation (Nozaki et al. 1999, Alibo and Nozaki 2000, 2004; Nozaki 2001; Nozaki and Alibo 2003b).

Figure 3.10 shows the NPDW normalized values for some water masses of this and other studies from the Southern Ocean and the western Pacific. All profiles of this study (Fig. 3.10a)

are depleted compared to NPDW except samples collected from the main body of LCDW (indicated in orange in figure 3.10a). LCDW show a prominent LREE enrichment compared to the NPDW reference. Although in the case of sample 9-3369 a part of this effect may result from a bottom sedimentary source (see section 3.4.4.1), a similar origin for this LREE enrichment is unlikely for the rest of the LCDW samples given that it is visible in the water column more than 1000 m above the bottom, therefore indicating this is a typical feature in the NPDW normalized pattern of LCDW. This LREE enrichment is also observed in deep samples from the Atlantic sector of the Southern Ocean at 39°S, 01°E (dashed brown lines in figure 3.10b; data from German et al., 1995). Nozaki and Alibo (2003b) suggested that AABW in low latitudes (40°S) close to its formation region, has undergone much less preferential scavenging of LREEs compared to older deep waters, therefore preserving its characteristic LREE enrichment with respect to NPDW.

In contrast, circumpolar deep waters from the Southeastern Indian Ocean exhibit MREE enrichments and strong depletions in LREE and Gd (dashed green lines in figure 3.10b), which, are thought to originate from admixture of southward flowing Indian Ocean deep waters affected by contributions from exchange with volcanic rocks of the Indonesian Archipelago, (Alibo and Nozaki, 2004). However, these Indian Ocean waters sampled at 40°S do not flow into the ACC and into the South Pacific Ocean where we have sampled for this study.

Samples influenced by North Pacific mid-depth waters of this study (indicated in blue in figure 3.10a) have a characteristic pattern with a relative LREE and MREE depletion: Pr to Eu depletion for SPGDW and Nd to Tb depletion for NPDW. This shape is consistent with samples from similar depths (dashed blue lines in figure 3.10b) in the Western South Pacific (27°S, 175°E) (Zhang and Nozaki, 1996; Alibo and Nozaki, 2004), indicating a pronounced homogeneity of waters of Pacific origin. These characteristic patterns reflect the preferential scavenging of LREEs and MREEs that these older water masses have undergone during advection from their source regions in the North and central Pacific (section 3.4.3).

The South Pacific AAIW patterns observed here (red patterns in figure 3.10a) fall within the NPDW normalised patterns observed elsewhere but are more similar to those of the S. Atlantic than to the Indian Ocean waters. A distinct REE pattern of AAIW may prove useful for separating the northern and southern sourced Pacific intermediate waters that have similar hydrographic properties.

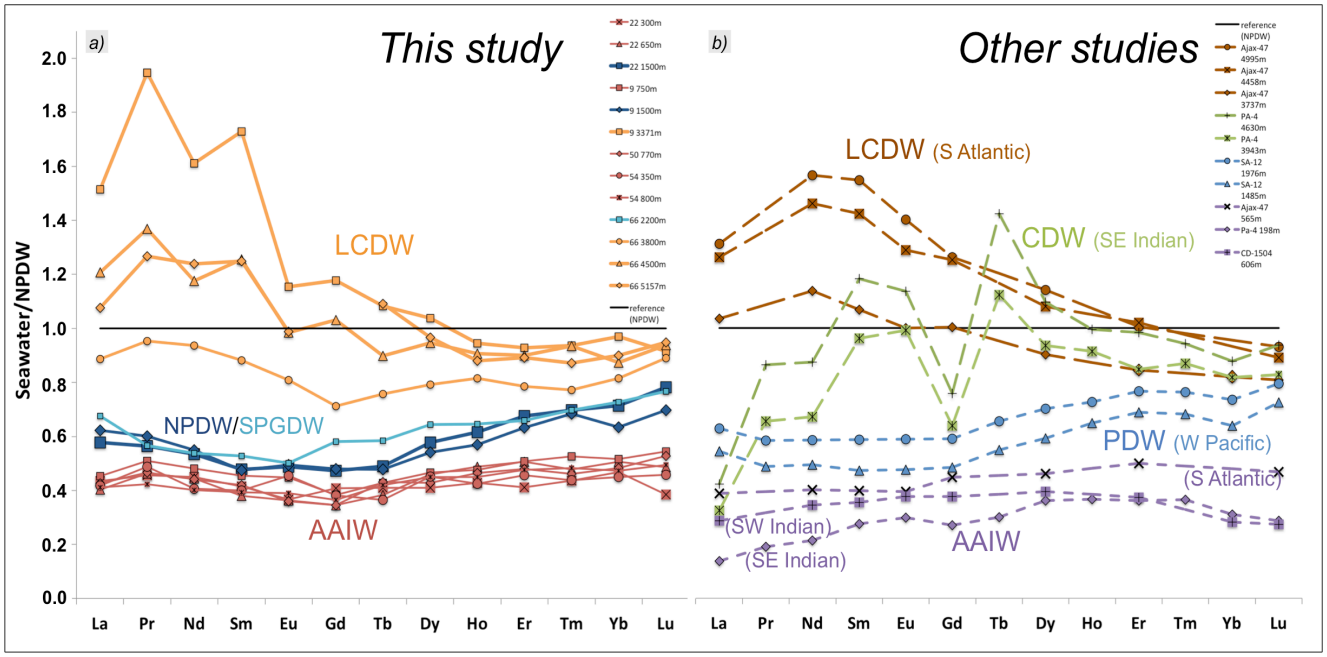


***Figure 3.10.*** *NPDW-normalized patterns for selected samples of this study (left panel) and previous studies (dashed patterns in the right panel) from the South Atlantic (AJAX-47, German et al. 1995), the Southeastern Indian Ocean (PA-4, Alibo and Nozaki 2004), the Southwestern Indian Ocean (CD-1504, Bertram and Elderfield 1993) and the Western South Pacific (SA-12, Zhang and Nozaki 1996). The different colours of the patterns reflect the dominance of a particular waters mass for each sample (indicated in the figure). NPDW reference concentrations after Alibo and Nozaki 1999.*

### 3.4.3. Biogeochemical cycling and the REE distribution

The primary productivity maximum at the equator seems to exert a considerable influence on the distribution of REEs in our study area, which we will discuss using Nd concentrations as an example. Profiles 22 and 66 show small (4 to 5 pmol/kg) mid-depth depletions in Nd concentrations compared to the other stations (Fig. 3.3). This occurs exactly at depths where the influence of North Pacific-derived waters is largest (sections 3.1.1. and 3.4.1.). North Pacific waters have previously been shown to have the highest Nd concentrations in deep waters of all major ocean basins ranging between 40 and 50 pmol/kg (e.g. Lacan et al., 2012 and references therein). These high concentrations should therefore be traceable in our study area if [Nd] conservatively follows the advection of water masses from the north, as for example captured in the model of Rempfer et al. (2011). Their modelled South Pacific [Nd] section presented in figure 3.9b predicts concentrations of up to 28 pmol/kg between 2000 and 3000 m in the eastern part of our study area while we observe Nd concentrations ranging from 13 to 21 pmol/kg for these depths.

We suggest that the reason for the discrepancy between the model and the data is the southward advection of the middepth north Pacific water masses underneath the eastern

equatorial high productivity area. The high rates of particle export will scavenge a significant amount of the dissolved Nd. This is consistent with the explanation of Grasse et al. (2012) for low concentrations in deep waters underneath the Peruvian upwelling area in the eastern equatorial Pacific. Jeandel et al (2013) also observed unexpectedly low concentrations of 14.6 to 18.8 pmol/kg in the depth range of 2000 to 3000 m in the Southeast Pacific that they attributed to scavenging by metalliferous particles originating from hydrothermal vent fluids. Based on our findings the observations of Jeandel et al. (2013) may, however, also be explained by the advection of Nd depleted modified NPDW (see section 3.4.1.2).

Scavenging processes especially affect the more particle reactive LREE, as reflected in the concentrations of La, Pr and Sm (Fig. 3.3), which are depleted similar to Nd in north Pacific derived middepths waters. The samples influenced by northern derived mid-depth waters also have the highest Er/Nd ratio at this depth level (Fig. 3.3), indicating depletion of LREEs. This is especially evident in profile 22 influenced by southward flowing NPDW and the upper part of profile 66, where SPGDW is present. In contrast, similarities between the profiles of dissolved silicate and HREEs (Bertram and Elderfield, 1993; Nozaki and Alibo, 2003a) have suggest the coupling of the HREEs to silicate cycling and diatom productivity (Akagi et al. 2011). This could also be the case in the South Pacific given that erbium (Er) and silicate concentrations appear to be well correlated ($R^2$ = 0.85) (Fig. 3.11), whereas the correlation with LREEs, such as Nd, is significantly weaker ($R^2$ = 0.52). Nevertheless, the positive intercept of both [Er] and [Nd] with [Si] and the weak correlation of all lanthanides with silicate below AAIW (red trend lines in figure 3.11) indicate that the life cycle of diatoms and dissolution of opal is not the main factor controlling the distribution of REEs in the South Pacific. This contrasts with the strong correlation ($R^2$ = 0.87) of silicate and [Nd] observed by Stichel et al. (2012) in the Atlantic sector of the Southern Ocean within the zone of high opal productivity (Sarmiento et al., 2007) and related dissolution processes.

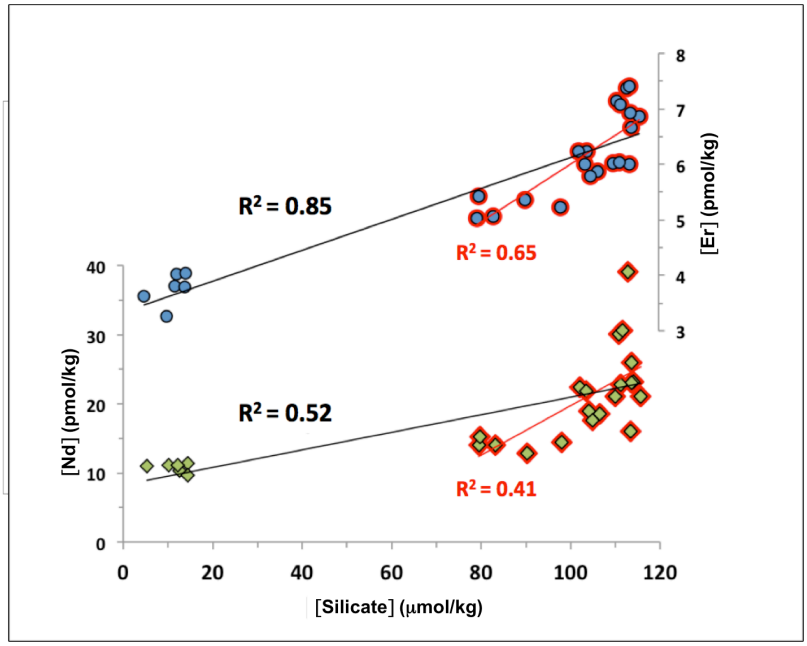


***Figure 3.11.*** *Nd (green diamonds) and Er concentrations (blue dots) (pmol/kg) versus dissolved silicate (pmol/kg) and their respective correlation coefficients ($R^2$) for all samples (black trend line) and for samples below the influence of AAIW (~1400 m) (red contoured samples and linear fit). Nd concentrations presented in this figure were obtained by the Isotope Dilution (ID) technique.*

### 3.4.4. Sediment – bottom water interactions.

#### 3.4.4.1 Release of REEs from the sediments of the Southeast Pacific Basin.

In our study area, the only example of sedimentary input of REEs can be found in the bottom waters of the Southeast Pacific basin, where sample 9-3769 shows relatively high LREE concentrations (e.g. [Nd]=39.1 pmol/kg)(Fig. 3.3). Without a considerable modification of the Nd isotope composition (-9.1 ±0.3, slightly less radiogenic than expected for LCDW) this cannot be explained by boundary exchange (e.g. Lacan and Jeandel, 2005).

The NPDW-normalised patterns (Fig. 3.10) clearly reveal the strong enrichment of LREE compared to other CDW samples, suggesting a significant sedimentary contribution of LREE to bottom waters. The PAAS-normalized pattern of this sample also clearly differs from that of the rest of the samples (Fig. 3.4), although it still shows a LREE to HREE enrichment and the negative Ce anomaly (Fig. 3.3), typical for seawater. The shape of the PAAS-normalized pattern is more indicative of the release of REE from oxides in the sediments than a detrital silicate component that would produce a generally flatter REE pattern (Haley et al., 2004). In addition, the relatively unradiogenic Nd isotope signature of this water sample (-9.1 ±0.3) precludes detrital (-2 to +5 for South America (Jeandel et al. 2007, GEOROC database and references therein)) and/or hydrothermal contributions. This suggests that although a significant sedimentary source of LREEs to the bottom water is identified at this location, probably the result of the sluggish

circulation (Reid, 1997; Schaffer et al., 2004) caused by the barrier of the East Pacific Rise and Chile Rise that hinders equatorward deep water flow, this LREE enrichment from oxides does not alter the isotopic composition of bottom waters as the oxides are releasing LREEs previously scavenged from the same water mass. Evidence for REE release from sedimentary iron oxides within LCDW that did not influence the Nd isotopic composition has recently been suggested in an experimental study (Wilson et al., 2013).

**3.4.4.2. Waters at the sediment-water interface.**

In contrast to the open ocean waters of this study, the bottom water samples from the Bounty Trough off New Zealand allow the evaluation of exchange processes between surface sediments and bottom waters from a slope setting located in the Deep Western Boundary Current (DWBC) of the South Pacific. The REE concentrations and PAAS-normalized REE patterns of the two multicorer seawater samples (MuC-78 and MuC-79) show a typical open ocean pattern (figures 3.3 and 3.4) indistinguishable from that of other samples of this study at similar depths. This suggests the absence of significant additions of sedimentary REEs to the bottom waters at this location. The only exception is Ce, which shows a slightly higher concentration (by 7 to 9 pmol/kg) that may point to a small sedimentary contribution of Ce to the bottom water.

Further confirmation of the absence of boundary exchange effects or input processes on our multicorer samples is obtained from the comparison between the dissolved Nd isotopic ratios of these two samples (-9.0 and -10.3) and the signatures of the detrital material supplied from New Zealand ($\varepsilon_{Nd}$ = -5 to +1 (Jeandel et al., 2007)). Although only based on two samples from one location these results suggest insignificant sedimentary contributions to the REE budget of bottom waters located in the Deep Western Boundary Current (DWBC) of the South Pacific. This contrasts with the observations along the flow path of the DWBC in the Indian Ocean (Wilson et al., 2012) and also with boundary exchange processes observed along the South American margin (Grasse et al., 2012; Jeandel et al., 2013) and other regions of the Pacific (Horikawa et al., 2011), which may be explainable by different prevailing rock types of the detrital particles.

The absence of REE contributions from the surface sediments to the bottom water is consistent with the observations of Haley et al. (2004) who also used multicorers to collect waters directly overlying the sediment off Peru and in the California basin. Dedicated studies of the interaction processes between the seafloor and bottom waters in different environments are needed to further elucidate the mechanisms leading to “boundary exchange”. This process has

been demonstrated to play a crucial role in the global budget and distribution of the REEs in the oceans (Lacan and Jeandel, 2005; Arsouze et al., 2009; Rempfer et al., 2011; Wilson et al., 2012; Pearce et al., 2013) but clearly is regionally variable, most likely as a function of the lithologies of the sediments and may also vary with time.

### 3.5. Conclusions

The first analyses of dissolved Nd isotopes and REE concentrations in the intermediate to deep-water column of the open mid-latitude South Pacific, overall confirm the reliability of Nd isotopes as water mass tracer in this region. Variations generally occur in correspondence with changes in hydrographic parameters, especially oxygen concentrations, which is the property that best distinguishes the Pacific water masses. The location and mixing of the different water masses could be tracked by combining Nd isotopes and hydrographic parameters: Pure circumpolar waters (AAIW and LCDW), occupying the shallowest and deepest areas of the analyzed depth range, respectively, reveal an $\varepsilon_{Nd}$ signature of -8.3 ±0.3, consistent with previous observations in the Atlantic and Pacific sectors of the Southern Ocean. Admixture of Pacific-derived waters partly replaces UCDW at middepths, except in isolated cases such as above the East Pacific Rise. Southward flowing Pacific derived waters are especially dominant at middepths of the eastern part of the study area, as well as in the Southwest Pacific basin where the main cores of NPDW and equatorial derived deep waters (SPGDW) are located and the most radiogenic $\varepsilon_{Nd}$ values of -5.4 ±0.4 and -6.0 ±0.2 are found. The influence of residual NADW in the westernmost South Pacific is documented by the least radiogenic Nd isotopic signatures ($\varepsilon_{Nd}$ = -10.3 ±0.3) and supported by low nutrient concentrations and high salinities. The Nd isotope distribution thus reliably fingerprints the most important water masses of the South Pacific and their mixtures, which will also serve as a basis for reconstructions of past deep water circulation using $\varepsilon_{Nd}$ signatures extracted from marine sediments in this important region of the world's ocean.

The resemblance of NPDW-normalized REE patterns of LCDW samples of this study to those from the deep South Atlantic suggests a strong influence of AABW on CDW of the deep South Pacific and South Atlantic basins. Distinct NPDW-normalized REE patterns are also found for LCDW, NPDW and AAIW in the South Pacific.

Scavenging processes underneath the eastern equatorial high productivity area diminish the LREE concentrations of NPDW during its southward advection to the circumpolar

region, producing non-conservative behaviour of Nd concentrations. Local sedimentary input is only observed in bottom waters of the Southeast Pacific Basin by release of LREE from oxides in the sediments without modification of the Nd isotope composition. On the other hand, the analysis of waters from the sediment-water interface located under the influence of the South Pacific deep western boundary current off New Zealand does not provide evidence for significant boundary exchange or sedimentary REE input. This suggests that boundary exchange is spatially and temporally discontinuous and further studies from different regions and settings are required to quantify and better understand this process.

**Acknowledgements**

We would like to thank the "Bundesministerium für Bildung und Forschung, Germany" for funding this project (No.: 03G0213B), the crew members and participants of expedition SO213, in particular D. Nürnberg and R. Tiedemann for organizing and leading the cruise, which was part of the collaborative SOPATRA (SOuth PAcific paleoceanographic TRAnsect) project between the GEOMAR Helmholtz Centre for Ocean Research Kiel and the Alfred Wegener Institute for Polar and Marine Research (AWI) in Bremerhaven. R. Tiedemann (AWI) provided the nutrient data. We also thank J. Rempfer, University of Berne, for providing the modelled section of the study area and Jutta Heinze for laboratory assistance. Comments by the associate editor Mark Rehkämper, as well as by David Wilson and two anonymous reviewers improved the quality of this paper significantly.

**References:**


Akagi T., Fu F.-F., Hongo Y. and Takahashi K. (2011) Composition of rare earth elements in settling particles collected in the highly productive North Pacific Ocean and Bering Sea: Implications for siliceous-matter dissolution kinetics and formation of two REE-enriched phases. *Geochim. Cosmochim. Acta* **75**, 4857–4876.

Alibo D.S. and Nozaki Y. (2000). Dissolved rare earth elements in the South China Sea: geochemical characterization of the water masses. *J. Geophys. Res.* **105**, 28771–28783.

Alibo D.S. and Nozaki Y. (2004). Dissolved rare earth elements in the eastern Indian Ocean. *Deep-Sea Res. I* **51**, 559-576.

Amakawa H., Nozaki Y., Alibo D. S., Zhang J., Fukugawa K. and Nagai H. (2004a) Neodymium isotopic variations in Northwest Pacific water. *Geochim. Cosmochim. Acta* **68**, 715–727.

Amakawa H., Sasaki K. and Ebihara M. (2009) Nd isotopic composition in the central North Pacific. *Geochim. Cosmochim. Acta* **73** (16), 4705–4719.

Antonov J. I., Seidov D., Boyer T. P., Locarnini R. A., Mishonov A. V., and Garcia H. E. (2010) World Ocean Atlas 2009 Volume 2: Salinity. S. Levitus, Ed., NOAA Atlas NESDIS 69, U.S. Government Printing Office, Washington, D.C., 184 pp.

Arsouze T., Dutay J.-C., Lacan F. and Jeandel C. (2009) Reconstructing the Nd oceanic cycle using a coupled dynamical biogeochemical model. *Biogeosciences* **6**(12), 2829–2846.

Barrat J. A., Keller F., Amosse´ J., Taylor R. N., Nesbitt R. W. and Hirata T. (1996) Determination of Rare Earth Elements in sixteen silicate reference samples by ICP-MS after Tm addition and ion exchange separation. *Geostand. Geoanal. Res.* **20**, 133–139.

Basak C., Martin E. E., Horikawa K. and Marchitto T. M. (2010) Southern Ocean source of 14C-depleted carbon in the North Pacific Ocean during the last deglaciation, *Nat. Geosci.,* **3**(11), 770-773.

Bertram C. J. and Elderfield H. (1993) The geochemical balance of the rare earth elements and neodymium isotopes in the oceans. *Geochim. Cosmochim. Acta* **57,** 1957–1986.

Bostock H. C., Opdyke B. N., Williams M. J. M. (2010) Characterising the intermediate depth waters of the Pacific Ocean using $\delta^{13}C$ and other geochemical tracers. *Deep-Sea Res. I* **57**, 847-859.

Byrne R. H. and Kim K. H. (1990) Rare Earth Elements scavenging in seawater. *Geochim. Cosmochim. Acta* **54**, 2645-2656.

Callahan J.E. (1972) The structure and circulation of deep water in the Antarctic. *Deep Sea Res.* **19**, 563–575.

Carter P., Vance D., Hillenbrand C. D., Smith J. A. and Shoosmith D. R. (2012) The neodymium isotopic composition of waters masses in the eastern Pacific sector of the Southern Ocean. *Geochim. Cosmochim. Acta* **79**, 41-59.

Elderfield H. (1988) The oceanic chemistry of the rare-earth elements. *Phil. Trans. Rov. Sac. London* A325, 105-126.

Elderfield H., Ferretti P., Greaves M., Crowhurst S., McCave I. N., Hodell D., and Piotrowski A. M. (2012) Evolution of ocean temperature and ice volume through the Mid-Pleistocene Climate Transition, *Science* **337**(6095), 704-709.

Frank M. (2002) Radiogenic isotopes: tracers of past ocean circulation and erosional input. *Rev. Geophys.* **40**, 1001.

Garcia H. E., Locarnini R. A., Boyer T. P. and Antonov J. I. (2010) World Ocean Atlas 2009 Volume 3: Dissolved Oxygen, Apparent Oxygen Utilization, and Oxygen Saturation. S. Levitus, Ed., NOAA Atlas NESDIS 70, U.S. Government Printing Office, Washington, D.C., 344 pp.

Garcia H. E., Locarnini R. A., Boyer T. P., and Antonov J. I. (2010) World Ocean Atlas 2009, Volume 4: Nutrients (phosphate, nitrate, and silicate). S. Levitus, Ed., NOAA Atlas NESDIS 71, U.S. Government Printing Office, Washington, D.C., 398 pp.

German C.R., Masuzawa T., Greaves M.J., Elderfield H. and Edmond J. (1995) Dissolved rare earth elements in the Southern Ocean: cerium oxidation and the influence of hydrography. *Geochim. Cosmochim. Acta* **59**, 1551–1558.

Goldstein S.L. and Hemming S.R. (2003) Long-lived Isotopic Tracers in Oceanography. Paleoceanography, and Ice-sheet Dynamics, *Treatise on Geochemistry. Pergamon, Oxford*, pp. 453–489

Grasse P., Stichel T., Stumpf R., Stramma L. and Frank M. (2012) The distribution of neodymium isotopes and concentrations in the Eastern Equatorial Pacific: Water mass advection versus particle exchange. *Earth Planet. Sci. Lett.* **353-354**, 198-207.

Grasshoff K., Kremling K. and Ehrhardt M. (1999) *Methods of Seawater Analysis.* Verlag Chemie, Weinheim (pp. 159–228).

Grenier M., Jeandel C., Lacan F., Vance D., Venchiarutti C., Cros A. and Cravatte S. (2013) From the subtropics to the central equatorial Pacific Ocean: Neodymium isotopic composition and rare earth element concentration variations. *J. Geophys. Res. Oceans* **118**, 1-27.

Haley B.A., Klinkhammer G.P. and McManus J. (2004) Rare earth elements in pore waters of marine sediments. *Geochim. Cosmochim. Acta* **68**, 1265–1279.

Hathorne E.C., Haley B.A., Stichel T., Grasse P., Zieringer M. and Frank M. (2013) Online preconcentration ICP-MS analysis of rare earth elements in seawater. *Geochem. Geophys. Geosyst.* **13**, Q01020, doi:10.1029/2011GC003907

Horikawa K., Martin E. E., Asahara Y., and Sagawa T. (2011) Limits on conservative behavior of Nd isotopes in seawater assessed from analysis of fish teeth from Pacific core tops, *Earth Planet. Sci. Lett.,* **310**, 119–130.

Jacobsen S.B. and Wasserburg G.J. (1980) Sm–Nd isotopic evolution of chondrites. *Earth Planet. Sci. Lett.* **50**, 139–155.

Jeandel C., Arsouze T., Lacan F., Téchine P. and Dutay J.-C. (2007) Isotopic Nd compositions and concentrations of the lithogenic inputs into the ocean: a compilation, with an emphasis on the margins. *Chem. Geol.* **239**, 156–164.

Jeandel C., Delattre H., Grenier M., Pradoux C. and Lacan F. (2013) Rare earth element concentrations and Nd isotopes in the Southeast Pacific Ocean. *Geochem. Geophys. Geosyst.* **14**, 328–341. doi:10.1029/GC004309

Johannesson K. H. and Burdige D. J. (2007) Balancing the global oceanic neodymium budget: evaluating the role of groundwater. *Earth Planet. Sci. Lett* **253**(1–2), 129–142.

Kawabe M. and Fujio S. (2010) Pacific Ocean circulation based on observation. *J. Oceanogr.* **66**, 389–403.

Lacan F. and Jeandel C. (2005) Neodymium isotopes as a new tool for quantifying exchange fluxes at the continent–ocean interface. *Earth Planet. Sci. Lett.* **232**, 245–257.

Lacan F., Tachikawa K. and Jeandel C. (2012) Neodymium isotopic composition of the oceans: A compilation of seawater data. *Chem. Geol.* **300-301**, 177-184.

Le Fevre B. and Pin C. (2005) A straightforward separation scheme for concomitant Lu–Hf and Sm–Nd isotope ratio and isotope dilution analysis. *Anal. Chim. Acta* **543**, 209–221.

Locarnini R. A., Mishonov A. V., Antonov J. I., Boyer T. P. and Garcia H. E. (2010) World Ocean Atlas 2009, Volume 1: Temperature. S. Levitus, Ed., NOAA Atlas NESDIS 68, U.S. Government Printing Office, Washington, D.C., 184 pp.

Mantyla A. W. and Reid J. L. (1983) Abyssal characteristics of the World Ocean waters. *Deep-Sea Res.*, **30**, 805–833.

Martin E. E., MacLeod K. G., Jiménez Berrocoso A. and Bourbon E. (2012) Water mass circulation on Demerara Rise during the late Cretaceous based on Nd isotopes. *Earth Planet. Sci. Lett.* **327-328**, 111–120.

Moffet J. W. (1990) Microbially mediated cerium oxidation in sea water. Nature 345,421-423.

Noble T. L., Piotrowski, A.M. and McCave, I. N. (2013) Neodymium isotopic composition of intermediate and deep waters in the glacial southwest Pacific. *Earth Planet. Sci. Lett.* **384**, 27-36.

Nozaki Y. (2001) *Encyclopedia of Ocean Sciences* (eds. J. H. Steel et al.). Vol. 2, Academic Press, pp. 840–845.

Nozaki Y. and Alibo D.S. (2003a) Importance of vertical geochemical processes in controlling the oceanic profiles of dissolved rare earth elements inferred from the study in the northeastern Indian Ocean. *Earth Planet. Sci. Lett.* **205**, 155–172.

Nozaki Y. and Alibo D.S. (2003b) Dissolved rare earth elements in the Southern Ocean, southwest of Australia: unique patterns compared to the South Atlantic data. *Geochemical Journal* **37**, 47–62.

Nozaki Y., Alibo D.-S., Amakwa H., Gamo T. and Hasumoto H. (1999) Dissolved rare earth elements and hydrography in the Sulu Sea. *Geochim. Cosmochim. Acta* **15,** 2171–2181.

Orsi A.H., Johnson G.C. and Bullister J.L. (1999) Circulation, mixing, and production of Antarctic Bottom Water. *Prog. Oceanogr.* **43**, 55–109.

Pahnke K., Goldstein S. L. and Hemming S. R. (2008) Abrupt changes in Antarctic Intermediate Water circulation over the past 25,000 years. *Nat. Geosci.* **1**, 870-874.

Pearce C. R., Jones M. T., Oelkers E. H., Pradoux C. and Jeandel C. (2013) The effect of particulate dissolution on the neodymium (Nd) isotope and Rare Earth Element (REE) composition of seawater. *Earth Planet. Sci. Lett.* **369-370**, 21-40

Piepgras D.J. and Jacobsen S.B. (1988) The isotopic composition of neodymium in the North Pacific. *Geochim. Cosmochim. Acta* **52**, 1373–1381

Piepgras D.J. and Jacobsen S.B. (1992) The behavior of rare earth elements in the seawater: precise determination of variations in the North Pacific water column. *Geochim. Cosmochim. Acta* **56**, 1851-1862.

Piepgras D.J. and Wasserburg G.J. (1982) Isotopic composition of neodymium in waters from the Drake Passage. *Science* **217**, 207–214.

Piepgras D. J. and Wasserburg G. J. (1987) Rare earth element transport in the western North Atlantic inferred from Nd isotopic observations. *Geochim. Cosmochim. Acta* 51, 1257–1271. *Earth Planet. Sci. Lett.* **357-358**, 289-297.

Piotrowski A. M., Galy A., Nicholl J. A. L., Roberts N., Wilson D. J., Clegg J. A. and Yu J. (2012) Reconstructing deglacial North and South Atlantic deep water sourcing using foraminiferal Nd isotopes.

Reid J. L. (1973) Transpacific hydrographic sections at Lats. 43°S and 28°S: the SCORPIO Expedition-III. Upper water and a note on southward flow at mid-depth. *Deep-Sea Res.* **20**, 39-49

Reid J. L. (1986) On the total geostrophic circulation of the South Pacific Ocean: Flow patterns, tracers and Transports. *Prog. Oceanog.* **16**, 1-61

Reid J. L. (1997) On the total geostrophic circulation of the Pacific Ocean: Flow patterns, tracers and Transports. *Prog. Oceanog.* **39**, 263-352

Reid J. L. and Lynn R. J. (1971) On the influence of the Norwegian-Greenland and Weddell seas upon the bottom waters of the Indian and Pacific oceans. *Deep-Sea Res.* **18**, 1063-1088.

Reid J. Jun., Stommel H., Dixon Stroup E. and Warren B. (1968) Detection of a Deep Boundary Current on the Western South Pacific. *Nature* **217**, 937.

Rempfer J., Stocker T. F., Joos F., Dutay J.-C. and Sidall M. (2011) Modelling Nd-isotopes with a coarse resolution ocean circulation model: Sensitivities to model parameters and source/sink distributions. *Geochim. Cosmochim. Acta* **75**, 5927-5950

Rickli J., Frank M. and Halliday A.N. (2009). The hafnium–neodymium isotopic composition of Atlantic seawater. *Earth Planet. Sci. Lett.* **280**, 118–127.

Roberts N. L., Piotrowski A. M., McManus J. F. and Keigwin L. D. (2009) Synchronous Deglacial Overturning and Water Mass Source Changes. *Science* **327**, 75

Sarmiento J.L., Simeon J., Gnanadesikan A., Gruber N., Key R.M. and Schlitzer R. (2007) Deep ocean biogeochemistry of silicic acid and nitrate. *Global Biogeochem. Cycles* **21**, doi:10.1029/2006GB002720.

Scher H. D. and Martin E. E. (2004) Circulation in the Southern Ocean during the Paleogene inferred from neodymium isotopes. *Earth Planet. Sci. Lett.* **228**, 391–405.

Schlitzer R. (2011) Ocean Data View. http://odv.awi.de

Shaffer G., Hormazabal S., Pizarro O. and Ramos M. (2004) Cirulation and variability in the Chile basin, *Deep Sea Res. I*, **51**, 1367-1386.

Siddall M., Khatiwala S., van de Flierdt T., Jones K., Goldstein S.L., Hemming S. and Anderson R.F. (2008) Towards explaining the Nd paradox using reversible scavenging in an ocean general circulation model. *Earth Planet. Sci. Lett.* **274**, 448–461.

Singh S.P., Singh S.K., Goswami V., Bhushan R., Rai V.K. (2012) Spatial distribution of dissolved neodymium and $\varepsilon_{Nd}$ in the Bay of Bengal: Role of particulate matter and mixing of water masses. *Geochim. Cosmochim. Acta* **94**, 38-56.

Sloyan B. M. and Rintoul S. R. (2001) Circulation, renewal, and modification of Antarctic mode and intermediate water. *J. Phys. Oceanogr.* **31**, 1005–1030.

Stichel T., Frank M., Rickli J. and Haley B. A. (2012) The hafnium and neodymium isotope composition of seawater in the Atlantic sector of the Southern Ocean. *Earth Planet. Sci. Lett.* **317-318**, 282-294.

Stommel H. and Arons A. B. (1960) On the abyssal circulation of the world ocean—I. Stationary planetary flow patterns on a sphere. *Deep-Sea Research*, **6**, 140–154.

Stommel H., Dixon Stroup E., Reid J. L. and Warren B. (1973) Transpacific hydrographic sections at Lats. 43°S and 28°S: the SCORPIO Expedition--I. Preface *. *Deep-Sea Res.* **20**, 1-7.

Tachikawa K., Athias V. and Jeandel C. (2003) Neodymium budget in the modern ocean and paleo-oceanographic implications. *J. Geoph. Res.* **108** (C8).

Tanaka T., Togashi S., Kamioka H., Amakawa H., Kagami H., Hamamoto T., Yuhara M., Orihasi Y., Yoneda S., Shimizu H., Kunimaru T., Takahashi K., Yanagi T., Nakano T., Fujimaki H., Shinjo R., Asahara Y., Tanimizu M. and Dragusanu C. (2000) JNdi-1: a neodymium isotopic reference in consistency with LaJolla neodymium. *Chem. Geol.* **168**, 279–281.

Taylor S. R. and McLennan S. M. (1985) *The Continental Crust*: *Its Composition and Evolution. An Examination of the Geochemical Record Preserved in Sedimentary Rocks*. Blackwell.

Tsimplis M. N., Bacon S. and Bryden H. L. (1998) The circulation of the subtropical South Pacific derived from hydrographic data. *J. Geophys. Res.* **103**, 21443-21468.

Tsuchiya M. and Talley L. D. (1996) Water-property distributions along an eastern Pacific hydrographic section at 135W. *J. Mar. Res.* **54**, 541-563.

Tsuchiya M. and Talley L. D. (1999) A Pacific hydrographic section at 88°W: Water-property distribution. *J. Geophys. Res.* **103**, 12899-12918.

van de Flierdt, T., et al. (2012) GEOTRACES intercalibration of neodymium isotopes and rare earth element concentrations in seawater and suspended particles. Part 1: reproducibility of results for the international intercomparison, *Limnol.Oceanogr.*, **10**, 234–251.

Warren B. A. (1973) Transpacific hydrographic sections at Lats. 43°S and 28°S: the SCORPIO Expedition-II. Deep water. *Deep-Sea Res.* **20**, 9-38.

Wijffels S. E. (2001) Revisiting the South Pacific subtropical circulation: A synthesis of World Ocean Circulation Experiment observations along 32°S. *J. Geophys. Res* **106**, 19481-19513.

Wilson D. J., Piotrowski A. M., Galy A. and McCave I. N. (2012) A boundary exchange influence on deglacial neodymium isotope records from the deep western Indian Ocean. *Earth Planet. Sci. Lett.* **341–344**, 35–47.

Wilson, D. J., A. M. Piotrowski, A. Galy, and J. A. Clegg (2013) Reactivity of neodymium carriers in deep sea sediments: Implications for boundary exchange an paleoceanography, *Geochim. Cosmochim. Acta*, **109**, 197-221.

# 4) Nd and Sr isotope compositions of different phases of surface sediments in the South Pacific: extraction of seawater signatures, boundary exchange, and detrital/dust provenance

**Abstract**

The radiogenic isotope composition of neodymium (Nd) and strontium (Sr) are useful tools to investigate present and past oceanic circulation or input of terrigenous material. We present Nd and Sr isotope compositions extracted from different sedimentary phases, including early diagenetic Fe-Mn coatings, 'unclean' foraminiferal shells, fossil fish teeth, and detritus of marine surface sediments (core-tops) covering the entire mid-latitude South Pacific. Comparison of detrital Nd isotope compositions to deep-water values from the same locations suggest that 'boundary exchange' has little influence on the Nd isotope composition of western South Pacific seawater. The concentrations of Rare Earth Elements (REE) and Al/Ca ratios of 'unclean' planktonic foraminifera suggest that this phase is a reliable recorder of seawater Nd isotope composition. The signatures obtained from fish teeth and 'non-decarbonated' leachates of bulk sediment Fe-Mn oxyhydroxide coatings also agree with the 'unclean' foraminifera. Direct comparison of Nd isotope compositions extracted using these methods with seawater Nd isotope compositions is complicated by the low accumulation rates of some of the core-top sediments yielding radiocarbon ages of up to 24 kyrs. This suggests integration of different past seawater Nd isotope compositions in sedimentary Nd isotope signatures from regions with low sedimentation rates. Combined detrital Nd and Sr isotope signatures indicate a dominant role of the Westerly winds in transporting lithogenic material from South New Zealand and Southeastern Australia to the open South Pacific. The proportion of this material decreases towards the east, where supply from the Andes increases and contributions from Antarctica cannot be ruled out.

*This chapter has recently been submitted to the journal Geochemistry, Geophysics, Geosystems, authored by Mario Molina-Kescher, Martin Frank and Ed Hathorne under the title: Nd and Sr isotope compositions of different phases of surface sediments in the South Pacific: extraction of seawater signatures, boundary exchange, and detrital/dust provenance*

## 4.1. Introduction

The radiogenic isotope compositions of Nd and Sr in seawater have been demonstrated to be useful tools to understand Earth surface processes given that they are not affected by biological fractionation or thermodynamic processes that potentially bias nutrient-based tracers (e. g. Frank, 2002). Thus they serve as tracers of present (e.g. von Blanckenburg, 1999; Goldstein and Hemming, 2003; Rickli et al., 2009; Stichel et al., 2012, Molina-Kescher et al., 2014) and past oceanic circulation regimes (e.g. Rutberg et al., 2000; Scher and Martin 2004; Piotrowski et al., 2005, 2008, 2012; Gutjahr et al., 2008; Pahnke et al., 2008; Basak et al., 2010; Martin et al., 2012), continental weathering inputs and regimes (e.g. Walter et al., 2000; Franzese et al., 2006; Roy et al., 2007; Hemming et al., 2007; Ehlert et al., 2011; Stumpf et al., 2011; Asahara et al., 2012; Dou et al., 2012; Soulet et al., 2013), or dust input to the oceans (e.g. Goldstein et al., 1984; Graves et al., 1994; Grousset and Biscaye, 2005 and references therein, Delmonte et al., 2004; Revel-Rolland et al., 2006; Noble et al., 2012). Radiogenic isotope signatures are obtained either directly from seawater, from authigenic seawater-derived phases such as carbonates, fish teeth, early diagentic Fe-Mn coatings of sediment particles, or from weathered terrigenous material.

The radiogenic isotope composition of Nd ($^{143}Nd/^{144}Nd$), is expressed in the epsilon ($\varepsilon_{Nd}$) notation: $\varepsilon_{Nd} = [(^{143}Nd/^{144}Nd_{sample}/^{143}Nd/^{144}Nd_{CHUR})-1]*10000$, where CHUR stands for Chondritic Uniform Reservoir ($^{143}Nd/^{144}Nd=0.512638$, (Jacobsen and Wasserburg, 1980)). The $\varepsilon_{Nd}$ and Sr isotope composition of continental rocks varies as a function of age and rock type, therefore allowing the distinction of regional and local sources of weathered material. Neodymium isotopes also serve as tracers in seawater as the characteristic Nd isotope composition of the different continental source rocks is supplied to the surrounding oceans via rivers or dissolution of particles thus transferring characteristic signatures to the ocean, which, together with the short oceanic residence time of Nd of 400-2,000 years (Tachikawa et al., 2003; Arsouze et al., 2009; Rempfer et al., 2011), permits to track the flow paths and mixing of major water masses. Nevertheless, the use of Nd isotopes is not without complications due to processes that affect their quasi-conservative behavior in seawater such as interactions with the sediments, particle dissolution and reversible scavenging in the water column. Processes that cause the seawater isotope composition to change with no significant increase in the dissolved Nd concentration are referred to as 'boundary exchange' (Lacan and Jeandel, 2005; Singh et al., 2012; Stichel et al., 2012b; Pearce et al., 2013). These processes have been demonstrated to play an important role in the REE budget of the oceans (e. g. Rempfer et al., 2011), although their

magnitude and the particular underlying mechanisms differ between oceanic regions and are an area of active research (e.g. Wilson et al., 2012, 2013; Huang et al., 2014; Molina-Kescher et al., 2014). Efforts have been made to resolve these issues, such as expanding the knowledge of the natural cycle of trace elements in the ocean through new dedicated investigations and data along ocean sections, such as in the frame of the international GEOTRACES program (SCOR working group, 2007), or through modeling studies applying different parameterizations (Siddall et al., 2008; Arsouze et al., 2009; Jones et al., 2008; Rempfer et al., 2011, 2012)

For palaeoceanographic studies the reliable extraction of the seawater signal from sedimentary records (Gutjahr et al., 2007; Elmore et al., 2009, Roberts et al., 2010; 2012; Piotrowski et al., 2012; Wilson et al., 2013; Kraft et al., 2013) is crucial. Different approaches to obtain the seawater $\varepsilon_{Nd}$ signal from authigenic, seawater-derived phases of marine sediments have been proposed, such as biogenic apatite of fish teeth (Martin and Haley, 2000; Martin and Scher, 2004), biogenic carbonates such as benthic foraminifera (Klevenz et al., 2008), deep sea corals (van de Flierdt et al., 2010) or authigenic Fe-Mn coatings of particles. The signatures contained in the latter are advantageous because they are widely available and allow high spatial and temporal coverage but have to be reliably separated from the "contaminant" detrital contributions. This has been achieved by only using authigenic Fe-Mn coatings of planktonic foraminifera (Roberts et al., 2010; 2012; Tachikawa et al., 2014) or by applying different leaching methods and reagents to bulk sediments (Rutberg et al., 2000; Bayon et al., 2002; Gutjahr et al., 2007; Charbonier et al., 2012; Wilson et al., 2013). Despite these effects, there have only been a few studies to date that directly compare bottom seawater Nd isotope compositions to those obtained from the sediments immediately below (Tachikawa et al., 2004; Elmore et al., 2011; Huang et al., 2014).

In this study we obtained $\varepsilon_{Nd}$ signatures from different authigenic and detrital fractions of sediment core tops in the South Pacific and compare them directly to the signatures overlying bottom seawater (Molina-Kescher et al., 2014). Two important questions can be elucidated from this comparison of water and sedimentary $\varepsilon_{Nd}$ data: 1) What role does seawater-sediment interaction play in the oceanic Nd cycle? This includes 'boundary exchange', for which continental margins are considered to be both an important source and sink of Nd in the oceans (Tachikawa et al., 2003; Lacan and Jeandel, 2005; Rempfer et al., 2011) and 2) Can the Nd isotope composition of bottom seawater in the South Pacific be reliably obtained from the sediments below in order to reconstruct past ocean circulation in this region? To resolve this second question, we compare results of four different extraction methods ('unclean' planktonic

foraminifera, fossil fish teeth/debris, 'decarbonated' and 'non-decarbonated' leachates of authigenic Fe-Mn coatings) to obtain seawater $\varepsilon_{Nd}$ signatures and evaluate the importance of the two end-members that contribute to the authigenic sediment $\varepsilon_{Nd}$ signatures: The detrital fraction of the sediment and the Nd dissolved in seawater. To corroborate the reliability of the extracting methods we also examine Al/Ca ratios, REE patterns and Sr isotope compositions to assess the absence of detrital contributions to the extracted solutions and to support the seawater origin of the Nd isotope ratios in the different phases.

Finally, by combining detrital Nd and Sr isotope compositions we track the provenance of the fine-grained terrigenous material to the surrounding continental source areas (New Zealand, Australia, South America and possibly also Antarctica).

#### 4.1.1. South Pacific background hydrology and sedimentology

The hydrography of the South Pacific is dominated by Southern Ocean derived water masses at intermediate (AAIW) and bottom (LCDW) depths ($\varepsilon_{Nd}$ ranging -8 to -9) whereas mid depths between 1000 and 3500 m are occupied by more radiogenic Pacific derived waters (Figure 4.1, see Molina-Kescher et al., 2014 for a detailed discussion). This is particularly the case in the eastern South Pacific where the main outflow of NPDW (average $\varepsilon_{Nd}$=-5.9 ±0.3) to the Southern Ocean occurs. In contrast, southeast of New Zealand, a Deep Western Boundary Current (DWBC) (e. g. Carter et al., 1996a) flowing to the north prevails that feeds the entire Pacific Ocean with circumpolar deep waters.

The South Pacific is one of the regions were the lowest sedimentation rates of all oceans have been observed. Below the carbonate compensation depth (CCD) located at around 4500 m water depth, areas such as the Southwest Pacific basin exhibit rates lower than 1 mm/kyr (e. g. Schmitz et al., 1986; Glasby et al., 1991, 2007; Rea et al., 2006). This is a consequence of the isolation and low atmospheric dust received compared to other oceanic regions (Rea, 1994; Prospero 2002). The small amount of dust that is supplied mainly consists of fine particles transported by the Southern Western Winds (SWW) or westerlies from Australia and New Zealand (Windom 1970; Thiede 1979; Fletcher and Moreno, 2012; Marx et al., 2014).

### 4.2. Samples and Methods

For this study, 31 core-top sediment samples were collected aboard the German RV SONNE during expedition SO213 that took place from December 2010 to March 2011 along a longitudinal transect between 36°S and 45°S extending over approximately 10 000 km from

central Chile to New Zealand (Figure 4.1). All core-top sediment samples represent undisturbed surface sediments as these were obtained using a multicore device, except sample 66-5 that corresponds to the first cm of the core-catcher of a piston core and thus its exact depth in the sediment is not known. Most samples were obtained above the carbonate compensation depth and are therefore mainly composed of foraminifera shells, except deepest samples 22-4 and 66-5, in which carbonates were absent.

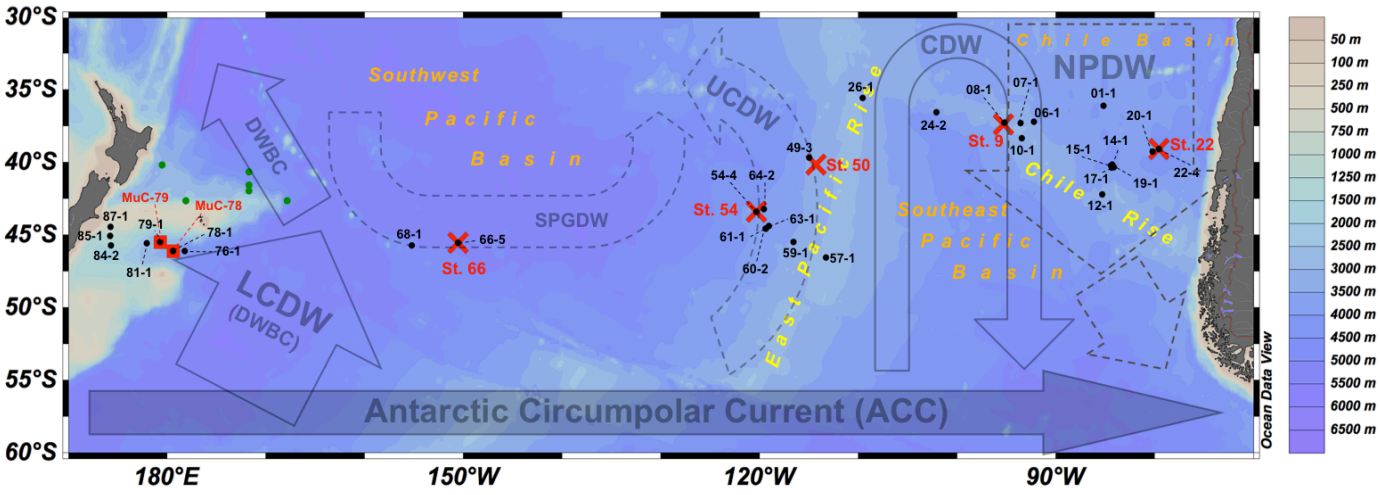


***Figure 4.1.*** *Study area with coarse bathymetry and the locations of the samples together with the schematic flowpaths and flow directions of the main water masses below 1500 m (circulation patterns after Kawabe and Fujio, 2005). Black dots represent core-top sediment samples, red crosses and squares represent locations for which seawater* $\varepsilon_{Nd}$ *analyses are available (data from Molina-Kescher et al., 2014) whereby crosses are CTD-profiles and squares are bottom water samples obtained from multicorers. Green dots represent sediment samples presented in Noble et al. (2013). Arrows represent water mass flow at middepths (dashed arrows), at the bottom (solid arrows) and occupying the entire water column (solid shaded arrow): AAC (Antarctic Circumpolar Current), LCDW (Lower Circumpolar Deep Water), DBWC (Deep Western Boundary Current), SPGDW (South Pacific Gyre derived Deep Water), UCDW (Upper Circumpolar Deep Water), CDW (Circumpolar Deep Water) and NPDW (North Pacific Deep Water).*

### 4.2.1. Methods applied to the extraction of Nd and Sr isotope signatures.

Four different techniques were applied for the extraction of seawater derived Nd and Sr isotope signatures from different phases of the sediment. In addition, detrital Nd and Sr isotope signatures were obtained from the same samples.

#### 4.2.1.1.Ferromanganese coatings of bulk sediments

The first technique employed was the extraction of the seawater Nd and Sr isotopic signatures from authigenic ferromanganese coatings of the bulk sediment (~3 g) applying the leaching protocol of Stumpf et al. (2010). The procedure consists of an initial double rinsing of the freeze-dried bulk sediment with de-ionised water followed by removal of the carbonate

fraction of the sediment using acetic acid buffered with Na-acetate. The ferromanganese coatings were subsequently dissolved in a 0.05 M-hydroxylamine hydrochloride/15%-acetic acid solution (HH) buffered to pH 3.6 with NaOH. This method was applied for 29 samples for Nd and Sr isotope analysis and for 3 samples only for Nd analysis. We will refer to this method as 'decarbonated leaching', which is distinct from the 'non-decarbonated leaching' method, hereafter referred as 'leaching', consisting of the same procedure described above but omitting the initial carbonate removal step. This second method was used for 19 samples only for analysis of Nd isotope compositions.

#### 4.2.1.2.Planktonic foraminifera with ferromanganese coatings

Between 25 and 75 mg of mixed species whole planktonic foraminifera shells were hand-picked from the >250 μm size fraction under a light microscope from 22 different locations. Samples were subsequently cracked between glass plates, observing with a binocular to ensure that all chambers were opened, and were ultrasonicated several times in deionized water and then in methanol to ensure the removal of most of the clays and silicate particles. The samples were then progressively dissolved in a weak acid (0.5 M $HNO_3$) until the carbonates and associated ferromanganese coatings were dissolved (~2 ml 0.5 M $HNO_3$). The final solution was then centrifuged to ensure removal of the smallest detrital particulates. A very similar procedure was named 'unclean forams' by Roberts et al. (2010) to clarify that the carbonate fraction was analysed together with Fe-Mn coatings. We will use the same term in our study to indicate that a reductive cleaning step for the dissolution of the coatings was not applied but that the $\varepsilon_{Nd}$ signature of the combined foraminiferal carbonate and coatings was measured. As demonstrated by many authors (e.g. Roberts et al., 2010; 2012, Kraft et al., 2013; Tachikawa et al., 2014) this method provides reliable bottom water signatures, as the Nd concentrations in the calcite are negligible compared to those in the coatings, which precipitate and equilibrate in deep waters.

#### 4.2.1.3. Fish teeth/debris.

Fish teeth and debris were found in the same size fraction as the foraminferal shells in five samples. These were hand-picked and separated from detrital and carbonate particles by rinsing with deionized water and methanol to be finally digested in 6M HCl (e.g. Martin and Scher 2004).

#### 4.2.1.4. Detrital fraction

After application of the 'decarbonated' leaching method described above a fine-grained detrital residue only consisting of the lithogenic fraction remained. This material was treated first with aqua regia and subsequently completely digested in a mixture of concentrated nitric

and hydrofluoric acid similar to Stumpf et al. (2011). In total 26 samples were prepared for analysis of Nd isotopes and 18 samples for Sr isotopes.

**4.2.2. Column chemistry and determination of isotopic signatures.**

Nd and Sr were separated from other elements applying a two-step ion chromatographic separation. The solutions resulting from the different extracting methods were brought through columns filled with 0.8 ml of Biorad® AG50W-X12 resin (200-400 µm mesh-size) (Barrat et al., 1996) to separate REEs and Sr. The solutions containing Nd and Sr were further purified using Eichrom® Ln Spec resin (50-100µm mesh-size, 2mL resin bed)(Le Fevre and Pin, 2005) and Eichrom Sr Spec resin (Horwitz et al., 1992), respectively. Isotopic ratios of both elements were measured on a Nu plasma MC-ICPMS at GEOMAR, using ratios of 0.7219 for $^{146}Nd/^{144}Nd$ and of 0.1194 for $^{88}Sr/^{86}Sr$ to correct for instrumental mass bias. Nd and Sr isotope ratios were corrected for Sm and $^{86}Kr$, $^{87}Rb$ interferences, respectively. The results were normalized to the accepted values of 0.512115 (JNdi-1 standard (Tanaka et al., 2000)) for $^{143}Nd/^{144}Nd$ and of 0.710245 (NIST NBS987) for $^{87}Sr/^{86}Sr$. The external reproducibilities (2σ) of the $^{143}Nd/^{144}Nd$ and $^{87}Sr/^{86}Sr$ measurements during each session ranged between 0.2 and 0.4 $\varepsilon_{Nd}$ units and between 0.00002 and 0.00006, respectively, as assessed by repeated measurements of the above standards matching sample concentrations (see tables 4.1 and 4.2).

**4.2.3. Determination of Al/Ca ratios and REE concentrations on 'unclean' foraminifera cuts.**

Al/Ca and REE concentrations on 'unclean' foraminifera were measured on an Agilent 7500ce ICP-MS in the same laboratory and using the same methods described in Kraft et al., (2013). Briefly, $^{27}Al$ was measured simultaneously with other elements on samples diluted to 10ppm Ca content following a first step to measure the Ca concentration of the samples. Element/Ca ratios were calculated from intensity ratios (Rosenthal et al., 1999) calibrated using standards with similar ratios to those found in foraminifera.. The 2σ uncertainty was 6-7% for Al/Ca ratios. REE concentrations were obtained using an online pre-concentration (OP) ICP-MS technique modified from Hathorne et al. (2012) using a "seaFAST" system (Elemental Scientific Inc.) coupled to the ICP-MS on samples diluted to a Ca concentration of 25ppm. The 2σ uncertainty based on repeated measurement of a sample averaged 9% (see Table 4.3 for all elements).

| | | | | *Detrital fraction* | | *Decarbonated leachates* | | *Non-decarb. leachates* | | *Uncleaned forams* | | *Fish teeth/debris* | |
|---|---|---|---|---|---|---|---|---|---|---|---|---|---|
| **Sample** | **Latitude** | **Longitude** | **Depth (m)** | **$\varepsilon_{Nd}$** | **2σ** | **$\varepsilon_{Nd}$** | **2σ** | **$\varepsilon_{Nd}$** | **2σ** | **$\varepsilon_{Nd}$** | **2σ** | **$\varepsilon_{Nd}$** | **2σ** |
| SO213- 01-1 | 36° 13' S | 85° 2' W | 2806 | -3.8 | 0.2 | -4.7 | 0.4 | - | - | -5.3 | 0.4 | - | - |
| SO213- 06-1 | 37° 21' S | 92° 23' W | 2791 | -4.5 | 0.2 | -5.2 | 0.3 | - | - | -5.3 | 0.4 | - | - |
| SO213- 07-1 | 37° 30' S | 93° 57' W | 2571 | - | - | -4.6 | 0.3 | - | - | - | - | - | - |
| SO213- 08-1 | 37° 29' S | 95° 21'W | 2171 | -4.8 | 0.2 | -4.9 | 0.4 | -4.5 | 0.3 | -5.4 | 0.4 | -4.9 | 0.7 |
| SO213- 10-1 | 38° 36' S | 93° 43' W | 2996 | -5.0 | 0.2 | -5.4 | 0.4 | - | - | -5.6 | 0.4 | - | - |
| SO213- 12-1 | 42° 23' S | 85° 28' W | 3016 | -3.0 | 0.2 | -4.0 | 0.4 | -4.6 | 0.2 | -4.6 | 0.4 | -4.6 | 0.7 |
| SO213- 14-1 | 40° 18' S | 84° 29' W | 4052 | -2.1 | 0.2 | -4.6 | 0.4 | -5.4 | 0.2 | -5.6 | 0.3 | - | - |
| SO213- 15-1 | 40° 24' S | 84° 39' W | 3246 | - | - | -4.3 | 0.4 | - | - | - | - | - | - |
| SO213- 17-1 | 40° 37' S | 84° 30' W | 2561 | -2.7 | 0.2 | -4.5 | 0.4 | - | - | -4.5 | 0.4 | - | - |
| SO213- 19-1 | 40° 34' S | 84° 13' W | 2951 | - | - | -4.2 | 0.4 | - | - | - | - | - | - |
| SO213- 20-1 | 39° 27'S | 80° 18' W | 2702 | -2.9 | 0.2 | -4.2 | 0.4 | - | - | -4.5 | 0.4 | -5.1 | 0.8 |
| SO213- 22-4 | 39° 12' S | 79° 55' W | 4125 | -1.4 | 0.2 | -2.0 | 0.2 | -4.3 | 0.2 | - | - | - | - |
| SO213- 24-2 | 36° 57' S | 102° 07' W | 3092 | -5.7 | 0.2 | -5.6 | 0.4 | -5.8 | 0.3 | -5.8 | 0.4 | - | - |
| SO213- 26-1 | 35° 60' S | 109° 55' W | 2830 | -5.6 | 0.2 | -5.6 | 0.4 | -5.7 | 0.2 | -5.9 | 0.4 | - | - |
| SO213- 49-3 | 39° 57' S | 114° 1' W | 3380 | -5.5 | 0.2 | - | - | -5.9 | 0.3 | -5.8 | 0.4 | -5.8 | 0.3 |
| SO213- 54-4 | 43° 42' S | 120° 30' W | 3840 | -5.6 | 0.2 | -5.6 | 0.2 | -5.9 | 0.2 | -6.0 | 0.3 | - | - |
| SO213- 57-1 | 46° 59' S | 113° 27' W | 1194 | -2.6 | 0.2 | -6.6 | 0.4 | -6.1 | 0.2 | -6.3 | 0.3 | - | - |
| SO213- 59-1 | 45° 50' S | 116° 53 'W | 3159 | -4.7 | 0.2 | -5.8 | 0.4 | -5.9 | 0.2 | -5.8 | 0.4 | - | - |
| SO213- 60-2 | 44° 58' S | 119° 33' W | 3468 | - | - | -5.8 | 0.4 | - | - | -6.3 | 0.3 | -5.1 | 0.3 |
| SO213- 61-1 | 44° 60' S | 119° 38' W | 3616 | - | - | -5.8 | 0.4 | - | - | - | - | - | - |
| SO213- 63-1 | 44° 40' S | 119° 05' W | 3938 | -5.6 | 0.2 | -6.3 | 0.4 | -5.9 | 0.2 | -6.1 | 0.4 | - | - |
| SO213- 64-2 | 43° 24' S | 119° 53' W | 3922 | - | - | -6.2 | 0.4 | - | - | -6.2 | 0.4 | - | - |
| SO213- 66-5 | 45° 23' S | 151° 42' W | 5133 | -5.2 | 0.2 | - | - | -6.6 | 0.3 | - | - | - | - |
| SO213- 68-1 | 45° 7' S | 155° 17' W | 1988 | -5.2 | 0.2 | -5.6 | 0.3 | - | - | -5.5 | 0.4 | - | - |
| SO213- 76-1 | 46° 13' S | 178° 2' W | 4337 | -3.6 | 0.2 | -3.7 | 0.3 | -7.2 | 0.3 | - | - | - | - |
| SO213- 78-1 | 46° 15' S | 179° 37' W | 3410 | -3.4 | 0.2 | -4.2 | 0.3 | -7.0 | 0.3 | -7.3 | 0.4 | - | - |
| SO213- 79-1 | 45° 51' S | 179° 34' E | 3143 | -4.0 | 0.2 | -5.7 | 0.3 | -8.1 | 0.3 | -7.7 | 0.4 | - | - |
| SO213- 81-1 | 45° 60' S | 178° 0' E | 2829 | -4.2 | 0.2 | -5.9 | 0.3 | -7.8 | 0.3 | -7.9 | 0.3 | - | - |
| SO213- 84-2 | 45° 7' S | 174° 35' E | 992 | -3.5 | 0.2 | -2.9 | 0.3 | -5.7 | 0.3 | -5.4 | 0.3 | - | - |
| SO213- 85-1 | 44° 46' S | 174° 32' E | 832 | -3.5 | 0.2 | -3.2 | 0.3 | -5.9 | 0.3 | -5.8 | 0.3 | - | - |
| SO213- 87-1 | 44° 5' S | 174° 6' E | 542 | -3.7 | 0.2 | -3.0 | 0.3 | -4.9 | 0.3 | - | - | - | - |

***Table 4.1.*** *Sample information and Nd isotope composition for the different core-top fractions analysed in ths study with external reproducibility (2σ).*

### 4.2.4. $^{14}C$ dating.

8 of the core-tops including at least one sample for each of the different areas and depths investigated in this study were radiocarbon dated (see areas in figure 4.4). The analyses were carried out by the Leibniz Labor at Christian-Albrechts University Kiel on 1 to 1.4 mg of handpicked mixed planktonic foraminiferal shells using accelerator mass spectrometry (AMS) and following the procedure after Stuiver and Polach (1977), which briefly consists in the

release of $^{14}C$, $^{13}C$ and $^{12}C$ in form of $CO_2$ gas of the samples and comparison to known concentrations of the same isotopes of a standard (Oxalic Acid II), correcting for isotope fractionation by simultaneously measuring the $^{13}C/^{12}C$ ratio. $^{14}C$ ages were converted to calendar age using the radiocarbon calibration program CALIB 7.0 (Stuiver and Reimer, 1993; Reimer et al., 2013) with a ΔR correction of 560 years (Bard, 1988).

## 4.3. Results

All the results presented in this study are available in the database of PANGAEA® (www.pangaea.de)

### .4.3.1. Neodymium and strontium isotope composition of the detrital fraction

Detrital $\varepsilon_{Nd}$ signatures (Table 4.1) show the most positive $\varepsilon_{Nd}$ signatures at the locations nearest to the continental landmasses (Fig. 4.2), ranging from -3 to -4 off New Zealand and from -1 to -4 in the Chile basin. The signatures become significantly less radiogenic as the distance from the continents increases, with the marked exception of station 57-1, located at the summit of the East Pacific Rise (EPR), which shows an $\varepsilon_{Nd}$ value of -2.6 pointing to a significant contribution of mantle-derived rocks. Compared to the seawater signatures at the same or nearby stations (Molina-Kescher et al., 2014), the detrital $\varepsilon_{Nd}$ signatures show more radiogenic values than the bottom waters for the entire study area (Fig. 4.3). The difference between bottom waters and detrital Nd isotopic compositions varies between 6 and 1 $\varepsilon_{Nd}$ units, with the largest difference found for sample 79-1 and the waters of MuC-79 in the Bounty Trough off New Zealand and the smallest difference occurring for sample 68-1 and water sample 66-2200, both obtained in the centre of the Southwest Pacific Basin near 2000 metres water depth.

The distribution pattern observed for Nd isotopes is mirrored by the detrital Sr isotope compositions (Fig. 4.2). The least radiogenic values occur near the continental margins: 0.70655 for the sample closest to Chile (22-2) and 0.70716 and 0.70766 for the two westernmost samples (87-1 and 85-1; respectively) located on the western Chatham Rise, whereas the values in the central South Pacific range from 0.709 to 0.710. The detrital Sr isotope signature of sample 57-1 is significantly less radiogenic than neighbouring samples also pointing to a contribution of mantle rocks, however, with a less pronounced difference than in the case of Nd isotopes. This exceptional and marked difference towards less (more) radiogenic Sr (Nd) isotope compositions of sample 57-1 is due to an increased abundance of black basaltic particles of around 5% as observed under a light microscope. These particles are in the same size range as the foraminifera

that compose around 95% of the sample and most likely originate from the Mid Oceanic Ridge (MORB). This finding points to submarine volcanic eruptions contributing to the sediment close to the active hydrothermal regions, in this case, the summit of the East Pacific Rise. This supports previous evidences of explosive eruptions at mid-ocean ridges (Clague et al., 2009; Helo et al., 2011). Similar particles were not found in the other samples of this study.

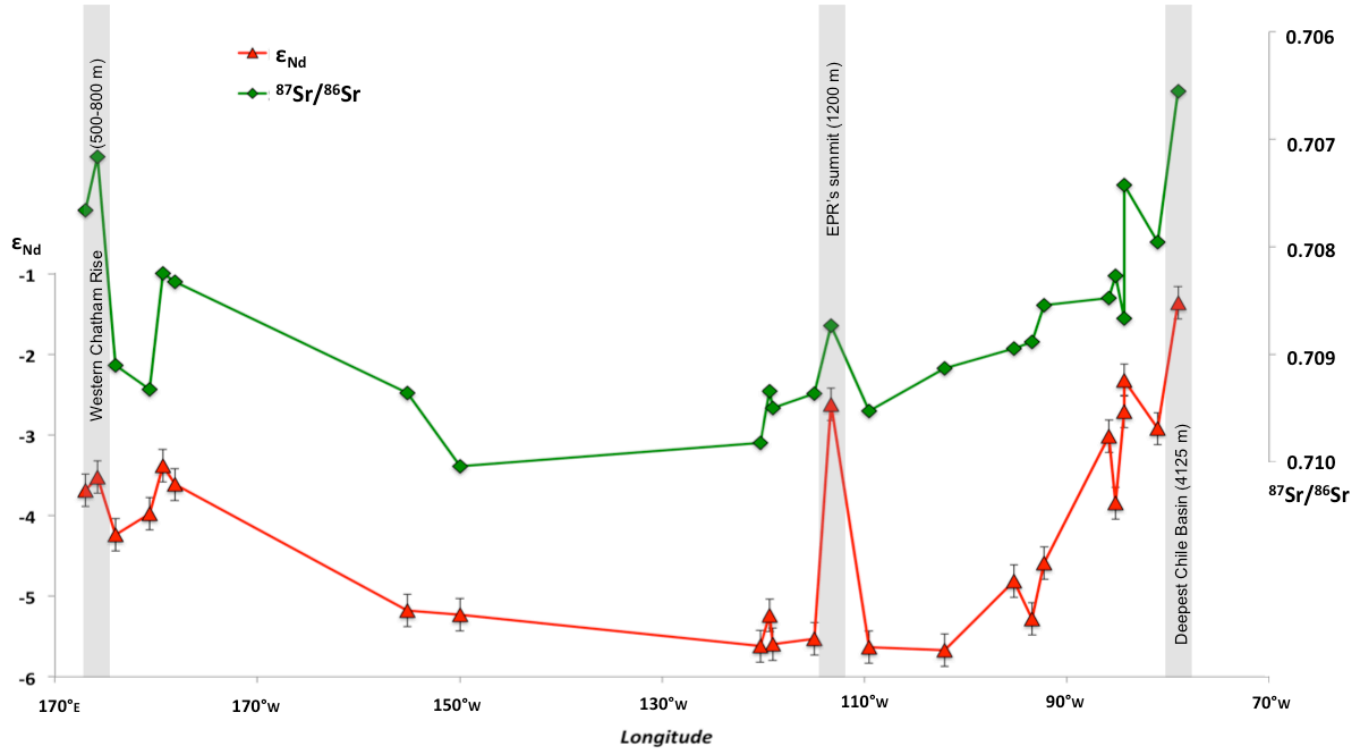


***Figure 4.2.*** *Spatial distribution of surface sediment detrital Nd and Sr isotope compositions in the South Pacific along the longitudinal section of SO213. The most radiogenic (unradiogenic) Nd (Sr) samples are highlighted by grey bars indicating their location and depth.*

| Sample | $^{87}Sr/^{86}Sr$ Detritus | 2σ s. d. | $^{87}Sr/^{86}Sr$ decarbonated Leachates | 2σ s. d. | Al/Ca unclean Foram (µmol/mol) | $^{14}C$ Date (Y.b.p.) |
|---|---|---|---|---|---|---|
| **01-1** | 0.70827 | 0.00002 | 0.70928 | 0.00003 | *B.d.l.* | 7982 ± 217 |
| **06-1** | - | - | 0.70919 | 0.00003 | *B.d.l.* | - |
| **07-1** | - | - | 0.70966 | 0.00003 | - | 16261 ± 542 |
| **08-1** | 0.70895 | 0.00002 | 0.70918 | 0.00002 | *B.d.l.* | 17267 ± 606 |
| **10-1** | - | - | 0.70918 | 0.00002 | *B.d.l.* | - |
| **12-1** | 0.70847 | 0.00002 | 0.70917 | 0.00003 | 1 | - |
| **14-1** | - | - | - | - | 42 | - |
| **15-1** | - | - | 0.70917 | 0.00003 | - | - |
| **17-1** | 0.70867 | 0.00002 | 0.70920 | 0.00003 | *B.d.l.* | 24226 ± 811 |
| **19-1** | - | - | 0.70920 | 0.00003 | - | - |
| **20-1** | 0.70796 | 0.00002 | 0.70914 | 0.00003 | 9 | 4142 ± 259 |
| **22-4** | 0.70655 | 0.00002 | 0.70920 | 0.00003 | - | - |
| **24-2** | - | - | 0.70920 | 0.00003 | *B.d.l.* | - |
| **26-1** | 0.70953 | 0.00002 | 0.70925 | 0.00003 | *B.d.l.* | - |
| **49-3** | - | - | - | - | *B.d.l.* | - |
| **54-4** | 0.70982 | 0.00002 | 0.70938 | 0.00003 | 7 | - |
| **57-1** | 0.70873 | 0.00002 | 0.70919 | 0.00003 | *B.d.l.* | - |
| **59-1** | - | - | - | - | *B.d.l.* | 8001 ± 210 |
| **60-2** | 0.70934 | 0.00004 | 0.70919 | 0.00003 | - | 11169 ± 246 |
| **61-1** | - | - | - | - | - | - |
| **63-1** | 0.70950 | 0.00002 | 0.70953 | 0.00003 | *B.d.l.* | - |
| **64-2** | | | 0.70920 | 0.00003 | 3 | |
| **66-5** | - | - | - | - | - | - |
| **68-1** | 0.70936 | 0.00002 | 0.70921 | 0.00002 | *B.d.l.* | - |
| **76-1** | 0.70832 | 0.00002 | 0.70906 | 0.00002 | - | - |
| **78-1** | 0.70825 | 0.00002 | 0.70919 | 0.00002 | 47 | - |
| **79-1** | 0.70933 | 0.00002 | 0.70941 | 0.00002 | 41 | - |
| **81-1** | 0.70910 | 0.00002 | 0.70940 | 0.00002 | *B.d.l.* | - |
| **84-2** | | | 0.70918 | 0.00002 | 362 | 4952 ± 238 |
| **85-1** | 0.70716 | 0.00002 | 0.70945 | 0.00002 | 229 | - |
| **87-1** | 0.70766 | 0.00002 | 0.70906 | 0.00002 | - | - |

***Table 4.2.*** *Sr isotope compositions, Aluminium to Calcium ratios for 'uncleaned' planktonic foraminifera and available radiocarbon ages for the core-top samples analysed in this study.*

### 4.3.2. Neodymium and strontium isotope signatures in leachates, foraminifera and fish teeth

The average $\varepsilon_{Nd}$ signatures from the four different methods used in this study to obtain authigenic seawater signatures from the sediment are as follows; -5.9 for 'non-decarbonated' leachates, -5.8 for 'unclean' planktonic foraminifera, -5.1 for fossil fish teeth and -4.8 for 'decarbonated' leachates. The average $\varepsilon_{Nd}$ signature of all water samples, obtained from the same depth range as the core tops, is systematically less radiogenic (-7.5) than of the signatures extracted from the sediments. This difference, however, varies substantially between different areas of our study. The best agreement is observed in the Chile Basin (Fig. 4.3e) and East Pacific Rise (Fig. 4.3c) where some of the authigenic sedimentary signatures agree within error with the bottom water compositions. The largest differences between seawater and 'unclean' forams are observed above the Chile Rise (Fig. 4.3d). Generally the results of the 'decarbonated' leaching method were most different from the seawater signatures.

The $^{87}Sr/^{86}Sr$ ratios obtained for the 26 'decarbonated' leachates differ substantially from that of the detritus (Fig. 4.4) and average 0.70925 (±0.0003). This is close to the established seawater value of 0.70918 (e.g. Henderson et al., 1994) and thus apparently supports that the $\varepsilon_{Nd}$ values obtained from the 'decarbonated' leachates are entirely seawater derived. However, as discussed below in section 4.4.2.2 the interpretation is more complex.

### 4.3.3. Elemental ratios and REE concentrations of the 'unclean' foraminifera

Al/Ca ratios and REE patterns were obtained on the dissolved 'unclean' foraminifera in order to detect any potential detrital contributions to the authigenic bottom water $\varepsilon_{Nd}$ signal recorded by the Fe-Mn coatings of the planktonic foraminifera shells.

Al/Ca ratios (table 4.2) were below detection limit in 13 of 22 samples and below 100 μmol/mol in the rest of the samples except 84-2 and 85-1. Values above 100 μmol/mol have been considered to indicate clay contamination of the samples (Ni et al., 2007; Kraft et al., 2013). Only samples 84-2 (362 μmol/mol) and 85-1 (229 μmol/mol), located very close to South Island of New Zealand on the Western Chatham Rise (Fig. 4.1) show Al/Ca ratios above 100 μmol/mol indicating that the extracted Nd isotope ratios of these two samples might be slightly contaminated by the detrital Nd isotope composition (see section 4.4.2.2.). The REE concentration patterns normalized to the Post Achaean Australian Sedimentary Rocks (PAAS) (Taylor and McLennan, 1985)(Table 4.3 and figure 4.5), show seawater-like patterns for all unclean foraminifera samples, including a marked Ce anomaly and a progressive light to heavy increase in REE abundance, although the HREE enrichment is less pronounced than in seawater.

The Ce anomaly is, however, smaller near the New Zealand Margin, such as in sample 84-2 (Fig. 4.5). In figure 4.5 the shape of the REE patterns of 'unclean' foraminifera and seawater of this and other studies (e.g. Martin et al., 2010) is compared and suggests that detrital contributions do not affect the REE concentrations of the Fe-Mn coatings extracted from 'unclean' foraminifera(R=0.86). These data generally support the bottom seawater origin of the $\varepsilon_{Nd}$ signatures obtained from 'unclean' foraminifera shells, except for samples 84-2 and 85-1.

| Sample | Latitude | Longitude | Depth (m) | La | Ce | Pr | Nd | Sm | Eu | Gd | Tb | Dy | Ho | Er | Tm | Yb | Lu |
|---|---|---|---|---|---|---|---|---|---|---|---|---|---|---|---|---|---|
| SO213- 01-1 | 36° 13' S | 85° 2' W | 2806 | 2.14 | 0.35 | 2.00 | 2.41 | 3.08 | 3.89 | 4.39 | 4.93 | 5.34 | 5.55 | 6.27 | 6.60 | 6.28 | 6.10 |
| SO213- 06-1 | 37° 21' S | 92° 23' W | 2791 | 2.22 | 0.15 | 2.10 | 2.63 | 3.31 | 4.23 | 4.74 | 5.04 | 5.61 | 5.60 | 6.34 | 6.80 | 6.49 | 5.89 |
| SO213- 08-1 | 37° 29' S | 95° 21'W | 2171 | 2.30 | 0.22 | 2.07 | 2.60 | 3.15 | 4.08 | 4.74 | 5.14 | 5.91 | 6.36 | 6.79 | 7.66 | 7.33 | 6.68 |
| SO213- 10-1 | 38° 36' S | 93° 43' W | 2996 | 2.70 | 0.23 | 2.75 | 3.38 | 4.17 | 5.22 | 6.08 | 6.50 | 7.20 | 7.18 | 7.77 | 8.25 | 7.89 | 7.09 |
| SO213- 12-1 | 42° 23' S | 85° 28' W | 3016 | 2.66 | 0.49 | 2.69 | 3.68 | 4.34 | 4.96 | 5.85 | 6.47 | 6.81 | 7.11 | 7.75 | 7.93 | 7.93 | 4.49 |
| SO213- 14-1 | 40° 18' S | 84° 29' W | 4052 | 1.33 | 0.20 | 1.71 | 2.06 | 2.60 | 3.07 | 3.41 | 3.48 | 3.37 | 3.17 | 3.28 | 3.55 | 3.22 | 2.91 |
| SO213- 17-1 | 40° 37' S | 84° 30' W | 2561 | 2.17 | 0.31 | 2.06 | 2.59 | 3.15 | 4.21 | 4.70 | 4.96 | 5.61 | 5.93 | 6.47 | 6.81 | 6.98 | 6.26 |
| SO213- 20-1 | 39° 27'S | 80° 18' W | 2702 | 2.52 | 0.31 | 2.15 | 2.67 | 3.28 | 3.97 | 4.75 | 5.24 | 5.97 | 5.99 | 6.46 | 7.33 | 7.11 | 6.62 |
| SO213- 24-2 | 36° 57' S | 102° 07' W | 3092 | 2.38 | 0.12 | 2.51 | 2.95 | 3.82 | 4.75 | 5.40 | 5.99 | 6.60 | 6.43 | 7.09 | 7.60 | 7.38 | 6.63 |
| SO213- 26-1 | 35° 60' S | 109° 55' W | 2830 | 1.70 | 0.04 | 1.74 | 2.13 | 2.82 | 3.51 | 4.12 | 4.52 | 5.07 | 5.26 | 5.69 | 6.03 | 5.78 | 5.38 |
| SO213- 49-3 | 39° 57' S | 114° 1' W | 3380 | 2.64 | 0.12 | 2.89 | 3.48 | 4.46 | 5.46 | 5.86 | 6.63 | 6.89 | 6.79 | 7.19 | 7.42 | 7.08 | 6.65 |
| SO213- 54-4 | 43° 42' S | 120° 30' W | 3840 | 2.93 | 0.49 | 3.51 | 4.10 | 5.35 | 6.16 | 6.58 | 6.97 | 6.95 | 6.50 | 6.82 | 7.01 | 6.40 | 6.11 |
| SO213- 57-1 | 46° 59' S | 113° 27' W | 1194 | 0.93 | 0.17 | 0.83 | 0.99 | 1.23 | 1.59 | 1.86 | 1.93 | 2.26 | 2.39 | 2.63 | 2.68 | 2.62 | 2.44 |
| SO213- 59-1 | 45° 50' S | 116° 53 'W | 3159 | 1.54 | 0.14 | 1.41 | 1.76 | 2.16 | 2.64 | 3.23 | 3.20 | 3.52 | 3.68 | 4.00 | 4.34 | 4.20 | 3.87 |
| SO213- 63-1 | 44° 40' S | 119° 05' W | 3938 | 2.09 | 0.27 | 2.43 | 2.90 | 3.70 | 4.40 | 4.71 | 4.93 | 5.01 | 4.77 | 4.83 | 4.70 | 4.62 | 4.02 |
| SO213- 64-2 | 43° 24' S | 119° 53' W | 3922 | 2.53 | 0.37 | 3.26 | 3.91 | 5.18 | 5.82 | 6.12 | 6.43 | 6.54 | 5.89 | 5.93 | 6.14 | 5.52 | 5.00 |
| SO213- 68-1 | 45° 7' S | 155° 17' W | 1988 | 2.11 | 0.31 | 1.74 | 2.15 | 2.65 | 3.27 | 3.97 | 4.42 | 4.99 | 5.33 | 5.83 | 6.25 | 6.20 | 5.77 |
| SO213- 78-1 | 46° 15' S | 179° 37' W | 3410 | 2.65 | 0.62 | 2.78 | 3.27 | 4.20 | 4.81 | 5.38 | 5.57 | 5.84 | 5.66 | 5.82 | 5.83 | 5.79 | 5.26 |
| SO213- 79-1 | 45° 51' S | 179° 34' E | 3143 | 1.79 | 0.37 | 1.75 | 2.06 | 2.65 | 3.01 | 3.56 | 3.68 | 3.90 | 3.90 | 4.06 | 4.26 | 4.01 | 3.81 |
| SO213- 81-1 | 45° 60' S | 178° 0' E | 2829 | 1.84 | 0.34 | 1.68 | 2.00 | 2.46 | 2.84 | 3.46 | 3.76 | 3.84 | 3.90 | 4.18 | 4.44 | 4.18 | 4.06 |
| SO213- 84-2 | 45° 7' S | 174° 35' E | 992 | 1.30 | 0.56 | 1.31 | 1.55 | 1.90 | 2.14 | 2.64 | 2.74 | 2.85 | 2.80 | 3.09 | 3.14 | 2.92 | 2.85 |
| SO213- 85-1 | 44° 46' S | 174° 32' E | 832 | 1.02 | 0.44 | 1.00 | 1.18 | 1.40 | 1.64 | 2.11 | 2.09 | 2.23 | 2.20 | 2.41 | 2.41 | 2.45 | 1.99 |
| | | | uncertainty (% 2s) -> | 8 | 8 | 8 | 8 | 9 | 9 | 6 | 8 | 6 | 7 | 7 | 33 | 8 | 2 |

***Table 4.3.*** *REE concentrations normalized to PAAS (Taylor and McLennan, 1985) measured on 'uncleaned' planktonic foraminifera samples*

### 4.3.4. $^{14}$C ages of core tops

The $^{14}$C ages of the 8 core-tops analysed (table 4.2) range between 4142 ±259 and 24226 ±811 years, as a consequence of very low sedimentation rates in the open South Pacific that range from less than 1 mm/kyr (Glasby et al., 2007) to 20 mm/kyr (SO213 cruise report). Rates are considerably higher at around 138 mm/kyr on the New Zealand Margin (Carter et al., 1996a), but the Bounty Trough has lower sedimentation rates than other parts of this margin: 3

to 27 mm/kyr (Griggs et al., 1983). This leads to core-tops with a mixed/average age as old as ~24 kyrs before present (17-1) corresponding to the Last Glacial Maximum (LGM) and only two samples (20-1 and 84-2) with middle Holocene ages (4142 ±259 and 4952 ±238 years BP, respectively). All other analysed samples represent the period of the last deglaciation and the early Holocene with an age range between ~8000 and ~17000 years. In addition to the low sedimentation rates, $^{230}$Th analyses performed in the area of this study (Schmitz et al., 1986) found evidence of sediment redistribution processes in the western and central South Pacific that especially influence the areas around the Valerie Passage, where the DWBC intensifies (Carter et al., 1996a).

### 4.4. Discussion

#### 4.4.1. Seawater-sediment interaction and the present day seawater Nd isotope signature

Direct comparison of bottom water $\varepsilon_{Nd}$ signatures with those of the detrital material of our study allows an estimation of the importance of sediment-water interaction including boundary exchange for the seawater Nd cycle in the South Pacific. The New Zealand Margin (Fig. 4.3a) is the area where the differences in $\varepsilon_{Nd}$ signatures between seawater and detritus are largest, reaching up to 6 $\varepsilon_{Nd}$ units. Sediment samples 78-1 and 79-1 are of particular interest for the purpose of this study given that they were obtained together with the overlying bottom water samples (MuC-78 and MuC-79) in the same multicorer tube. In a previous study these water samples were found to be relatively unradiogenic at $\varepsilon_{Nd}$ values of -9.0±0.3 and -10.3±0.3, which was attributed to admixed North Atlantic Deep Water (NADW) (Molina-Kescher et al., 2014). This remnant of NADW has also been documented in this region based on elevated salinity and low nutrient contents (Reid and Lynn 1971; Warren, 1973; Gordon, 1975), which identified upper Lower Circumpolar Deep Water (uLCDW) between 2800 m and 3900 m water depth (Gordon, 1975; Warren, 1981; McCave et al., 2008; Noble et al., 2013). The large difference between the Nd isotope compositions of detritus and seawater observed in our study shows that sedimentary contributions do not play a significant role for setting the dissolved Nd isotope signature of the bottom waters of this region and confirm the advective origin of these relatively unradiogenic seawater signatures. This suggests the absence of boundary exchange in the Deep Western Boundary Current (DWBC) of the Southwest Pacific (Molina-Kescher et al., 2014), in contrast to the observations in the DWBC of the Southwestern Indian Ocean (Wilson et al., 2012).

The relatively unradiogenic residual $\varepsilon_{Nd}$ signature of NADW observed on the southern flank of the Chatham Rise disappears quickly to the north of our sampling sites as documented by Holocene 'unclean' planktonic foraminifera $\varepsilon_{Nd}$ data of -6.8 ±0.4 obtained at the northern flank of the Chatham Rise (Noble et al. 2013). This suggests a clear separation of the hydrography on both sides of it in terms of dissolved Nd isotope compositions with a clear dominance of Pacific derived waters on the northern flank of Chatham Rise, similar to observations based on hydrographic parameters (McCave et al., 2008; Bostock et al., 2011). The difference may also be the result of a recent change in the circulation (see section 4.4.2.1). However, the absence of dissolved seawater $\varepsilon_{Nd}$ measurements from the northern Chatham Rise does not allow verification of these hypotheses as yet and although boundary exchange (Noble et al., 2013) may be responsible for significant modifications of seawater $\varepsilon_{Nd}$ signatures, its absence in this study suggests these processes are spatially and temporally variable.

Hydrothermal contributions to seawater Nd isotope compositions of the East Pacific Rise are also insignificant given that the highly radiogenic Nd contributions of MORB to the detrital fraction of sample 57-1 (see section 4.3.1) are not reflected in the corresponding seawater signatures of profiles 50 and 54 between 700 m and 1900 m (Fig. 4.3c).

### 4.4.2. Reliable extraction of the seawater Nd isotope signatures from the sediments

One of the main goals of this study is a comparison of the results of the different methods to extract bottom water Nd isotope compositions to the signatures of the overlying water column and of the detrital fraction in order to identify the most appropriate technique for future paleoceanographic reconstructions of the deep water circulation in this area. This comparison, presented in figure 4.3, shows that the reliability of the different methods changes considerably between locations, although 'unclean' planktonic foraminifera, leachates and fish teeth display $\varepsilon_{Nd}$ values close to the respective seawater signatures and are therefore considered the best techniques. Although mostly yielding trends and changes with water depth similar to seawater $\varepsilon_{Nd}$, the results of all sediment extraction techniques applied here are offset to more radiogenic Nd isotope compositions and thus towards the compositions of the detrital material. It might be argued that the offset between sedimentary and seawater $\varepsilon_{Nd}$ signatures is a consequence of partial dissolution of the detrital fraction, which during the extraction procedures biased the extracted seawater Nd isotope compositions. This is most probably the case for samples 84-2 and 85-1 and for the 'decarbonated' leachates in near coastal areas (see sections 4.4.2.2 and 4.4.2.3) but cannot explain the foraminifera and fish teeth data. In addition, based on Al/Ca and

REE patterns obtained for the same samples this offset is most likely the result of the relatively old mixed age of the core-top sediments (see section 4.4.2.1)

The presence of basaltic material in the sediment of sample 57-1 on the East Pacific Rise (Fig. 4.3c) is not reflected in the leached authigenic Nd isotope signatures of the same samples. This suggests an insignificant hydrothermal contribution to these sediments and documents that the seawater signature can be extracted reliably despite the presence of basaltic material in the sediments.

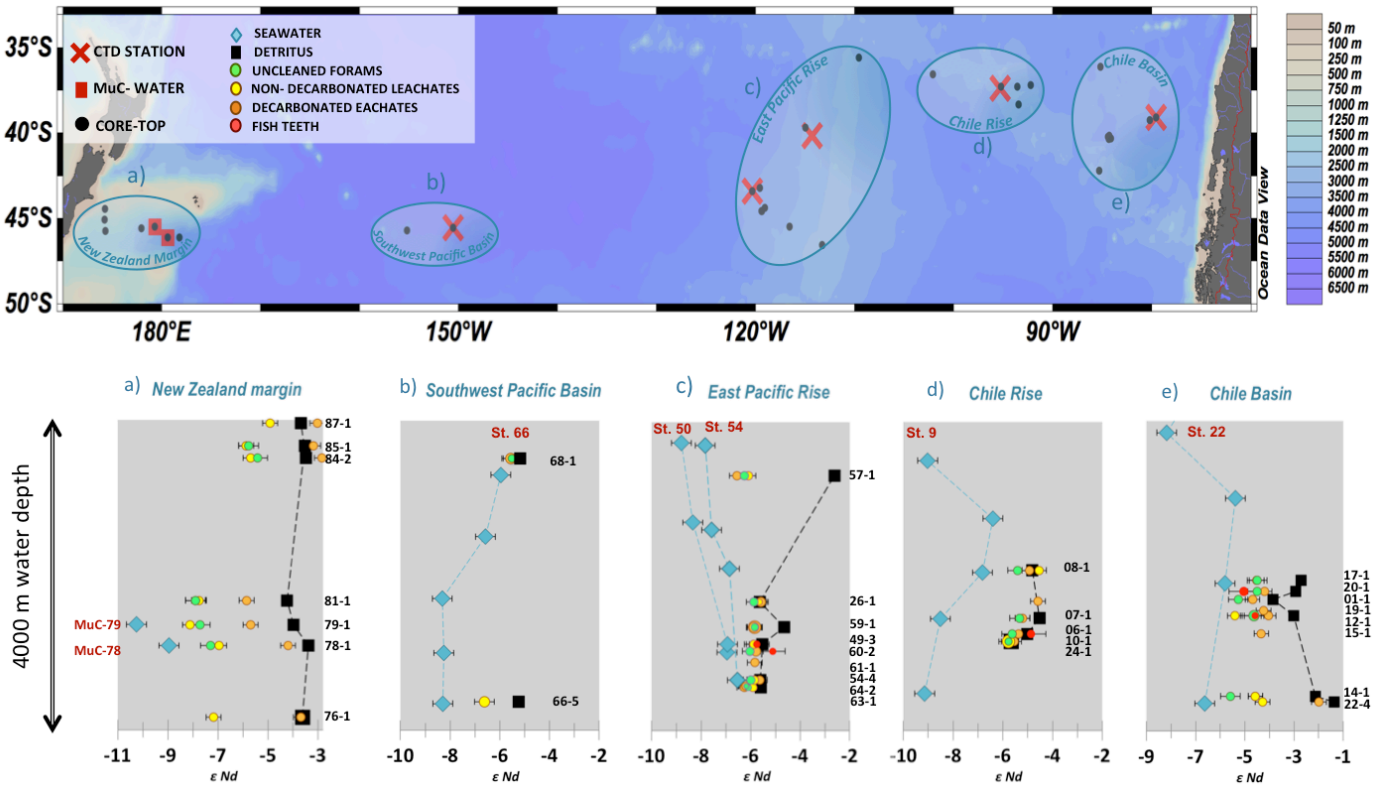


***Figure 4.3.*** *Nd isotope compositions with corresponding 2σ external reproducibilities for seawater (data from Molina-Kescher et al., 2014), detrital fractions and the different methods applied for the extraction of authigenic, seawater derived $\varepsilon_{Nd}$ signatures plotted against water depth. The data are grouped in five different plots that correspond to specific regions marked by blue circles on the map on top. Every sample is identified to the right of the plots. Symbols are defined on the legend at the top-left corner of the figure. The nomenclature of the samples on the map is provided on figure 4.1.*

### 4.4.2.1. Integration of $\varepsilon_{Nd}$ values from seawater subject to different circulation states

The extremely low sedimentation rates in the South Pacific result in the integration of seawater $\varepsilon_{Nd}$ values reflecting different circulation states of the past up to ~24000 years. Al/Ca ratios and REE patterns (section 4.3.3.) measured in 'unclean' foraminifera in almost all cases clearly support an essentially pure seawater origin of the $\varepsilon_{Nd}$ signatures for the latter method, which consequently also supports the same origin for Nd extracted from the fish teeth and 'non-

decarbonated' leachates given that all three methods generally yield identical Nd isotope compositions within error.

Figure 4.5 shows that the REE concentration patterns of our 'unclean' foraminifera are more similar to seawater than in other studies. Authigenic sedimentary REE extractions usually present a characteristic middle REE enrichment ('MREE-bulge') as a consequence of diagenesis (Martin et al., 2010 and references therein; Kraft et al., 2013). In contrast, we observe lower MREE/MREE* ratios compared to other studies. This suggests a lower pore water contribution than in other regions despite the old ages of the core tops, which is probably consequence of prevailing oxic conditions in the bottom waters (Haley et al., 2004).

The integration of signatures from different periods of time results in some important observations: In the case of the water and sediment samples simultaneously retrieved within the same multicore tube from the New Zealand margin (MuC-78, 78-1 and MuC-79, 79-1)(Fig. 4.3a), the relatively unradiogenic seawater $\varepsilon_{Nd}$ signal (-9.0 and -10.3 respectively) does not match 'unclean' foraminifera $\varepsilon_{Nd}$ signatures (-7.3 ±0.4 and -7.7 ±0.4, respectively) but agrees with Holocene 'unclean' foram data (-6.8 ±0.4) from the northern flank of the Chatham Rise (Noble et al., 2013), obtained at 500 to 1000 km to the north of our location on similar depths (~ 3200 m)(see Fig. 4.1). This suggests that the remnant of NADW identified by the seawater Nd isotope composition (see section 4.4.1) only represents a 'snapshot' of today's seawater composition, most probably caused by a recent change in the circulation of the area that has not yet been transferred to the sedimentary record. A similar observation was made in the Chile Rise area (Fig. 4.3 d), where an offset between the integrated LGM-Holocene sedimentary $\varepsilon_{Nd}$ signatures and the prevailing seawater Nd isotope compositions (~ 4 $\varepsilon_{Nd}$ units) is found that is considerably larger than the offsets in the adjacent Chile Basin and East Pacific Rise areas (Fig. 4.3 c and e). Today the deeper part of the Chile Rise area between 90°W and 110°W is occupied by CDW and thus relatively negative seawater Nd isotope compositions prevail. A deepening of NPDW during glacial periods as already deduced in many paleoceanographic studies (Matsumoto et al., 2002 and references therein) may thus explain the large seawater-sediment $\varepsilon_{Nd}$ offset in this compared to the adjacent areas.

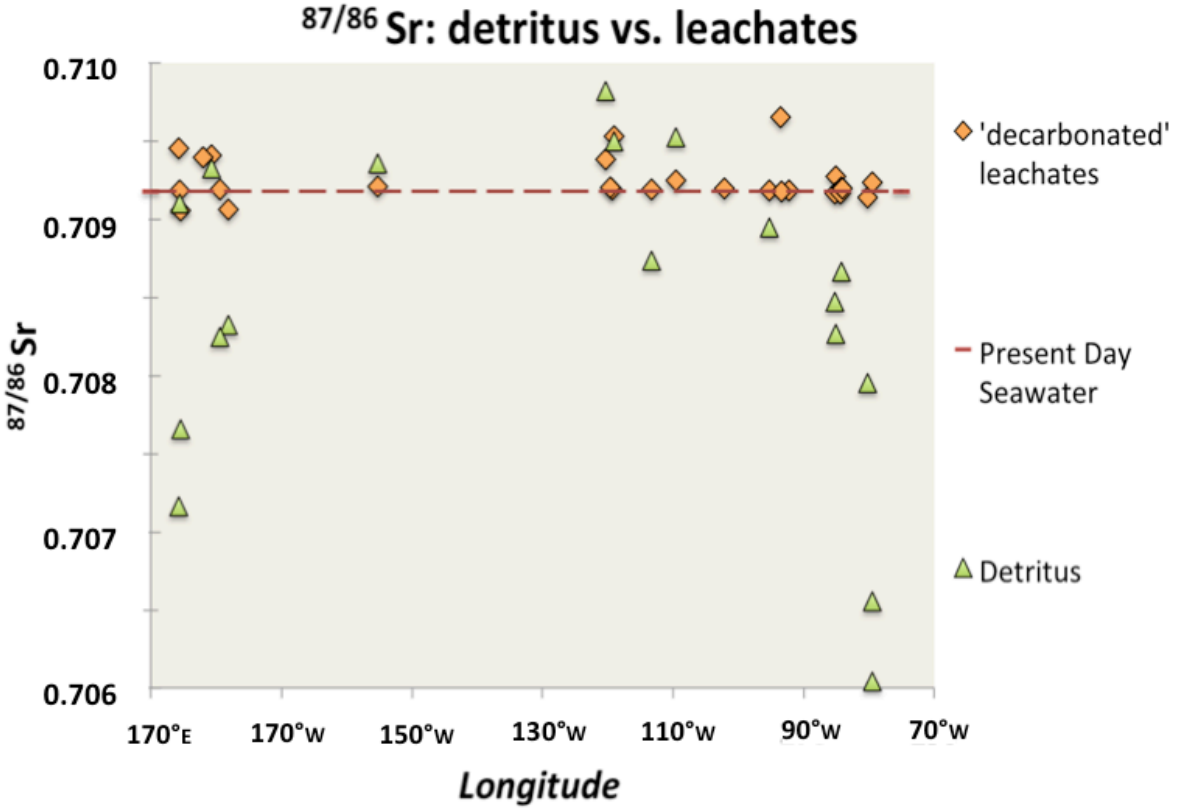


***Figure 4.4.*** *Sr isotope compositions of detritus and 'decarbonated' leachates against longitude. The present day seawater ratio is marked by the dashed line.*

#### 4.4.2.2. Detrital contributions.

Although 'unclean' foraminifera have generally proven to be reliable recorders of seawater Nd isotope compositions (e.g. Roberts et al., 2010; Tachikawa et al., 2014), in this study the two samples from locations closest to land, namely 84-2 (995 m depth) and 85-1 (832 m depth), show relatively high Al/Ca ratios of 362 μmol/mol and 229 μmol/mol. This indicates that the extracted Nd isotope signatures were slightly affected by lithogenic clay contributions from nearby New Zealand and thus show $\varepsilon_{Nd}$ signatures more radiogenic (-5.4 ±0.3 and -5.8 ±0.3 respectively) than expected for Antarctic Intermediate Water (AAIW) prevailing at the water depths of these two samples. Foraminiferal Nd isotope data obtained from settings close to the coast may generally be biased and therefore should be accompanied by elemental data to ensure that the removal of detrital material was sufficient. Similar observations have been made in other near coastal areas, such as the Gulf of Guinea (Kraft et al., 2013).

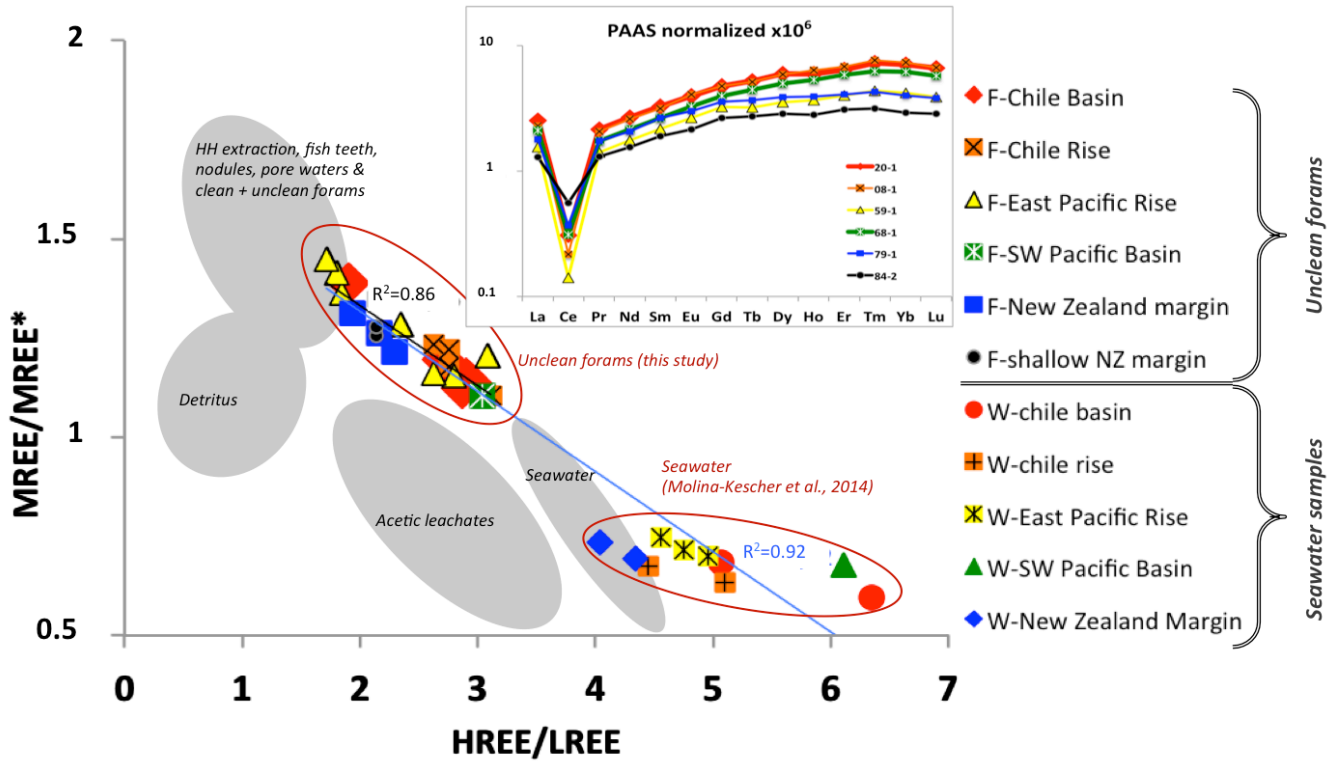


***Figure 4.5.*** *HREE/LREE (Tm+Yb+Lu/La+Pr+Nd) versus MREE/MREE* (Gd+Tb+Dy/LREE+HREE) of the REE concentrations normalized to Post-Achaean Australian Sedimentary Rocks (PAAS) (Taylor and McLennan, 1985) measured on 'unclean' planktonic foraminifera samples of the different areas analyzed in this study (see legend: areas defined in figure 4.3) and from seawater samples obtained for the same locations and depths (Molina-Kescher et al., 2014). Shaded grey areas from Martin et al., (2010) (references therein) and Kraft et al., (2013) are shown for comparison. PAAS normalized patterns from selected samples of each area are also presented in the smaller subplot.*

#### 4.4.2.3. Failure of 'decarbonated' leachates as recorders of seawater Nd isotope compositions in near coastal regions.

A decarbonation step prior to the HH-leach of the bulk sediment has been a commonly used procedure of the seawater Nd isotope extraction methods for the reconstructions of past deep water circulation regimes (e. g. Piotrowski et al., 2005, 2008; Gutjahr et al, 2007; 2008). In our study area, 'decarbonated' leachates are, however, clearly biased toward lithogenic signatures in near coastal locations, such as the New Zealand Margin (Fig. 4.3a) and the Chile Basin (Fig. 4.3e). The $\varepsilon_{Nd}$ signatures of the unclean forams and leachates are significantly different from the 'decarbonated' leachates, with the latter in most cases being similar to or indistinguishable from the signatures of the detrital fraction. As shown by Wilson et al. (2013), the use of an acetic acid decarbonation step prior to the HH leach results in the partial dissolution of remaining non-authigenic phases, in our case mostly of readily acid-soluble particles of volcanic origin, which alter the signatures extracted by 'decarbonated' leaching. It is evident that this procedure fails to provide reliable bottom water $\varepsilon_{Nd}$ signatures in near coastal

regions of the South Pacific, whereas at the open ocean sites the results of all extraction methods applied, including 'decarbonated' leaching, are identical within error and are thus considered reliable. This complements results from the North Atlantic (Elmore et al., 2011), where 'decarbonated' leaching failed to produce the seawater Nd isotope composition near active volcanic settings such as Iceland. On the other hand, 'decarbonated' leaching has been shown to be a reliable technique in other open ocean regions such as the Western North Atlantic (Gutjahr et al., 2008), the Indian Ocean (Piotrowski et al., 2009) or the Atlantic sector of the Southern Ocean (Piotrowski et al., 2005; 2012) among other regions. The success of this technique may therefore be related to the absence of active volcanism in the studied area. And, as shown in section 4.3.2. and figure 4.4, obtaining a Sr isotope signature close to that of modern seawater in the 'decarbonated' leachates does not serve as a proof for a seawater Nd isotope signature.

### 4.4.3. Provenance of detrital material in the South Pacific deduced from Nd-Sr isotope compositions.

The clear general trend to more positive (negative) Nd (Sr) isotope signatures of the detritus at the ocean margins shown in figure 4.2 demonstrates the importance of the erosion of young volcanogenic material from South America and New Zealand. Figures 4.6 and 4.7 compare combined Nd and Sr isotope compositions of the samples of this study (symbols) with those of the lithologies and fine particles from the surrounding landmasses, which are the most likely source regions of the weathered terrigenous material supplied to the South Pacific (shaded areas).

#### 4.4.4.1 New Zealand Margin

Figure 4.6 compares the isotopic compositions of the samples obtained from the New Zealand Margin sediments (orange diamonds) with the lithologies of the two dominant rock types of these islands: volcanoclastic rocks predominant in North Island (red), where active volcanic regions such as the Taupo Volcanic Zone are present and therefore similar in isotope composition to MORB; and Torelesse Terrane metasediment (blue), a dominant New Zealand sedimentary sequence that dominates the eastern flank of New Zealand's Alps of the South Island (Adams et al., 2005). Combined detrital Nd-Sr isotope compositions of West Antarctica and Ross sea sediments are also shown (green).

We observe essentially the same Nd isotope compositions for all detrital samples in this area, whereas the $^{87}Sr/^{86}Sr$ ratios vary between 0.7072 and 0.7093. The samples obtained at Western Chatham Rise, 87-1 and 85-1, are the shallowest (542 and 842 m) and closest to the

South Island (~200 km from the coast). These samples clearly overlap with the lithological range of the Torelesse rocks of the eastern New Zealand Alps, which is the source region for the weathered material to the entire Bounty Trough sedimentary system (Carter and Carter, 1996). The volcanic material from the North Island apparently does not reach our study area.

Samples 76-1, 78-1, 79-1 and 81-1, obtained in the Bounty Trough between 500 and 850 km off the coast from water depths between ~2800 and ~4400 m, show higher $^{87}Sr/^{86}Sr$ ratios than the sediments from the Western Chatham Rise and their expected source (eastern NZ Alps). This most probably indicates a fractionation of Sr isotopes due to grain size effects (Innocent et al., 2000; Tütken et al., 2002), which has been shown to result in more radiogenic $Sr^{87}/Sr^{86}$ ratios as particle grain size decreases. This is consistent with the fact that these locations are most distant from the coast and are the deepest samples, which are expected to be primarily composed of finer particles due to longer transport. These four samples show similar bulk detrital Sr isotope composition to samples obtained from the northern flank of the Chatham Rise (Graham et al., 1997; Noble et al., 2013) characterized by $Sr^{87}/Sr^{86}$ ratios > 0.709. Variations in the source provenance, which seems less probable due to the short distance to New Zealand, could also explain the mismatch between New Zealand's Torelesse rocks and samples 76-1, 78-1, 79-1 and 81-1. The similarity of the isotopic composition of these samples to circumantarctic detritus may suggest that a part of the lithogenic material that reaches the Bounty Trough may originate from Antarctica and has been transported in suspension in circumpolar waters and the DWBC. Where this current originates, south of the Bounty Trough, it initially decelerates because of its loss of momentum when it detaches from the ACC (Carter et al., 1996a). This effect could be the cause for the settling of the transported fine particles. A similar mechanism has also been invoked for sediments in the Atlantic sector of the Southern Ocean (Franzese et al., 2006).

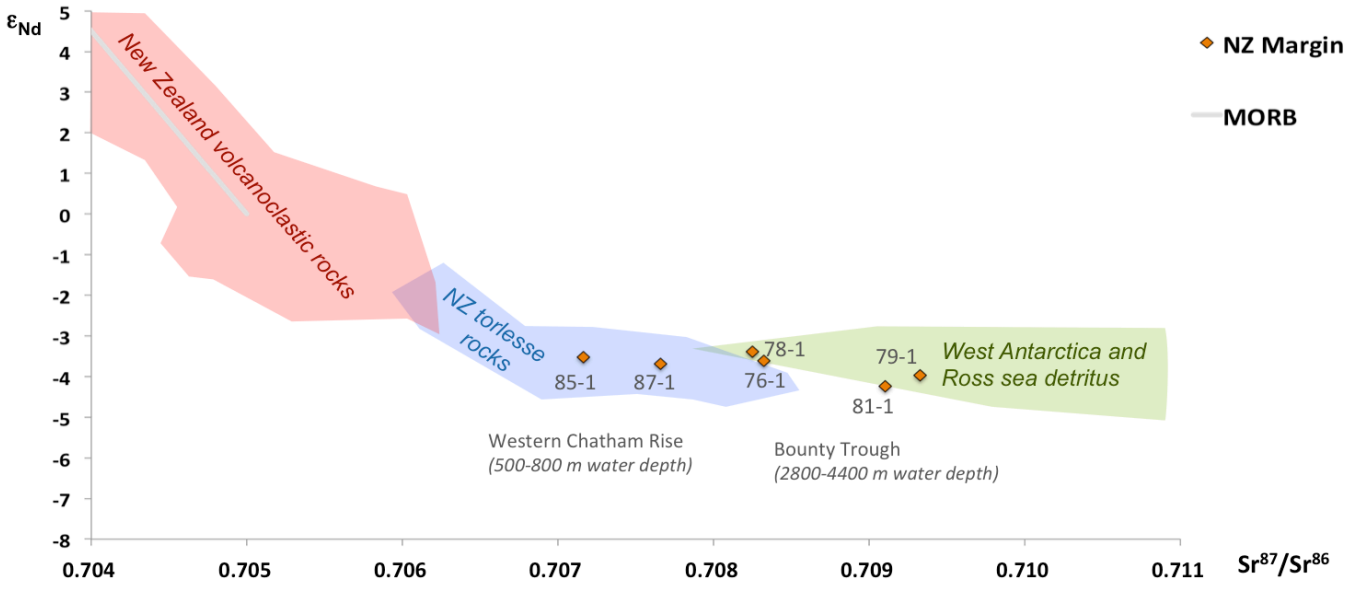


***Figure 4.6.*** *Combined Nd and Sr isotope signatures of detrital core-tops obtained on the New Zealand Margin (orange symbols)(see locations in figures 4.1 and 4.3a), which are subdivided in two groups as a function of distance to New Zealand (Western Chatham Rise < Bounty Trough), and their most probable sources represented by the coloured areas:Volcanoclastic rocks, most representative of North Island (New Zealand) in red (data from: Wandres et al., 2004; Adams et al., 2005); Torlesse metasedimentary rocks, dominant in South Island (New Zealand) in blue (Wandres et al., 2004; Adams et al., 2005); and detrital surface sediments from offshore West Antarctica and the Ross sea (combined from Roy et al., 2007 and Hemming et al., 2007)*

#### 4.4.4.2 Open South Pacific

Figure 4.7 shows the detrital Nd-Sr isotope compositions of this study (diamonds) and that of material that is likely to reach the South Pacific, excluding the samples from the New Zealand Margin (shown in Fig. 4.6),. These are the lithologies of the southern and austral Andes (red field), which will play an important role for the Chile Basin; dust and fine particles from Australia and New Zealand's North and South Islands (blue, yellow and purple fields respectively) brought by the dominant westerlies; and circumantarctic detritus to the south and southwest of the study area (West Antarctica, Ross sea and Wilkes Land) (green and orange fields), from where the dominant oceanic currents may have transported lithogenic material.

Long distance transport from the continental sources allows only very fine-grained particles to reach these distal locations and therefore provenance rather than grain size has apparently been the most important factor controlling the Sr isotope composition of the detrital material in this area. This is also demonstrated by the significant correlation with the Nd isotope compositions of $R^2$=0.81 (excluding sample 57-1, clearly affected by MORB contributions (see section 4.3.1.)). This correlation is geographically consistent given that $\varepsilon_{Nd}$ signatures ($^{87}Sr/^{86}Sr$ ratios) generally decrease (increase) from near South American sites towards the open ocean:

Chile Basin >(<) Chile Rise >(<) EPR and SWP, confirming the Andes as one of the source endmembers. Fine-grain dust from North Island (New Zealand) also falls in the same field as Andean rocks because of its mainly volcanic origin, but it seems less probable that its presence in the detritus increases with distance from New Zealand. Furthermore, the North Island is not under the direct influence of the westerlies as it extends into the subtropical ridge of high pressure (Delmonte et al., 2004) and therefore it is likely only a minor source region of detritus to the eastern South Pacific.

Besides the south and Austral Andes, a second and robust endmember cannot be clearly deduced from figure 4.7 as circumantarctic detritus and aeolian dust from Australia and South Island (NZ) display similar Sr-Nd fields. Nevertheless, almost all samples follow a trend that clearly diverges from the West Antarctica and Ross Sea detritus, except for a few samples from the Chile Basin, which may indeed have been influenced by Antarctic derived material transported to this location by surface currents such as the Humboldt Current.

Therefore the main source candidates for the detritus arriving in the South Pacific remain Australian and South Island (NZ) dust, as suggested by other authors before (e. g. Rea, 1994; Stacin et al., 2008). The large arid continent of Australia, the eastern part of which is affected by the westerlies that move toward the South Pacific (e.g. Leinen et al., 1986; Hesse, 1994), has been even considered as the greatest contributor to atmospheric dust in the Southern Hemisphere (Tanaka and Chiba, 2006). Central and east Australia present a huge variety of lithologies and therefore also display a large Nd-Sr field; nevertheless, the main area providing dust to the South Pacific are the Lake Eyre and Murray River Basins (McTanish, 1989; McGowan and Clark, 2008; Albani et al., 2012), the Nd-Sr isotope composition of which ranges between -3 and -8 and 0.7090 and 0.7019, respectively (Revel-Rolland et al. 2006).

On the other hand, eastern South Island (NZ), although being smaller and wetter, also represents a major dust source to the South Pacific because of its proximity and because it has large loess deposits (Berger et al., 2002; Eden and Hammond, 2003) susceptible to transport by wind, especially during glacial periods when a large part of the New Zealand continental shelf was exposed. During the glacial period the dust deposition in the Pacific sector of the Southern Ocean was higher (e. g. Lamy et al., 2014) and as a consequence of the low sedimentation rates in our study area (see section 4.3.4) significant amounts of southern New Zealand glacial-detritus probably reached our study sites.

In summary, both South Island (NZ) and southeastern Australia probably contribute similar amounts of dust (see also Stancin et al., 2008) and can be considered the major sources of

lithogenic material found in the SW Pacific Basin and Chile Rise near 45°S, confirming the absolute predominance of these dust sources until at least ~110°W in this latitude (McGowan and Clark, 2008; Albani et al., 2012). In contrast, east of this longitude, the influence of these two sources in the detritus decreases, especially in the Chile Basin, where South American material contributes significantly, potentially also receiving supplies from the Antarctic.

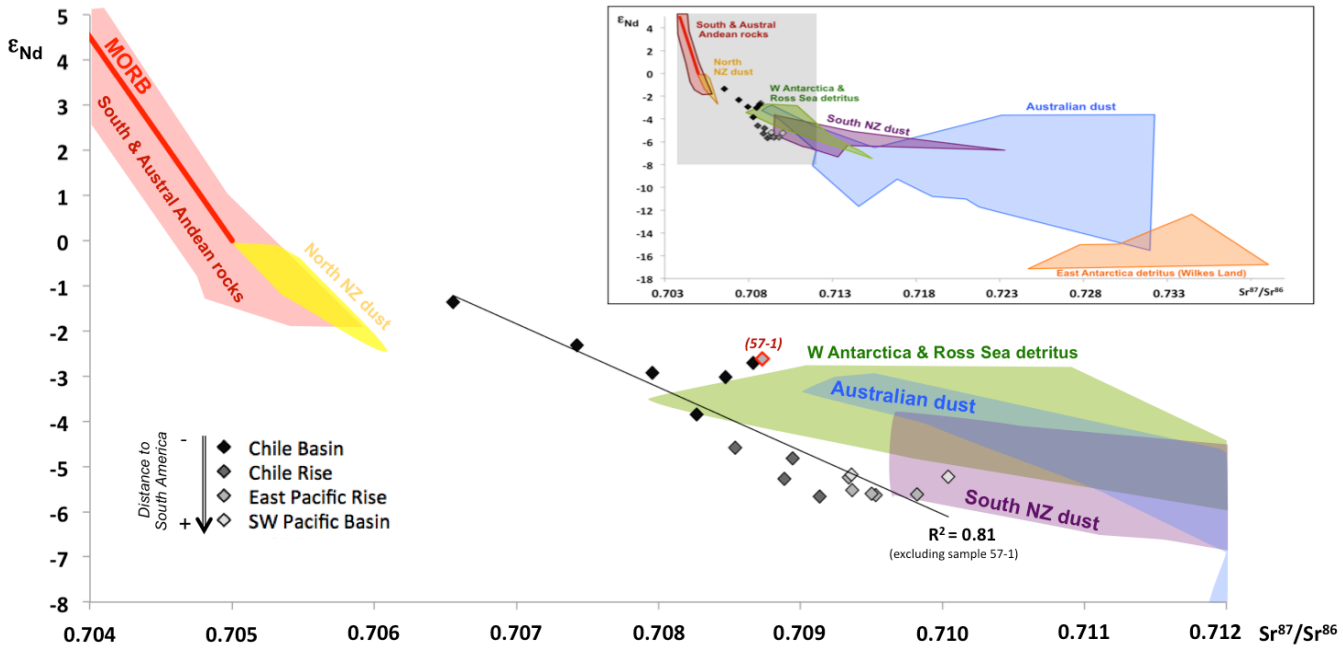


***Figure 4.7.*** *Combined Nd and Sr isotope signatures of detrital core-tops from the open South Pacific (diamonds) grouped by areas (as defined in fig. 4.3) and coded in black to light grey tones as a function to the distance to South America (see legend on figure). The most probable sources that surround the South Pacific are presented as coloured Sr-Nd areas: The Southern (Hickey et al., 1986; Futa and Stern, 1988) and Austral Andes (Futa and Stern, 1988; Stern and Kilian, 1996) combined, in red. Fine-grained particles (<5 μm) susceptible to be transported by wind from: North Island (New Zealand) in yellow (data from Delmonte et al., 2004); South Island (New Zealand) in purple (Taylor et al., 1985; Delmonte et al., 2004); and Eastern Australia in blue (Revel-Rolland et al., 2006). Circumantarctic surface sediments (detritus) from Wilkes Land, in orange; and West Antarctica and Ross Sea, in green (combined from Roy et al., 2007 and Hemming et al., 2007). Note that the smaller subplot shows a larger Nd-Sr area. The grey square on it is shown in detail in the big plot.*

## 4.5. Conclusions

The results of this study suggest that 'boundary exchange' does not play a significant role for the Nd isotope composition of bottom waters of the western South Pacific. No alteration of the bottom waters could be found by comparing core-top detritus with its directly overlying seawater (Molina-Kescher et al., 2014) on a continental margin with high terrigenous input such as the Bounty Trough off New Zealand.

We compared authigenic and detrital core-top $\varepsilon_{Nd}$ signatures to those of bottom waters immediately above in order to identify the most reliable method to extract seawater Nd signatures from South Pacific sediments. Authigenic seawater signatures extracted from 'unclean' planktonic foraminifera; fossil fish teeth and 'non-decarbonated' leachates are offset to more radiogenic vales from seawater $\varepsilon_{Nd}$ signatures. Independent evidence, such as REE patterns and Al/Ca measurements on 'unclean' foraminifera indicate, however, that these three extraction methods effectively record bottom seawater signatures. We suggest that the observed offset between sediment and seawater Nd isotope compositions originates from the low sedimentation rates observed in this area, confirmed by $^{14}C$ ages of up to 24 kyr. Thus the authigenic $\varepsilon_{Nd}$ signature obtained from the core-top sediments integrates the Nd isotope signal of the Holocene and the last glacial to differing extents.

Detrital Nd and Sr isotopes indicate that the dominant sources of terrigenous material reaching the South Pacific between 35°S and 50°S are southeastern Australia and the South Island of New Zealand, the fine grained material of which is transported by the dominant Westerlies. The influence of these two sources decreases towards the west, especially in the Chile Basin, where the detritus contains increased amounts of weathered material from the Southern and Austral Andes. Antarctica may also be a contributing source to the deposited lithogenic material of the South Pacific, especially in the domains of the Deep Western Boundary Current and the Humboldt Current.

**Acknowledgements**

We would like to thank the "Bundesministerium für Bildung und Forschung, Germany" for funding this project (No.: 03G0213B) as well as the crew members and participants of expedition SO213, in particular D. Nürnberg, R. Tiedemann and F. Lamy for organizing and leading the cruise, which was part of the collaborative SOPATRA (SOuth PAcific paleoceanographic TRAnsect) project between the GEOMAR Helmholtz Centre for Ocean Research Kiel and the Alfred Wegener Institute for Polar and Marine Research (AWI) in Bremerhaven. D. Nürnberg provided the $^{14}C$ dating. We also want to thank Chandranath Basak and Ellen E. Martin for helping with the identification of the fish teeth and Jutta Heinze for laboratory assistance.

**References:**


Adams C. J., Pankhurst R. J., Maas R. and Millar I. L. (2005) Nd and Sr isotopic signatures of metasedimentary rocks around the South Pacific margin and implications for provenance. *Geological Society, London*, Special Publications 2005, **246**, 113-141

Albani S., Mahowald N. M., Delmonte B., Maggi V. and Winckler G. (2012) Comparing modeled and observed changes in mineral dust transport and deposition to Antarctica between the Last Glacial Maximum and current climates. *Clym Din*, **38**, 1731–1755

Arsouze T., Dutay J. C., Lacan F. and Jeandel C. (2009) Reconstructing the Nd oceanic cycle using a coupled dynamical – biogeochemical model, *Biogeosciences*, **6**, 2829–2846.

Asahara Y., Takeuchi F., Nagashima K., Harada N., Yamamoto K., Oguri K. and Tadai O. (2012) Provenance of terrigenous detritus of the surface sediments in the Bering and Chukchi Seas as derived from Sr and Nd isotopes: Implications for recent climate change in the Arctic regions, *Deep-Sea Research II*, **61-64**, 155-171.

Bard E. (1988) Correction of accelerator mass spectrometry 14C ages measured in planktonic foraminifera: Paleoceanographic implications, *Paleoceanography*, **3(6),** 635–645, doi:10.1029/PA003i006p00635.

Barrat J. A., Keller F., Amossé J., Taylor R. N., Nesbitt R. W., and Hirata T. (1996) Determination of Rare Earth Elements in sixteen silicate reference samples by ICP-MS after Tm addition and ion exchange separation. *Geostand. Geoanal. Res*. **20**, 133–139.

Basak C., Martin E. E., Horikawa K., and Marchitto T. M. (2010) Southern Ocean source of 14C-depleted carbon in the North Pacific Ocean during the last deglaciation, *Nat. Geosci.,* **3(11**), 770-773.

Bayon G., German C. R., Boella R. M., Milton J. A., Taylor R. N. and Nesbitt R. W. (2002) An improved method for extracting marine sediment fractions and its application to Sr and Nd isotopic analysis. *Chem. Geol.* **187**, 179–199. http://dx.doi.org/10.1016/s0009-2541(01)00416-8.

Berger G.W., Pillans B.J., Bruce J.G. and McIntosh P.D. (2002) Luminescence chronology of loess–paleosol sequences from southern South Island, New Zealand. *Quaternary Science Reviews* **21**, 1899–1913.

Bostock H. C., Hayward B. W., Neil H. L., Currie K. I. and Dunbar G. B. (2011) Deep-water carbonate concentrations in the southwest Pacific. *Deep-Sea Res.*, Part 1, Oceanogr. Res. Pap. 58, 72–85.

Carter R.M. and Carter L. (1996) The abyssal Bounty Fan and lower Bounty Channel: evolution of a rifted-margin sedimentary system. *Mar. Geol.* **130**, 181-202.

Carter L., Carter R.M., McCave I.N. and Gamble J. (1996a) Regional sediment recycling in the abyssal Southwest Pacific Ocean. *Geology* **24**, 735-738.

Carter L., Carter R.M. and McCave I.N. (2004) Evolution of the sedimentary system beneath the deep Pacific inflow off eastern New Zealand. *Marine Geology* **205**, 9–27.

Charbonnier G., Pucéat E., Bayon G., Desmares D., Dera G., Durlet C., Deconinck J-F., Amédro F., Gourlan A. T., Pellenard P. and Bomou B. (2012) Reconstruction of the Nd isotope composition of seawater on epicontinental seas: Testing the potential of Fe-Mn

oxyhydroxide coatings on foraminifera test for deep-time investigations, *Geochim. Cosmochim. Acta,* **99**, 39-56.

Delmonte B., Basile-Doelsch I., Petit J.-R., Maggi V., Revel-Rolland M., Michard A., Jagoutz E. and Grousset F. (2004) Comparing the Epica and Vostok dust records during the last 220,000 years: stratigraphical correlation and provenance in glacial periods. *Earth-Science Reviews* **66**, 63–87.

Dou Y., Yang S., Liu Z., Shi X., Li J., Yu H. and Berne S. (2012) Sr-Nd isotopic constrains on terrigenous sediment provenances and Kuroshio Current variabilita in the Okinawa Trough during the late Quaternary, *Palaeogeography, Palaeoclimatology, Palaeoecology*, **356-366**, 38-47.

Eden D.N. and Hammond A.P. (2003) Dust accumulation in the New Zealand region since the last glacial maximum. *Quaternary Science Reviews* **22**, 2037–2052.

Ehlert C., Frank M., Haley B. A., Böniger U., De Deckker P. and Gingele F. X. (2011) Current transport versus continental inputs in the eastern Indian Ocean: Radiogenic isotope signatures of clay size sediments, *Geochem. Geophys. Geosyst.* **12**, Q06017, doi:10.1029/2011GC003544

Elderfield H., Ferretti P., Greaves M., Crowhurst S., McCave I. N., Hodell D., and Piotrowski A. M. (2012) Evolution of ocean temperature and ice volume through the Mid-Pleistocene Climate Transition, *Science* **337**(6095), 704-709.

Elmore A.C., Piotrowski A.M., Wright J.D. and Scrivner A.E. (2011) Testing the extraction of past seawater Nd isotopic composition from North Atlantic marine sediments. *Geochem. Geophys. Geosyst.* **12**, Q09008, http://dx.doi.org/ doi:09010.01029/02011GC003741.

Fletcher M-S. and Moreno P., I. (2012) Have the Southern Westerlies changed in a zonally symmetric manner over the last 14,000 years? A hemisphere-wide take on a controversial problem. *Quaternary International* **253**, 32-46

Frank M. (2002) Radiogenic isotopes: Tracers of past ocean circulation and erosional input, *Rev. Geophys.,* **40**(1), 1001, doi:10.1029/2000RG000094.

Franzese A. M., Hemming S. R., Goldstein S. L. and R. F. Anderson (2006) Reduced Agulhas leakage at the LGM inferred from an integrated provenance and flux study, *Earth Planet. Sci. Lett.,* **250**, 72–88.

Futa K. and Stern C. R. (1988) Sr and Nd isotopic and trace element compositions of Quaternary volcanic centers of the southern Andes, *Earth Planet. Sci. Lett.,* **88**, 253-262.

Tiedemann R., Lamy F., cruise participants (2014) FS Sonne Fahrtbericht/Cruise Report SO213 - SOPATRA: South Pacific Paleoceanographic Transects - Geodynamic and Climatic Variability in Space and Time, Leg 1: Valparaiso/Chile - Valparaiso/Chile, 27.012.2010 - 12.01.2011, Leg 2: Valparaiso/Chile - Wellington/New Zealand, 12.01.2011 - 07.03.2011. doi:10.2312/cr_so213

Glasby G.P. (1991) Mineralogy, geochemistry, and origin of Pacific red clays; A review: *New Zealand J. of Geol. and Geoph.*, **34**, 167–176.

Glasby G. P. (2007) Broad region of no sediment in the Southwest Pacific Basin: COMMENT AND REPLAY: COMMENT. *Geology* **35**; e132. doi:10.1130/G23843C.1

Goldstein S. L., O'Nions R. K. and Hamilton P. J. (1984) A Sm-Nd isotopic study of atmospheric dusts and particulates from major river systems, *Earth Planet. Sci. Lett.,* **70**, 221–236, doi:10.1016/0012-821X(84)90007-4.

Goldstein S. and S. R. Hemming (2003) Long Lived isotopic tracers in oceanography, paleoceanography and ice-sheet dynamics, *Treatise on Geochemistry*, 6.17, pp. 453–489, Elsevier, New-York.

Gordon A. L. (1975) An Antarctic oceanographic section along 170°E. *Deep-Sea Res.* **22**, 357–377

Graham I.J., Glasby G.P. and Churchman G.J. (1997) Provenance of the detrital component of deep-sea sediments from the SW Pacific Ocean based on mineralogy, geochemistry and isotopic composition. *Marine Geology* **140**, 75–96.

Greaves M. J., Statham P. J. and Elderfield H. (1994) Rare earth element mobilization from marine atmospheric dust into seawater. *Mar. Chem.* **46,** 255–260.

Griggs G. B., Carter L., Kennett J. P. and Carter R. M. (1983) Late Quaternary marine stratigraphy southeast of New Zealand: *Geological Society of America Bulletin*, **94**, 791–797.

Grousset F. and Biscaye P. (2005) Tracing dust sources and transport patterns using Sr, Nd and Pb isotopes. *Chemical Geology* **222**, 149-167.

Gutjahr M., Frank M., Stirling C. H., Klemm V., van de Flierdt T. and A. N. Halliday (2007) Reliable extraction of a deepwater trace metal isotope signal from Fe-Mn oxyhydroxide coatings of marine sediments, *Chem. Geol*., **242**, 351–370, doi:10.1016/j.chemgeo.2007.03.021.

Gutjahr M., Frank M., Stirling C. H., Keigwin L. D. and Halliday A. N. (2008) Tracing the Nd isotope evolution of North Atlantic Deep and Intermediate Waters in the western North Atlantic since the Last Glacial Maximum from Blake Ridge sediments, *Earth Planet. Sci. Lett.,* **266**, 61–77, doi:10.1016/ j.epsl.2007.10.037.

Haley B.A., Klinkhammer G.P. and McManus J. (2004) Rare earth elements in pore waters of marine sediments. *Geochim. Cosmochim. Acta* **68**, 1265–1279.

Hathorne E.C., Haley B.A., Stichel T., Grasse P., Zieringer M. and Frank M. (2012) Online preconcentration ICP-MS analysis of rare earth elements in seawater. *Geochem. Geophys. Geosyst.* **13**, Q01020, doi:10.1029/2011GC003907

Hemming S.R., van der Flierdt T., Goldstein S.L., Franzese A. M., Roy M., Gastineu G. and Landrot G. (2007) Strontium isotope tracing of terrigenous sediment dispersal in the Antarctic Circumpolar Current: Implications for constraining frontal positions, *Geochem. Geophys. Geosyst.* **8**, Q06N13, doi:10.1029/2006GC001441

Henderson G.M., Martel D.J., O'Nions R.K. and Shackleton N.J. (1994) Evolution of seawater $^{87}Sr/^{86}Sr$ over the last 400 ka: the absence of glacial/interglacial cycles, *Earth and Planetary Science Letters* **128**, 643-651, http://dx.doi.org/10.1016/0012-821X(94)90176-7.

Hergt J. M., Chappell B. W., Faure G. and Mensing T. M. (1989) The geochemistry of Jurassic dolerites from Portal Peak Antarctica, *Contributions to Mineralogy and Petrology*, **102**, 198-305

Hesse P.P. (1994) The record of continental dust from Australia in Tasman Sea sediments. *Quaternary Science Reviews* **13**, 257–272.

Hickey R. L., Frey F. A. and Gerlach D. C. (1986) Multiple sources for basaltic arc rocks from the Southern Volcanic Zone of the Andes (34°-41° S): Trace element and isotopic evidence for

contributions from subducted oceanic crust, mantle and continental crust, *J. of Geophysical Research*, **91**, 5963-5983

Horwitz E. P., Chiarizia R. and Dietz M. L. (1992) A novel strontium-selective extraction chromatographic resin. *Solvent Extr. Ion Exch.* **10**, 313–336. http://dx.doi.org/10.1080/07366299208918107.

Huang K-F., Oppo D. W. and Curry W. B. (2014) Decreased influence of Antarctic intermediate water in the tropical Atlantic during North Atlantic cold events. *Earth and Planetary Science Letters* **384**, 200-208

Innocent C., Fagel N. and Hillaire-Marcel C. (2000) Sm-Nd isotope systematics in deep-sea sediments: clay-size versus coarser fractions. *Marine Geology* **168**, 79–87.

Jacobsen S. B. and Wasserburg G. J. (1980) Sm-Nd isotopic evolution of chondrites, *Earth Planet. Sci. Lett.,* **50**, 139–155.

Jones K. M., Khatiwala S. P., Goldstein S. L., Hemming S. R. and van de Flierdt T. (2008) Modeling the distribution of nd isotopes in the oceans using an ocean general circulation model. *Earth and Planetary Science Letters* **272**(3–4), 610–619.

Kamp P. J. J., Green P. F. and White S. H. (1989) Fission track analysis reveals character of collisional tectonics in New Zealand: *Tectonics*, **8**, 169–185.

Kawabe M. and Fujio S. (2010) Pacific Ocean circulation based on observation. *J. Oceanogr.* **66**, 389–403.

Klevenz V., Vance D., Schmidt D.N. and Mezger K. (2008) Neodymium isotopes in benthic foraminifera: core-top systematics and a down-core record from the Neogene south Atlantic. *Earth Planet. Sci. Lett*. **265**, 571–587. doi:10.1016/j.epsl.2007.10.053.

Kraft S., Frank M., Hathorne E. C. and Weldeab S. (2013) Assessment of seawater Nd isotope signatures extracted from foraminiferal shells and authigenic phases of Gulf of Guinea sediments, *Geochim. Cosmochim. Acta* **121**, 414-435.

Lacan F. and Jeandel C. (2005) Neodymium isotopes as a new tool for quantifying exchange fluxes at the continentocean interface, *Earth Planet. Sci. Lett.,* **232**, 245–257.

Lamy F., Gersonde R., Winckler G., Esper O., Jaeschke A., Kuhn G., Ullermann J., Martinez-Garcia A., Lambert F. and Kilian R. (2014) Increased Dust Deposition in the Pacific Southern Ocean During Glacial Periods. *Science* **343**, 403. DOI: 10.1126/science.1245424

Le Fevre B. and Pin C. (2005) A straightforward separation scheme for concomitant Lu–Hf and Sm–Nd isotope ratio and isotope dilution analysis. *Anal. Chim. Acta* **543**, 209–221.

Leinen M., Cwienk D., Heath G.R., Biscay P.E., Kolla V., Thiede J. and Dauphin J.Pl. (1986) Distribution of biogenic silica and quartz in recent deep-sea sediments. *Geology* **14**, 199–203.

Martin E.E. and Scher H.D. (2004) Preservation of seawater Sr and Nd isotopes fossil fish teeth: bad news and good news. *Earth Planet. Sci. Lett.* **220**, 25–39.

Martin E. E., MacLeod K. G., Jiménez Berrocoso A. and Bourbon E. (2012) Water mass circulation on Demerara Rise during the late Cretaceous based on Nd isotopes. *Earth Planet. Sci. Lett.* **327-328**, 111–120.

Marx S. K., Lavin K. S., Hageman K. J., Kamber B. S., O'Loingsigh T. and McTainsh G. H. (2014). Trace elements and metal pollution in aerosols at an alpine site, New Zealand: sources, concentrations and implications. *Atmospheric Environment*, **82**, 206-217.

McCave I. N., Carter L. and Hall I. R. (2008) Glacial–interglacial changes in water mass structure and flow in the SW Pacific Ocean. *Quat. Sci. Rev.* **27**,1886–1908, http://dx.doi.org/10.1016/j.quascirev.2008.07.010

McTainsh G.H. (1989) Quaternary aeolian dust processes and sediments in the Australian region. *Quaternary Science Reviews* **8**, 235–253.

Matsumoto K., Oba T., Lynch-Stieglitz J. and Yamamoto H. (2002) Interior hydrography and circulation of the glacial Pacific Ocean. *Quaternary Science Reviews* **21**, 1693–1704.

McGowan H. and Clark A. (2008) Identification of dust transport pathways from Lake Eyre, Australia using Hysplit. *Atmospheric environment* **42**, 6915–6925

Molina-Kescher M., Frank M. and Hathorne E. (2014) South Pacific dissolved Nd isotope compositions and rare earth element distributions: Water mass mixing versus biogeochemical cycling. *Geochim. Cosmochim. Acta* **127**, 171-189.

Ni Y. Y., Foster G. L., Bailey T., Elliott T., Schmidt D. N., Pearson P., Haley B. and Coath C. (2007) A core top assessment of proxies for the ocean carbonate system in surface-dwelling foraminifers. *Paleoceanography* **22**, Pa3212, http://dx.doi.org/10.1029/2006pa001337.

Noble T. L. Piotrowski A. M., Robinson L. F., McManus J. F., Hillenbrand C-D. and Bory A. J.-M. (2012) Greater supply of Patagonian sourced detritus and transport by the ACC to the Atlantic sector of the Southern Ocean during the last glacial period. *Earth Planet. Sci. Lett.* **317**, 374–385.

Noble T. L., Piotrowski, A.M. and McCave, I. N. (2013) Neodymium isotopic composition of intermediate and deep waters in the glacial southwest Pacific. *Earth Planet. Sci. Lett.* **384**, 27-36.

Pahnke K., Goldstein S. L. and Hemming S. R. (2008) Abrupt changes in Antarctic Intermediate Water circulation over the past 25,000 years, *Nat. Geosci.,* **1**, 870–874, doi:10.1038/ngeo360.

Pearce C. R., Jones M. T., Oelkers E. H., Pradoux C. and Jeandel C. (2013) The effect of particulate dissolution on the neodymium (Nd) isotope and Rare Earth Element (REE) composition of seawater. *Earth Planet. Sci. Lett.* **369-370**, 21-40

Pena L. D., Goldstein S. L., Hemming S. R., Jones K. M., Calvo E., Pelejero C. and Cacho I. (2013) Rapid changes in meridional advection of Southern Ocean intermediate waters to the tropical Pacific during the last 30 kyr. *Earth Planet. Sci. Lett.*, **368**, 20-32

Piotrowski A. M., Goldstein S. L., Hemming S. R. and Fairbanks R. G. (2005) Temporal relationships of carbon cycling and ocean circulation at glacial boundaries, *Science*, **307**, 1933–1938, doi:10.1126/science.1104883.

Piotrowski A. M., Goldstein S. L., Hemming S. R., Fairbanks R. G. and Zylberberg D. R. (2008) Oscillating glacial northern and southern deep water formation from combined neodymium and carbon isotopes, *Earth Planet. Sci. Lett.,* **272**(1–2), 394–405, doi:10.1016/j.epsl.2008.05.011.

Piotrowski A. M., Galy A., Nicholl J. A. L., Roberts N., Wilson D. J., Clegg J. A. and Yu J. (2012) Reconstructing deglacial North and South Atlantic deep water sourcing using foraminiferal Nd isotopes. *Earth Planet. Sci. Lett.,* **357-358**, 289–297, http://dx.doi.org/10.1016/j.epsl.2012.09.036

Prospero J. M., Ginoux P., Torres O., Nicholson S. E. and Gill T. E. (2002) Environmental Characterization of global sources of atmospheric soil dust identified with the nimbus 7 total ozone mapping spectrometer (TOMS) absorbing aerosol product, *Reviews of Geophysics*, **40**, DOI: 10.1029/2000RG000095

Rea D.K. (1994) The paleoclimatic record provided by eolian deposition in the deep sea: the geologic history of wind. *Reviews of Geophysics* **32** (2), 159–195.

Rea D.K., Lyle M.W., Liberty L.M., Hovan S.A., Bolyn M.P., Gleason J.D., Hendy I.L., Latimer J.C., Murphy B.M., Owen R.M., Paul C.F., Rea T.H.C., Stancin A.M., Thomas D.J. (2006) Broad region of no sediment in the southwest Pacific Basin. *Geology* **34** (10), 873–876.

Reid J. L. and Lynn R. J. (1971) On the influence of the Norwegian-Greenland and Weddell seas upon the bottom waters of the Indian and Pacific oceans. *Deep-Sea Res.* **18**, 1063-1088.

Reimer P.J., Bard E., Bayliss A., Beck J.W., Blackwell P.G., Bronk Ramsey C., Buck C.E., Cheng H., Edwards R.L., Friedrich M., Grootes P.M., Guilderson T.P., Haflidason H., Hajdas I., HattÃ C., Heaton T.J., Hogg A.G., Hughen K.A., Kaiser K.F., Kromer B., Manning S.W., Niu M., Reimer R.W., Richards D.A., Scott E.M., Southon J.R., Turney C.S.M., van der Plicht J. (2013) IntCal13 and MARINE13 radiocarbon age calibration curves 0-50000 years calBP, *Radiocarbon* **55**(4). DOI: 10.2458/azu_js_rc.55.16947

Rempfer J., Stocker T. F., Joos F., Dutay J. C. and Siddall M. (2011) Modelling Nd isotopes with a coarse resolution ocean circulation model: Sensitivities to model parameters and source/sink distributions, *Geochim. Cosmochim. Acta*, **75**, 5927–5950.

Rempfer J., Stocker T. F., Joos F. and Dutasy J-C. (2012) Sensitivity of Nd isotopic composition in seawater to changes in Nd sources and paleoceanographic implications, *J. of Geophysical Research*, **117**, C12010, doi:10.1029/2012JC008161.

Revel-Rolland M., De Deckker P., Delmonte B., Hesse P.P., Magee J.W., Basile-Doelsch I., Grousset F. and Bosch D. (2006) Eastern Australia: a possible source of dust in East Antarctica interglacial Ice. *Earth Planet. Sci. Lett.,***249**, 1–13.

Rickli J., Frank M. and Halliday A. N. (2009) The hafnium neodymium isotopic composition of Atlantic seawater, *Earth Planet. Sci. Lett.,* **280**, 118–127, doi:10.1016/j.epsl.2009. 01.026.

Roberts N. L., Piotrowski A. M., McManus J. F. and Keigwin L. D. (2010) Synchronous deglacial overturning and water mass source changes, *Science*, **327**, 75–78, doi:10.1126/ science.1178068.

Roberts N. L., Piotrowski A. M., Elderfield H., Eglinton T. I. and Lomas M. W. (2012) Rare earth element association with foraminifera. *Geochim. Cosmochim. Acta* **94**, 57–71.

Rosenthal Y., Field M. P. and Sherrell R. M. (1999) Precise determination of element/calcium ratios in calcareous samples using sector field inductively coupled plasma mass spectrometry. *Anal. Chem.* **71**, 3248–3253. http://dx.doi.org/10.1021/ac981410x.

Roy M., van der Flierdt T., Hemming S. R. and Goldstein S. L (2007) $^{40}Ar/^{39}Ar$ ages of hornblade grains and bulk Sm/Nd isotopes of circum-Antarctic glacio-marine sediments: Impications for sediment provenance in the southern ocean, Chemical *Geology*, **244**, 507-519.

Rutberg R. L., Hemming S. R. and Goldstein S. L. (2000) Reduced North Atlantic Deep Water flux to the glacial Southern Ocean inferred from neodymium isotope ratios, *Nature*, **405**, 935–938, doi:10.1038/35016049.

Scher H. D. and Martin E. E. (2004) Circulation in the Southern Ocean during the Paleogene inferred from neodymium isotopes, *Earth Planet. Sci. Lett.,* **228**, 391–405, doi:10.1016/j.epsl.2004.10.016

Schmitz W., Mangini A., Stoffers P., Glasby G.P. and Pluger W.L. (1986) Sediment accumulation rates in the Southwestern Pacific Basin and Aitutaki Passage. *Marine Geology* **73**, 181–190.

Siddall M., Khatiwala S., van de Flierdt T., Jones K., Goldstein S. L., Hemming S. and Anderson R. F. (2008) Towards explaining the Nd paradox using reversible scavenging in an ocean general circulation model, *Earth Planet. Sci. Lett.,* **274**, 448–461.

Singh S.P., Singh S.K., Goswami V., Bhushan R., Rai V.K. (2012) Spatial distribution of dissolved neodymium and $\varepsilon_{Nd}$ in the Bay of Bengal: Role of particulate matter and mixing of water masses. *Geochim. Cosmochim. Acta* **94**, 38-56.

SCOR Working Group: (2007) Geotraces – an international study of the global marine biogeochemical cycles of trace elements and their isotopes. *Chemie der Erde – Geochemistry* **67(2)**, 85–131.

Soulet G., Ménot G., Bayon G., Rostek F., Ponzevera E., Toucanne S., Lericolais G. and Bard E. (2013) Abrupt drainage cycles of the Fennoscandian Ice Sheet, *Proceedings of the National Academy of Sciences of the United States of America*, 10.1073/pnas.1214676110

Stancin A. M., Gleason J. D., Hovan S. A., Rea D. K., Owen R. M., Moore Jr. T. C., Hall C. M. and Blum, J. D. (2008) Miocene to recent eolian dust record from the Southwest Pacific Ocean at 40°S latitude. *Palaeogeography, Palaeoclimatology, Palaeoecology*, **261**, 218-233

Stern C. R. and Kilian R. (1996) Role of the subducted slab, mantle wedge and continental crust in the generation of adakites from the Andean Austral Volcanic Zone. *Contrib. Mineral Petrol,* **123**, 163-281.

Stichel T., Frank M., Rickli J. and Haley B. A. (2012) The hafnium and neodymium isotope composition of seawater in the Atlantic sector of the Southern Ocean, *Earth Planet. Sci. Lett.,* **317**, 282–294.

Stichel T., Frank M., Rickli J., Hathorne E. C., Haley B. A., Jeandel C. and Pradoux C. (2012) Sources and input mechanisms of hafnium and neodymium in surface waters of the Atlantic sector of the Southern Ocean, *Geochim. Cosmochim. Acta,* **94**, 22-37

Stuiver M. and Polach H. A. (1977) Reporting of C-14 Data - Discussion, *Radiocarbon*, **19(3)**, 355–363.

Stuiver M. and Reimer P. J. (1993) Extended C-14 Data-Base and Revised Calib 3.0 C-14 Age Calibration Program, *Radiocarbon*, **35(1)**, 215–230.

Stumpf R., Frank M., Schönfeld J. and Haley B.A. (2010) Late Quaternary variability of Mediterranean Outflow Water from radiogenic Nd and Pb isotopes. *Quat. Sci. Rev.* **29** (19/20), 2462–2472. doi:10.1016/j.quascirev.2010.06.021

Stumpf R., Frank M., Schönfeld J. and Haley B. A. (2011) Climatically driven changes in sediment supply on the SW Iberian shelf since the Last Glacial Maximum, *Earth Planet. Sci. Lett.,* 312, 80-90.

Tachikawa K., Athias V. and Jeandel C. (2003) Neodymium budget in the modern ocean and paleo-oceanographic implications. *J. Geoph. Res.* **108** (C8).

Tachikawa K., Roy-Barman M., Michard A., Thouron D., Yeghicheyan D. and Jeandel C. (2004) Neodymium isotopes in the Mediterranean Sea : Comparison between seawater and sediment signals, *Geochim. Cosmochim. Acta*, **68**-14, 3095-3106

Tachikawa K., Piotrowski A. M. and Bayon G. (2014) Neodymium associated with foraminiferal carbonate as a recorder of seawater isotopic signatures. *Quaternary Science Reviews* **88** 1-13. doi: http://dx.doi.org/10.1016/j.quascirev.2013.12.027

Tanaka T. et al. (2000) JNdi-1: A neodymium isotopic reference in consistency with LaJolla neodymium, *Chem. Geol*., **168**(3–4), 279–281, doi:10.1016/S0009-2541(00)00198-4.

Tanaka T.Y. and Chiba M. (2006) A numerical study of the contributions of dust source regions to the global dust budget. *Global and Planetary Change* **52**, 88–104.

Taylor S. R., McLennan S. M. and McCulloch M. T. (1983) Geochemistry of loess, continental crustal composition and crustal model ages, *Cosmochim. Acta*, **47**, 1897-1905.

Taylor S. R. and McLennan S. M. (1985) *The Continental Crust*: *Its Composition and Evolution. An Examination of the Geochemical Record Preserved in Sedimentary Rocks*. Blackwell.

Thiede J. (1979) Wind regimes over the late Quaternary southwest Pacific Ocean. *Geology* **7**, 259–262.

Tütken T., Eisenhauer A., Wiegand B. and Hansen B.T. (2002) Glacial–interglacial cycles in Sr and Nd isotopic composition of Arctic marine sediments triggered by the Svalbard/Barents Sea ice sheet. *Marine Geology* **182**, 351–372.

van der Flierdt T. (2010) Neodymium isotopes in paleoceanography. *Quaternary Science Reviews* **29**, 2439-2441. doi:10.1016/j.quascirev.2010.07.001

von Blanckenburg, F. (1999) Tracing Past Ocean Circulation?, *Science*, **286**, 1862b–1863.

Wandres A. M., Bradshaw J. D., Weaver S., Maas R., Ireland T. and Eby N. (2004) Provenance analysis using conglomerate clast lithologies: a case study from the Pahau terrane of New Zealand, *Sedimentary Geology*, **167**, 57-89

Walter H. J., Hegner E., Diekmann B., Kuhn G. and Rutgers Van Der Loeff M. M. (2000) Provenance and transport of terrigenous sediment in the South Atlantic Ocean and their relations to glacial and interglacial cycles: Nd and Sr isotopic evidence, *Geochim. Cosmochim. Acta*, **64**, 3813–3827.

Warren B. A. (1973) Transpacific hydrographic sections at latitudes 43°S and 28°S, the SCORPIO Expedition II. Deep Water. *Deep-Sea Res*. **20**, 9–38.

Wilson D. J., Piotrowski A. M., Galy A. and McCave I. N. (2012) A boundary exchange influence on deglacial neodymium isotope records from the deep western Indian Ocean. *Earth Planet. Sci. Lett.* **341–344**, 35–47.

Wilson, D. J., A. M. Piotrowski, A. Galy, and J. A. Clegg (2013) Reactivity of neodymium carriers in deep sea sediments: Implications for boundary exchange an paleoceanography, *Geochim. Cosmochim. Acta*, **109**, 197-221.

Windom H.L. (1970) Contribution of atmospherically transported trace metals to South Pacific Sediments. *Geochim. Cosmochim. Acta,* **34**: 509-514.

# 5) Changes of the deep-water circulation in the central South Pacific during the last two glacial-interglacial cycles deduced from Nd, Pb, and C isotopes.

**Abstract**

The global thermohaline ocean circulation has been one of the principal drivers of climatic variability on Earth. It is therefore crucial to decipher its natural changes during Earth's history in order to understand the mechanisms responsible for climate change. The South Pacific has played an important role for the global oceanic circulation given that deep waters from the Atlantic Ocean, the Southern Ocean, and the Pacific basin are exchanged and mixed in this area, hence it has remained poorly investigated due to its remote location. In this study we present a deep-water circulation reconstruction of the central South Pacific for the last two glacial cycles (from 240,000 years ago to the Holocene) based on three different and independent proxies: Radiogenic neodymium (Nd) and lead (Pb), and stable benthic carbon isotopes. All three proxies indicate consistent variations in the composition of Circumpolar Deep Water (CDW) as a consequence of reduced proportions of North Atlantic Deep Water (NADW) during cold stages. In addition, a reconstruction of the variation of the sources of lithogenic material arriving the central South Pacific by wind and/or oceanic circulation based on combined detrital Nd and strontium (Sr) isotope compositions suggests that Australian and New Zealand dust has remained the principal contributor of detritus to the central South Pacific but that the supply of lithogenic material from the Antarctic continent was enhanced through ice rafting during glacial periods.

*This chapter will be prepared for submission to the journal Earth and Planetary Science Letters in the following months.*

## 5.1. Introduction

For being able to predict future climate change it is essential to understand the natural processes that have controlled the environment of our planet in the past on different time scales. The ocean has played a key role in controlling Earth's climate by 1) redistributing heat, 2) influencing the albedo as a consequence of changes of the sea-ice extent, and 3) modulating $CO_2$ exchange through the 'biological pump', that results in uptake of $CO_2$ from the atmosphere and which is directly dependent on the availability of continent-derived micronutrients, such as iron, brought to the surface ocean by wind.

The global thermohaline circulation (THC) has been one of the main mechanisms regulating Earth's climate because it redistributes heat from lower to higher latitudes and also transports and/or accumulates nutrients, oxygen and $CO_2$ in the deep ocean (e. g. Broecker, 1982; Rahmstorf, 2002; Sigman et al., 2010; Adkins, 2013). The main deep-water formation regions driving the THC are the North Atlantic and the area surrounding Antarctica, where North Atlantic Deep Water (NADW) and Antarctic Bottom Water (AABW) form, respectively. These two major deep and bottom water masses mix in the Southern Ocean within the eastward flowing Antarctic Circumpolar Current (ACC) to form Circumpolar Deep Water (CDW), in which also deep waters of Pacific origin are entrained. CDW fills the Indian and Pacific oceans with oxygenated, nutrient depleted waters that finally return to the Southern ocean at intermediate and middepths as nutrient-rich and oxygen depleted waters. The South Pacific represents the entrance and exit of deep-water masses feeding the Pacific Ocean, which is the largest nutrient and $CO_2$ reservoir on Earth.

The carbon isotope composition ($\delta^{13}C$) of benthic foraminifera has been widely used as recorder of past changes of the deep-water circulation (Boyle and Keigwin, 1986; Duplessy et al., 1988; Charles and Fairbanks, 1992; Matsumoto and Lynch-Stieglitz, 1999; Matsumoto et al., 2002; Ninneman and Charles, 2002; McCave et al., 2008). Its dissolved distribution follows the major nutrients in the present day ocean and is governed by the age and mixing of water masses along the thermohaline circulation. Young, nutrient-depleted water masses, such as North Atlantic Deep Water (NADW) are characterized by high $\delta^{13}C$ values whereas the oldest least ventilated deep water masses, such as in the North Pacific, are marked by low or even negative $\delta^{13}C$ signatures (Lynch-Stiglitz, 2006; Ravelo and Hillaire-Marcel, 2007). However, several factors other than water mass mixing influence this tracer, such as: Isotopic disequilibrium between the atmosphere and the surface ocean (Charles et al, 1993) or; Changes in the primary

production of surface waters that alter the pre-formed $\delta^{13}C$ signal of water masses before they are subducted into the deep ocean, remineralisation of organic material at the sediment water interface where the benthic foraminifera calcify (biological effects) (Mackensen et al., 1993) as well as the glacial-interglacial balance between terrestrial and oceanic carbon storage. (Oliver et al., 2010; Petersen et al., 2014).

Radiogenic Nd isotope compositions ($^{143}Nd/^{144}Nd$) of deep waters have been recorded in authigenic Fe-Mn coatings of the sediment particles and have been shown to be a reliable paleo-circulation tracer, independent of biological and thermodynamic fractionation effects (Rutberg et al., 2000; Piotrowski et al., 2004; 2005). Water masses acquire their Nd isotope compositions in their formation region as a consequence of weathering of continental rocks with distinct isotopic signatures (expressed as $\varepsilon_{Nd}$ values: $\varepsilon_{Nd}=[(^{143}Nd/^{144}Nd_{(sample)}/ (^{143}Nd/^{144}Nd_{(CHUR)} -1]*10^4$, whereby CHUR stands for the Chondritic Uniform Reservoir ($^{143}Nd/^{144}Nd=0.512638$, Jacobsen and Wasserburg, 1980)). Consequently, deep water masses formed in the North Atlantic (NADW) are characterized by a highly negative (unradiogenic) $\varepsilon_{Nd}$ signature near -13.5 (Piepgras and Wasserburg, 1987; Rickli et al., 2009) due to weathering contributions from the old cratonic rocks of Canada and Greenland, whereas the $\varepsilon_{Nd}$ signatures of North Pacific waters such as North Pacific Deep Water (NPDW) range from -2 to -4 (Piepgras and Jacobsen, 1988; Amakawa et al., 2004, 2009) as a consequence of the more positive (radiogenic) Nd isotope composition of the volcanic rocks that surround the Pacific. Waters originating from these source areas mix in the Southern Ocean producing an $\varepsilon_{Nd}$ signature of around -8.5 for CDW (Piepgras and Wasserburg, 1982; Carter et al., 2012; Stichel et al., 2012a; Garcia-Solsona et al., 2013; Molina-Kescher et al., 2014). Tracing the mixing of water masses along the thermohaline circulation pathway in the open ocean is possible due to the intermediate oceanic residence time of Nd between 400 and 2000 years (Tachikawa et al., 2003; Arsouze et al., 2009; Rempfer et al., 2011), which is similar to the global ocean mixing time. In the water column of near coastal regions, where Nd is introduced into seawater or in high productivity areas with high particulate fluxes, dissolved Nd isotopes are affected by non-conservative behavior that complicates or sometimes prevents their use as water mass tracers (Lacan and Jeandel, 2005; Rempfer et al., 2011; Singh et al., 2012; Stichel et al., 2012b; Grasse et al., 2012; Pearce et al., 2013). In addition, the reliable extraction of the authigenic, sea-water-derived signature recorded in the sediment is sometimes complicated (Gutjahr et al., 2007; Elmore et al., 2009, Roberts et al., 2010; 2012; Piotrowski et al., 2012; Wilson et al., 2013; Kraft et al., 2013; Tachikawa et al., 2014). These issues have been studied in detail for the South Pacific basins including the core locations of this study and have been

demonstrated not to bias the water mass signatures registered by the sedimentary Nd isotopes (Molina-Kescher et al., 2014a, 2014b).

Lead (Pb) isotopes behave similarly to Nd isotopes in seawater in that water masses from different oceanic basins present characteristic isotopic ratios as a consequence of the inputs from weathered rocks of different type and ages, although Pb isotopes undergo incongruent weathering producing that the radiogenic Pb isotopes ($^{206}Pb$, $^{207}Pb$ and $^{208}Pb$) are preferentially mobilized during weathering with respect to primordial $^{204}Pb$ (Chow and Paterson, 1959, 1962; Frank, 2002). In the case of Pb, also hydrothermal inputs play a role for the oceanic Pb budget, as well as the short residence time of this element in the ocean (~50 to 200 years) (Schaule and Patterson, 1981; von Blanckenburg and Igel, 1999). However, differentiation of admixed deep-water signatures from the Pacific and Atlantic basins is possible along the pathway of Circumpolar Deep Water (CDW) due to the very high current speeds and volume transport of the ACC (Abouchami and Goldstein, 1995).

Radiogenic isotopes of Nd; Pb and Sr can also be used for studying the provenance of lithogenic material (detritus) deposited on the seafloor transported over long distances by wind (dust input) or oceanic currents (e. g. Frank, 2002). Here we combine the evidence obtained from detrital Sr and Nd isotopes to analyze past source changes of the detritus that arrived in the central South Pacific.

### 5.1.1. Hydrography of the deep South Pacific

The area of the mid-latitude (35°S to 50°S) South Pacific between New Zealand and South America presents a complex deep-water circulation pattern, which is schematically shown in figure 5.1. While a Deep Western Boundary Current (DWBC) that detaches from the Antarctic Circumpolar Current (ACC) represents the entrance of deep waters into the Pacific in the western part of the South Pacific, the exit and reintroduction of old mid-depth waters coming from the North Pacific into the ACC occurs in the eastern South Pacific, close to South America (see Molina-Kescher et al., 2014a for a detailed hydrographic description). The ACC mainly consists of Circumpolar Deep Water (CDW), a homogeneous mixture of deep waters from all major ocean basins containing large contributions of NADW and AABW, which dominates the deep central South Pacific (Kawabe and Fujio, 2010), although central Pacific waters also exert some influence in this area (Reid, 1986). The Ross Sea is one of the main formation regions of AABW, which occupies the abyssal Southeast Pacific Basin but is not able to cross the East Pacific Rise (EPR) towards the Southwest Pacific Basin due to its high density (Orsi et al., 1999).

## 5.2. Samples and Methods

Two gravity cores, SO213-59-2 and SO213-60-1, from 3161 m and 3471 m water depth respectively, obtained in the western flank of the East Pacific Rise in the central South Pacific (44-46°S, 117-119°W) (Fig. 5.1) aboard the German RV SONNE during expedition SO213 (Dec. 2010 – Mar. 2011) were analysed for stable oxygen ($\delta^{18}O$) and carbon ($\delta^{13}C$) isotopes, and for radiogenic neodymium ($\varepsilon_{Nd}$), strontium ($^{88}Sr/^{86}Sr$) and lead isotope compositions.

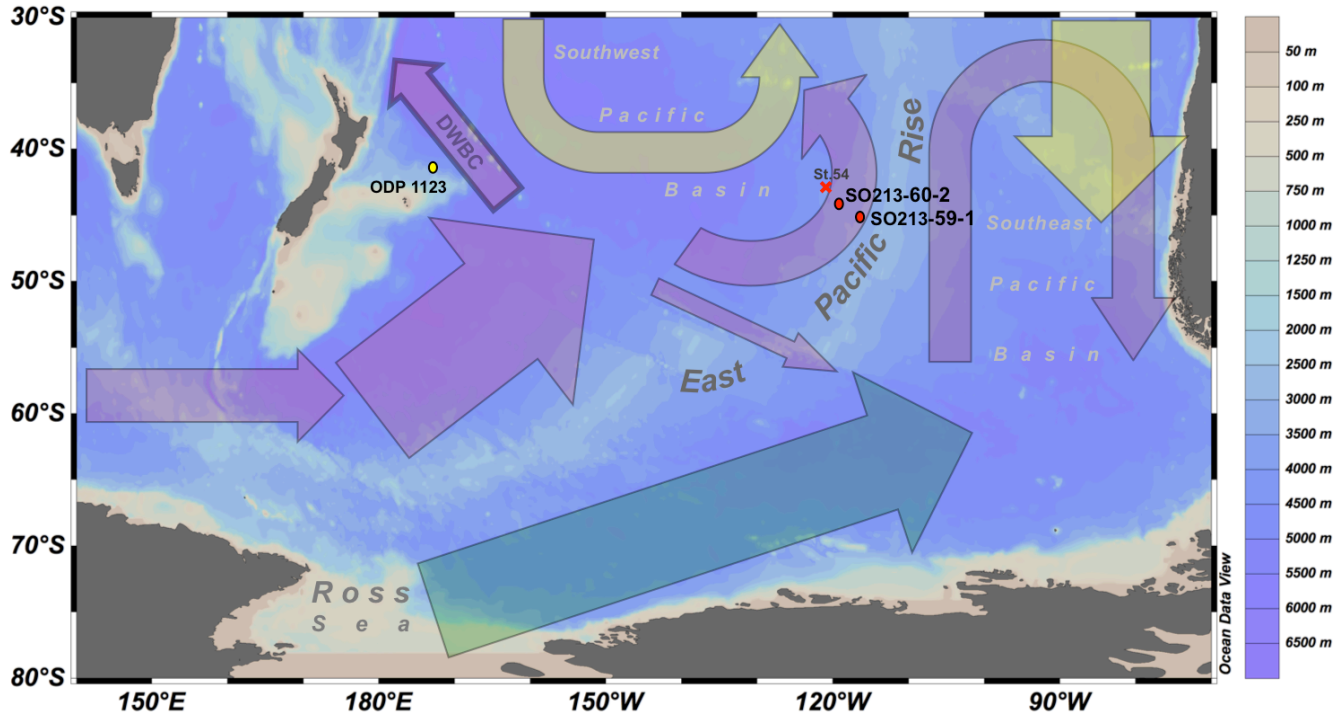


***Figure 5.1.*** *Map of the study area with coarse bathymetry and the locations of the cores of this study (red dots) and of another two study referred to in the text (yellow dot: Elderfield et al., 2012; Noble et al., 2013) together with the schematic flow-paths and flow directions of the main water masses between 3000 and 4000 m water depth (circulation patterns after Reid, 1986; Kawabe and Fujio, 2005). Arrows represent water mass flow coded by colours: Circumpolar Deep Water (red), Pacific derived water (yellow) and Antarctic Bottom Water (greenish). DBWC stands for: Deep Western Boundary Current. The red cross represents the station with seawater Nd isotope analysis (St. 54 at 3842 m water depth: Molina-Kescher et al., 2014) closest to the location of the cores of this study. Water depth of Cores SO213-59-2, SO213-60-1 and ODP 1123: 3161 m, 3471 m, and 3290 m, respectively.*

### 5.2.1. Stable isotopes Oxygen ($\delta^{18}O$) and Carbon ($\delta^{13}C$) analysis

Stable isotopic ($\delta^{18}O$ and $\delta^{13}C$) analyses were performed on the benthic foraminiferal species *Cibicidoides wuellerstorfi* and *Uvigerina peregrina* (~10 individuals of the size fraction > 250 µm) from the cores SO213-59-2 and SO213-60-1, respectively. Isotopic analyses were performed on a Thermo Finnigan MAT 253 mass spectrometer (Thermo Scientific, Germany)

coupled with a KIEL IV Carbonate device. Results were referenced to the NBS19 standard and calibrated to VPDB. Analytical errors were ± 0.06 for $\delta^{18}O$ and ± 0.07 for $\delta^{13}C$.

**5.2.2. Nd, Pb and Sr isotope analysis.**

For the extraction of deep water Nd isotope signatures recorded by early diagenetic, authigenic Fe-Mn coatings that precipitate on sediment particles, we used the 'unclean' planktonic foraminifera technique (e. g. Roberts et al., 2010; Tachikawa et al., 2014) in 63 samples of Core 59-2 and 40 samples of Core 61-1. This method has proven to faithfully represent the Nd isotope composition of seawater in our study area (Molina-Kescher et al., 2014b) and other oceanographic regions (e. g. Roberts et al., 2010; Kraft et al., 2013; Tachikawa et al., 2014). The extraction consists in the dissolution of clay-free mixed planktonic foraminifera without a previous isolation of Fe-Mn coatings. We also applied a 'non-decarbontaed' bulk sediment leaching technique (Wilson et al., 2013; Molina-Kescher et al., 2014b) on 12 samples for each of the two cores as an alternative method for the extraction of seawater derived Nd and Pb isotope compositions. This method consists in the leaching of bulk sediment using hydroxylamine hydrochloride without a previous carbonate removal and has proven to be the most reliable leaching method for the isolation of the authigenic Nd of the coatings (Wilson et al., 2013; Molina-Kescher et al., 2014b). In addition, two fish teeth found in cores 60-1 and 1 for 59-2 were analysed to confirm the validity of the seawater origin of the Nd isotope compositions (e.g. Martin and Scher, 2004).

Detrital Nd and Sr isotope signatures were obtained on the 24 previously leached bulk sediment samples of Cores 59-2 and 60-1, and two more for the latter core, to track changes in the provenance of the lithogenic material. These 26 samples, after a second hydroxylamine leach of 24 hours, were totally digested using a mixture of concentrated $HNO_3$ and HF.

After dissolution all samples underwent a two-step ion chromatographic separation following previous studies to isolate and purify Nd (Barrat et al., 1996, Le Fevre and Pin, 2005), Sr (Horwitz et al., 1992) and Pb (Galer and O'Nions, 1989; Lugmair and Galer, 1992)

To measure the isotopic ratios of Nd, Sr and Pb, we used a Nu plasma MC-ICPMS at GEOMAR using ratios of 0.7219 for $^{146}Nd/^{144}Nd$ and 0.1194 for $^{88}Sr/^{86}Sr$ to correct for instrumental mass bias. Pb isotope compositions were measured using a standard bracketing method (Albarède et al., 2004). Nd and Sr isotope ratios were corrected for Sm and $^{86}Kr$, $^{87}Rb$ interferences, respectively. The results were normalized to the accepted values of 0.512115 (JNdi-1 standard (Tanaka et al., 2000)) for $^{143}Nd/^{144}Nd$, 0.710245 (NIST NBS987) for $^{87}Sr/^{86}Sr$ and for the accepted values of NBS981 (Abouchami et al., 1999) for Pb isotopes. The external

reproducibilities (2σ) of the Nd, Sr and Pb isotope measurements during each session were assessed by repeated measurements of the above standards matching sample concentrations and ranged between 0.2 and 0.4 $\varepsilon_{Nd}$ units, between 0.00004 and 0.00012 for $^{87}Sr/^{88}Sr$, and 0.015 for $^{206}Pb/^{204}Pb$, 0.0001 for $^{207}Pb/^{206}Pb$ and 0.015 for $^{208}Pb/^{204}Pb$ (see table 5.1).

| ***SO213-59-2*** | **$\delta^{18}O$ benthic** | **2σ** | **$\delta^{13}C$ benthic** | **2σ** | **$\varepsilon_{Nd}$ forams** | **2σ** | **$\varepsilon_{Nd}$ leachates** | **2σ** | **$\varepsilon_{Nd}$ detritus** | **2σ** | **$^{206}Pb/^{204}Pb$ leach** | **2σ** | **$^{207}Pb/^{206}Pb$ leach** | **2σ** | **$^{87}Sr/^{86}Sr$ detritus** | **2σ** |
|---|---|---|---|---|---|---|---|---|---|---|---|---|---|---|---|---|
| Holocene | 3.15 | ±0.06 | 0.34 | ±0.07 | -5.78 | ±0.25 | -5.95 | ±0.40 | -5.24 | ±0.24 | 18.771 | ±0.015 | 0.8324 | ±0.0001 | 0.70925 | 0.00004 |
| Last Glacial Maximum | 4.21 | ±0.06 | -0.05 | ±0.07 | -5.22 | ±0.25 | -5.33 | ±0.40 | -3.76 | ±0.24 | 18.738 | ±0.015 | 0.8333 | ±0.0001 | 0.70933 | 0.00004 |
| Last Interglacial (MIS 3+4+5) | 3.79 | ±0.06 | 0.13 | ±0.07 | -5.80 | ±0.25 | -5.52 | ±0.40 | -4.70 | ±0.24 | 18.758 | ±0.015 | 0.8327 | ±0.0001 | 0.70935 | 0.00004 |
| MIS 6 | 4.19 | ±0.06 | -0.36 | ±0.07 | -5.29 | ±0.25 | -4.06 | ±0.40 | -4.28 | ±0.24 | 18.748 | ±0.015 | 0.8333 | ±0.0001 | 0.70935 | 0.00004 |
| MIS 7 | 3.90 | ±0.06 | -0.20 | ±0.07 | -5.69 | ±0.25 | -4.96 | ±0.40 | -5.34 | ±0.24 | 18.746 | ±0.015 | 0.8319 | ±0.0001 | 0.70937 | 0.00004 |
| average INTERGLACIALS* | 3.75 | ±0.06 | 0.08 | ±0.07 | -5.76 | ±0.25 | -5.37 | ±0.40 | -5.08 | ±0.24 | 18.757 | ±0.015 | 0.8325 | ±0.0001 | 0.70935 | 0.00004 |
| average GLACIALS | 4.20 | ±0.06 | -0.18 | ±0.07 | -5.26 | ±0.25 | -4.73 | ±0.40 | -4.11 | ±0.24 | 18744 | ±0.015 | 0.8333 | ±0.0001 | 0.70934 | 0.00004 |
| | | | | | | | | | | | | | | | | |
| ***SO213-60-1*** | **$\delta^{18}O$ benthic** | **2σ** | **$\delta^{13}C$ benthic** | **2σ** | **$\varepsilon_{Nd}$ forams** | **2σ** | **$\varepsilon_{Nd}$ leachates** | **2σ** | **$\varepsilon_{Nd}$ detritus** | **2σ** | **$^{206}Pb/^{204}Pb$ leach** | **2σ** | **$^{207}Pb/^{206}Pb$ leach** | **2σ** | **$^{87}Sr/^{86}Sr$ detritus** | **2σ** |
| Holocene | 3.65 | ±0.06 | -0.47 | ±0.07 | -5.79 | ±0.32 | -6.02 | ±0.40 | -5.24 | ±0.24 | 18751 | ±0.015 | 0.8331 | ±0.0001 | 0.70934 | 0.00004 |
| Last Glacial Maximum | 4.28 | ±0.06 | -0.43 | ±0.07 | -5.77 | ±0.32 | - | ±0.40 | -4,07 | ±0.24 | - | ±0.015 | - | ±0.0001 | 0.71023 | 0.00012 |
| Last Interglacial (MIS 3+4+5) | 4.21 | ±0.06 | -0.42 | ±0.07 | -5.81 | ±0.32 | -5.85 | ±0.40 | -5.53 | ±0.24 | 18760 | ±0.015 | 0.8328 | ±0.0001 | 0.70938 | 0.00004 |
| MIS 6 | 4.48 | ±0.06 | -0.91 | ±0.07 | -5.48 | ±0.32 | -5.71 | ±0.40 | -5.09 | ±0.24 | 18753 | ±0.015 | 0.8335 | ±0.0001 | 0.70964 | 0.00004 |
| MIS 7 | 4.07 | ±0.06 | -0.76 | ±0.07 | -5.88 | ±0.32 | -6.03 | ±0.40 | -5.87 | ±0.24 | 18771 | ±0.015 | 0.8329 | ±0.0001 | 0.70931 | 0.00008 |
| average INTERGLACIALS* | 4.15 | ±0.06 | -0.50 | ±0.07 | -5.82 | ±0.32 | -5.91 | ±0.40 | -5.60 | ±0.24 | 18.762 | ±0.015 | 0.8328 | ±0.0001 | 0.70937 | 0.00004 |
| average GLACIALS | 4.44 | ±0.06 | -0.81 | ±0.07 | -5.58 | ±0.32 | -5.71 | ±0.40 | -4.75 | ±0.24 | 18.753 | ±0.015 | 0.8335 | ±0.0001 | 0.70970 | 0.00010 |

***Table 5.1.*** *Results of this study averaged for isotopic stages. The averages for each stage were calculated using all available data points (see table S1). *Including here glacial MIS 4.*

## 5.3. Results

### 5.3.1. Stratigraphy

The age models of both cores (SO213-59-2 and SO213-60-1) are based on the $\delta^{18}O$ records of the benthic foraminifera tuned to the global benthic $\delta^{18}O$ stack LR04 (Lisiecki and Raymo, 2005). The age model of core SO213-59-2 (Fig. 5.2)(details in Tapia et al. submitted) is supported by two $^{14}C$ accelerator mass spectrometer (AMS) ages at 11 and 36 kilo years before present, further on referred to as ka. The sediments of this core, were deposited with low sedimentation rates between 0.4 cm $ka^{-1}$ and 1.5 cm $ka^{-1}$ averaging 0.87 cm $ka^{-1}$. Albeit the age model of the second Core, SO213-60-1, lack of $^{14}C$ dating, biostratigraphic and paleomagnetic

data confirm and support the $\delta^{18}O$ stratigraphy (details in Tapia et al., in prep). This core present sedimentation rates between 0.4 cm $ka^{-1}$ and 1.0 cm $ka^{-1}$ averaging 0.68 cm $ka^{-1}$. The low sedimentation rates of the study area (0.5 – 2 cm/Ka (Tiedemann et al., 2014)) result in bioturbation affecting the benthic oxygen isotope records obtained of Core 60-1 more strongly (Fig. 5.3), in that the amplitude of its $\delta^{18}O$ curve is reduced and the record considerably more smoothed than that of core 59-2 (Fig. 5.2) resulting in a less precise stratigraphy and lower age resolution. Thus, the interpretations of this study focus on the results obtained from better resolved core SO213-59-2. Because both core sites are bathed by the same water mass, the data from SO213-60-1 will be used to support our findings at particular intervals, such as the transitions from MIS 5 to MIS 6 and from the LGM to the Holocene, which can be clearly identified in the $\delta^{18}O$ curve of core 60-1.

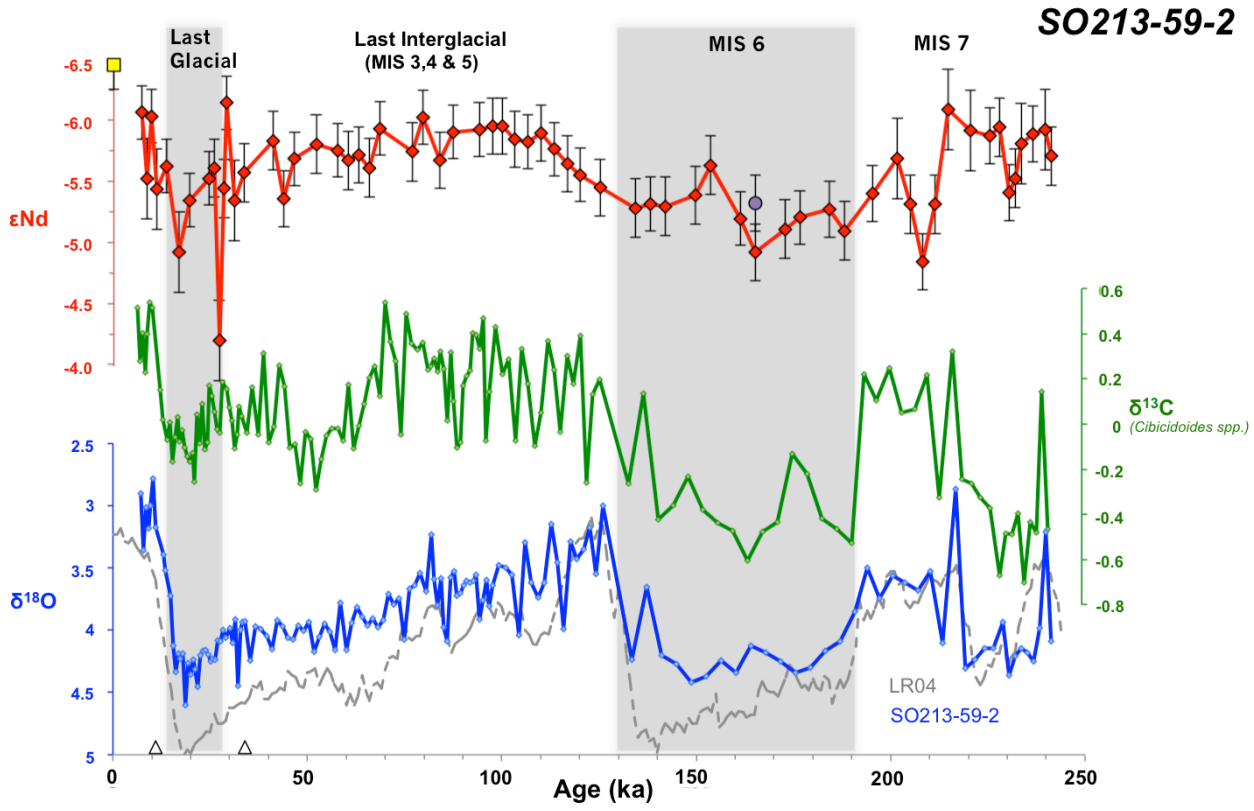


***Figure 5.2.*** *Nd (red), carbon (green) and oxygen (blue) isotope compositions of Core SO213-59-2, which covers the past ~240 ka. Nd isotope compositions ($\varepsilon_{Nd}$) with error bars (2σ) correspond to: Fe-Mn coatings of 'unclean' planktonic foraminifera (red diamonds), a fish tooth (purple dot), and present day seawater (yellow square: data from Molina-Kescher et al., 2014). Carbon ($\delta^{13}C$) and oxygen ($\delta^{18}O$) isotopes were obtained from benthic foraminifera (Cibicidoides wuellerstorfi). The global $\delta^{18}O$ stack LR04 (grey dashed line: Lisiecki and Raymo, 2005) is shown for comparison. Grey bars indicate glacial periods identifiable in the $\delta^{18}O$ data of core SO213-59-2.*

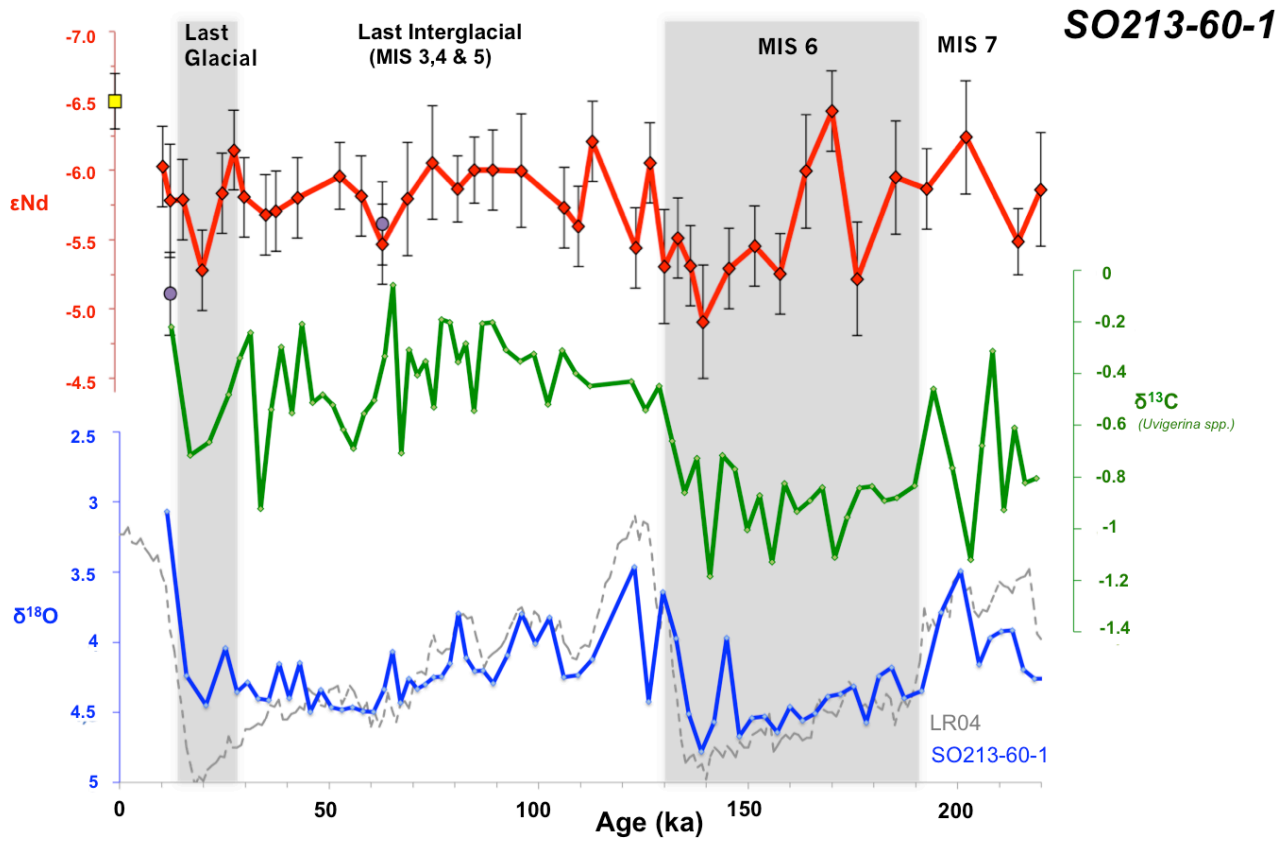


***Figure 5.3.*** *Nd (red), carbon (green) and oxygen (blue) isotope compositions of Core SO213-59-2, which covers the past ~240 ka. Nd isotope compositions ($\varepsilon_{Nd}$) with error bars (2σ) correspond to: Fe-Mn coatings of 'unclean' planktonic foraminifera (red diamonds), a fish tooth (purple dot), and present day seawater (yellow square: data from Molina-Kescher et al., 2014). Carbon ($\delta^{13}C$) and oxygen ($\delta^{18}O$) isotopes were obtained from benthic foraminifera (Cibicidoides wuellerstorfi). The global $\delta^{18}O$ stack LR04 (grey dashed line: Lisiecki and Raymo, 2005) is shown for comparison. Grey bars indicate glacial periods identifiable in the $\delta^{18}O$ data of core SO213-59-2.*

### 5.3.2. Oxygen and carbon isotopes of benthic foraminifera

The $\delta^{18}O$ record of Core 59-2 (Fig. 5.2) allows a clear differentiation of the most prominent transitions of the last two glacial cycles (from Termination III, at ~240 ka , to the early Holocene at 7.2 ka ). The variations in the benthic $\delta^{13}C$ signature recorded by *Cibicidoides wuellerstorfi* of Core 59-2 (Fig. 5.2) follow trends similar to those of benthic $\delta^{18}O$. The glacial Marine Isotope Stages MIS 6 and 2, present an average benthic $\delta^{18}O$ value of 4.2‰, identical to average global and South Pacific LGM values (Matsumoto and Lynch-Stieglitz, 1999), whereas benthic $\delta^{13}C$ displays average values for these two glacial stages that differ considerably of -0.05 (LGM), -0.36 (MIS 6), similarly than in other studies of the southern hemisphere (Oliver et al., 2010; Petersen et al., 2014). The $\delta^{18}O$ difference between Holocene and glacial periods MIS 2 (LGM) and MIS 6 is around 1.1 ‰, similar to the expected global ice volume change of 1.2‰ (Elderfield et al., 2012), whereas the $\delta^{13}C$ LGM-Holocene difference reaches 0.38‰, identical within error to recent estimates of terrestrial carbon reservoir changes for the South Pacific of 0.39‰ (Peterson et al.,

2014). The last interglacial, including here MIS 3, MIS 5 and the short glacial MIS 4, which cannot be clearly identified in this record, displays a progressive transition from minimum $\delta^{18}O$ values of ~3‰ at MIS 5e (126 ka) to maximum values of ~4.6‰ recorded for the LGM and from ~0.39‰ to ~-0.26‰ in terms of $\delta^{13}C$, displaying a similar pattern to other Pacific records compiled by Oliver et al. (2010). Interglacial stage MIS 7 is known to have been a weak interglacial that included a period of fully developed glacial conditions (sub-stage 7d) between approximately 240 ka and 220 ka (Lang and Wolf, 2001). Although in our benthic $\delta^{18}O$ record of core 59-2 the sub-stages of MIS 7 are not very well defined, a clear glacial excursion from 241 to 219 Ka corresponding to sub-stage 7d can be distinguished in both $\delta^{18}O$ and $\delta^{13}C$ data, averaging values of 4.1‰ and -0.40 for that period, respectively, after which these increased to 3.6‰ and 0.11, similar to other interglacial periods of this record.

Benthic $\delta^{18}O$ and $\delta^{13}C$ signatures of Core 60-1 (Fig. 5.3), obtained from *Uvigerina peregrina* species, display less pronounced changes than Core 59-2 and overall lower values in terms of carbon isotopes as infaunal species, such as *Uvigerina peregrina,* register $\delta^{13}C$ signatures of pore waters, which are depleted due to respiration processes in the sediment (Ravelo and Hillare-Marcel, 2007). The Holocene is almost absent in this core as it is represented by only one sample, which presents $\delta^{18}O$ and $\delta^{13}C$ signatures of 3.07 and -0.22 respectively, varying 1.2‰ and 0.28‰ with respect to the LGM ($\delta^{18}O$=4.27‰ and $\delta^{13}C$=-0.50‰), which corresponds to the global ice volume change in terms of oxygen isotopes (Elderfield et al., 2012) and, in terms of carbon isotopes, to the terrestrial-oceanic carbon reservoir balance, although the $\delta^{13}C$ Holocene-LGM variation in Core 60-1 is smaller than the expected change of 0.38 for this area (Petersen et al., 2014). There are no clear $\delta^{13}C$ variations between isotopic stages 2 and 5. Only MIS 6 shows distinctly lighter values (at an average of -0.89) compared with a more positive value of -0.42 during MIS 3 to5. This amplitude of change is similar to Core 59-2.

### 5.3.3. Nd isotopes

Deep water Nd isotope compositions obtained from 'unclean' foraminifera of Cores 59-2 and 60-1 yield the same average $\varepsilon_{Nd}$ signatures within error of -5.6 and -5.7, respectively. Both cores show relatively small variations during the entire investigated period of time, which are in part due to the low sedimentation rates of the area that produce the smearing of the Nd isotope signal, as it integrates the $\varepsilon_{Nd}$ signatures from different circulation stages (Molina-Kescher et al., 2014b), but also derives from the hydrographic conditions of the setting (section 5.4.2.1).

In general, less radiogenic $\varepsilon_{Nd}$ signatures prevailed during interglacial periods (including here glacial sub-stage 7d), which average -5.8 in both cores and show typical minimum $\varepsilon_{Nd}$

values of ~-6.1. In contrast, the most radiogenic $\varepsilon_{Nd}$ signatures occurred during glacials with averages of -5.3 for 59-2 and -5.6 for 60-1, and maximum $\varepsilon_{Nd}$ values around -5.8. In Core 59-2 also two radiogenic peaks of -5 and -4.2 were found at 17 and 27 ka, respectively (Fig. 5.2). The first one coincided with Heinrich event 1 and the second one may correspond to Heinrich event 2 (24 ka) taking into account the uncertainty of the oxygen isotope based age model, which is supported by only two radiocarbon dated samples (11 and 36 ka.).

The difference between $\varepsilon_{Nd}$ averages calculated for glacial and interglacial periods (table 5.1) is small for both cores but significant (outside error) at least in the case of core 59-2. The glacial-interglacial variations of both cores are also consistent with each other when taking a closer look at details of the two $\varepsilon_{Nd}$ records (figure 5.2 and 5.3). The data of Core 60-1 (Fig. 5.3) generally follow the same trend as Core 59-2 including a radiogenic peak near the LGM and a clear transition from more radiogenic, Pacific-like (-4.9) to less radiogenic, Southern Ocean-like (-6.1) $\varepsilon_{Nd}$ values at the MIS 6 to MIS 5 transition. Only in the interval between 159 and 181 ka in core 60-1 (Fig. 5.3) two samples clearly deviate towards less radiogenic values (-6 and -6.4 $\varepsilon_{Nd}$ units) and thus do not match the trend displayed by core 59-2. Despite that this is hard to envisage in view of the small difference in water depth of the two cores, this might be due to a difference of the deep-water circulation regime between both sites at that time and might have been linked to enhanced advection of Southern Ocean-derived deep waters only affecting the deeper site. A fish tooth Nd isotope signature with an age of 164 ka in core 59-2 confirms the overall more positive $\varepsilon_{Nd}$ signatures obtained from the unclean foraminifera of glacial stage MIS 6 compared with MIS 5 or MIS 7.

The 'Non-decarbonated' leachate $\varepsilon_{Nd}$ signatures of core 59-2 (Fig. 5.4a) are within error identical to those of the unclean foraminifera in the younger part of the core between MIS 5 and the present. For MIS 6 and most of MIS 7 the leachate data are significantly more radiogenic and closely match the detrital data. Leachate Nd isotope signatures of core 60-2 (Fig. 5.4b) are identical within error to the detrital and 'unclean' foraminfera for most samples and there are no systematic offsets between the two extraction methods of the seawater signatures.

Except for two samples of the last interglacial at 62.7 ka (corresponding to the time interval of MIS 4, although this glacial is not appreciated in the $\delta^{18}O$ data) and at 93.5 Ka (MIS 5c), the detrital $\varepsilon_{Nd}$ curve of Core 59-2 (Fig. 5.4a) shows glacial-interglacial variations oscillating from more radiogenic glacial signatures between -3.5 and -4.5 and less radiogenic interglacial signatures between -5 and -6 suggesting systematic changes in the provenance of the lithogenic

material that reached the central South Pacific during cold and warm periods (see section 5.4.3). A higher proportion of mantle-like volcanic source rocks prevailed during glacial periods. Except for a radiogenic peak value near -4 at the LGM, there are less pronounced glacial/interglacial differences in the detrital $\varepsilon_{Nd}$ data of core 60-1 (fig. 5.4b).

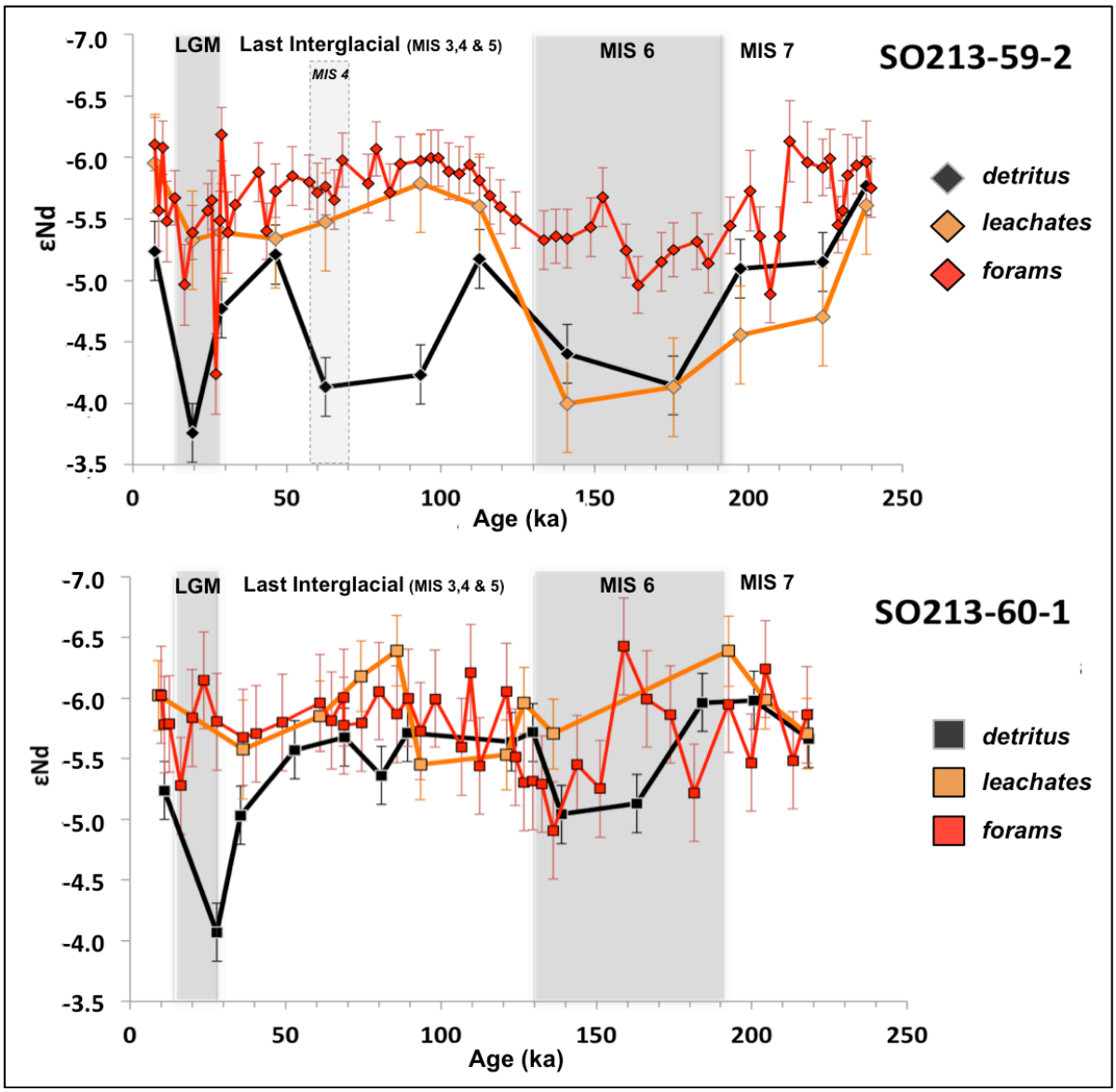


***Figure 5.4.*** *Nd isotope compositions ($\varepsilon_{Nd}$) for cores SO213-59-2 (a) and SO213-60-1 (b) for the last 240 and 220 ka., respectively, of the detrital fraction of the sediment (blue), 'non-decarbonated' leachates (green) and 'unclean' forams (red). Grey bars indicate glacial periods distinguishable in the $\delta^{18}O$ data. The time interval of Glacial MIS 4 (light grey dashed bar) is also shown for core 59-2 (a) to match with the positive detrital-$\varepsilon_{Nd}$ peak at 67.2 ka. Nevertheless this glacial period is not noticeable in the benthic oxygen isotopes of this core.*

### 5.3.4. Pb isotopes

$^{206}Pb/^{204}Pb$ and $^{207}Pb/^{206}Pb$ leachate results of both cores chosen for display in figure 5.5 (see also tables 5.1, S1 and S2) show values similar to Fe-Mn nodules obtained from the central South Pacific at similar latitudes (Abouchami and Goldstein, 1995). The glacial-interglacial variations in the Pb isotope ratios in both records are relatively small, but clearly significant. They consistently show very similar glacial/interglacial changes of essentially the same amplitudes between the two locations (Fig. 5.5). The variability also follows the same direction as the seawater-derived $\varepsilon_{Nd}$ signatures and the benthic $\delta^{13}C$ values, in that more 'Pacific-like' signatures prevailed during glacial stages, suggesting a common factor controlling the changes observed in the three different deep water circulation proxies (see section 5.4.2).

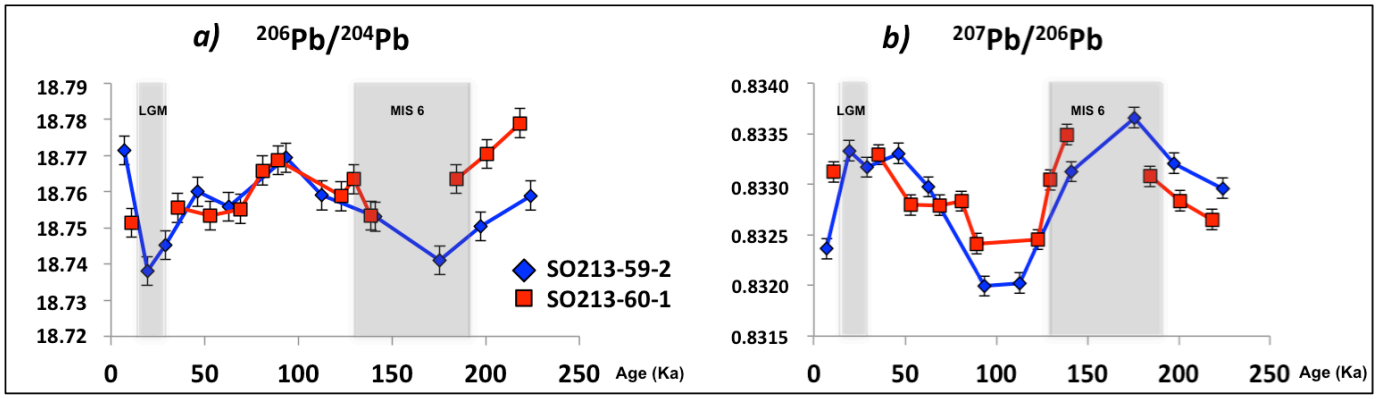


***Figure 5.5.*** *Pb isotope compositions with error bars (2σ) for cores SO213-59-2 (red squares) and SO213-60-1 (blue diamonds) for the last 240 and 220 ka., respectively. a) $^{206}Pb/^{204}Pb$ ratios b) $^{207}Pb/^{206}Pb$ ratios. Grey bars indicate glacial periods distinguishable in the $\delta^{18}O$ data.*

### 5.3.5. Detrital Sr isotopes

Detrital Sr isotope ratios ($^{87}Sr/^{86}Sr$) vary between 0.7092 and 0.7095 for core 59-2 and 0.7092 and 0.7102 for core 60-1 (Fig 5.6). While Core 59-1 does not reveal systematic glacial-interglacial detrital $^{87}Sr/^{86}Sr$ variations, core 60-1 shows the less radiogenic (lower) values during glacials consistent with a higher proportion of mantle derived source rocks.

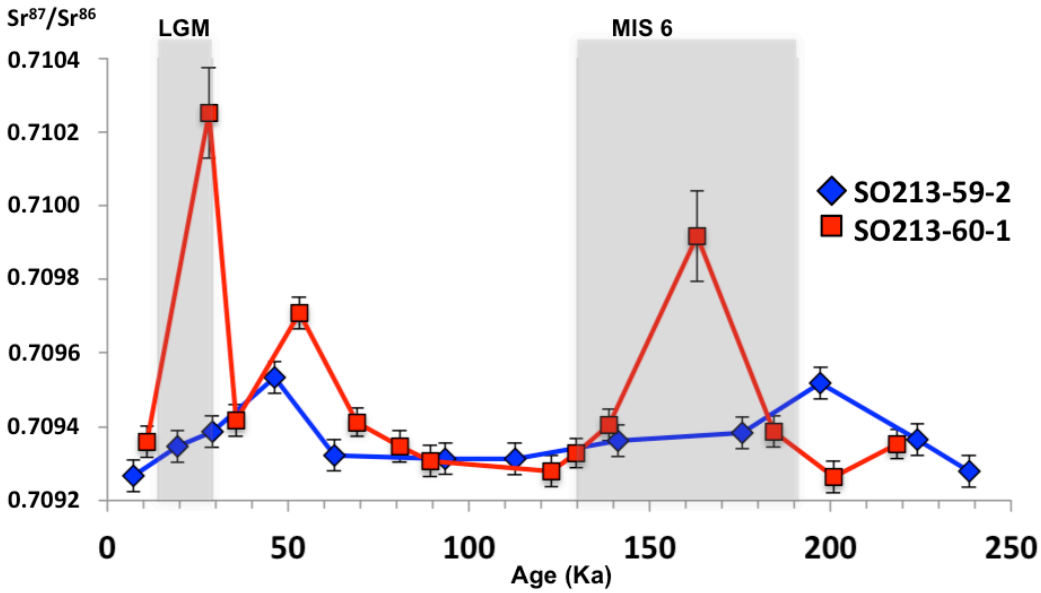


***Figure 5.6.*** *Detrital Sr isotope compositions with error bars (2σ) for cores SO213-59-2 (red squares) and SO213-60-1 (blue diamonds) for the last 240 and 220 ka., respectively. Grey bars indicate glacial periods distinguishable in the $\delta^{18}O$ data.*

## 5.4. Discussion

### 5.4.1. Reliability of the $\varepsilon_{Nd}$ data as recorder of past deep water circulation

Before we start the interpretation of the data, we evaluate the reliability of our extracted deep water Nd isotope compositions. Fossil fish teeth are known to faithfully record the Nd isotope composition of bottom waters of the past (Martin and Scher, 2004). For our new data the three available fossil fish teeth display within error the same $\varepsilon_{Nd}$ signatures as unclean forams from the same age, although one fish tooth data point corresponding to 13 ka obtained from core 60-1, shows an LGM-like signature (-5.1), which most probably is an artefact resulting from bioturbation and the low age resolution of this core (see section 5.3.1). The youngest unclean foraminifera samples of both cores display within error the same $\varepsilon_{Nd}$ signatures (-6.1 ±0.3 at 7.1 ka for 59-2 and -6.0 ±0.3 at 11.3 ka for 60-1) as present day seawater (-6.5 ±0.2, 3842 m water depth) at the same location (see Molina-Kescher et al., 2014). Comparison to the Nd isotope compositions of the detritus (Fig. 5.5) shows that there was no significant contamination of the seawater signal extracted from the foraminifera (e. g. Kraft et al., 2013; Molina-Kescher et al., 2014b). In particular, the detrital $\varepsilon_{Nd}$ signatures of Core 59-2 (Fig. 5.4a) in most cases show considerably more radiogenic $\varepsilon_{Nd}$ values than the 'unclean' forams, which is most pronounced during glacial periods, when the detritus reached the most positive values and the difference to

'unclean' foram data amounted up to 1.6 $\varepsilon_{Nd}$ units. In the case of core 60-2 (Fig. 5.4b), most of the detrital and 'unclean' forams Nd isotope compositions present similar values. In addition to the above considerations, both cores also recorded a consistent LGM-Holocene and MIS6-MIS5 trend from more radiogenic to less radiogenic signatures of the unclean foraminifera (Figs. 5.2 and 5.3).

The 'non-decarbonated' leachates do not always seem to have recorded the seawater signal as reliably as the 'unclean' forams. This is most evident in core 59-2 (Fig. 5.5a), where leachates faithfully follow the seawater curve of the foraminifera back to 130 ka, whereas prior to that, the similarity between the detrital and leachate signatures suggest a contamination of the latter by partially dissolving the lithogenic fraction during the leaching process. Leachates of Core 60-2 (Fig. 5.5b) show values similar than forams and detritus. Therefore, we will only use 'unclean' foram data for the paleoceanographic interpretations of this study as these faithfully record seawater signatures, unlike leachates.

### 5.4.2. Changes in the deep-water circulation of the last two glacial cycles

Nd, Pb and C isotopes of core 59-2 (Figures 5.2 and 5.5) show consistent glacial-interglacial variations (except for sub-stage 7d as discussed in section 5.4.2.3), which indicate more 'Pacific-like' signatures during glacial periods. Paleoceanographic changes in the Pacific Ocean have been poorly studied compared to other oceanic regions such as the Atlantic, but some evidences suggest a deepening of NPDW during the last glacial period (Keigwin, 1998; Matsumoto and Lynch-Stieglitz, 1999; Matsumoto et al., 2002; Huang et al., 2014a) or even a strong production of deep waters in the North Pacific during Heinrich events (Okazaki et al., 2010). Although these processes could explain the glacial-interglacial variations observed in our data, the flow of NPDW from the Pacific into the Southern Ocean principally occurs at middepths of the eastern South Pacific (e. g. Molina-Kescher et al., 2014a), whereas the central South Pacific is not an exit of pacific deep waters to the ACC nowadays, and rather represents a main entrance of UCDW flowing into the Pacific, although this occurs at shallower depth than the location of our cores (see Kawabe and Fujio, 2010). Therefore, it is improbable that a deepening or stronger production of NPDW during glacial stages could have been the trigger of the deep-water circulation changes observed in the central South Pacific. Instead, these processes would be appreciable in the eastern South Pacific, where a vigorous glacial-NPDW could have occupy areas of the Southeast Pacific basin that are today dominated by circumpolar deep waters (e. g. Molina-Kescher et al., 2014b).

It is also very unlikely that very dense AABW formed in the Ross Sea reached the western flank of the East Pacific Rise in the past given the position of our cores (44°-46°S), the bathymetry of the South Pacific and the eastward flow of the ACC (see circulation scheme on figure 5.1), therefore, this possibility is also discarded as an explanation for the glacial-interglacial changes observed in this study. Our data also do not support a hypothetical increment in AABW formation of the Weddell Sea during glacials as this water mass presents more unradiogenic $\varepsilon_{Nd}$ signatures (-9.5) (van der Flierdt, 2007; Stichel et al 2012; Noble et al., 2012).

On the other hand, a lot of paleoceanographic evidence deduced either from carbon isotopes (e. g. Boyle and Keigwin, 1986; Duplessy et al., 1988; Charles and Fairbanks, 1992; Ninneman and Charles, 2002; Curry and Oppo, 2005) or from Nd isotopes (Rutgers et al., 2000; Piotrowski et al., 2004, 2005, 2008, 2009, 2012; Noble et al., 2013) has suggested that during glacial stages the production of NADW was reduced, implying that the proportion of this water mass in CDW was lowered during cold periods. Hence, the reduction of NADW production during cold stages is the most probable explanation for the variations observed in our Nd and Pb isotope data and in part of the $\delta^{13}C$ change recorded in this study as explained below.

**5.4.2.1. Nd isotope evidence.**

At the present day, the western flank of the East Pacific Rise between 3000 and 3500 m, where our cores are located, is mainly bathed in CDW (see figure 5.1). Nevertheless, the present-day hydrographic properties indicate also a significant influence of Pacific-derived waters at this location and depth as reflected by relatively radiogenic Nd isotope compositions (-6.5) as well as decreased oxygen (~3.8 ml/l) and elevated phosphate concentrations (2.16 mmol/l) (Molina-Kescher et al., 2014a). For comparison, pure Lower CDW (LCDW) in the Southwest Pacific Basin is characterized by $\varepsilon_{Nd}$=-8.3, [$O_2$]=4.4 ml/l, [Phosphate]=2.07 mmol/l (Molina-Kescher et al., 2014a). Therefore, the admixture of Pacific central waters to the deep waters of this region dilutes the fraction of NADW present in CDW, which partly explains the relatively small glacial-interglacial variations observed at this location in terms of Nd isotopes, also affected by the low sedimentation rates (section 5.3.3). This dilution effect is also evident when comparing our $\varepsilon_{Nd}$ record of Core 59-2 to Holocene and LGM Nd isotope compositions obtained at ODP Site 1123 (Fig. 5.7) on Chatham Rise in the western South Pacific from a water depth of 3290 m (Elderfield et al., 2012; Noble et al., 2013), which is located at the main entrance of CDW into the Pacific basin and consequently still contains a higher proportion of NADW compared to the central S. Pacific (Reid and Lynn, 1971; Warren, 1973; Gordon, 1975; McCave et al., 2008). The LGM to

Holocene amplitude of the change in Nd isotope compositions of ODP 1123 (~2 $\varepsilon_{Nd}$ units) is significantly larger than observed for Core SO213-59-2 (1 to 1.5 $\varepsilon_{Nd}$ units) reflecting the higher proportion of NADW within CDW in the Southwest Pacific. Another piece of evidence that links the strength in NADW formation to the deep circulation changes observed in this study is the correspondence of radiogenic Nd isotope peaks in Core 59-2 (Fig. 5.2) during Heinrich events, which have been associated with essential shut downs of NADW production (Elliot et al., 1998; Hemming, 2004; McManus et al., 2004; Piotrowski et al., 2008). Core 59-2 (Fig. 5.2) shows the most radiogenic $\varepsilon_{Nd}$ values at 16.8 Ka bp (H1) and particularly at 27 ka, which may correspond to H2 (24 ka bp) taking into account the uncertainty of the age model and the low sedimentation rates. The magnitude of these two radiogenic peaks could have been enhanced by a stronger deep-water formation in the North Pacific during Heinrich events (Okazaki et al., 2010).

The influence of changes in the production rate of NADW on deep waters of the Southern Hemisphere is reflected in the overall progressively more radiogenic $\varepsilon_{Nd}$ signatures and the decrease of the glacial/interglacial Nd isotope difference along the thermohaline circulation pathway (Fig. 5.7) from the South Atlantic (Piotrowski et al., 2008) and the Indian Ocean (Piotrowski et al., 2009) via the Western South Pacific (Elderfield et al, 2012; Noble et al., 2013) to the central South Pacific (core 59-2, this study). Therefore reflecting the progressive dilution of NADW as it mixes with other water masses. As the pre-formed Nd isotope composition of NADW has not changed during glacial-interglacial scales as Fe-Mn crust and coral evidences suggest (Foster and Vance, 2006; van de Flierdt et al., 2006), a reduction in the production rate of NADW during cold stages is therefore the most probable explanation for the variations observed in the locations presented in figure 5.7, as also argued by the authors of these studies.

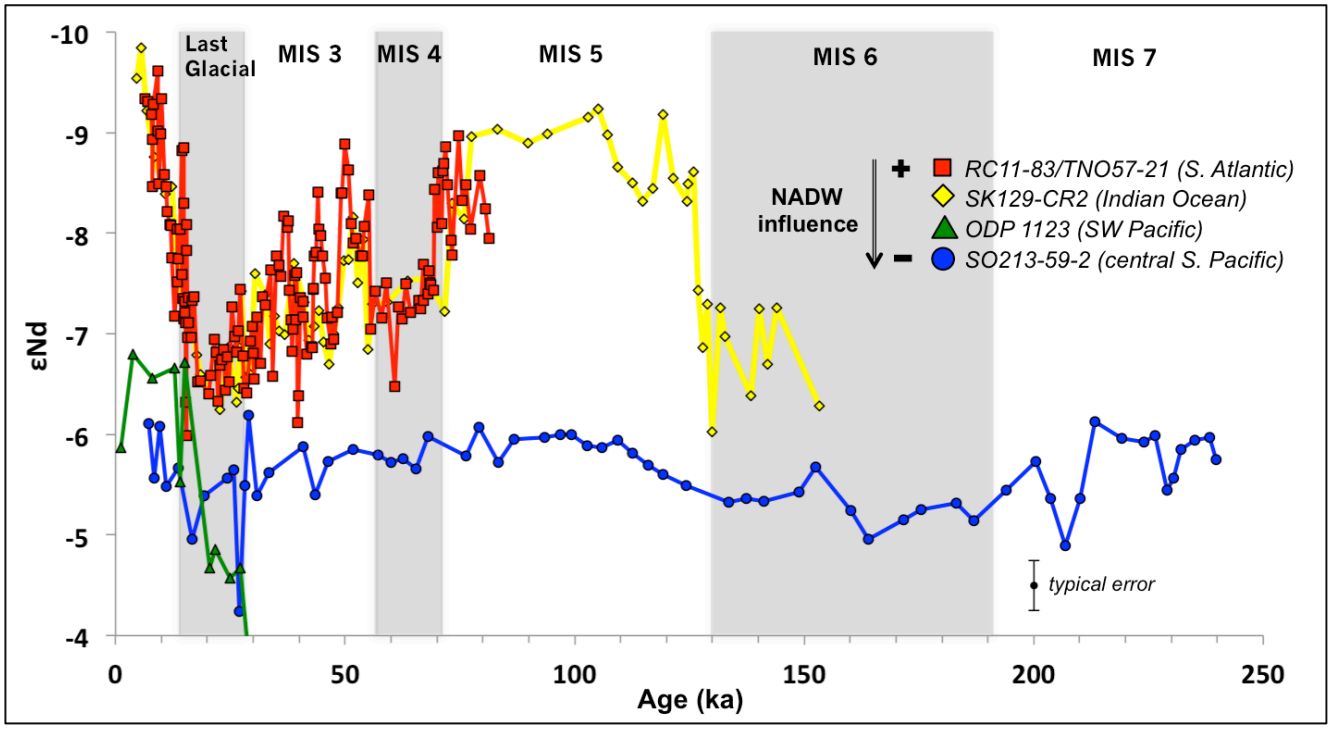


***Figure 5.7.*** *Comparison of Nd isotope ($\varepsilon_{Nd}$) records from similar depths and from different oceanic settings of the Southern Hemisphere (see legend) covering similar time scales. Water depth and references of the cores: 4718/4981 (RC11-83 / TNO57-21 (Piotrowski et al., 2005; 2008)), 3800 m (SK129-CR2 (Piotrowski et al., 2009)), 3290 m (ODP 1123 Elderfield et al., 2012; Noble et al., 2013) and 3161 m (SO213-59-2 (this study)). Grey bars indicate glacial periods.*

#### 5.4.2.2. Pb isotope evidence

The small but significant variations observed in the $^{206}Pb/^{204}Pb$ and $^{207}Pb/^{206}Pb$ records (Fig. 5.5) further confirm the decreased proportion of North Atlantic derived deep waters in CDW. Abouchami and Goldstein (1995) presented a detailed study of the evolution of Pb isotope signatures of circumpolar deep waters along the ACC, showing a constant decrease in the $^{206}Pb/^{204}Pb$ ratio towards the West (Indian > Pacific > Atlantic) largely reflecting the dilution of NADW along the pathway of CDW, with maximum values of 19.10 in the Southern Indian Ocean and minimum values of 18.70 in the eastern South Atlantic. Core 59-2 shows minimum values of ~18.74 in the LGM and beginning of MIS 6 and maxima of ~18.77 during the Holocene and MIS 5, responding again to changes in NADW admixture to CDW.

#### 5.4.2.3. $\delta^{13}C$ evidence

As recently shown in the compilation by Petersen et al., (2014), the LGM-Holocene variation in $\delta^{13}C$ signatures due to changes in the global carbon reservoir between land and ocean reaches 0.39‰ for deep waters of the South Pacific region, which explains the $\delta^{13}C$ change in this period of time for our records. There are few $\delta^{13}C$ compilations for longer periods of time, with the more recent being that from Oliver et al. (2010) for the last 150 ka. This study indicates

higher and similar values for interglacials MIS 1 and 5 and lower values for glacial MIS 2 and MIS 6, whereas the latter presents even lower $\delta^{13}C$ signatures. The authors assign most of the glacial-interglacial variation to changes in biosphere carbon storage but modulated by changes in ocean circulation, productivity, and air-sea gas exchange. Figure 5.8 compares the $\delta^{13}C$ data from this study (SO213-59-2) to similar records from the western South Pacific (Elderfield et al., 2012), the equatorial central Pacific (Mix et al., 1995), and the equatorial Indian Ocean (Piotrowski et al., 2009). The variations in benthic carbon isotopes of core 59-2 are very similar to those observed in other locations of the Pacific and even the interior of the Indian Ocean, further suggesting a dominant role of terrestrial-oceanic carbon transfers in modulating the e $\delta^{13}C$ variations. Nevertheless, as Oliver et al. (2010) do not assign specific values to this factor in their compilation, here we analyze, for the period prior to the LGM, how circulation changes, and perhaps productivity during glacial sub-stage MIS 7d, could have affected the $\delta^{13}C$ signal in the central South Pacific, although the variations are predominantly imprinted by the variation in biosphere carbon storage.

The benthic $\delta^{13}C$ signal variations of core 59-2 overall support the deep water circulation changes deduced from Nd isotope compositions (Fig. 5.2), as the former shows more negative values during cold periods, indicating larger contributions of old, nutrient-rich water masses from the deep Pacific to circumpolar waters, while during interglacials, younger and nutrient-depleted water masses, such as NADW, played a more important role for the mixture of waters composing CDW. However, during sub-glacial stage MIS 7d (~240 to 220 ka), there is a reversed relationship between $\varepsilon_{Nd}$ and $\delta^{13}C$ signatures (Fig. 5.2), which coincides with a remarkable offset towards more negative $\delta^{13}C$ values between our Core 59-2 and other $\delta^{13}C$ records from the Southern Hemisphere (Fig. 5.8). We suggest that the anomalously low $\delta^{13}C$ values observed during sub-stage MIS 7d on Core 59-2 could be an artefact related to high productivity that is known to alter the $\delta^{13}C$ signatures registered in benthic foraminifera (Mackensen et al., 1993). There is no benthic $\delta^{13}C$ for this period of time but evidences (Chase et al., 2003; Matsumoto and Lynch-Stieglitz, 1999) indicate that during the Holocene and the LGM, the primary productivity remained at similar levels in the central South Pacific. Matsumoto and Lynch-Stieglitz (1999) deduced this by the low concentrations of authigenic uranium found on core E25-10, only 5° south of our location. This circumstance may have been different during sub-stage 7d as inferred from the data of this study, implying an increase in surface water productivity of the central South Pacific at this location during this glacial sub-stage.

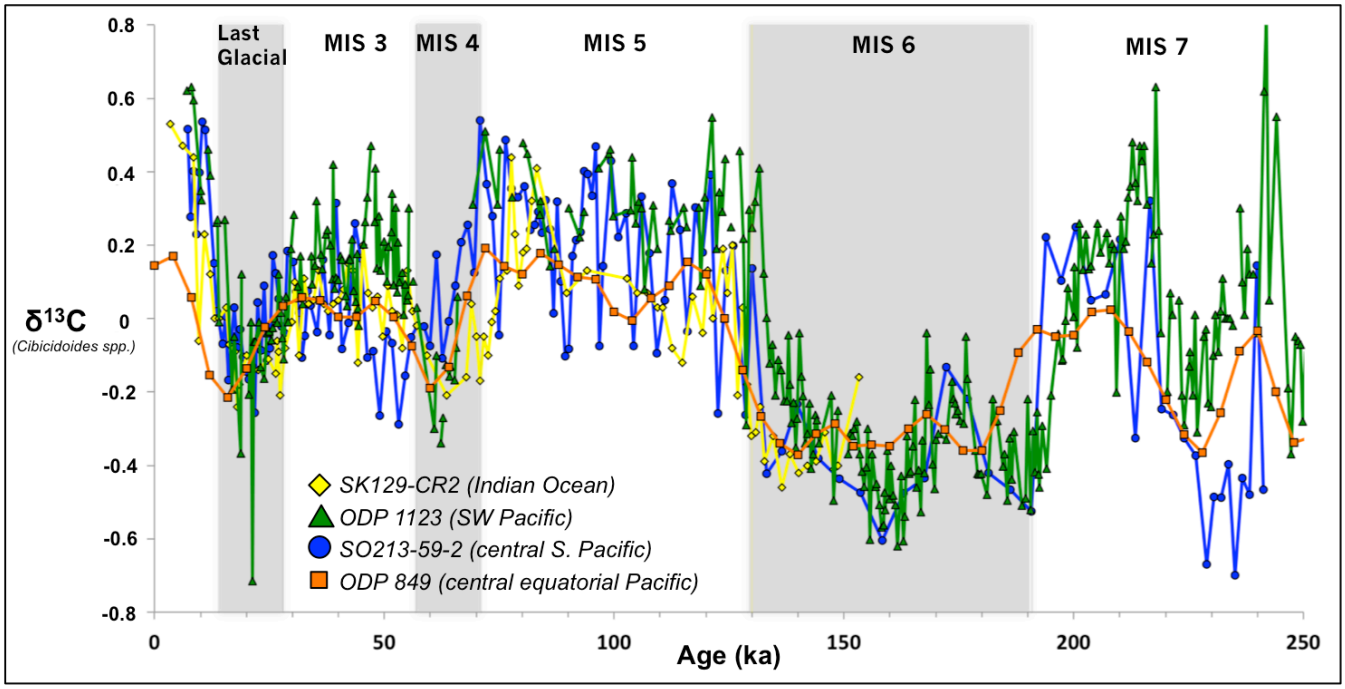


***Figure 5.8.*** *Comparison of benthic C isotope ($\delta^{13}C$) records of similar depths from the Indian Ocean and nearby oceanic settings (see legend) covering similar time scales. Water depth and references of the cores: 3800 m (SK129-CR2 (Piotrowski et al., 2009), 3290 m (ODP 1123 (Elderfield et al., 2012)), 3161 m (SO213-59-2 (this study)) and 3851 m (ODP 849 (Mix, 1995). Grey bars indicate glacial periods.*

### 5.4.3. Changes in the detrital provenance

In Molina-Kescher et al. (2014b) we presented data on the provenance of the detrital material, mainly dust, arriving in the South Pacific along 40°S using Nd-Sr isotope compositions of the lithogenic fraction of the surface sediments. We were able to show that the Nd-Sr isotope distribution mainly reflect the dominant westerly winds, with dust from Australia and New Zealand dominating the Southwest Pacific Basin and the Chile Rise, whereas weathered material from South America was also contributed to the eastern part of the study area. The Nd-Sr isotope variability of the detrital material in cores 59-2 and 60-1 is also applied to track past changes in the supply and provenance of the dust. The interglacial data closely match the Nd-Sr isotope signatures of the core-tops obtained on the East Pacific Rise reflecting the dominance of the westerly winds as carriers of dust to the central South Pacific during warm periods (Fig. 5.9). The glacial signatures are shifted towards more radiogenic $\varepsilon_{Nd}$ values and in the case of core 60-1 also have more radiogenic Sr isotope ratios. Although the arrays of South New Zealand and Australian dust (blue and purple fields on figure 5.9) partially overlap with Nd-Sr isotope signatures from West Antarctica and detritus from the Ross sea (green field on figure 5.9), the more restricted isotopic field of the latter, suggest that this change towards more radiogenic Nd-Sr isotope compositions was caused by an increase in the supply of detrital material from the

Antarctic continent. Ice Rafted Debris (IRD) were not found in neither of the two investigated cores, therefore it can be discarded that this material has been brought by drifting icebergs. Chase et al. (2003) observed a stronger supply from detrital material north of 66°S in the South Pacific, which they attributed to suspended load transported by CDW in suspension to the central South Pacific, similar to observations of the South Atlantic (Franzese et al., 2006). This was probably a consequence of the larger ice-sheet extent in Western Antarctica during glacial stages (Anderson et al., 2002; Denton and Hughes, 2002), which increased erosion, releasing fine grained weathered material to the Southern Ocean. Although the observed shift towards Antarctic derived material appears small, the contributions from this source must have been large to produce this variation, given that Lamy et al., (2014) demonstrated a threefold increase of the deposition of dust from Australia and New Zealand in the Pacific sector of the Southern Ocean during glacial periods of the past million years.

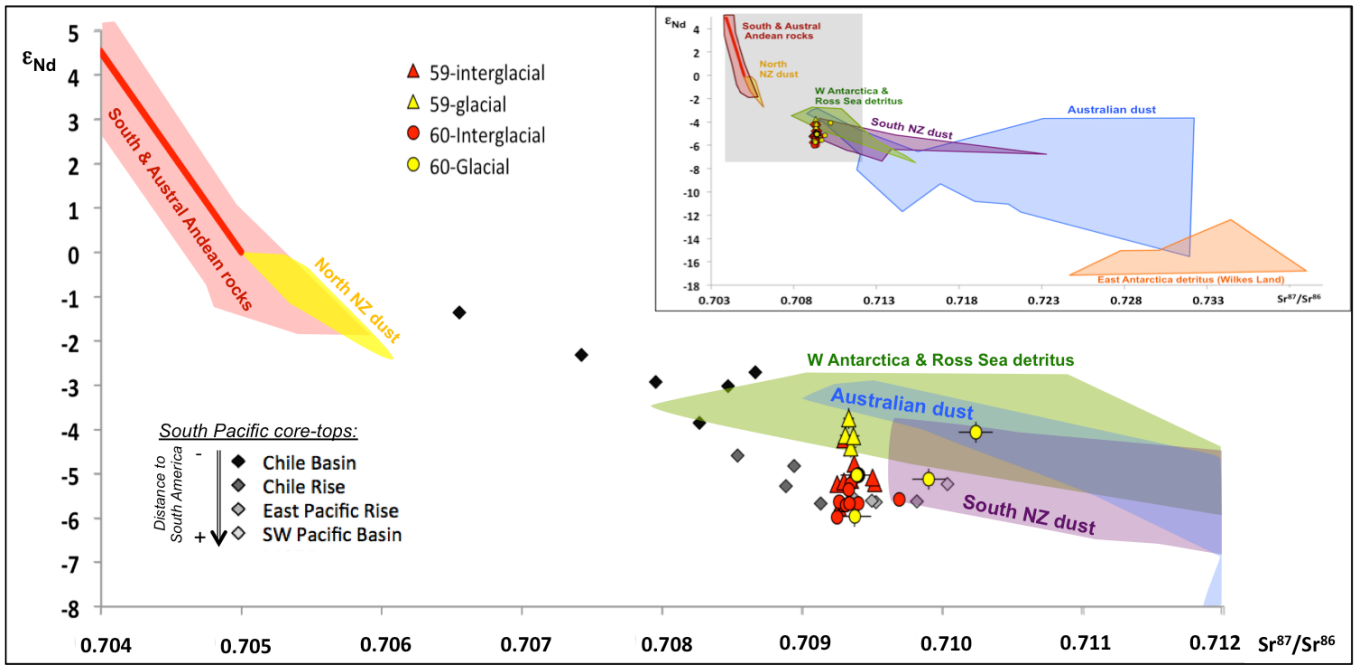


***Figure 5.9.*** *Combined Nd and Sr isotope signatures of detrital analysis on cores SO213-59-2 (triangles) and SO213-60-1 (circles) coded for glacial (yellow) and interglacial (red) periods. Core-top analysis from the open South Pacific (diamonds) coded in black to light grey as a function of the distance to South America (see legend on figure) are also shown for comparison. The most probable detrital sources that surround the South Pacific are presented as coloured Sr-Nd arrays: The Southern (Hickey et al., 1986; Futa and Stern, 1988) and Austral Andes (Futa and Stern, 1988; Stern and Kilian, 1996) combined, in red. Fine-grained particles (<5 μm) susceptible to be transported by wind from: the North Island (New Zealand) in yellow (data from Delmonte et al., 2004); the South Island (New Zealand) in purple (Taylor et al., 1983; Delmonte et al., 2004); and Eastern Australia in blue (Revel-Rolland et al., 2006). Circumantarctic sediments from Wilkes Land, in light yellow (only on the inset figure); and West Antarctica and Ross Sea, in green (combined from Roy et al., 2007 and Hemming et al., 2007).Note that the inset shows a larger range of potential source areas for Nd-Sr isotopes. The grey square marks the range of the big plot.*

## 5.5. Conclusions

The results of our study based on two sediment cores from the central South Pacific indicate a reduction of NADW admixture to the Southern Ocean during glacial stages and support the relevance of this water mass in controlling the composition of deep waters globally given that all three deep-water circulation proxies used in this study (Nd, C and Pb isotopes) show consistent variations: 1) More radiogenic and thus more Pacific like Nd and Pb isotopic signatures of deep waters prevailed during glacials, which is consistent with a reduction in the contribution of the least radiogenic endmember (NADW) of CDW, which has prevailed in the mid-latitude (~43°S) central South Pacific at 3000/3500 m water depth; 2) Although mostly influenced by changes in the biosphere carbon reservoir, $\delta^{13}C$ data show lighter values during glacial periods, also indicating a reduction in the admixture of nutrient-depleted NADW to CDW. The small amplitude of the observed Nd and Pb isotope variability is fully consistent with the expected dilution of NADW in the central South Pacific via mixing with Southern Ocean and Pacific waters.

Combined detrital Nd-Sr isotope compositions indicate that the provenance of lithogenic material arriving the central South Pacific changed significantly during the past 240 ka in that Australian and New Zealand dust has remained the main source of continental derived material brought to this region by the dominant Westerlies. However, the glacial signatures were shifted towards more radiogenic isotope compositions suggesting markedly increased contributions of Antarctic derived material during glacial periods as a consequence of enhanced erosion and weathering due to larger ice sheets. The glacial detritus was most probably transported northwards as suspended load of oceanic currents.

**Acknowledgements**

We would like to thank the “Bundesministerium für Bildung und Forschung, Germany” for funding this project (No.: 03G0213B) as well as the crew members and participants of expedition SO213. This cruise was part of the collaborative SOPATRA (SOuth PAleoceanografic TRAnsects) project of GEOMAR and the Alfred Wegener Institute (AWI).

**References:**


Abouchami W. and Goldstein S. L. (1995) A lead isotopic study of Circum-Antarctic manganese nodules, *Geochim. Cosmochim. Acta,* **59**, 1809–1820,

Abouchami W., Galer S.J.G. and Koschinski A. (1999) Pb and Nd isotopes in NE Atlantic Fe–Mn crusts: proxies for trace metal paleosources and paleocean circulation. Geochim. *Cosmochim. Acta* **63** (10), 1489–1505.

Adkins J.F. (2013) The role of deep ocean circulation in setting glacial climates. *Paleoceanography* **28**, 1–23.

Albarède F., Telouk P., Blichert-Toft J., Boyet M., Agranier A. and Nelson B. (2004) Precise and accurate isotopic measurements using multiple-collector ICPMS. *Geochim. Cosmochim. Acta* **68** (12), 2725–2744.

Amakawa H., Nozaki Y., Alibo D. S., Zhang J., Fukugawa K. and Nagai H. (2004a) Neodymium isotopic variations in Northwest Pacific water. *Geochim. Cosmochim. Acta* **68**, 715–727.

Amakawa H., Sasaki K. and Ebihara M. (2009) Nd isotopic composition in the central North Pacific. *Geochim. Cosmochim. Acta* **73** (16), 4705–4719.

Anderson J. B., Shipp S. S., Lowe A. L., Wellner J. S. and Mosola A. B. (2002) The Antarctic Ice Sheet during the Last Glacial Maximum and its subsequent retreat history: a review. *Quaternary Science Reviews*, **21**, 49-70

Arsouze T., Dutay J.-C., Lacan F. and Jeandel C. (2009) Reconstructing the Nd oceanic cycle using a coupled dynamical biogeochemical model. *Biogeosciences* **6**(12), 2829–2846.

Barrat J. A., Keller F., Amosse´ J., Taylor R. N., Nesbitt R. W. and Hirata T. (1996) Determination of Rare Earth Elements in sixteen silicate reference samples by ICP-MS after Tm addition and ion exchange separation. *Geostand. Geoanal. Res.* **20**, 133–139

Broecker W.S. (1982) Ocean chemistry during glacial time. *Geochim. Cosmochim. Acta* **46**, 1689–1705.

Boyle E.A. and Keigwin L.D. (1986) Comparison of Atlantic and Pacific paleochemical records for the last 215,000 years: changes in deep ocean circulation and chemical inventories. *Earth Planet. Sci. Lett*. **76** (1–2), 135–150.

Carter P., Vance D., Hillenbrand C. D., Smith J. A. and Shoosmith D. R. (2012) The neodymium isotopic composition of waters masses in the eastern Pacific sector of the Southern Ocean. *Geochim. Cosmochim. Acta* **79**, 41-59.

Charles C.D. and Fairbanks R.G. (1992) Evidence from Southern Ocean sediments for the effect of North Atlantic deep water flux on climate. *Nature* **355**, 416–419.

Charles C.D., Wright J.D. and Fairbanks R.G. (1993). Thermodynamic influences on the marine carbon isotope record. *Paleoceanography* **8** (6), 691–698.

Chase Z., Anderson R. F., Fleisher M. Q. and Kubik P. W. (2003) Accumulation of biogenic and lithogenic material in the Pacific sector of the Southern Ocean during the past 40,000 years. *Deep-Sea Res. II*, **50**, 799-832

Chow T. J. and Patterson C. C. (1959) Lead isotopes in manganese nodules. *Geochim. Cosmochim. Acta* **17**,21-31

Chow T. J. and Patterson C. C. (1962) The occurrence and significance of lead isotopes in pelagic sediments. *Geochim. Cosmoihim. Acta* **26**, 263-308.

Curry W.B. and Oppo D. W. (2005) Glacial water mass geometry and the distribution of $\delta^{13}C$ of ∑CO2 in the western Atlantic Ocean. *Paleoceanography* **20**, PA1017, http://dx.doi.org/doi:1010.1029/2004PA001021.

Delmonte B., Basile-Doelsch I., Petit J.-R., Maggi V., Revel-Rolland M., Michard A., Jagoutz E. and Grousset F. (2004) Comparing the Epica and Vostok dust records during the last 220,000 years: stratigraphical correlation and provenance in glacial periods. *Earth-Science Reviews* **66**, 63–87.

Denton G. H. and Hughes T. J. (2002) Reconstructing the Antarctic Ice Sheet at the Last Glacial Maximum. *Quaternary Science Rev*. **21**, 193-202

Duplessy J.-C., Shackleton N.J., Fairbanks R.G., Labeyrie L., Oppo D.W. and Kallel N. (1988) Deepwater source variations during the last climatic cycle and their impact on the global deepwater circulation. *Paleoceanography* **3**, 343–360.

Elderfield H., Ferretti P., Greaves M., Crowhurst S., McCave I. N., Hodell D., and Piotrowski A. M. (2012) Evolution of ocean temperature and ice volume through the Mid-Pleistocene Climate Transition, *Science* **337**(6095), 704-709.

Elliot M., et al. (1998) Millennial-scale iceberg discharges in the Irminger Basin during the last glacial period: relationship with the Heinrich Events and environmental settings. *Paleoceanography* **13** (5), 433–446.

Elmore A.C., Piotrowski A.M., Wright J.D. and Scrivner A.E. (2011) Testing the extraction of past seawater Nd isotopic composition from North Atlantic marine sediments. *Geochem. Geophys. Geosyst.* **12**, Q09008, http://dx.doi.org/doi:09010.01029/02011GC003741.

Foster G.L. and Vance D. (2006) Negligible glacial–interglacial variation in continental chemical weathering rates. *Nature* **444**, 918–921.

Frank M. (2002) Radiogenic isotopes: Tracers of past ocean circulation and erosional input, *Rev. Geophys.,* **40**(1), 1001, doi:10.1029/2000RG000094.

Franzese A. M., Hemming S. R., Goldstein S. L. and R. F. Anderson (2006) Reduced Agulhas leakage at the LGM inferred from an integrated provenance and flux study, *Earth Planet. Sci. Lett.,* **250**, 72–88.

Futa K. and Stern C. R. (1988) Sr and Nd isotopic and trace element compositions of Quaternary volcanic centers of the southern Andes, *Earth Planet. Sci. Lett.,* **88**, 253-262.

Tiedemann R., Lamy F., cruise participants (2014) FS Sonne Fahrtbericht/Cruise Report SO213 - SOPATRA: South Pacific Paleoceanographic Transects - Geodynamic and Climatic Variability in Space and Time, Leg 1: Valparaiso/Chile - Valparaiso/Chile, 27.012.2010 - 12.01.2011, Leg 2: Valparaiso/Chile - Wellington/New Zealand, 12.01.2011 - 07.03.2011. doi:10.2312/cr_so213

Galer S.J.G. and O'Nions R.K. (1989) Chemical and isotopic studies of ultramafic inclusions from the San Carlos volcanic field, Arizona: a bearing on their petrogenesis. *J. Petrol.* **30** (4), 1033–1064.

Garcia-Solsona E., Jeandel C., Labatut M., Lacan F., Vance D., Chavagnac V. and Pradoux C. (2014) Rare earth elements and Nd isotopes tracing water mass mixing and particle-seawater interactions in the SE Atlantic. *Geochim. Cosmochim. Acta* **125**, 351–372

Gordon A. L. (1975) An Antarctic oceanographic section along 170°E. *Deep-Sea Res.* **22**, 357–377

Grasse P., Stichel T., Stumpf R., Stramma L. and Frank M. (2012) The distribution of neodymium isotopes and concentrations in the Eastern Equatorial Pacific: Water mass advection versus particle exchange. *Earth Planet. Sci. Lett.* **353-354**, 198-207.

Gutjahr M., Frank M., Stirling C. H., Klemm V., van de Flierdt T. and A. N. Halliday (2007) Reliable extraction of a deepwater trace metal isotope signal from Fe-Mn oxyhydroxide coatings of marine sediments, *Chem. Geol*., **242**, 351–370, doi:10.1016/j.chemgeo.2007.03.021.

Hemming S.R. (2004) Heinrich Events: massive late Pleistocene detritus layers of the North Atlantic and their global climate imprint. *Rev. Geophys*. **42** (1), RG1005.

Hemming S.R., van der Flierdt T., Goldstein S.L., Franzese A. M., Roy M., Gastineu G. and Landrot G. (2007) Strontium isotope tracing of terrigenous sediment dispersal in the Antarctic Circumpolar Current: Implications for constraining frontal positions, *Geochem. Geophys. Geosyst.* **8**, Q06N13, doi:10.1029/2006GC001441

Hickey R. L., Frey F. A. and Gerlach D. C. (1986) Multiple sources for basaltic arc rocks from the Southern Volcanic Zone of the Andes (34°-41° S): Trace element and isotopic evidence for contributions from subducted oceanic crust, mantle and continental crust, *J. of Geophysical Research*, **91**, 5963-5983

Horwitz E. P., Chiarizia R. and Dietz M. L. (1992) A novel strontium-selective extraction chromatographic resin. *Solvent Extr. Ion Exch.* **10**, 313–336. http://dx.doi.org/10.1080/07366299208918107.

Huang K-F., You C-F., Chung C-H., Lin Y-H. and Liu Z. (2014) Tracing the Nd isotope evolution of North Pacific Intermediate and Deep Waters through the last deglaciation from South China Sea sediments*. J Asian Earth Sci.,* **79**, 564-573

Jacobsen S.B. and Wasserburg G.J. (1980) Sm–Nd isotopic evolution of chondrites. *Earth Planet. Sci. Lett.* **50**, 139–155.

Kawabe M. and Fujio S. (2010) Pacific Ocean circulation based on observation*. J. Oceanogr.* **66**, 389–403.

Keigwin L.D. (1998) Glacial-age hydrography of the north west Pacific Ocean. *Paleoceanography* **13** (4), 323–339.

Kraft S., Frank M., Hathorne E. C. and Weldeab S. (2013) Assessment of seawater Nd isotope signatures extracted from foraminiferal shells and authigenic phases of Gulf of Guinea sediments, *Geochim. Cosmochim. Acta* **121**, 414-435.

Lacan F. and Jeandel C. (2005) Neodymium isotopes as a new tool for quantifying exchange fluxes at the continentocean interface, *Earth Planet. Sci. Lett.,* **232**, 245–257.

Lang N. and Wolff E. W. (2011) Interglacial and glacial variability from the last 800 ka in marine, ice and terrestrial archives. *Clim. Past*, **7**, 361–380. doi:10.5194/cp-7-361-2011

Lamy F., Gersonde R., Winckler G., Esper O., Jaeschke A., Kuhn G., Ullermann J., Martinez-Garcia A., Lambert F. and Kilian R. (2014) Increased Dust Deposition in the Pacific Southern Ocean During Glacial Periods. *Science* **343**, 403. DOI: 10.1126/science.1245424

Le Fevre B. and Pin C. (2005) A straightforward separation scheme for concomitant Lu–Hf and Sm–Nd isotope ratio and isotope dilution analysis. *Anal. Chim. Acta* **543**, 209–221..

Lisiecki L. E. and Raymo M. E. (2005) A Pliocene-Pleistocene stack of 57 globally distributed benthic δ 18O records, *Paleoceanography*, **20**(1), doi:10.1029/2004PA001071.

Lugmair G.W. and Galer S.J.G. (1992) Age and isotopic relationships among the angrites Lewis Cliff 86010 and Angra dos Reis. *Geochim. Cosmochim. Acta* **56**, 1673–1694.

Lynch-Stieglitz J. (2006) Tracers of past ocean circulation. In: Elderfield, H. (Ed.), The Oceans and Marine Geochemistry. Treatise on Geochemistry, vol. 6. Elsevier- Pergamon, Oxford, pp. 433–451 (Chapter 6.16).

Mackensen A., Hubberton H.W., Bickert T., Fischer G. and Futterer D.K. (1993) The d13C in benthic foraminiferal tests of Fontbotia wuellerstorfi (Schwager) relative to the d13C of dissolved inorganic carbon in Southern Ocean deep water: implications for glacial ocean circulation models. *Paleoceanography* **8**, 587–610.

Martin E.E. and Scher H.D. (2004) Preservation of seawater Sr and Nd isotopes in fossil fish teeth: bad news and good news. *Earth Planet. Sci. Lett.* **220**, 25–39.

Matsumoto K. and Lynch-Stieglitz J. (1999) Similar glacial and Holocene deepwater circulation inferred from southeast Pacific benthic foraminiferal carbon isotope composition. *Paleoceanography* **14** (2), 149–163.

Matsumoto K., Oba T., Lynch-Stieglitz J. and Yamamoto H. (2002) Interior hydrography and circulation of the glacial Pacific Ocean. *Quaternary Science Reviews* **21**, 1693–1704.

McCave I. N., Carter L. and Hall I. R. (2008) Glacial–interglacial changes in water mass structure and flow in the SW Pacific Ocean. *Quat. Sci. Rev.* **27**,1886–1908, http://dx.doi.org/10.1016/j.quascirev.2008.07.010

McManus J.F., Francois R., Gherardi J.-M., Keigwin L. and Brown-Leger S. (2004) Collapse and rapid resumption of Atlantic meridional circulation linked to deglacial climate changes. *Nature* **428**, 834–837.

Mix A.C. (1995) Benthic foraminifer stable isotope record from Site 849 (0–5 Ma): local and global climate changes. *Proc. Ocean Drill. Program Sci. Results* **138**, 371–412.

Molina-Kescher, M., Frank, M., Hathorne, E., 2014. South Pacific dissolved Nd isotope compositions and rare earth element distributions: Water mass mixing versus biogeochemical cycling. *Geochim. Cosmochim. Acta* **127**, 171-189.

Molina-Kescher, M., Frank, M., Hathorne, E., Nd and Sr isotope compositions of different phases of surface sediments in the South Pacific: extraction of seawater signatures, boundary exchange, and detrital/dust provenance. *Geochem. Geophys. Geosyst. submitted*

Ninnemann U.S. and Charles C.D. (2002) Changes in the mode of Southern Ocean circulation over the last glacial cycle revealed by foraminiferal stable isotopic variability. *Earth Planet. Sci. Lett.* **201** (2), 383.

Noble T. L., Piotrowski A. M., Robinson L. F., McManus J. F., Hillenbrand C-D. and Bory A. J.-M. (2012) Greater supply of Patagonian sourced detritus and transport by the ACC to the Atlantic sector of the Southern Ocean during the last glacial period. Earth Planet. Sci. Lett. 317, 374–385.

Noble T. L., Piotrowski, A.M. and McCave, I. N. (2013) Neodymium isotopic composition of intermediate and deep waters in the glacial southwest Pacific. *Earth Planet. Sci. Lett.* **384**, 27-36.

Okazaki Y., Timmermann A., Menviel L., Harada N., Abe-Ouchi A., Chikamoto M.O., Mouchet A. and Asahi H. (2010) Deep water formation in the North Pacific during the last glacial termination. *Science* **329**, 200–204.

Oliver K. I. C., Hoogakker B. A. A., Crowhurst S., Henderson G. M., Rickaby R. E. M., Edwards N. R. and Helderfield H. (2010) A synthesis of marine sediment core $\delta^{13}C$ data over the last 150 000 years. *Clim. Past*, **6**, 645-673

Orsi A.H., Johnson G.C. and Bullister J.L. (1999) Circulation, mixing, and production of Antarctic Bottom Water. *Prog. Oceanogr.* **43**, 55–109.

Pearce C. R., Jones M. T., Oelkers E. H., Pradoux C. and Jeandel C., 2013. The effect of particulate dissolution on the neodymium (Nd) isotope and Rare Earth Element (REE) composition of seawater. *Earth Planet. Sci. Lett.* **369-370**, 21-40

Peterson C. D., Lisiecki L. E. and Stern J. V. (2014) Deglacial whole-ocean $\delta^{13}C$ change estimated from 480 benthic foraminiferal records. *Paleoceanography*. doi: 10.1002/2013PA002552

Piepgras D.J. and Jacobsen S.B. (1988) The isotopic composition of neodymium in the North Pacific. *Geochim. Cosmochim. Acta* **52**, 1373–1381

Piepgras D.J. and Wasserburg G.J. (1982) Isotopic composition of neodymium in waters from the Drake Passage. *Science* **217**, 207–214.

Piepgras D. J. and Wasserburg G. J. (1987) Rare earth element transport in the western North Atlantic inferred from Nd isotopic observations. *Geochim. Cosmochim. Acta* 51, 1257–1271. *Earth Planet. Sci. Lett.* **357-358**, 289-297.

Piotrowski A.M., Banakar V.K., Scrivner A.E., Elderfield H., Galy A. and Dennis A. (2009) Indian Ocean circulation and productivity during the last glacial cycle. *Earth Planet. Sci. Lett.* **285**, 179–189.

Piotrowski A. M., Galy A., Nicholl J. A. L., Roberts N., Wilson D. J., Clegg J. A. and Yu J., 2012. Reconstructing deglacial North and South Atlantic deep water sourcing using foraminiferal Nd isotopes. *Earth Planet. Sci. Lett*. **357-358**, 289-297.

Piotrowski A.M., Goldstein S.L., Hemming S.R. and Fairbanks R.G. (2004) Intensification and variability of ocean thermohaline circulation through the last deglaciation*. Earth Planet. Sci. Lett.* **225**, 205–220.

Piotrowski A. M., Goldstein S. L., Hemming S. R. and Fairbanks R. G. (2005) Temporal relationships of carbon cycling and ocean circulation at glacial boundaries, *Science*, **307**, 1933–1938, doi:10.1126/science.1104883.

Piotrowski A. M., Goldstein S. L., Hemming S. R., Fairbanks R. G. and Zylberberg D. R. (2008) Oscillating glacial northern and southern deep water formation from combined neodymium and carbon isotopes, *Earth Planet. Sci. Lett.,* **272**(1–2), 394–405, doi:10.1016/j.epsl.2008.05.011.

Rahmstorf S. (2002) Ocean circulation and climate during the past 120,000 years. *Nature* **419**, 207-214 doi:10.1038/nature01090

Ravelo C. and Hillaire-Marcel C. (2007) Developments in Marine Geology, Volume 1. doi:10.1016/S1572-5480(07)01023-8

Reid J. L. and Lynn R. J. (1971) On the influence of the Norwegian-Greenland and Weddell seas upon the bottom waters of the Indian and Pacific oceans. *Deep-Sea Res.* **18**, 1063-1088.

Reid J. L. (1986) On the total geostrophic circulation of the South Pacific Ocean: Flow patterns, tracers and Transports. *Prog. Oceanog.* **16**, 1-61

Rempfer J., Stocker T. F., Joos F., Dutay J. C. and Siddall M. (2011) Modelling Nd isotopes with a coarse resolution ocean circulation model: Sensitivities to model parameters and source/sink distributions, *Geochim. Cosmochim. Acta*, **75**, 5927–5950.

Revel-Rolland M., De Deckker P., Delmonte B., Hesse P.P., Magee J.W., Basile-Doelsch I., Grousset F. and Bosch D. (2006) Eastern Australia: a possible source of dust in East Antarctica interglacial Ice. *Earth Planet. Sci. Lett.,* **249**, 1–13.

Rickli J., Frank M. and Halliday A. N. (2009) The hafnium neodymium isotopic composition of Atlantic seawater, *Earth Planet. Sci. Lett.,* **280**, 118–127, doi:10.1016/j.epsl.2009. 01.026.

Roberts N. L., Piotrowski A. M., McManus J. F. and Keigwin L. D. (2010) Synchronous deglacial overturning and water mass source changes, *Science*, **327**, 75–78, doi:10.1126/ science.1178068.

Roberts N. L., Piotrowski A. M., Elderfield H., Eglinton T. I. and Lomas M. W. (2012) Rare earth element association with foraminifera. *Geochim. Cosmochim. Acta* **94**, 57–71.

Roy M., van der Flierdt T., Hemming S. R. and Goldstein S. L (2007) $^{40}Ar/^{39}Ar$ ages of hornblade grains and bulk Sm/Nd isotopes of circum-Antarctic glacio-marine sediments: Impications for sediment provenance in the southern ocean, Chemical *Geology*, **244**, 507-519.

Rutberg R. L., Hemming S. R. and Goldstein S. L. (2000) Reduced North Atlantic Deep Water flux to the glacial Southern Ocean inferred from neodymium isotope ratios, *Nature*, **405**, 935–938, doi:10.1038/35016049.

Sigman D. M., Hain M. P., Haug G. H. (2010) The polar ocean glacial cycles in atmospheric $CO_2$ conentration. *Nature* **466**, 47–55**.** doi:10.1038/nature09149

Singh S.P., Singh S.K., Goswami V., Bhushan R., Rai V.K. (2012) Spatial distribution of dissolved neodymium and $\varepsilon_{Nd}$ in the Bay of Bengal: Role of particulate matter and mixing of water masses. *Geochim. Cosmochim. Acta* **94**, 38-56.

Stern C. R. and Kilian R. (1996) Role of the subducted slab, mantle wedge and continental crust in the generation of adakites from the Andean Austral Volcanic Zone. *Contrib. Mineral Petrol,* **123**, 163-281.

Stichel T., Frank M., Rickli J. and Haley B. A. (2012) The hafnium and neodymium isotope composition of seawater in the Atlantic sector of the Southern Ocean, *Earth Planet. Sci. Lett.,* **317**, 282–294.

Stichel T., Frank M., Rickli J., Hathorne E. C., Haley B. A., Jeandel C. and Pradoux C. (2012) Sources and input mechanisms of hafnium and neodymium in surface waters of the Atlantic sector of the Southern Ocean, *Geochim. Cosmochim. Acta,* **94**, 22-37

Tachikawa K., Athias V. and Jeandel C. (2003) Neodymium budget in the modern ocean and paleo-oceanographic implications. *J. Geoph. Res.* **108** (C8).

Tachikawa K., Piotrowski A. M. and Bayon G. (2014) Neodymium associated with foraminiferal carbonate as a recorder of seawater isotopic signatures. *Quaternary Science Reviews* **88** 1-13. doi: http://dx.doi.org/10.1016/j.quascirev.2013.12.027

Tanaka T. et al. (2000) JNdi-1: A neodymium isotopic reference in consistency with LaJolla neodymium, *Chem. Geol.*, **168**(3–4), 279–281, doi:10.1016/S0009-2541(00)00198-4.

Tapia R., Nürnberg D., Ronge T. and Tiedemann R. Glacial disparities in Intermediate Mode Water advection in the South Pacific Gyre. *Earth Planet. Sci. Lett. Submitted.*

Taylor S. R., McLennan S. M. and McCulloch M. T. (1983) Geochemistry of loess, continental crustal composition and crustal model ages, *Cosmochim. Acta*, **47**, 1897-1905.

Tiedemann R., Lamy F., cruise participants (2014) FS Sonne Fahrtbericht/Cruise Report SO213 - SOPATRA: South Pacific Paleoceanographic Transects - Geodynamic and Climatic Variability in Space and Time, Leg 1: Valparaiso/Chile - Valparaiso/Chile, 27.012.2010 - 12.01.2011, Leg 2: Valparaiso/Chile - Wellington/New Zealand, 12.01.2011 - 07.03.2011. doi:10.2312/cr_so213

van de Flierdt T., Robinson L.F., Adkins J.F., Hemming S.R. and Goldstein S.L. (2006) Temporal stability of the neodymium isotope signature of the Holocene to glacial North Atlantic. *Paleoceanography* **21**, PA4102, http://dx.doi.org/doi:4110.1029/ 2006PA001294

van der Flierdt T., et al. (2007) Global neodymium - hafnium isotope systematics – revisited. *Earth Planet. Sci. Lett.* **259**, 432–441.

Warren B. A. (1973) Transpacific hydrographic sections at latitudes 43°S and 28°S, the SCORPIO Expedition II. Deep Water. *Deep-Sea Res*. **20**, 9–38.

Wilson, D. J., A. M. Piotrowski, A. Galy, and J. A. Clegg (2013) Reactivity of neodymium carriers in deep sea sediments: Implications for boundary exchange an paleoceanography, *Geochim. Cosmochim. Acta*, **109**, 197-221.

# 6) Summary and outlook

The principal conclusions of this thesis are:

1) Nd isotopes serve as a reliable proxy to study past deep-water circulation regimes in the South Pacific as they faithfully trace the principal intermediate and deep-water masses of todays water column and these $\varepsilon_{Nd}$ signatures can be reliably extracted from surface sediments despite some problems such as the low sedimentation rates of this area.

The principal water masses of the South Pacific are recognizable by their oxygen concentrations and Nd isotope compositions: Southern Ocean derived water masses (AAIW, UCDW and LCDW), which occupy intermediate and deep waters, present high oxygen concentrations and typical $\varepsilon_{Nd}$ signatures of around -8.3 whereas Pacific derived waters (NPDW and SPGDW), flowing at middepths, have low oxygen concentrations and more positive $\varepsilon_{Nd}$ values ranging from -5.3 to -6. The most reliable techniques to extract these signatures from the sediment, where they are stored in early diagenetic Fe-Mn oxydroxide coatings of the sediment particles, are: dissolution of clay-free ('unclean') planktonic foraminifera, leaching of the bulk sediment without previous de-carbonation and dissolution of fossil fish teeth. The low sedimentation rates of this area result in the integration of Nd isotope composition from different circulation regimes of the past, which can complicate paleocirculation studies in this area.

2) The advection of NADW reaches locations far from its formation regions, such as the South Pacific, and has played a crucial role for the thermohaline circulation of the last 240 000 years.

Nutrient poor NADW has been identified in terms of Nd isotope composition (~-9.7) at the western end of the South Pacific, where it forms part of the Deep Western Boundary Current (DWBC) that flows northwards to the east of New Zealand. The Nd isotope composition of the DWBC is apparently not affected by 'boundary exchange' processes with the continental margin. The shoaling and reduced production of NADW during glacial periods has been a principal mechanism that has modified the deepwater circulation of the central South Pacific during the last 240 000 years as indicated by Nd and Pb isotope records that indicate a decreased proportion of NADW in CDW, the water mass that dominates the water column above the East Pacific Rise.

3) The lithogenic material found in the sediment of the South Pacific predominantly originates from Southeastern Australia and southern New Zealand. This source has dominated the continental derived material of the central South Pacific over the last 240 000 years.

The detrital material consists of fine particles brought to the South Pacific by the dominant Southern Westerly Winds (SWW) or westerlies. The influence of these sources is reduced in the eastern South Pacific, where the proportions of Andean derived material increases. The presence of detritus from west Antarctica and the Ross Sea at the New Zealand Margin and in the southeastern Pacific Basin supplied by oceanic currents cannot be excluded. During glacial stages the central South Pacific experienced enhanced supply of Antarctic derived material, most likely transported in suspension by oceanic currents. Evidences of submarine explosive eruptions on the summit of the East Pacific Rise were also found. These pieces of evidence are based on combined Nd-Sr isotope compositions of the detrital fraction of the sediment.

Besides these and other findings presented in this thesis, some open questions remained that should be subject of future work:

1) The role of NPDW for the THC in the past is controversial given that it is not clear whether or not this water mass deepened during glacial periods or if its production in the North Pacific was enhanced during Heinrich events. Therefore, the detailed study of sedimentary records from the eastern South Pacific, where these water mass exits the Pacific today, will help to solve these issues. Although, as noticed in this work, NPDW is exposed to pronounce scavenging processes at the equator, Nd isotopes could be very useful for these investigations. Nevertheless, this task will be difficult as became obvious from the material recovered as part of cruise SO213, during which, as a consequence of the low sedimentation rates in this area, only the recovery of very old (up to 4 Ma) sediments was possible, in which pronounced glacial-interglacial variations were not enough resolute.

2) Another important investigation should include a detailed sampling of seawater samples on the pathway of NPDW from the North Pacific to the Drake's Passage in order to find out if Nd isotopes faithfully track its advection and to what extent the scavenging processes near the equator affect their quasi-conservative behaviour. Such transect has so far not been considered within the international GEOTRACES program but would be worth pursuing for this and a number of other reasons.

3) Sediment core SO213-60-1, which has been analysed in this thesis in terms of Nd, Pb, Sr O and C isotopes for the past 220 ka, covers the past 1 million years. Therefore, a detailed

investigation of the entire core would be very helpful to understand circulation regimes of the central South Pacific during this interval, especially the Mid-Pleistocene Transition, the period between the 41 ka and 100 ka orbital cycles.

# Appendix

***Table S1.*** *Data obtained from core SO213-59-2 with 2σ uncertainties.*
*2σ uncertainty for benthic $\delta^{18}O$ and $\delta^{13}C$ are 0.06 and 0.07 respectively for all samples*

| Depth top [cm] | Age [Kyr] | $\delta^{18}O$ benthic | $\delta^{13}C$ benthic | $\varepsilon_{Nd}$ forams | 2σ | $\varepsilon_{Nd}$ leachates | 2σ | $\varepsilon_{Nd}$ detritus | 2σ | $^{208}Pb/^{204}Pb$ leach | 2σ | $^{207}Pb/^{204}Pb$ leach | 2σ | $^{206}Pb/^{204}Pb$ leach | 2σ | $^{208}Pb/^{206}Pb$ leach | 2σ | $^{207}Pb/^{206}Pb$ leach | 2σ | $^{87}Sr/^{86}Sr$ detritus | 2σ |
|---|---|---|---|---|---|---|---|---|---|---|---|---|---|---|---|---|---|---|---|---|---|
| 4 | 7,17 | 2,903 | 0,516 | -6,11 | 0,22 | -5,95 | 0,4 | -5,24 | 0,24 | 38,677 | 0,015 | 15,626 | 0,005 | 18,771 | 0,004 | 2,060 | 0,001 | 0,8324 | 0,0001 | 0,709246 | 0,00004 |
| 5 | 7,81 | 3,359 | 0,278 | | | | | | | | | | | | | | | | | | |
| 6 | 8,44 | 3,014 | 0,401 | -5,57 | 0,33 | | | | | | | | | | | | | | | | |
| 7 | 9,08 | 3,183 | 0,230 | | | | | | | | | | | | | | | | | | |
| 8 | 9,72 | 3,002 | 0,398 | -6,08 | 0,22 | | | | | | | | | | | | | | | | |
| 9 | 10,36 | 2,78 | 0,537 | | | | | | | | | | | | | | | | | | |
| 10 | 11,00 | 3,173 | 0,514 | -5,48 | 0,33 | | | | | | | | | | | | | | | | |
| 13 | 12,92 | 3,391 | 0,150 | | | | | | | | | | | | | | | | | | |
| 14 | 13,56 | 3,52 | 0,020 | -5,67 | 0,22 | | | | | | | | | | | | | | | | |
| 16 | 14,83 | 3,723 | -0,068 | | | | | | | | | | | | | | | | | | |
| 17 | 15,47 | 4,122 | 0,006 | | | | | | | | | | | | | | | | | | |
| 18 | 16,11 | 4,332 | -0,167 | | | | | | | | | | | | | | | | | | |
| 19 | 16,75 | 4,186 | 0,060 | -4,96 | 0,33 | | | | | | | | | | | | | | | | |
| 20 | 17,39 | 4,229 | -0,030 | | | | | | | | | | | | | | | | | | |
| 21 | 18,03 | 4,19 | -0,079 | | | | | | | | | | | | | | | | | | |
| 22 | 18,67 | 4,605 | -0,029 | | | | | | | | | | | | | | | | | | |
| 23 | 19,31 | 4,263 | -0,104 | -5,39 | 0,22 | -5,33 | 0,4 | -3,76 | 0,24 | 38,601 | 0,015 | 15,616 | 0,005 | 18,738 | 0,004 | 2,060 | 0,001 | 0,8333 | 0,0001 | 0,709326 | 0,00004 |
| 24 | 19,94 | 4,359 | -0,143 | | | | | | | | | | | | | | | | | | |
| 25 | 20,58 | 4,237 | -0,165 | | | | | | | | | | | | | | | | | | |
| 26 | 21,22 | 4,312 | -0,129 | | | | | | | | | | | | | | | | | | |
| 27 | 21,86 | 4,456 | 0,256 | | | | | | | | | | | | | | | | | | |
| 28 | 22,50 | 4,2 | -0,044 | | | | | | | | | | | | | | | | | | |
| 29 | 23,14 | 4,169 | 0,086 | | | | | | | | | | | | | | | | | | |
| 30 | 23,78 | 4,16 | -0,089 | | | | | | | | | | | | | | | | | | |
| 31 | 24,42 | 4,194 | -0,114 | -5,57 | 0,22 | | | | | | | | | | | | | | | | |
| 32 | 25,06 | 4,253 | 0,080 | | | | | | | | | | | | | | | | | | |
| 33 | 25,69 | 4,228 | 0,172 | -5,65 | 0,24 | | | | | | | | | | | | | | | | |
| 34 | 26,33 | 4,236 | 0,122 | | | | | | | | | | | | | | | | | | |
| 35 | 26,97 | 4,085 | -0,053 | -4,24 | 0,33 | | | | | | | | | | | | | | | | |
| 36 | 27,61 | 4,092 | -0,022 | | | | | | | | | | | | | | | | | | |
| 37 | 28,25 | 3,997 | 0,039 | -5,49 | 0,24 | | | | | | | | | | | | | | | | |
| 39 | 28,89 | 4,063 | 0,185 | -6,19 | 0,22 | -5,39 | 0,4 | -4,77 | 0,24 | 38,621 | 0,015 | 15,619 | 0,005 | 18,745 | 0,004 | 2,060 | 0,001 | 0,8332 | 0,0001 | 0,709367 | 0,00004 |
| 40 | 30,17 | 3,986 | 0,154 | | | | | | | | | | | | | | | | | | |
| 41 | 30,81 | 4,106 | 0,073 | -5,39 | 0,33 | | | | | | | | | | | | | | | | |
| 42 | 31,44 | 3,915 | 0,017 | | | | | | | | | | | | | | | | | | |
| 43 | 32,08 | 4,45 | -0,107 | | | | | | | | | | | | | | | | | | |
| 44 | 32,72 | 3,999 | 0,047 | | | | | | | | | | | | | | | | | | |

| Depth top [cm] | Age [Kyr] | $\delta^{18}O$ benthic | $\delta^{13}C$ benthic | $\varepsilon_{Nd}$ forams | 2σ | $\varepsilon_{Nd}$ leachates | 2σ | $\varepsilon_{Nd}$ detritus | 2σ | $^{208}Pb/^{204}Pb$ leach | 2σ | $^{207}Pb/^{204}Pb$ leach | 2σ | $^{206}Pb/^{204}Pb$ leach | 2σ | $^{208}Pb/^{206}Pb$ leach | 2σ | $^{207}Pb/^{206}Pb$ leach | 2σ | $^{87}Sr/^{86}Sr$ detritus | 2σ |
|---|---|---|---|---|---|---|---|---|---|---|---|---|---|---|---|---|---|---|---|---|---|
| 45 | 33,36 | 3,937 | 0,076 | -5,62 | 0,24 | | | | | | | | | | | | | | | | |
| 46 | 34,00 | 3,925 | 0,035 | | | | | | | | | | | | | | | | | | |
| 47 | 35,37 | 4,243 | -0,037 | | | | | | | | | | | | | | | | | | |
| 48 | 36,73 | 3,972 | 0,161 | | | | | | | | | | | | | | | | | | |
| 49 | 38,10 | 3,992 | -0,045 | | | | | | | | | | | | | | | | | | |
| 50 | 39,46 | 4,048 | 0,314 | | | | | | | | | | | | | | | | | | |
| 51 | 40,83 | 4,151 | -0,082 | -5,88 | 0,24 | | | | | | | | | | | | | | | | |
| 52 | 42,20 | 3,924 | -0,012 | | | | | | | | | | | | | | | | | | |
| 53 | 43,56 | 3,972 | 0,259 | -5,40 | 0,23 | | | | | | | | | | | | | | | | |
| 54 | 44,93 | 4,063 | 0,165 | | | | | | | | | | | | | | | | | | |
| 55 | 46,29 | 4,075 | -0,106 | -5,73 | 0,22 | -5,34 | 0,4 | -5,21 | 0,24 | 38,671 | 0,015 | 15,634 | 0,005 | 18,760 | 0,004 | 2,061 | 0,001 | 0,8333 | 0,0001 | 0,709512 | 0,00004 |
| 56 | 47,66 | 3,964 | -0,088 | | | | | | | | | | | | | | | | | | |
| 57 | 49,02 | 4,005 | -0,264 | | | | | | | | | | | | | | | | | | |
| 58 | 50,39 | 3,936 | -0,035 | | | | | | | | | | | | | | | | | | |
| 59 | 51,76 | 4,175 | -0,067 | -5,85 | 0,24 | | | | | | | | | | | | | | | | |
| 60 | 53,12 | 4,054 | -0,289 | | | | | | | | | | | | | | | | | | |
| 61 | 54,49 | 3,948 | -0,156 | | | | | | | | | | | | | | | | | | |
| 62 | 55,85 | 4,012 | -0,052 | | | | | | | | | | | | | | | | | | |
| 63 | 57,22 | 4,159 | -0,020 | -5,80 | 0,22 | | | | | | | | | | | | | | | | |
| 64 | 58,59 | 3,779 | -0,021 | | | | | | | | | | | | | | | | | | |
| 65 | 59,95 | 4,159 | -0,074 | -5,72 | 0,24 | | | | | | | | | | | | | | | | |
| 66 | 61,32 | 3,941 | 0,175 | | | | | | | | | | | | | | | | | | |
| 67 | 62,68 | 3,816 | -0,108 | -5,76 | 0,23 | -5,47 | 0,4 | -4,13 | 0,24 | 38,638 | 0,015 | 15,624 | 0,005 | 18,756 | 0,004 | 2,060 | 0,001 | 0,8330 | 0,0001 | 0,709303 | 0,00004 |
| 68 | 64,05 | 3,895 | -0,008 | | | | | | | | | | | | | | | | | | |
| 69 | 65,41 | 3,963 | 0,090 | -5,66 | 0,24 | | | | | | | | | | | | | | | | |
| 70 | 66,78 | 3,906 | 0,207 | | | | | | | | | | | | | | | | | | |
| 71 | 68,15 | 3,977 | 0,256 | -5,98 | 0,22 | | | | | | | | | | | | | | | | |
| 72 | 69,51 | 3,918 | 0,124 | | | | | | | | | | | | | | | | | | |
| 73 | 70,88 | 3,709 | 0,540 | | | | | | | | | | | | | | | | | | |
| 74 | 72,24 | 3,792 | 0,366 | | | | | | | | | | | | | | | | | | |
| 75 | 73,61 | 3,748 | 0,280 | | | | | | | | | | | | | | | | | | |
| 76 | 74,98 | 4,075 | -0,045 | | | | | | | | | | | | | | | | | | |
| 77 | 76,34 | 3,666 | 0,487 | -5,79 | 0,24 | | | | | | | | | | | | | | | | |
| 78 | 77,71 | 3,64 | 0,355 | | | | | | | | | | | | | | | | | | |
| 79 | 79,07 | 3,544 | 0,331 | -6,07 | 0,22 | | | | | | | | | | | | | | | | |
| 80 | 80,44 | 3,688 | 0,361 | | | | | | | | | | | | | | | | | | |
| 81 | 81,80 | 3,231 | 0,241 | | | | | | | | | | | | | | | | | | |
| 82 | 82,64 | 3,593 | 0,256 | | | | | | | | | | | | | | | | | | |
| 83 | 83,47 | 3,799 | 0,291 | -5,72 | 0,23 | | | | | | | | | | | | | | | | |
| 84 | 84,31 | 3,587 | 0,233 | | | | | | | | | | | | | | | | | | |
| 85 | 85,14 | 3,98 | 0,323 | | | | | | | | | | | | | | | | | | |

| Depth top [cm] | Age [Kyr] | $\delta^{18}O$ benthic | $\delta^{13}C$ benthic | $\varepsilon_{Nd}$ forams | 2σ | $\varepsilon_{Nd}$ leachates | 2σ | $\varepsilon_{Nd}$ detritus | 2σ | $^{208}Pb/^{204}Pb$ leach | 2σ | $^{207}Pb/^{204}Pb$ leach | 2σ | $^{206}Pb/^{204}Pb$ leach | 2σ | $^{208}Pb/^{206}Pb$ leach | 2σ | $^{207}Pb/^{206}Pb$ leach | 2σ | $^{87}Sr/^{86}Sr$ detritus | 2σ |
|---|---|---|---|---|---|---|---|---|---|---|---|---|---|---|---|---|---|---|---|---|---|
| 86 | 85,97 | 4,089 | 0,243 | | | | | | | | | | | | | | | | | | |
| 87 | 86,81 | 3,577 | 0,014 | -5,95 | 0,22 | | | | | | | | | | | | | | | | |
| 88 | 87,64 | 3,525 | 0,319 | | | | | | | | | | | | | | | | | | |
| 89 | 88,47 | 3,727 | 0,101 | | | | | | | | | | | | | | | | | | |
| 90 | 89,31 | 3,706 | -0,103 | | | | | | | | | | | | | | | | | | |
| 91 | 90,14 | 3,64 | -0,083 | | | | | | | | | | | | | | | | | | |
| 92 | 90,97 | 3,606 | 0,170 | | | | | | | | | | | | | | | | | | |
| 93 | 91,81 | 3,619 | 0,214 | | | | | | | | | | | | | | | | | | |
| 94 | 92,64 | 3,602 | 0,236 | | | | | | | | | | | | | | | | | | |
| 95 | 93,47 | 3,555 | 0,402 | -5,97 | 0,22 | -5,79 | 0,4 | -4,23 | 0,24 | 38,623 | 0,015 | 15,617 | 0,005 | 18,769 | 0,004 | 2,058 | 0,001 | 0,8320 | 0,0001 | 0,709294 | 0,00004 |
| 96 | 94,31 | 3,912 | 0,394 | | | | | | | | | | | | | | | | | | |
| 97 | 95,14 | 3,761 | 0,335 | | | | | | | | | | | | | | | | | | |
| 98 | 95,97 | 3,6 | 0,468 | | | | | | | | | | | | | | | | | | |
| 99 | 96,81 | 3,807 | -0,074 | -6,00 | 0,23 | | | | | | | | | | | | | | | | |
| 100 | 97,64 | 3,643 | 0,142 | | | | | | | | | | | | | | | | | | |
| 102 | 99,31 | 3,476 | 0,429 | -6,00 | 0,23 | | | | | | | | | | | | | | | | |
| 104 | 100,98 | 3,501 | 0,222 | | | | | | | | | | | | | | | | | | |
| 106 | 102,64 | 3,554 | 0,288 | -5,89 | 0,23 | | | | | | | | | | | | | | | | |
| 108 | 104,31 | 4,038 | -0,075 | | | | | | | | | | | | | | | | | | |
| 110 | 105,98 | 3,295 | 0,332 | -5,87 | 0,22 | | | | | | | | | | | | | | | | |
| 112 | 107,64 | 3,621 | 0,179 | | | | | | | | | | | | | | | | | | |
| 114 | 109,31 | 3,739 | -0,095 | -5,94 | 0,23 | | | | | | | | | | | | | | | | |
| 116 | 110,98 | 3,616 | 0,049 | | | | | | | | | | | | | | | | | | |
| 118 | 112,64 | 3,15 | 0,368 | -5,81 | 0,22 | -5,60 | 0,4 | -5,17 | 0,24 | 38,605 | 0,015 | 15,608 | 0,005 | 18,759 | 0,004 | 2,058 | 0,001 | 0,8320 | 0,0001 | 0,709292 | 0,00004 |
| 120 | 114,31 | 3,459 | 0,242 | | | | | | | | | | | | | | | | | | |
| 122 | 115,98 | 3,988 | -0,036 | -5,69 | 0,23 | | | | | | | | | | | | | | | | |
| 124 | 117,64 | 3,292 | 0,302 | | | | | | | | | | | | | | | | | | |
| 126 | 119,31 | 3,429 | 0,180 | -5,60 | 0,22 | | | | | | | | | | | | | | | | |
| 128 | 120,98 | 3,354 | 0,392 | | | | | | | | | | | | | | | | | | |
| 130 | 122,65 | 3,173 | -0,258 | | | | | | | | | | | | | | | | | | |
| 132 | 124,31 | 3,545 | 0,131 | -5,49 | 0,23 | | | | | | | | | | | | | | | | |
| 134 | 125,98 | 3,001 | 0,198 | | | | | | | | | | | | | | | | | | |
| 138 | 133,49 | 4,234 | -0,262 | -5,33 | 0,24 | | | | | | | | | | | | | | | | |
| 140 | 137,31 | 3,655 | 0,137 | -5,36 | 0,22 | | | | | | | | | | | | | | | | |
| 142 | 141,13 | 4,201 | -0,423 | -5,34 | 0,24 | -4,00 | 0,4 | -4,40 | 0,24 | 38,638 | 0,015 | 15,625 | 0,005 | 18,753 | 0,004 | 2,060 | 0,001 | 0,8331 | 0,0001 | 0,709342 | 0,00004 |
| 144 | 144,95 | 4,274 | -0,361 | | | | | | | | | | | | | | | | | | |
| 146 | 148,77 | 4,418 | -0,233 | -5,43 | 0,24 | | | | | | | | | | | | | | | | |
| 148 | 152,59 | 4,367 | -0,381 | -5,68 | 0,24 | | | | | | | | | | | | | | | | |
| 150 | 156,41 | 4,244 | -0,437 | | | | | | | | | | | | | | | | | | |
| 152 | 160,23 | 4,341 | -0,474 | -5,24 | 0,22 | | | | | | | | | | | | | | | | |
| 154 | 164,05 | 4,121 | -0,604 | -4,96 | 0,23 | | | | | | | | | | | | | | | | |
| 156 | 167,87 | 4,179 | -0,477 | | | | | | | | | | | | | | | | | | |

| Depth top [cm] | Age [Kyr] | $\delta^{18}O$ benthic | $\delta^{13}C$ benthic | $\varepsilon_{Nd}$ forams | 2σ | $\varepsilon_{Nd}$ leachates | 2σ | $\varepsilon_{Nd}$ detritus | 2σ | $^{208}Pb/^{204}Pb$ leach | 2σ | $^{207}Pb/^{204}Pb$ leach | 2σ | $^{206}Pb/^{204}Pb$ leach | 2σ | $^{208}Pb/^{206}Pb$ leach | 2σ | $^{207}Pb/^{206}Pb$ leach | 2σ | $^{87}Sr/^{86}Sr$ detritus | 2σ |
|---|---|---|---|---|---|---|---|---|---|---|---|---|---|---|---|---|---|---|---|---|---|
| 158 | 171,69 | 4,254 | -0,435 | -5,15 | 0,24 | -4,13 | 0,4 | -4,15 | 0,24 | 38,632 | 0,015 | 15,625 | 0,005 | 18,741 | 0,004 | 2,061 | 0,001 | 0,8337 | 0,0001 | 0,709362 | 0,00004 |
| 160 | 175,51 | 4,34 | -0,133 | -5,25 | 0,22 | | | | | | | | | | | | | | | | |
| 162 | 179,33 | 4,298 | -0,219 | | | | | | | | | | | | | | | | | | |
| 164 | 183,15 | 4,168 | -0,420 | -5,32 | 0,23 | | | | | | | | | | | | | | | | |
| 166 | 186,97 | 4,088 | -0,466 | -5,14 | 0,24 | | | | | | | | | | | | | | | | |
| 168 | 190,78 | 3,847 | -0,526 | | | | | | | | | | | | | | | | | | |
| 170 | 194,02 | 3,501 | 0,222 | -5,45 | 0,23 | -4,55 | 0,4 | -5,10 | 0,24 | 38,637 | 0,015 | 15,624 | 0,005 | 18,750 | 0,004 | 2,061 | 0,001 | 0,8332 | 0,0001 | 0,709497 | 0,00004 |
| 172 | 197,25 | 3,745 | 0,103 | | | | | | | | | | | | | | | | | | |
| 174 | 200,48 | 3,562 | 0,249 | -5,73 | 0,33 | | | | | | | | | | | | | | | | |
| 176 | 203,72 | 3,616 | 0,049 | -5,36 | 0,24 | | | | | | | | | | | | | | | | |
| 178 | 206,95 | 3,684 | 0,065 | -4,89 | 0,23 | | | | | | | | | | | | | | | | |
| 180 | 210,18 | 3,528 | 0,215 | -5,36 | 0,24 | | | | | | | | | | | | | | | | |
| 182 | 213,42 | 4,105 | -0,325 | -6,13 | 0,33 | | | | | | | | | | | | | | | | |
| 184 | 216,65 | 2,867 | 0,321 | | | | | | | | | | | | | | | | | | |
| 186 | 219,12 | 4,304 | -0,246 | -5,96 | 0,33 | | | | | | | | | | | | | | | | |
| 188 | 221,59 | 4,234 | -0,262 | | | | | | | | | | | | | | | | | | |
| 190 | 224,05 | 4,146 | -0,326 | -5,92 | 0,23 | -4,70 | 0,4 | -5,15 | 0,24 | 38,642 | 0,015 | 15,626 | 0,005 | 18,759 | 0,004 | 2,060 | 0,001 | 0,8330 | 0,0001 | 0,709345 | 0,00004 |
| 192 | 226,51 | 4,142 | -0,373 | -5,99 | 0,24 | | | | | | | | | | | | | | | | |
| 194 | 228,98 | 3,934 | -0,669 | -5,45 | 0,23 | | | | | | | | | | | | | | | | |
| 196 | 230,54 | 4,363 | -0,485 | -5,57 | 0,24 | | | | | | | | | | | | | | | | |
| 198 | 232,08 | 4,206 | -0,488 | -5,85 | 0,33 | | | | | | | | | | | | | | | | |
| 200 | 233,63 | 4,147 | -0,397 | | | | | | | | | | | | | | | | | | |
| 202 | 235,17 | 4,184 | -0,700 | -5,94 | 0,23 | | | | | | | | | | | | | | | | |
| 204 | 236,72 | 4,254 | -0,435 | | | | | | | | | | | | | | | | | | |
| 206 | 238,26 | 3,987 | -0,479 | -5,97 | 0,33 | -5,61 | 0,4 | -5,77 | 0,24 | | | | | | | | | | | 0,709259 | 0,00004 |
| 208 | 239,81 | 3,208 | 0,145 | -5,75 | 0,24 | | | | | | | | | | | | | | | | |
| 210 | 241,35 | 4,088 | -0,466 | | | | | | | | | | | | | | | | | | |

***Table S2.*** *Data obtained from core SO213-60-1 with 2σ uncertainties.*
*2σ uncertainty for benthic $\delta^{18}O$ and $\delta^{13}C$ are 0.06 and 0.07 respectively for all samples*

| Depth top [cm] | Age [Kyr] | $\delta^{18}O$ benthic | $\delta^{13}C$ benthic | $\varepsilon_{Nd}$ forams | 2σ | $\varepsilon_{Nd}$ leachates | 2σ | $\varepsilon_{Nd}$ detritus | 2σ | $^{208}Pb/^{204}Pb$ leach | 2σ | $^{207}Pb/^{204}Pb$ leach | 2σ | $^{206}Pb/^{204}Pb$ leach | 2σ | $^{208}Pb/^{206}Pb$ leach | 2σ | $^{207}Pb/^{206}Pb$ leach | 2σ | $^{87}Sr/^{86}Sr$ detritus | 2σ |
|---|---|---|---|---|---|---|---|---|---|---|---|---|---|---|---|---|---|---|---|---|---|
| 1 | 11,3 | 3,068 | -0,219 | -5,78 | 0,29 | -6,02 | 0,4 | -5,24 | 0,24 | 38,657 | 0,015 | 15,623 | 0,005 | 18,751 | 0,004 | 2,061 | 0,001 | 0,833 | 0,0001 | 0,70934 | 0,00004 |
| 3 | 16,0 | 4,238 | -0,716 | -5,79 | 0,41 | | | | | | | | | | | | | | | | |
| 5 | 20,6 | 4,448 | -0,666 | -5,28 | 0,29 | | | | | | | | | | | | | | | | |
| 7 | 25,2 | 4,043 | -0,482 | -5,84 | 0,29 | | | | | | | | | | | | | | | | |
| 9 | 28,0 | 4,353 | -0,339 | -6,15 | 0,29 | | | -4,07 | 0,19 | | | | | | | | | | | 0,71023 | 0,00012 |
| 11 | 30,5 | 4,284 | -0,242 | -5,81 | 0,29 | | | | | | | | | | | | | | | | |
| 13 | 33,0 | 4,403 | -0,924 | | | | | | | | | | | | | | | | | | |
| 15 | 35,5 | 4,411 | -0,539 | -5,68 | 0,29 | -5,58 | 0,4 | -5,03 | 0,24 | 38,666 | 0,015 | 15,630 | 0,005 | 18,756 | 0,004 | 2,062 | 0,001 | 0,833 | 0,0001 | 0,70940 | 0,00004 |
| 17 | 38,0 | 4,156 | -0,297 | -5,71 | 0,29 | | | | | | | | | | | | | | | | |
| 19 | 40,5 | 4,399 | -0,552 | | | | | | | | | | | | | | | | | | |
| 21 | 43,0 | 4,147 | -0,209 | -5,80 | 0,29 | | | | | | | | | | | | | | | | |
| 23 | 45,5 | 4,494 | -0,513 | | | | | | | | | | | | | | | | | | |
| 25 | 48,0 | 4,338 | -0,481 | | | | | | | | | | | | | | | | | | |
| 27 | 50,5 | 4,463 | -0,522 | | | | | | | | | | | | | | | | | | |
| 29 | 53,0 | 4,481 | -0,616 | -5,96 | 0,29 | -5,85 | 0,4 | -5,57 | 0,24 | 38,637 | 0,015 | 15,618 | 0,005 | 18,753 | 0,004 | 2,060 | 0,001 | 0,833 | 0,0001 | 0,70969 | 0,00004 |
| 31 | 55,6 | 4,463 | -0,691 | | | | | | | | | | | | | | | | | | |
| 33 | 58,1 | 4,491 | -0,554 | -5,82 | 0,24 | | | | | | | | | | | | | | | | |
| 35 | 60,6 | 4,496 | -0,503 | | | | | | | | | | | | | | | | | | |
| 37 | 63,1 | 4,336 | -0,333 | -6,00 | 0,29 | | | | | | | | | | | | | | | | |
| 39 | 65,1 | 4,068 | -0,057 | | | | | | | | | | | | | | | | | | |
| 41 | 67,1 | 4,431 | -0,707 | | | | | | | | | | | | | | | | | | |
| 43 | 69,0 | 4,258 | -0,308 | -5,80 | 0,41 | -6,18 | 0,4 | -5,68 | 0,24 | 38,639 | 0,015 | 15,620 | 0,005 | 18,755 | 0,004 | 2,060 | 0,001 | 0,833 | 0,0001 | 0,70939 | 0,00004 |
| 45 | 71,0 | 4,334 | -0,405 | | | | | | | | | | | | | | | | | | |
| 47 | 73,0 | 4,299 | -0,352 | | | | | | | | | | | | | | | | | | |
| 49 | 74,9 | 4,25 | -0,531 | -6,06 | 0,41 | | | | | | | | | | | | | | | | |
| 51 | 76,9 | 4,244 | -0,191 | | | | | | | | | | | | | | | | | | |
| 53 | 78,9 | 4,149 | -0,202 | | | | | | | | | | | | | | | | | | |
| 55 | 80,8 | 3,793 | -0,355 | -5,87 | 0,41 | -6,39 | 0,4 | -5,36 | 0,24 | 38,671 | 0,015 | 15,630 | 0,005 | 18,766 | 0,004 | 2,061 | 0,001 | 0,833 | 0,0001 | 0,70933 | 0,00004 |
| 57 | 82,8 | 4,11 | -0,283 | | | | | | | | | | | | | | | | | | |
| 59 | 84,7 | 4,205 | -0,543 | -6,00 | 0,24 | | | | | | | | | | | | | | | | |
| 61 | 86,7 | 4,202 | -0,206 | | | | | | | | | | | | | | | | | | |
| 63 | 89,2 | 4,293 | -0,202 | -5,73 | 0,29 | -5,45 | 0,4 | -5,72 | 0,24 | 38,660 | 0,015 | 15,624 | 0,005 | 18,769 | 0,004 | 2,060 | 0,001 | 0,832 | 0,0001 | 0,70929 | 0,00004 |
| 65 | 92,5 | 4,094 | -0,307 | | | | | | | | | | | | | | | | | | |
| 67 | 95,9 | 3,797 | -0,352 | -6,00 | 0,41 | | | | | | | | | | | | | | | | |
| 69 | 99,3 | 4,009 | -0,323 | | | | | | | | | | | | | | | | | | |

| Depth top [cm] | Age [Kyr] | $\delta^{18}O$ benthic | $\delta^{13}C$ benthic | $\varepsilon_{Nd}$ forams | 2σ | $\varepsilon_{Nd}$ leachates | 2σ | $\varepsilon_{Nd}$ detritus | 2σ | $^{208}Pb/^{204}Pb$ leach | 2σ | $^{207}Pb/^{204}Pb$ leach | 2σ | $^{206}Pb/^{204}Pb$ leach | 2σ | $^{208}Pb/^{206}Pb$ leach | 2σ | $^{207}Pb/^{206}Pb$ leach | 2σ | $^{87}Sr/^{86}Sr$ detritus | 2σ |
|---|---|---|---|---|---|---|---|---|---|---|---|---|---|---|---|---|---|---|---|---|---|
| 71 | 102,6 | 3,823 | -0,519 | | | | | | | | | | | | | | | | | | |
| 73 | 106,0 | 4,249 | -0,31 | -5,60 | 0,29 | | | | | | | | | | | | | | | | |
| 75 | 109,4 | 4,236 | -0,4 | -6,21 | 0,29 | | | | | | | | | | | | | | | | |
| 77 | 112,7 | 4,12 | -0,449 | -5,44 | 0,29 | | | | | | | | | | | | | | | | |
| 83 | 122,8 | 3,466 | -0,431 | -6,06 | 0,29 | -5,53 | 0,4 | -5,64 | 0,24 | 38,642 | 0,015 | 15,617 | 0,005 | 18,759 | 0,004 | 2,060 | 0,001 | 0,832 | 0,0001 | 0,70926 | 0,00004 |
| 85 | 126,2 | 4,422 | -0,541 | -5,51 | 0,29 | | | | | | | | | | | | | | | | |
| 87 | 129,6 | 3,642 | -0,447 | -5,31 | 0,41 | -5,96 | 0,4 | -5,72 | 0,24 | 38,686 | 0,015 | 15,631 | 0,005 | 18,763 | 0,004 | 2,062 | 0,001 | 0,833 | 0,0001 | 0,70931 | 0,00004 |
| 89 | 132,8 | 3,972 | -0,662 | -5,31 | 0,29 | | | | | | | | | | | | | | | | |
| 91 | 135,8 | 4,512 | -0,862 | -5,29 | 0,29 | | | | | | | | | | | | | | | | |
| 93 | 138,8 | 4,778 | -0,728 | -4,91 | 0,41 | -5,71 | 0,4 | -5,04 | 0,24 | 38,668 | 0,015 | 15,632 | 0,005 | 18,753 | 0,004 | 2,062 | 0,001 | 0,833 | 0,0001 | 0,70939 | 0,00004 |
| 95 | 141,8 | 4,567 | -1,186 | | | | | | | | | | | | | | | | | | |
| 97 | 144,9 | 3,969 | -0,717 | -5,45 | 0,29 | | | | | | | | | | | | | | | | |
| 99 | 147,9 | 4,671 | -0,769 | | | | | | | | | | | | | | | | | | |
| 101 | 150,9 | 4,54 | -1,006 | -5,25 | 0,29 | | | | | | | | | | | | | | | | |
| 103 | 153,9 | 4,53 | -0,871 | | | | | | | | | | | | | | | | | | |
| 105 | 157,0 | 4,642 | -1,13 | -6,43 | 0,29 | | | | | | | | | | | | | | | | |
| 107 | 160,0 | 4,461 | -0,826 | | | | | | | | | | | | | | | | | | |
| 109 | 163,0 | 4,557 | -0,935 | -5,99 | 0,41 | | | -5,13 | 0,19 | | | | | | | | | | | 0,70990 | 0,00012 |
| 111 | 166,0 | 4,506 | -0,891 | | | | | | | | | | | | | | | | | | |
| 113 | 169,1 | 4,386 | -0,841 | -5,86 | 0,29 | | | | | | | | | | | | | | | | |
| 115 | 172,1 | 4,367 | -1,113 | | | | | | | | | | | | | | | | | | |
| 117 | 175,1 | 4,314 | -0,956 | -5,22 | 0,41 | | | | | | | | | | | | | | | | |
| 119 | 178,1 | 4,572 | -0,843 | | | | | | | | | | | | | | | | | | |
| 121 | 181,2 | 4,242 | -0,836 | | | | | | | | | | | | | | | | | | |
| 123 | 184,2 | 4,18 | -0,893 | -5,95 | 0,41 | -6,39 | 0,4 | -5,96 | 0,24 | 38,678 | 0,015 | 15,632 | 0,005 | 18,763 | 0,004 | 2,061 | 0,001 | 0,833 | 0,0001 | 0,70937 | 0,00004 |
| 125 | 187,2 | 4,398 | -0,88 | | | | | | | | | | | | | | | | | | |
| 127 | 191,5 | 4,347 | -0,835 | -5,47 | 0,29 | | | | | | | | | | | | | | | | |
| 129 | 196,1 | 3,788 | -0,458 | | | | | | | | | | | | | | | | | | |
| 131 | 200,7 | 3,493 | -0,765 | -6,24 | 0,41 | -5,99 | 0,4 | -5,98 | 0,24 | 38,690 | 0,015 | 15,633 | 0,005 | 18,770 | 0,004 | 2,061 | 0,001 | 0,833 | 0,0001 | 0,70924 | 0,00004 |
| 133 | 205,1 | 4,158 | -1,121 | | | | | | | | | | | | | | | | | | |
| 135 | 207,8 | 3,968 | -0,68 | | | | | | | | | | | | | | | | | | |
| 137 | 210,4 | 3,923 | -0,312 | | | | | | | | | | | | | | | | | | |
| 139 | 213,1 | 3,914 | -0,927 | -5,49 | 0,24 | | | | | | | | | | | | | | | | |
| 141 | 215,7 | 4,196 | -0,61 | | | | | | | | | | | | | | | | | | |
| 143 | 218,3 | 4,259 | -0,823 | -5,86 | 0,41 | -5,71 | 0,4 | -5,67 | 0,24 | 38,703 | 0,015 | 15,637 | 0,005 | 18,779 | 0,004 | 2,061 | 0,001 | 0,833 | 0,0001 | 0,70933 | 0,00004 |
| 145 | 221,0 | 4,258 | -0,806 | | | | | | | | | | | | | | | | | | |

# Acknowledgements

First of all I want to thank Martin for giving me this opportunity, for his guidance and motivation during these years and for giving me free rein in my research.

I also want to thank Dirk for his support, especially during my first days at GEOMAR and during the cruise. Same for Raul, who was also a very nice office mate. The long cruise across the Pacific and the time in New Zealand afterwards was a very good and enriching experience, in part thanks to the people involved, most of them from AWI, including Ralf and Frank, who leaded the cruise perfectly.

I thank the entire working group of Martin for teaching me and guiding me in the labs and the mass spectrometer, especially Roland, Cecile, Clauschi, Steffie and Moritz, who helped me a lot in the beginning. but also the others I don't mention here. And especially, Jutta, who makes the entire work possible in our working group, as well as Chris and Ed, who take care of the 'baby-Nu'. Ed gave me a lot of ideas while writing our manuscripts, which improved them a lot.

A special mention to Ingmar, who picked a lot of forams for me!

I learned very much about paleoclimate and geochemistry in the congresses I visited as well as during the talks at GEOMAR and the visits to the AWI (Bremerhaven). I am very glad I had these opportunities.

I am also very happy that I shared this time with a lot of nice people I met in GEOMAR, especially the paleoceanography group, from where I take many good friends.

Finally I want to thank my family for their support and constant interest on my work during these period, my friends in Kiel who enriched my experience here considerably, and very specially, to Idoia, who is always there, accompanying, believing and sharing. This wouldn't have been possible without you.